CALIFORNIA INSTITUTE OF TECHNOLOGY

EARTHQUAKE ENGINEERING RESEARCH LABORATORY

AN INVESTIGATION OF THE DYNAMIC CHARACTERISTICS OF AN EARTH DAM

BY

A. M. ABDEL-GHAFFAR AND R. F. SCOTT

REPORT NO. EERL 78-02

A Report on Research Conducted under Grants
from the National Science Foundation and
the Earthquake Research Affiliates Program
at the California Institute of Technology

PASADENA, CALIFORNIA

AUGUST, 1978

This report is based on research conducted under Grant No. ATA 74-19135 from the National Science Foundation and with support from the Earthquake Research Affiliates. Any opinions, findings, and conclusions or recommendations expressed in this publication are those of the authors and do not necessarily reflect the views of the National Science Foundation.

CALIFORNIA INSTITUTE OF TECHNOLOGY

EARTHQUAKE ENGINEERING RESEARCH LABORATORY

AN INVESTIGATION OF THE DYNAMIC CHARACTERISTICS OF AN EARTH DAM

By

A. M. Abdel-Ghaffar and R. F. Scott

Report No. EERL 78-02

A Report on Research Conducted under Grants from
the National Science Foundation and
the Earthquake Research Affiliates Program at
the California Institute of Technology

Pasadena, California

August, 1978

TABLE OF CONTENTS

ACKNOWLEDGMENTS

The authors wish to acknowledge the work of Dr. John B. Berrill who calculated the time differences between the crest and the base records of the Santa Felicia Dam from the 1971 San Fernando earthquake.

The authors are grateful to Kinemetrics Inc. of Pasadena, California, for providing the instruments for the wave-velocity measurements and to the United Water Conservation District of Ventura County, California for giving permission to make the tests on Santa Felicia Dam. The assistance provided by R. Relles, P. Spanos and J-H Prevost in conducting the tests is greatly appreciated. Gratitude is also extended to Sai-Man Li for the time and effort he contributed to the digitization and computer processing of the 1976 earthquake records.

This research was supported by grants from the National Science Foundation and the Earthquake Research Affiliates program at the California Institute of Technology.

ABSTRACT

An investigation has been made to analyze observations of the effect of two earthquakes (with $M_L = 6.3$ and 4.7) on Santa Felicia Dam, a rolled-fill embankment located in Southern California. The dam is 236.5 ft. high and 1,275 ft. long by 30 ft. wide at the crest. The purpose of the investigation is: (1) to study the nonlinear behavior of the dam during the two earthquakes, (2) to provide data on the in-plane dynamic shear moduli and damping factors for the materials of the dam during real earthquake conditions, and (3) to compare these properties with those previously available from laboratory investigations.

From the recorded motions of the dam, amplification spectra were computed to indicate the natural frequencies of the dam and to estimate the relative contribution of different modes of vibrations. A comparison between these natural frequencies and those obtained by two elastic shear-beam models was made to obtain representative dam material properties. In addition, field wave-velocity measurements were carried out as a further check as well as to study the variation of shear wave velocity at various depths in the dam. The amplification spectra showed a predominant frequency of 1.45 Hz in the upstream/downstream direction; in this direction the response was treated as that of a single-degree-of-freedom hysteretic structure. Three types of digital band-pass filtering of the crest and abutment records were used to enhance the hysteresis loops which show the relationship between the relative displacement of the crest with respect to the abutment and the absolute acceleration of the dam. A method is described which, using some of the existing elastic-response theories, enables the shear stresses and

strains, and consequently the shear moduli, to be evaluated from the hysteresis loops. The equivalent viscous damping factors were calculated from the areas inside the hysteresis loops. The shear moduli and the damping factors were determined as functions of the induced strains in the dam. Finally, the shear moduli and damping factors obtained for the dam were compared with previously available laboratory data for sands and saturated clays.

INTRODUCTION

As far as the field of Earthquake Engineering is concerned, there are very few "complete" instrumental records to indicate the nature of the response of earth dams to strong earthquakes; however, there are limited records available for smaller shocks. The term "complete" records means records that are capable of providing a completely adequate definition of input ground motion as well as dam structural response. The input motion can be measured by strong-motion accelerographs, often mounted on dam abutments or at an appropriate site in the immediate vicinity of the dam that is not obviously influenced in a major way by local geologic structural features, as indicated by Bolt and Hudson (1975). The instruments to measure dam response can usually be mounted at different locations (at least two) on the crest, avoiding special superstructures which may introduce localized dynamic behavior.

The limited instrumental records available for smaller shocks and microtremors, in both the United States and Japan, indicate that the ground motion is increasingly magnified with increasing elevation over the height of the dam. Consequently, an earth dam does not behave as a rigid body during an earthquake, but rather the magnitude and distribution of acceleration on the dam are influenced by its dynamic response characteristics. Clearly, the behavior during these smaller shocks and microtremors would be a poor indication of a dam's performance during strong earthquake shaking because of the nonlinear behavior of soils.

Much effort and progress have been made in the development of

analytical as well as numerical techniques for evaluating the response of earth dams subjected to earthquake motions. Successful application of all these existing techniques is essentially dependent on the incorporation of representative dam-material properties in the analyses. Because the behavior of earth dams during earthquakes is governed by their dynamic response characteristics, it is possible to learn much about the dynamic properties of such structures from examination of their response to strong earthquake shaking. Unfortunately direct measurements are infrequent, since moderately large earthquakes are rare. It is difficult, without measurements, to compare behavior with earthquake design requirements (Bolt and Hudson, 1975), in order to estimate the performance of other dams and to make rational design decisions for repair and strengthening of the structures.

It is the purpose of this investigation to: (1) discuss the problem of analyzing the behavior of earth dams during earthquakes, (2) provide some data, from the earthquake-response observations, on the dynamic shear moduli and damping factors for earth dam materials, (3) correlate this data with that obtained for sands and saturated clays (most of the data available to date have been developed for sands and saturated clays only) and finally (4) permit better understanding of the response characteristics of earth dams to earthquakes.

This study deals with results from observations of the effect of two earthquakes (one with $M_L = 6.3$ and an epicentral distance of 33.0 Km and the other with $M_L = 4.7$ and an epicentral distance of 14.0 Km, see Fig. 1) on an actual earth dam: Santa Felicia Dam; it is a rolled-fill embankment located in Santa Paula, Ventura County, California and built in 1954-55. The dam is 236.5 ft high, 1,275 ft long at the crest, 450 ft long

across the valley at the base, 30 ft. wide at the crest and approximately 1,400 ft. wide at the base. The dam was equipped with two accelerographs (AR-240) in June 1967; one accelerograph was located at the central section of the dam crest (55 feet east of the crest midpoint), and an abutment accelerograph was placed in the caretaker's shop at the downstream end of the dam. Recently (in early 1977) the existing AR-240 accelerograph on the abutment was replaced with a new and improved instrument (SMA-1) that will give better information on the timing of recorded ground motion through greater reliability and earlier triggering. Records from two earthquakes were recovered and analyzed in this study; that from the San Fernando earthquake of February 9, 1971 ($M_L = 6.3$) and that from the Southern California earthquake of April 8, 1976 ($M_L = 4.7$). Amplification spectra of the dam were computed for the two earthquakes by dividing the Fourier amplitude spectrum of the acceleration recorded at the crest by that recorded at the abutment. Analysis of the observed records reveals that the acceleration amplitude is amplified mostly at the dam crest. In the upstream/downstream direction the spectra show a predominant single peak at the fundamental frequency of 1.45Hz. In addition, a visual inspection of the amplification spectra obtained from the two earthquakes reveals that the values of the resonant frequencies vary slightly from one earthquake to the other. Certain existing elastic shear-beam theories were used to check the values of the resonant frequencies corresponding to peak values of the amplification spectra and to estimate the shear wave velocity of the dam material. Field wave-velocity measurements were carried out for Santa Felicia Dam to: (1) further check the suggested shear wave velocity which was estimated from the observed resonant frequencies

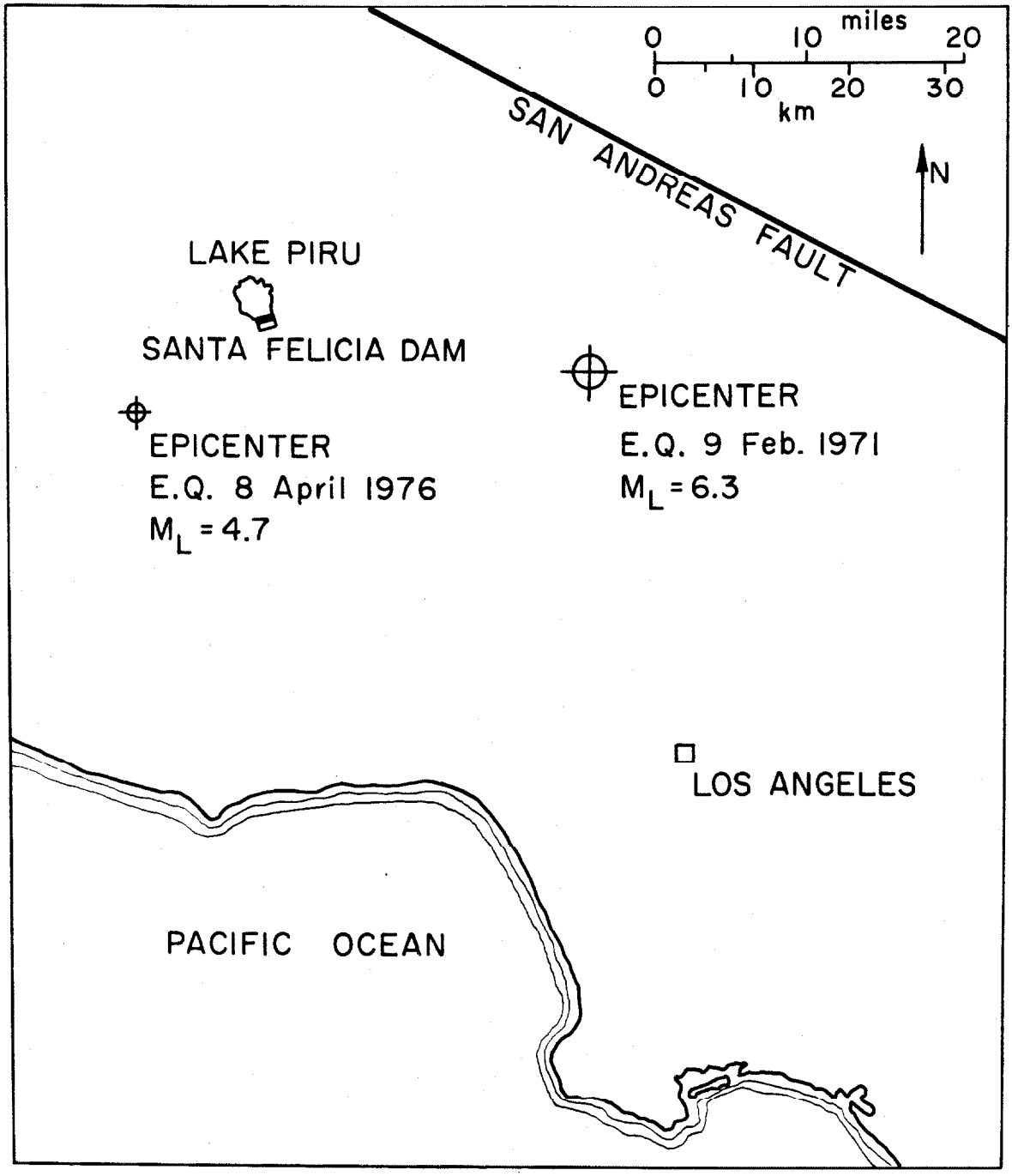

Fig. 1 Overall location map showing Santa Felicia Dam and the epicenters of the two earthquakes

as well as from use of the existing shear-beam theories, (2) study the variation of the shear wave velocity at various depths in the dam, and finally (3) establish a representative and reliable mean value of the material constants for use in earthquake response analysis.

In this investigation, the response of the upstream/downstream fundamental mode is treated as that of a single-degree-of-freedom hysteretic structure, as suggested for a building structure by Iemura and Jennings (1973). Three types of digital band-pass filtering of the crest and the abutment records were used to give hysteresis loops which show the relationship between the relative displacement of the crest with respect to the abutment and the absolute acceleration of the dam. In evaluating the earthquake response of the dam, one-dimensional shear-beam theory with shear modulus varying with depth was used to estimate dynamic shear strains and stresses. However, a two-dimensional theory with constant shear modulus was used to compare the results. An effort was made to simplify the presentation of the mathematics necessary for dynamic analysis of the dam models. Using two existing elastic-response theories, a method was outlined whereby the shear stresses and strains could be determined as functions of the maximum absolute acceleration and maximum relative displacement, respectively, for each hysteresis loop; this enables evaluation of the shear moduli. The equivalent linear shear modulus was expressed as the secant modulus determined by the slope of the line joining the extreme points of the hysteresis loop. Although the assumption of elastic behavior during earthquakes is not strictly correct for earth dams, it was used to provide a basis for establishing the natural frequencies of the dam, and in addition to give at least a qualitative picture

of the dynamic response characteristics of the dam for each hysteresis loop. Then, the damping factor value was evaluated from the area inside the hysteresis loop. Since each of the shear moduli and damping factors depends on the magnitude of strain for which the hysteresis loop is determined, these dynamic properties were determined, for the gravelly material of the dam, as functions of the induced strains in the dam. Finally, the data obtained on the dynamic shear moduli and damping factors were compared with previously available data for sands and saturated clays.

A. INPUT INFORMATION

A-I DESCRIPTION OF SANTA FELICIA DAM

Santa Felicia Dam (Fig. 2) is located on Piru Creek, about 4.5 miles (7.25 Km) northeast of the town of Piru in Ventura County, Southern California, which is 65 Km north-west of Los Angeles. It is owned by the United Water Conservation District (UWCD) of Ventura County, California and was designed by the UWCD and Bechtel Corporation; it was begun in April 1954 and completed in December 1955. The dam was built to provide a supplemental water supply to meet the growing agricultural, municipal and industrial needs of District lands in the Santa Clara River Valley and Coastal Plain by storing the flood waters of Piru Creek which otherwise would be wasted in the ocean.

The dam consists of a rolled-fill embankment, a low-level outlet works and an ungated chute spillway. The dam is about 273 ft. high above its lowest foundation and approximately 200 ft. above the original stream bed; it is about 450 ft. long across the valley at the base and approximately 1,400 ft. wide at the base. The crest has a width of 30 ft. and a length of approximately 1,275 ft.; upstream and downstream slopes are 2.25:1 and 2:1, respectively. An impervious core with 0.33:1 slopes is carried up from bedrock which is at an estimated average depth of 75 ft. below the stream bed. An open, concrete-lined spillway channel with ungated crest 20 ft. lower than the top of the dam is located on the terrace, west of the western abutment. Figure 3 shows structural details of the dam cross-section, a longitudinal cross-section and a plan view of the dam. The dam's reservoir, Lake Piru, extends upstream for 5 miles at full supply

level and has a capacity of 100,000 acre feet (Ref. 1).

From the geological point of view, the Santa Felicia Dam site lies within a series of sandstones and shales of Miocene Age which have been conspicuously folded and tilted. The sandstones are predominantly medium-grained and loosely cemented. The shales are variable in character, ranging from silty to clay. The geological formations are interstratified in a great variety of combinations. Thus, the bedrock at Santa Felicia Dam consists of sandstone strata of varying degrees of hardness interlayered with shale seams of varying thickness. In general, the geological conditions were favorable for the construction of the dam (Ref. 21).

The geology of the site was utilized to provide a sound, watertight and economical section and to assure a firm seal between the bedrock and the impervious central core throughout the dam's length. The sands and gravel of the stream bed, 70 to 90 ft in thickness at the dam site, were used as a foundation for the pervious shells of the dam, up- and down-stream from the impervious core.

The embankment has a total of about 3,400,000 cubic yards of core and shell material which is basically of an alluvial nature and which was obtained from borrow pits at the reservoir site and from sites up- and down-stream. The alluvium consists of clay, sand, gravel and boulders. Suitable gravelly materials from the core cut-off trench excavation were used for construction of the pervious shell embankments. The core material (824,500 cubic yards) was selected from the upstream impervious borrow pit areas on the basis of laboratory tests. In the construction of the embankment, the impervious core materials were spread in almost horizontal layers not more than 8 inches thick before compaction, and

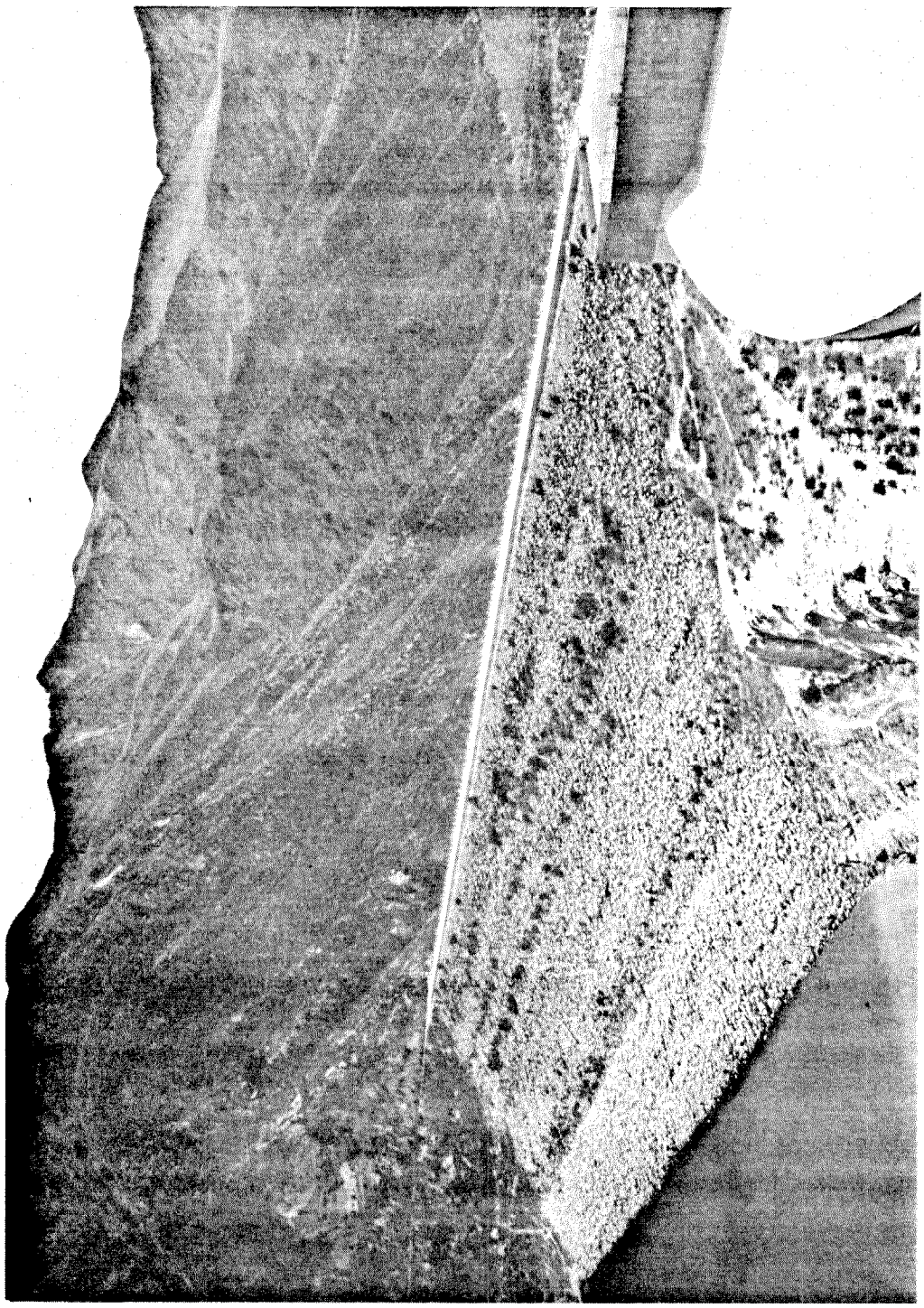

Fig. 2 General view showing the upstream side of Santa Felicia Dam and part of the spillway at the right (western) abutment

SANTA FELICIA DAM
SANTA PAULA , CALIFORNIA

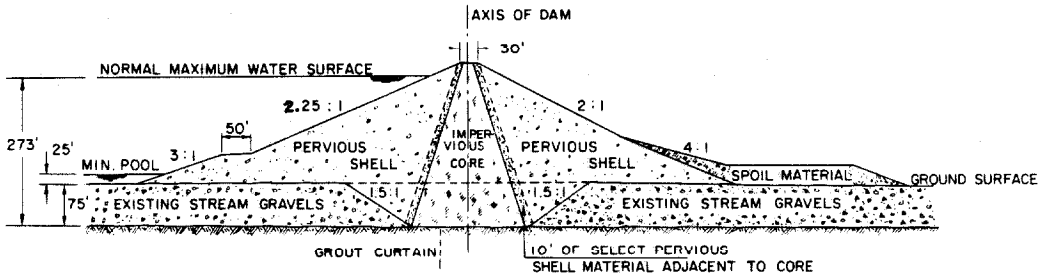

CROSS SECTION OF THE DAM

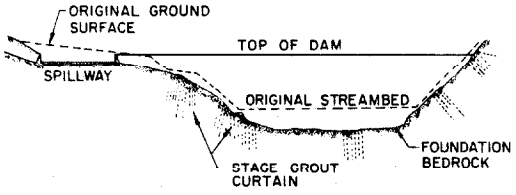

DEVELOPED PROFILE ON AXIS DAM LOOKING UPSTREAM

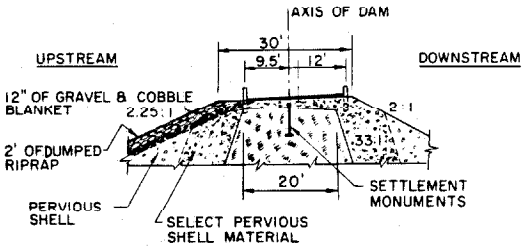

CREST DETAIL

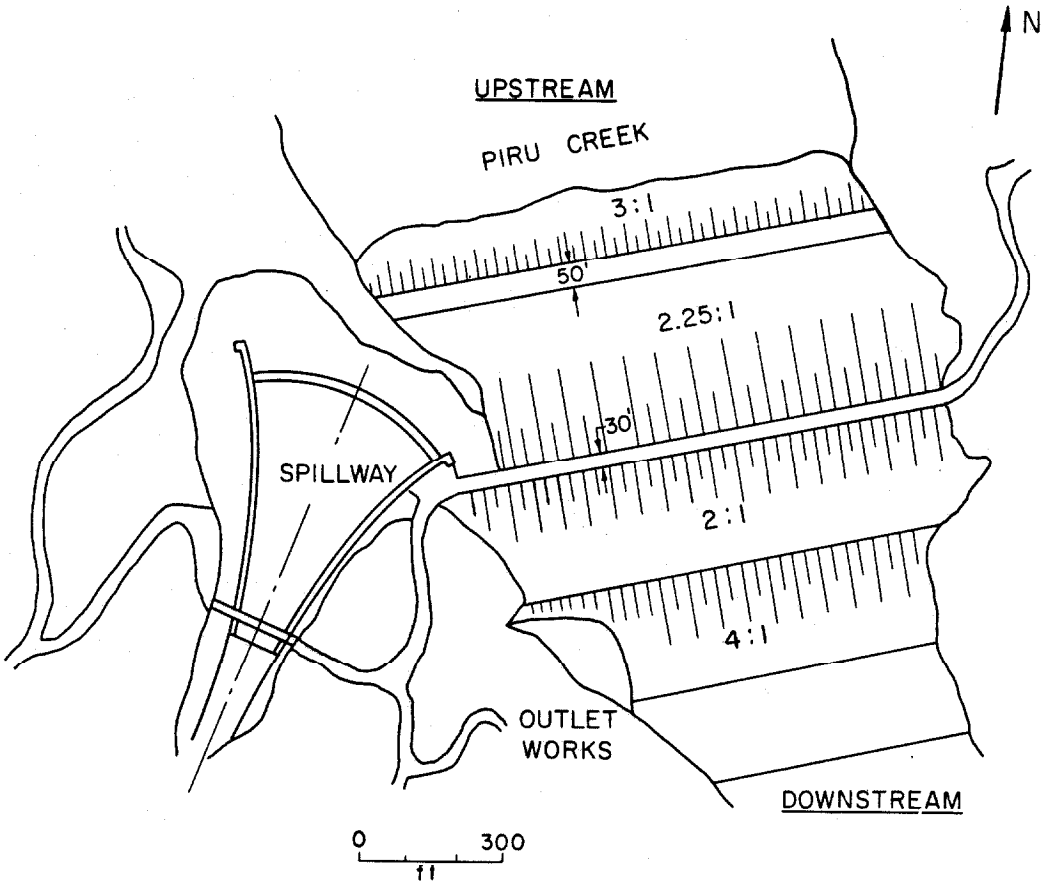

PLAN VIEW

Fig. 3 Structural details of Santa Felicia Dam

pervious shell materials in layers not over 18 inches in thickness. Fifty-ton four-wheel pneumatic-tired rollers were used for compacting the impervious core and the pervious shell. After all suitable materials from the core trench excavation had been utilized, the sands and gravels of the river bed were used in the pervious fills. The core material has a high degree of impermeability, is granular in nature and possesses considerable strength. A one-foot layer of gravel and cobble was placed on the downstream slope of the dam and on the upstream face. The latter was designed to serve as both a bed and a drain for the riprap. The purpose of the layer on the downstream face of the dam was to prevent erosion of the face of the dam from rain.

The laboratory and field tests, during and before construction, included moisture determinations, density-in-place tests, particle size analyses, specific gravity determinations, and permeability tests. Table 1 indicates design values conservatively assumed to be representative of the typical soils as determined from results of the soil testing program in the field and laboratory.

In order to prevent leakage through the rock formations underlying the dam and to insure a good cut off from the reservoir, a continuous grout curtain was provided in the bedrock throughout the entire length of the dam approximately parallel to the axis, and to a depth of 120 ft. below the surface bedrock. A similar curtain of grout was placed beneath the crest of the spillway and joined to the main curtain of the dam.

The ungated concrete spillway of the dam has a discharge capacity of 105,000 cubic feet per second with the water surface five feet below the top of the dam. This allows for the "maximum possible flood"

estimated for the stream and is three times the greatest flood that has occurred during the period of record.

The outlet works structure, which extends through the base of the dam, is built primarily on the rock bench which forms a part of the right or west abutment at about stream bed level. The function of the outlet works is to release, control the flow of stored water for spreading and and to recharge the ground water for domestic and industrial water supply, irrigation and other downstream uses.

More detailed information concerning the design and construction is given by Price (1956).

TABLE 1

Characteristics of Santa Felicia Dam Materials (Ref. 1)

Property	Core	Shell	Foundation
Dry unit weight	114 pcf	125 pcf	116 pcf
Moist unit weight	131 pcf	131 pcf	122 pcf
Saturated unit weight	134 pcf	141 pcf	135 pcf
Submerged unit weight	73 pcf	79 pcf	73 pcf
Coefficient of friction	0.60	0.84	0.81
Permeability	0.001 ft/day	20 ft/day	150 ft/day
Specific gravity	2.68	2.69	2.69

A-II STRONG-MOTION INSTRUMENTATION OF THE DAM

A-II-1. Location of Strong-Motion Instrumentation

Two strong-motion accelerographs (AR-240) and six seismoscopes were installed in June 1967, on and around Santa Felicia Dam. The crest accelerograph was located at the center section of the dam crest, 20 ft. south of the dam axis and 55 ft. east of the crest mid-point (see Fig. 4). The small building shown in Fig. 5 housed the crest accelerograph and one of the six seismoscopes. The abutment accelerograph was placed in the caretaker's shop at the downstream end of the outlet tunnel as shown in Fig. 7-a; this also provided a shelter for the second seismoscope. The time trace circuits of both the base and the crest accelerograms were tied together. Two seismoscopes were located on the east and west abutments of the dam. Figure 6 shows the east abutment seismoscope. Another seismoscope was near the end of the downstream slope close to bedrock, and the last one was placed on the crest one-fourth of the way from the spillway. The accelerographs were not moved until recently (early 1977) when the AR-240 on the abutment was replaced by an SMA-1 equipped with WWVB receiver. Figure 7-a shows the seismoscope array of Santa Felicia Dam.

A-II-2 Up-grading of the Strong-Motion Accelerographs

Recent concern about the so-called "Palmdale Uplift" along the San Andreas Fault has led both seismologists and earthquake engineers to re-examine the strong-motion earthquake recorders in that general area, as indicated by Housner[2]. In particular, the Lake Hughes array of strong-motion accelerographs is being upgraded and extended. This array starts with an instrument by the San Andreas Fault near Lake Hughes and extends in a southwesterly direction with four accelerographs spaced a couple of miles apart. The strong-motion accelerograph below Santa Felicia Dam makes a logical extension of this area. As mentioned before, the abutment accelerograph was replaced with a new and improved instrument; however, the crest accelerograph has not been replaced since it was installed in June 1967. Generally, this improvement will give better information on the timing of the recorded ground motion through greater reliability, earlier triggering, and higher compatibility with the radio time receivers. In addition, if the accelerograph on the crest of the dam is replaced with a new, improved instrument, this would provide much better information for analyzing the structural behavior of the dam, especially if a strong earthquake originates on the San Andreas Fault.

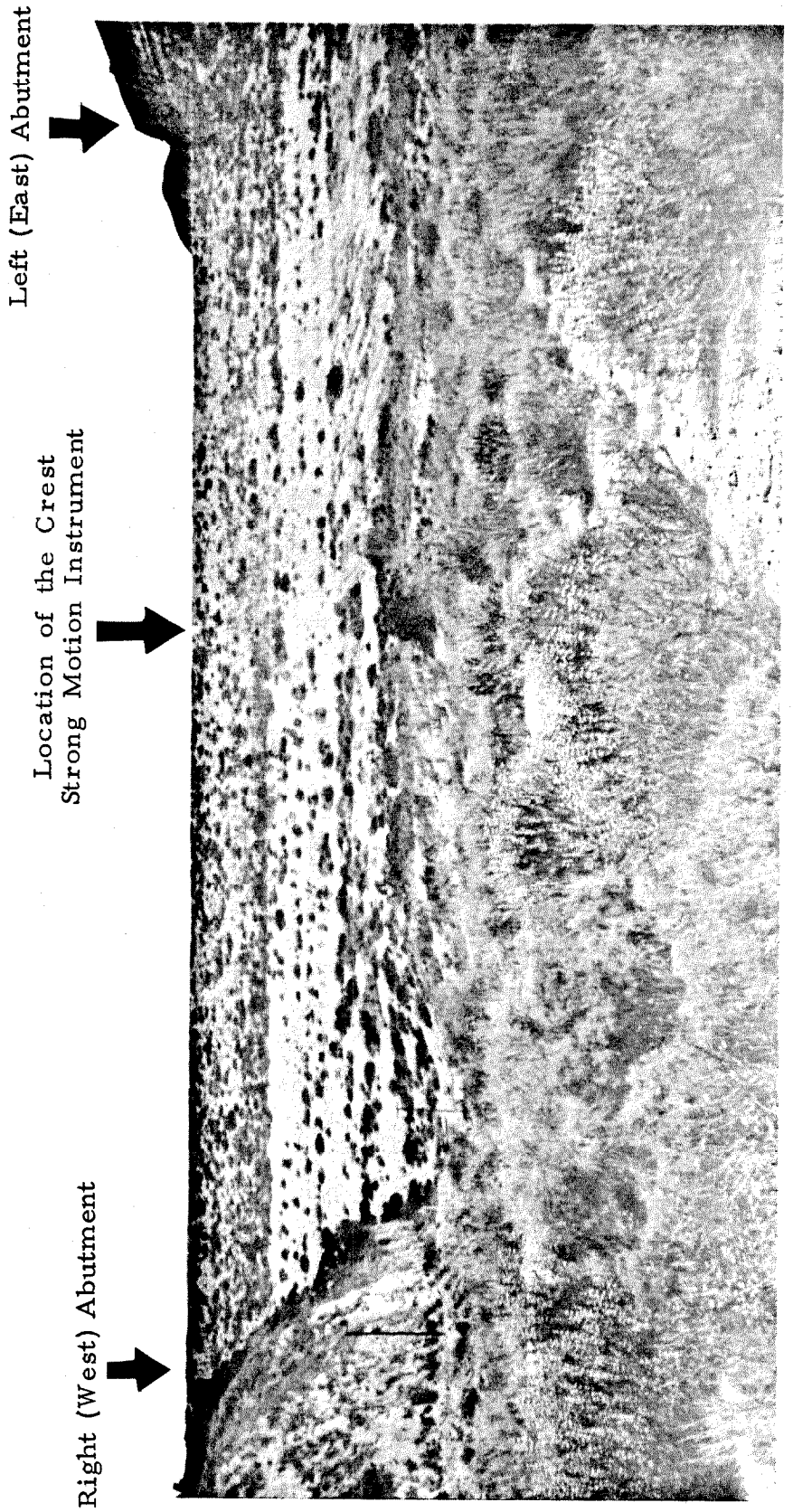

Fig. 4 A view looking upstream to show the location of the crest strong-motion instrument

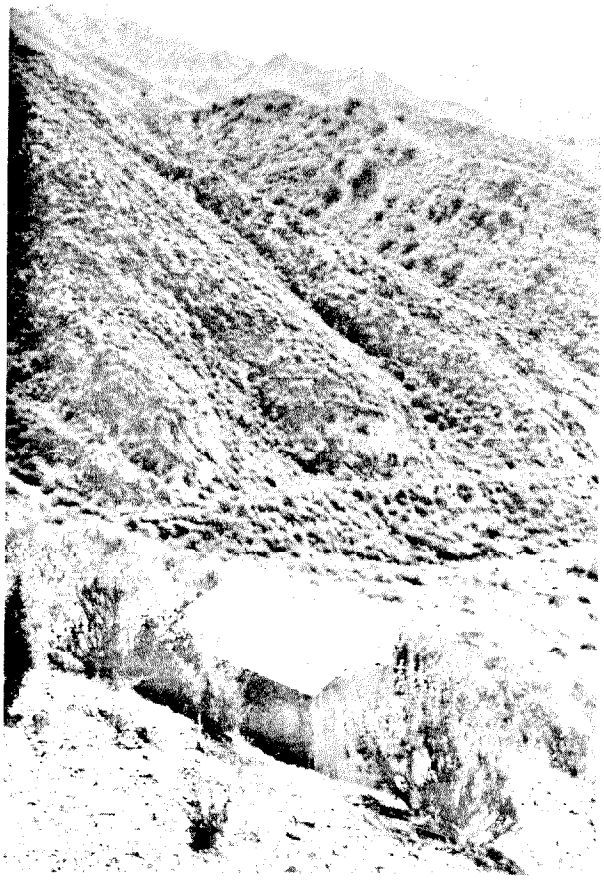

Fig. 5 Location of the crest accelerograph

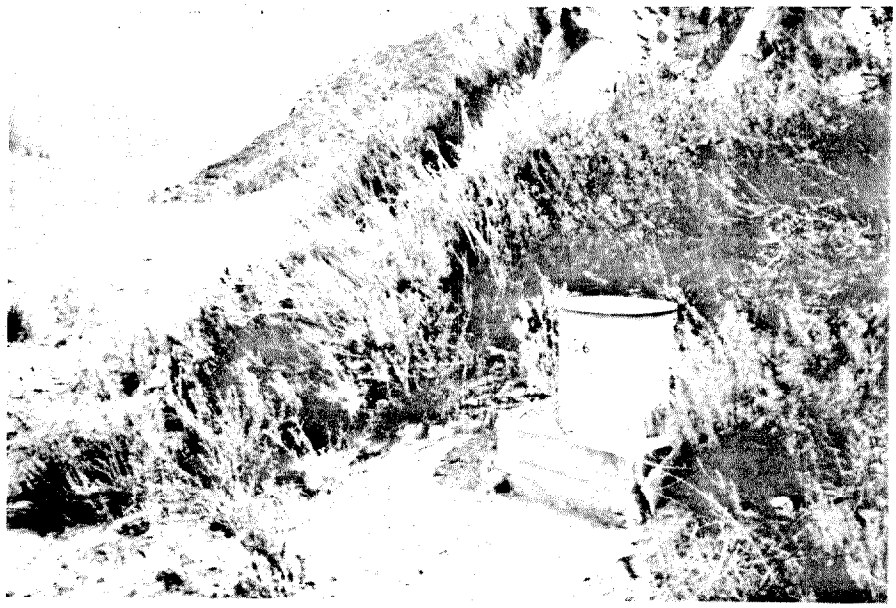

Fig. 6 East (left) abutment seismoscope

SANTA FELICIA DAM , CALIFORNIA
LOCATIONS OF THE STRONG-MOTION INSTRUMENTS
DURING THE SAN FERNANDO EARTHQUAKE OF FEB. 9 , 1971

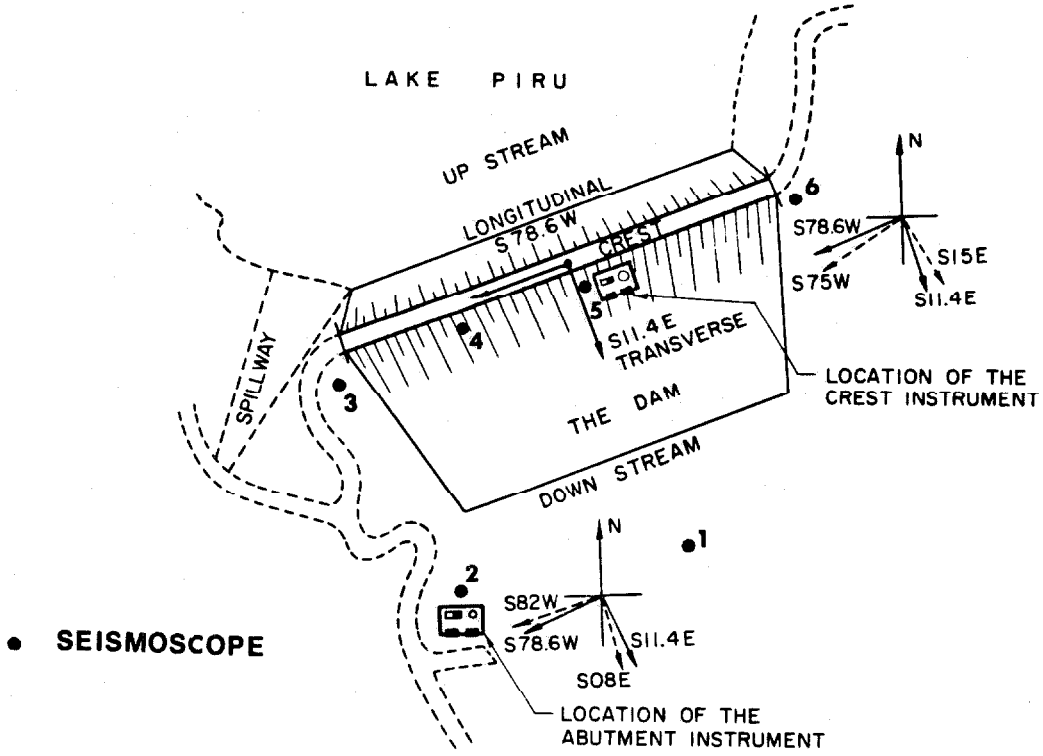

(a) GENERAL VIEW

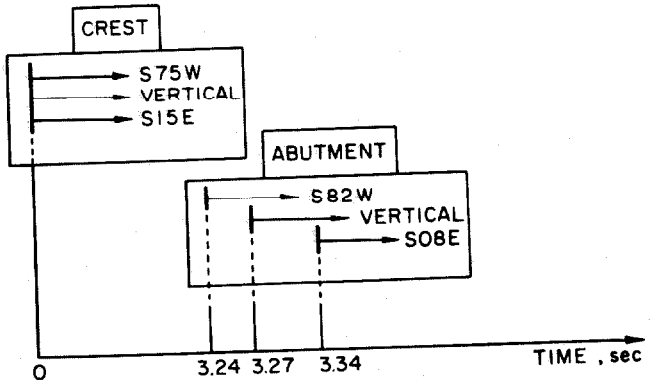

(b) TIME DIFFERENCES BETWEEN THE RECORDS

Fig. 7

A-III PERFORMANCE OF THE DAM DURING TWO EARTHQUAKES

Two accelerograms, each composed of three components, one at the abutment and one at the crest, were obtained at Santa Felicia Dam during two recent earthquakes. One record was recovered from the San Fernando earthquake of February 9, 1971 which had a local magnitude of 6.3, and the other record was recovered from the Southern California earthquake of April 8, 1976 which had a local magnitude of 4.7. In this section, the performance of the dam during these two earthquakes is examined.

A-III-1 San Fernando Earthquake of February 9, 1971

On February 9, 1971, at approximately 6:00 a.m. the six seismoscopes and the two accelerometers at the crest and the base (Figs. 6-a and 7) of Santa Felicia Dam were activated by a strong shake. Afterwards, inspection of the east abutment seismoscope indicated that the motion was roughly northwest - southeast. Figure 8 shows the oscillations which were scratched on the smoked glass of the six seismoscopes. The dam was about 33.4 Km west of the San Fernando epicenter; the precise direction between epicenter and dam was N80^{o}W. Table 2-a lists all six recovered seismoscope records. For each record, the maximum displacement on the plate was measured (from the initial zero point), and the maximum relative displacement response spectrum, S_d, was calculated (Hudson, 1971).

Both the abutment and the crest accelerograms were recorded on AR-240 accelerographs. Figures 9 through 11 show the crest and abutment records, and Table 2-b is a summary of both of the accelerograph records.

262 SANTA FELICIA DAM - TOE, S-1

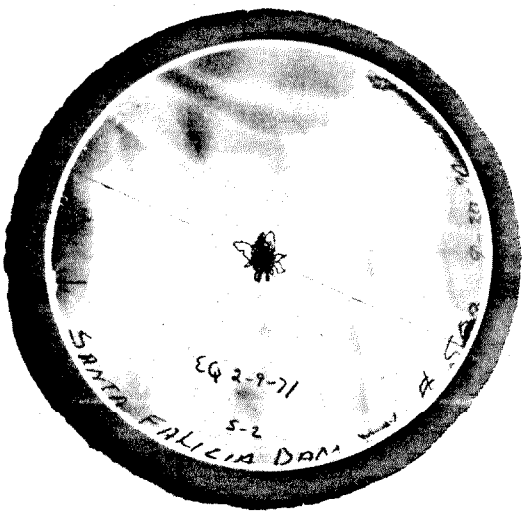

263 SANTA FELICIA DAM - OUTLET WORKS, S-2

NORTH

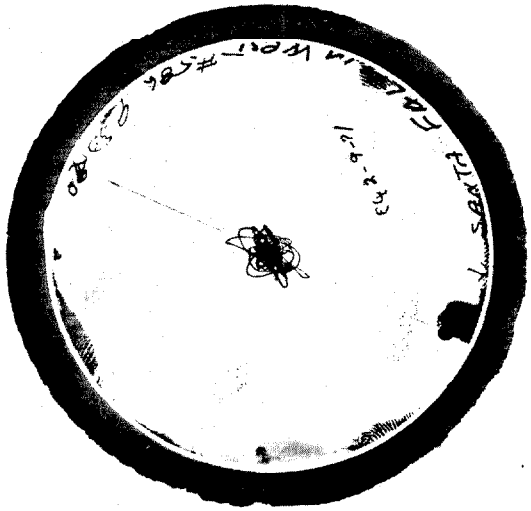

264 SANTA FELICIA DAM - RIGHT ABUT., S-3

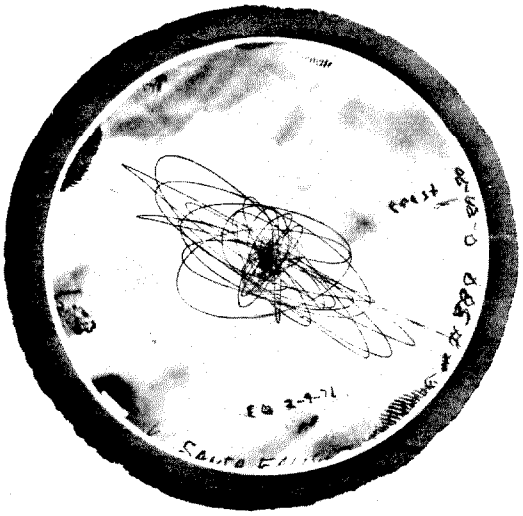

265 SANTA FELICIA DAM - RIGHT CREST, S-4

2 CM

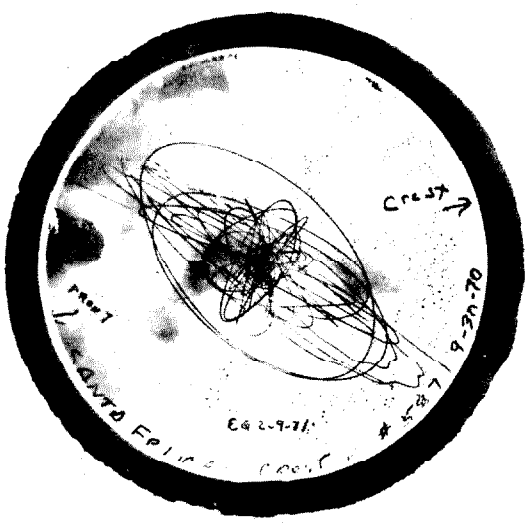

266 SANTA FELICIA DAM - CREST, S-5

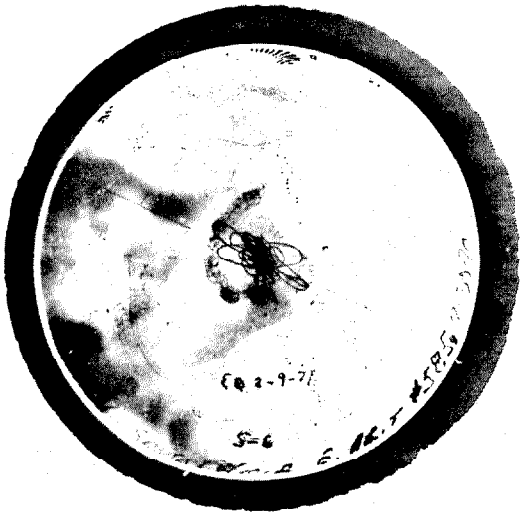

267 SANTA FELICIA DAM - LEFT ABUT., S-6

Fig. 8

TABLE 2-a

Seismoscope Records of Santa Felicia Dam

Location	Seismoscope	Location from Epicenter		Max. Rel. Displacement	
		Direction (N-C. W. -Deg.*)	Distance (Km)	Direction (N-C. W. -Deg.*)	S_d (cm)
Dam toe	S-1	282	33.4	290	2.10
Outlet works	S-2	282	33.4	295	1.24
Right abutment	S-3	282	33.4	288	1.82
Right crest	S-4	282	33.4	302	5.63
Dam crest	S-5	282	33.4	305	6.28
Left abutment	S-6	282	33.4	303	2.30

* Means direction in degrees from North clockwise

TABLE 2-b

Summary of the Santa Felicia Dam Accelerograph Records

Event	Station Location		Component	Volume I (Uncorrected Accelerograms) Max. Accel. (g)	Volume II (Corrected Accelerograms) Max. Accel. (g)
	Name	Coordinate			
February 9 1971 San Fernando Earthquake Local magnitude 6.3	Crest	34.46 N 118.75 W	S15E S75W Down	0.211 0.184 0.070	0.207 0.177 0.066
	Outlet works (Abutment)	34.46 N 118.75 W	S08E S82W Down	0.231 0.231 0.087	0.217 0.202 0.065

Standard data processing, including the uncorrected digitized accelerograms, the corrected accelerograms, integrated velocity and displacement records, the response spectrum curves and finally the Fourier amplitude spectra, of these records can be found in Caltech Reports Nos. EERL 71-22, 73-50, 73-83 and 73-103.

It is important to indicate that the time trace circuits were interconnected, so that the timing pips on both the abutment and the crest accelerograms represent the same absolute time, plus or minus some multiple of 0.5 seconds (since the instruments did not necessarily trigger simultaneously). The first 3 to 3.5 seconds of the abutment record have been lost due to double exposure. Furthermore, the edge of the doubly-exposed area is not normal to the axis of the film and hence the recoverable traces in each of the three directional components start at different times, as illustrated in Fig. 7-b.

However, by comparing peaks in the Caltech-digitized Vol. II record with the same peaks in a copy of the original record, it appears that, in the digitization process, the time scale of the digitized record was reset to zero at the beginning of each trace, so that the relation between the components was eradicated.

The time differences, to the nearest .02 secs, between the Vol. II time scales of the crest and abutment (outlet works) records are given in Table 3. They were found by first comparing displacement peaks in the two records to find the approximate time difference to the nearest timing mark. An allowance of approximately 0.2 secs was made for the displacement pulse to travel the height of the dam (273 ft.). Knowing the time differences to the nearest 0.5 secs, corresponding acceleration peaks in the digitized and in the original records were compared to find

TABLE 3

Time Differences Between the Digitized Volume II Records
Santa Felicia Dam, February 9, 1971

Abutment Record Component	Time of Crest Record at Start of Abutment Record (Seconds)
S82W	3.24
S08E	3.34
Down	3.27

the precise time differences.

Finally, since neither instrument was exactly aligned with the dam axis (S78.6°W) the horizontal components of each record were rotated to be parallel and normal to the dam axis (see Fig.6-a). The rotations were small; 3.4° at the abutment and 3.6° in the opposite direction at the crest. The difference between the starting times of the base record components were taken into account, and rotated horizontal components were obtained starting at 3.34 secs on the crest record time scale as shown in Fig.6-b.

A further complication in the base record developed due to the fact that the floor of the valve house, to which the instrument was fixed, apparently rested on a concrete standpipe rather than on firm ground. Presumably this is the cause of the peaks in the Fourier amplitude spectra of the abutment record, near 10 Hz (this will be shown later in this report).

a - Interpretation of the Recorded Accelerograms

The two digitized and filtered accelerograms of the abutment and of the crest obtained at Santa Felicia Dam during the San Fernando earthquake, along with the calculated velocities and displacements, are shown in Figs. 9 through 11. In these figures, it is important to note the different time origins of the accelerograms.

In the upstream/downstream component (S11.4°E) of both the crest and the abutment records (Fig. 9), there is a region (from 0 to about 20 seconds) which has a high acceleration level with relatively high predominant frequencies, whereas the remainder of the records (from about 20 to 50 seconds) show a low acceleration level and lower predominant frequencies. Thus, possibly there is a greater contribution from surface waves in the latter portion of both the crest and the abutment accelerograms.

The first part (0 to 20 seconds) of the crest accelerogram, shown in Fig. 9-a, consists of the first mode response of the dam, with an apparent period of about 0.7 secs, superimposed on long-period surface waves. In addition, the displacement curve in Fig. 9-a consists of the 0.7 secs short-period portion and fluctuations at longer periods. Since the acceleration at the crest reflects the absolute motion of the structure, the displacement curve is considered to show a combination of the motion of the crest with respect to the abutment (structural motion), which is the motion of shorter period, superimposed upon a longer-period motion which represents the displacement of the bedrock of the dam (ground motion). Therefore, the crest record shows that in the upstream/downstream direction the dam responded mainly in its fundamental mode.

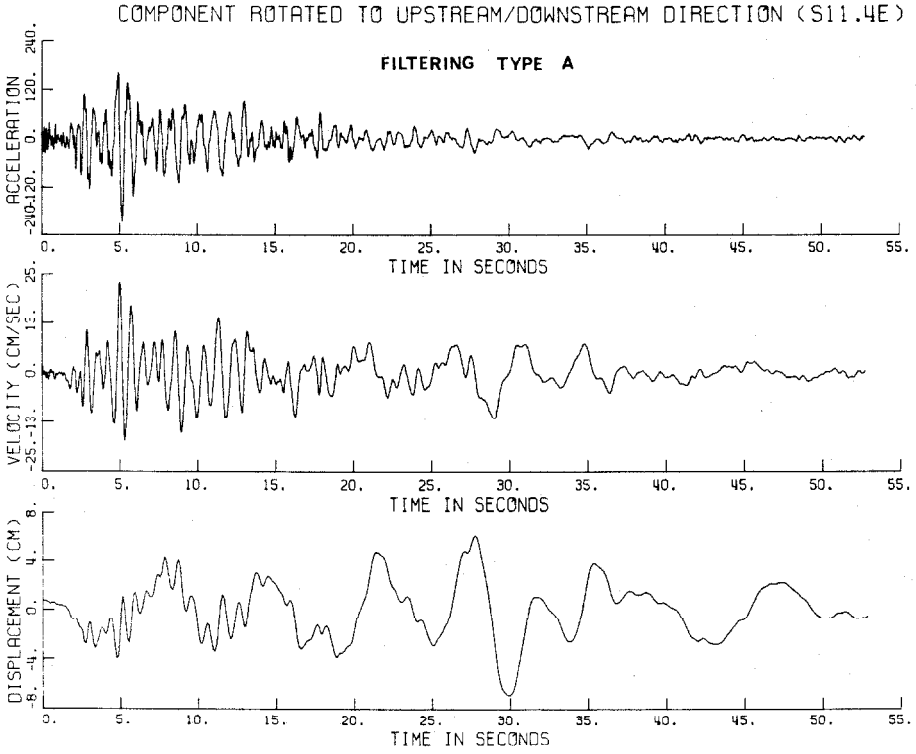

(a) Crest

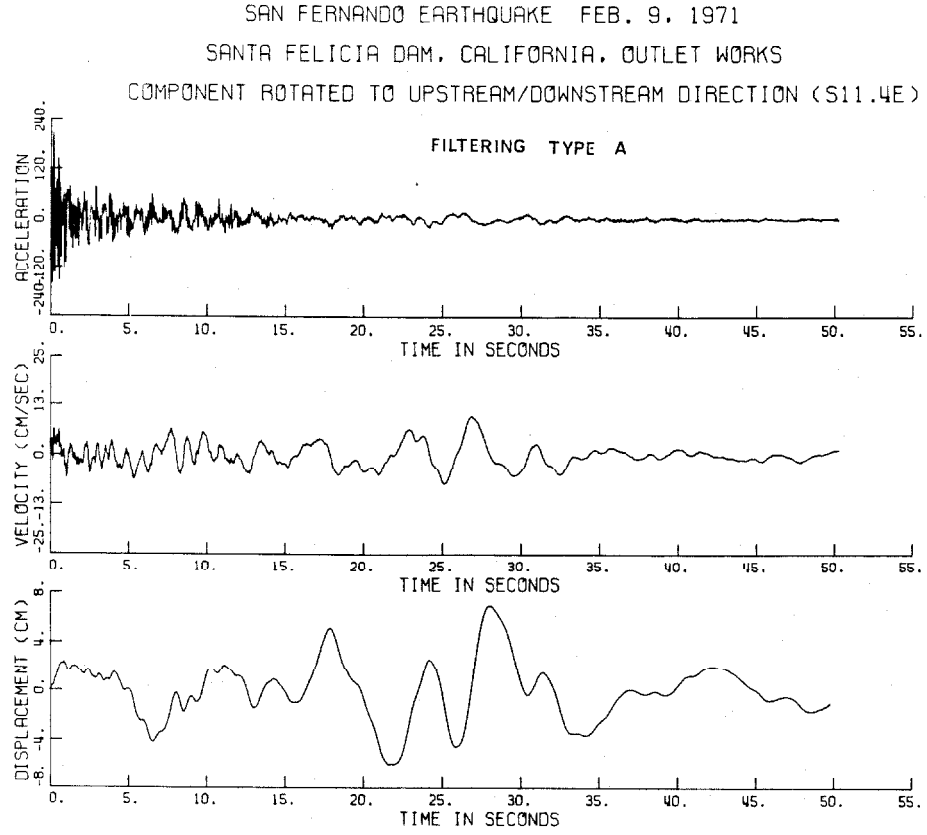

(b) Right Abutment

Fig. 9

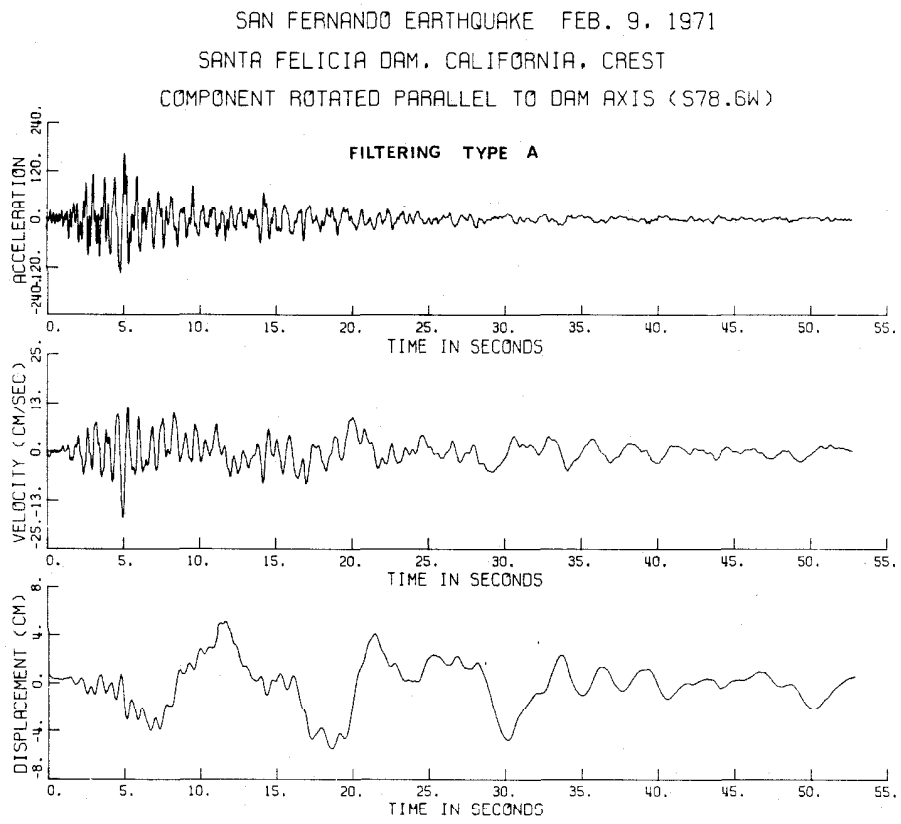

(a) Crest

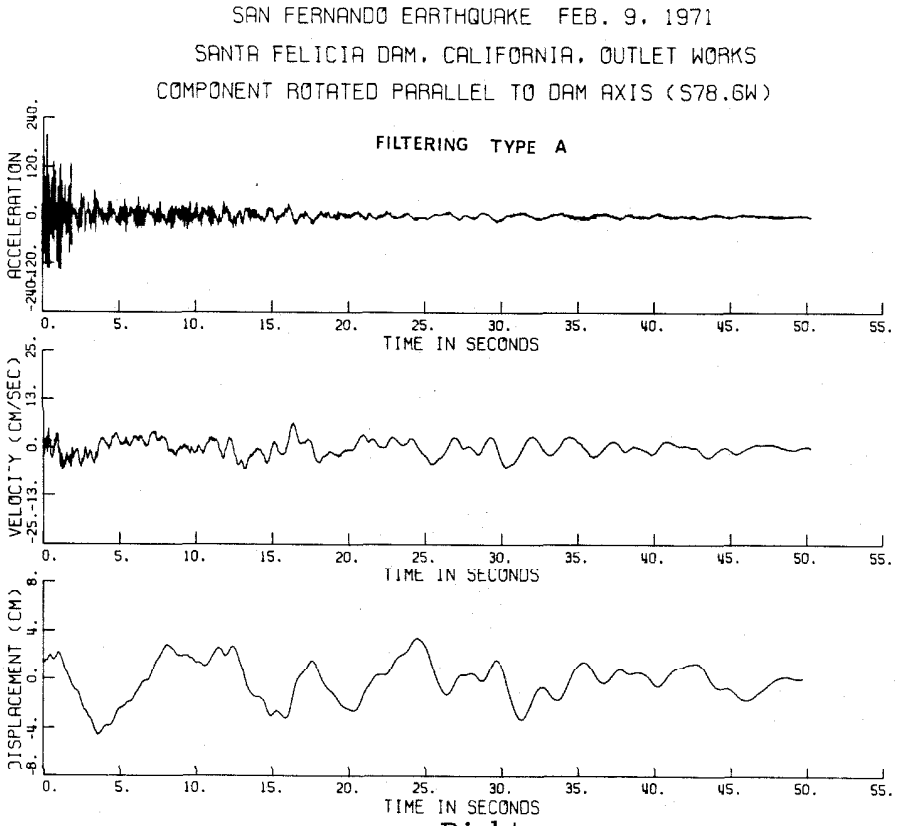

(b) Right Abutment

Fig. 10

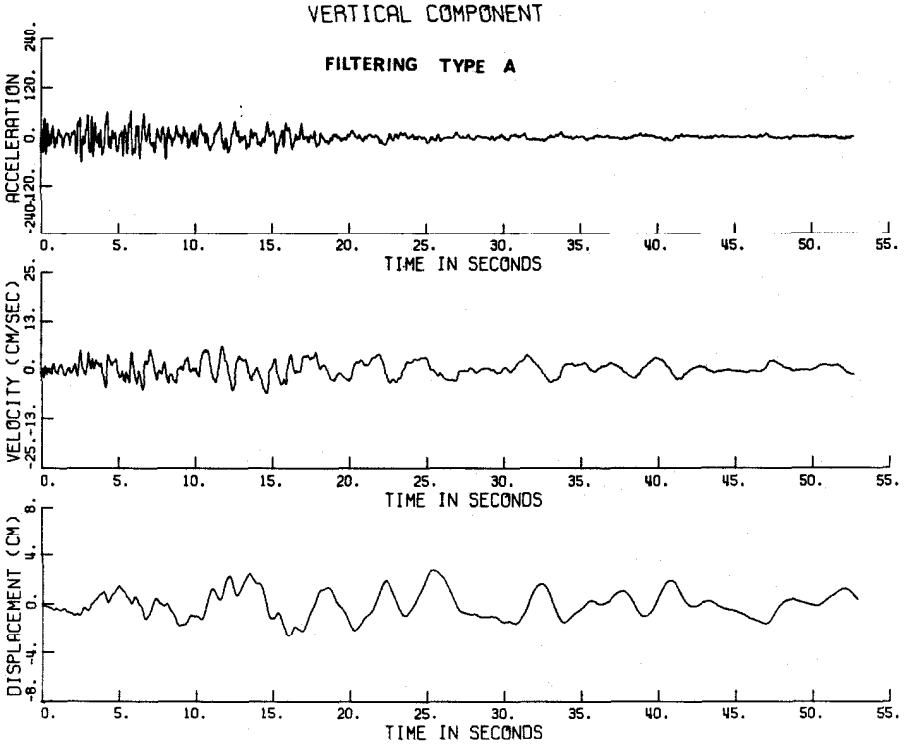

(a) Crest

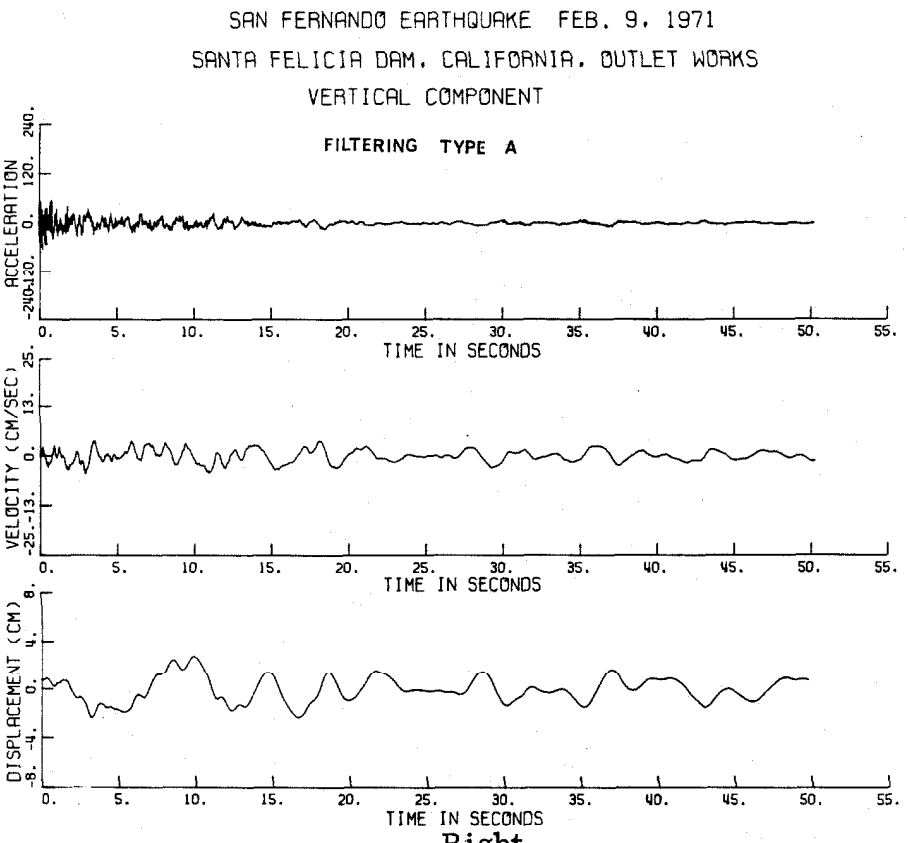

(b) Right Abutment

Fig. 11

Actually there is some contribution from the higher modes apparent in the first part of the response, but this contribution is generally small compared to the response of the fundamental mode.

The observed response of the crest component parallel to the dam axis (S78.6°W) showed a fundamental period of about 0.75 secs as well as significant contribution from the higher modes, as shown in Fig. 10.

The vertical components of the earthquake motion measured at the abutment and crest of the dam did not exhibit any predominant period of vibration as indicated by Fig. 11. The maximum amplitude of dynamic displacement of the bedrock at the site in the direction perpendicular to the dam axis appears in Figs. 9(a) and (b) to be about 8 cm. Superimposed on this, the amplitude of fundamental mode displacements of the dam crest with respect to the base seems to be in the order of approximately 1.3 cm upstream and downstream. It is apparent, therefore, that relatively small deformations and strains must have been generated in the structure during the earthquake.

b - Cracks at the East Abutment

The 6.3 magnitude earthquake of February 9, 1971 caused longitudinal stresses that created a crack on the road surface of the dam crest at the east abutment (Ref. 2). The crack, approximately one-sixteenth of an inch in width, ran through the roadway pavement, nearly perpendicular to the dam axis. Extension of the crack was traced to the natural overburden northeast of the dam as shown in Fig. 12. The depth of the crack is not known. Close observations

on February 9, 1971 of both abutments, upstream and downstream, revealed no other cracking or seepage which might indicate a hazardous condition. This narrow meandering crack across the crest at the east abutment appears to have no structural significance since it is in a portion of the roadway which is east of the dam proper.

Nonetheless, investigations have implied that there has been a continuous small longitudinal movement of the dam crest toward the east abutment, which indicates a compression of the dam against this abutment, but the 1/16-inch lateral crack which occurred during the earthquake indicates tension at this point, which is close to the point of contact of the dam crest with the abutment. So while this may be only an insignificant surface crack, it is possible that the sharp ridge forming the abutment has been sheared, possibly leaving an essentially loose block of rock. Perhaps the depth and extent of this crack should be investigated to make sure that it will not be a hazard when the reservoir is full and spilling.

In general, the performance of the dam and the outlet works appeared quite satisfactory; in spite of an indicated seismic acceleration of nearly 0.25g, the earthquake had only minor effects. Apart from the earthquake, the total settlements and lateral movements to date of the dam are well within normal limits and the additional amounts caused by the earthquake are quite normal.

Copies of various drawings, a post-San Fernando inspection report and miscellaneous correspondence between Professor Housner and UWCD are filed in the Earthquake Engineering Library at Caltech.[1,2]

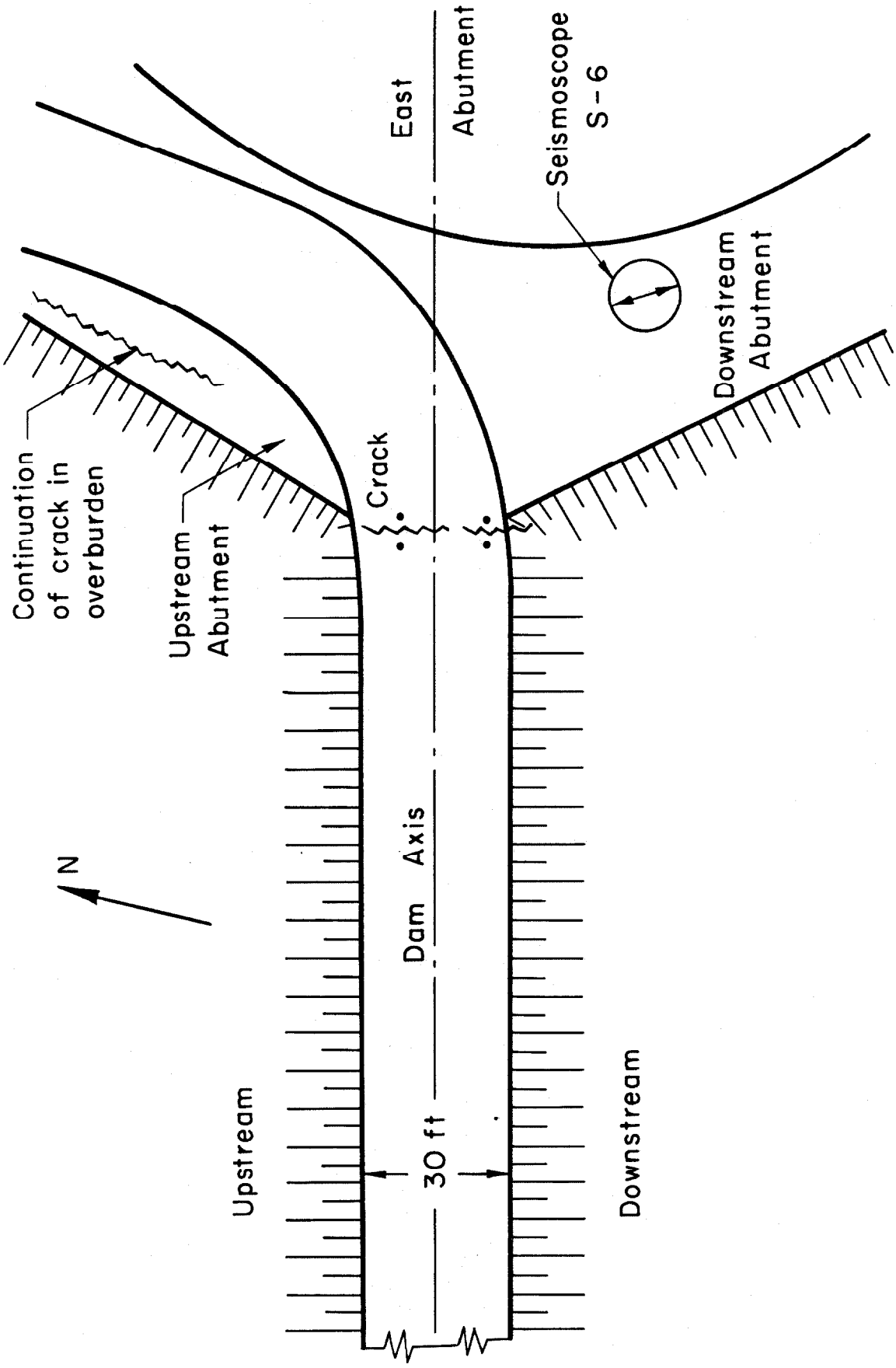

Fig. 12 The crack at the East Abutment of Santa Felicia Dam as a result of the San Fernando earthquake of February 9, 1971

A-III-2 Southern California Earthquake of April 8, 1976

Two accelerograph records were recovered at the Santa Felicia Dam from the U.S. Geological Survey's national network of strong-motion instrumentation[7] following the Southern California earthquake of April 8, 1976. One was recorded at the base and the other at the crest. The maximum indicated acceleration during this 4.7 local magnitude event was 0.05g. The dam was 14 Km northeast of the epicenter. Table 4 is a summary of the accelerograph records of Santa Felicia Dam.

The seismoscope records from this small earthquake show so little motion that they are indistinguishable from plates left on a seismoscope for an extended period of time. However, the accelerograph recordings are very interesting in the analysis of the behavior of the dam in spite of the relatively small amplitude of motion. Unlike the recordings during the San Fernando earthquake, the two horizontal components of the 1976 earthquake motion (S12°E and S78°W) were recorded almost perpendicular to the dam axis (S11.4°E) and the longitudinal axis of the dam (S78.6°W). In addition, the recovered record of the crest has a duration of about 18 secs, while the recovered record of the right abutment has only 6 seconds duration. The corrected accelerogram and integrated velocity and displacement traces (Vol. II data) of the two records are shown in Figs. 13 through 15; the standard data processing of the other three volumes (I, III and IV) can be found in Appendix A.

The observed responses of both the crest and the abutment show long period motions in the integrated velocity and displacement; this could be due to human digitization error, to the shortness of

the records or to a contribution from surface waves. The response of the fundamental mode in the upstream/downstream direction (component S12°E) with an apparent period of about 0.7 seconds is indicated by the computed velocity plot of Fig. 13. Similarly, the component parallel to the dam axis showed a fundamental period of about 0.73 seconds superimposed on long-period surface waves.

In this event, the amplitude of the dynamic displacement of the crest with respect to the base (component S12° E) in the fundamental mode was only about 1 mm.

TABLE 4

Summary of the Santa Felicia Dam Accelerograph

Event	Station Location		Component	Max. Acceleration (g)
	Name	Coordinate		
8 April 1976 1521 GMT Southern California Earthquake Local Magnitude 4.7	Crest	34.46N 118.75W	S12E S78W Down	0.05 0.05 0.03
	Right Abutment	34.46N 118.75W	S12E S78W Down	0.05 0.04 0.03

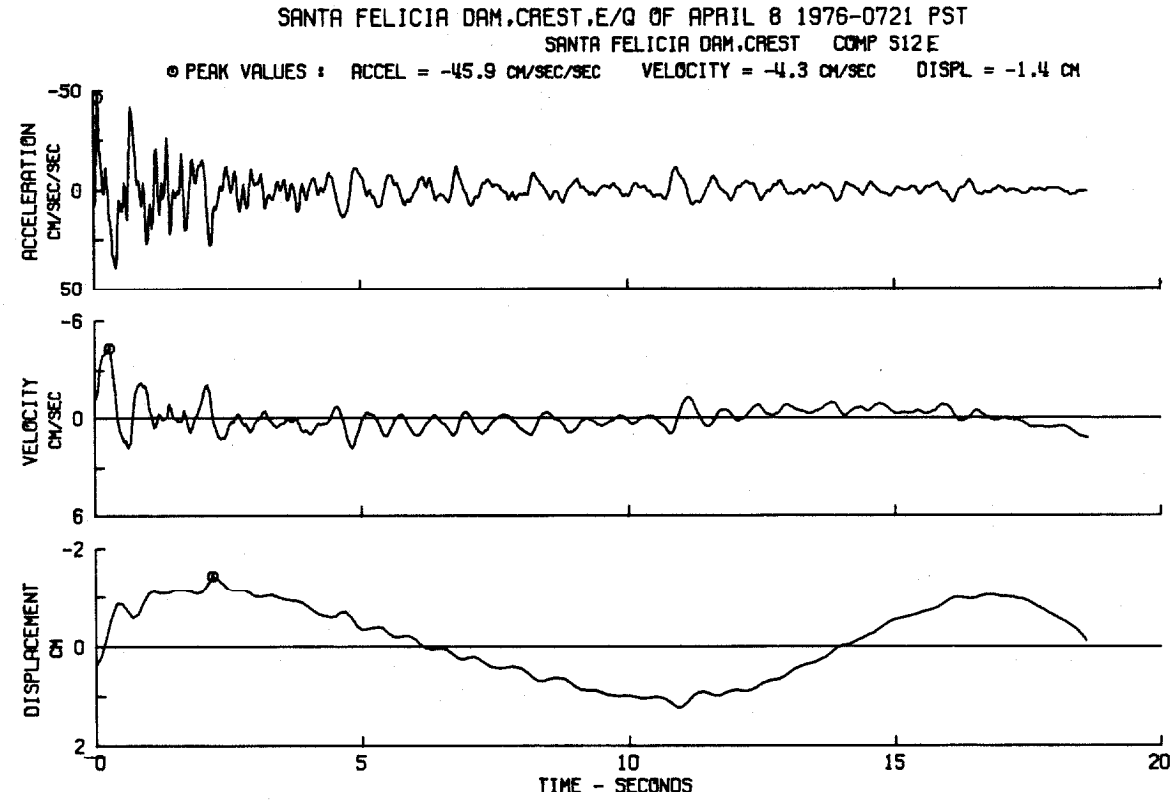

(a) Crest

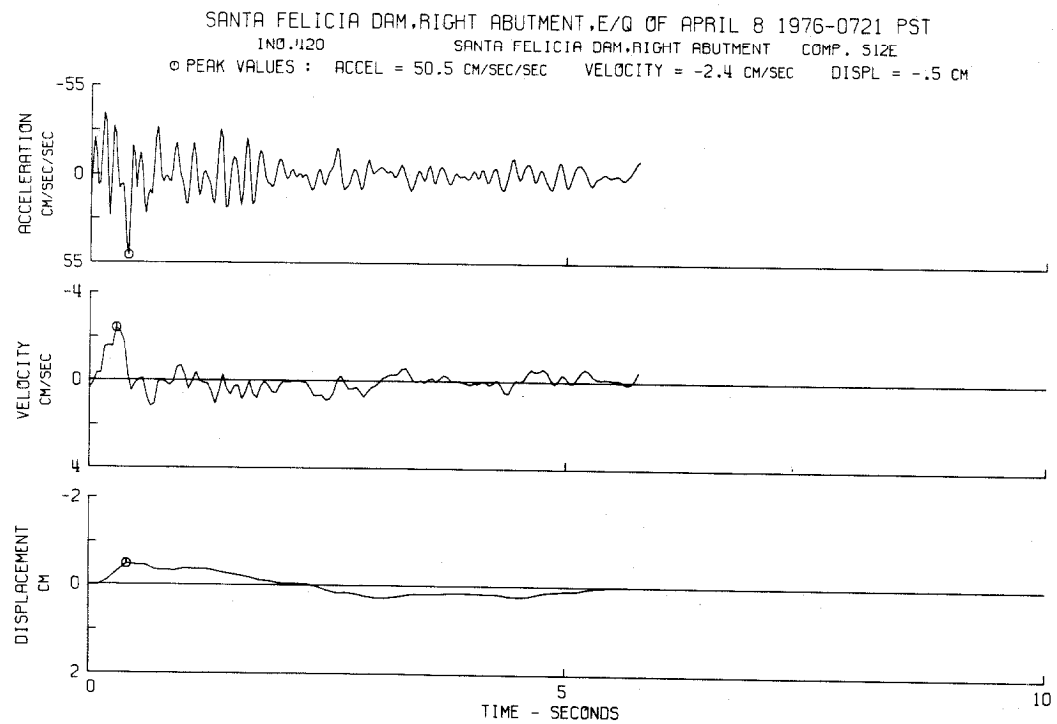

(b) Right Abutment

Fig. 13 Corrected accelerograms and computed velocities and displacements in the upstream/downstream direction

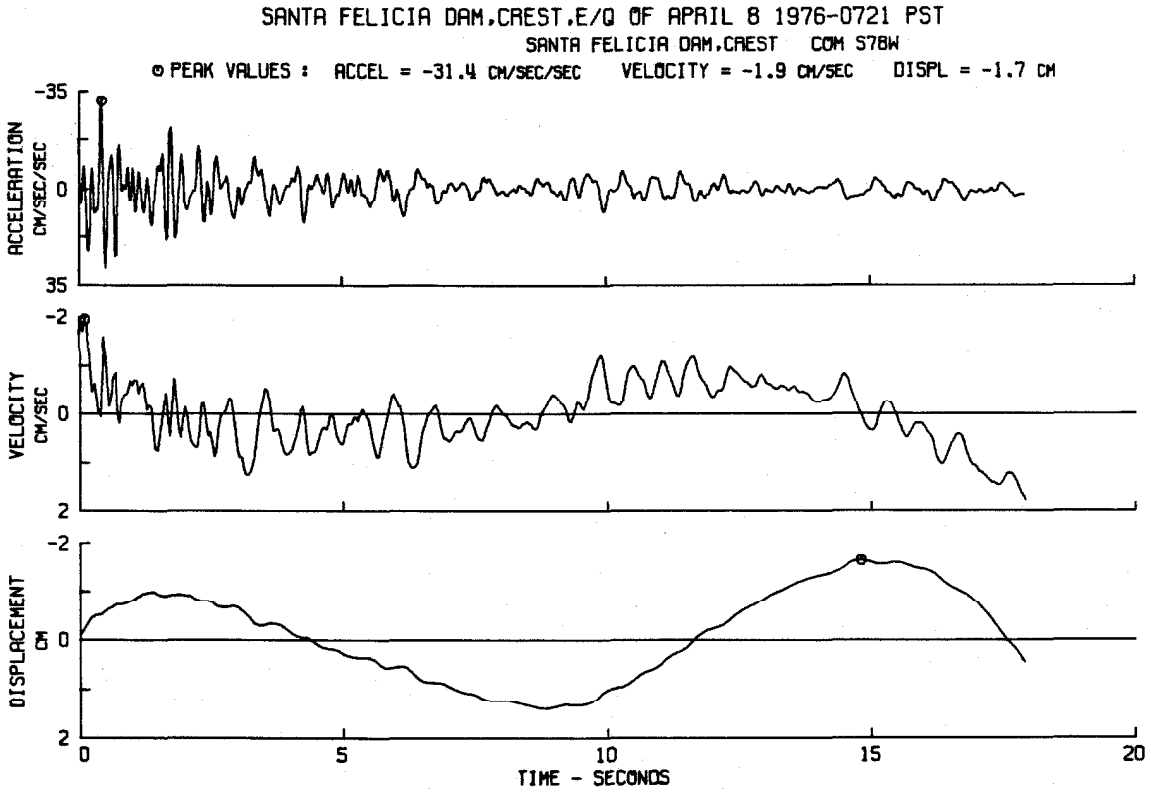

(a) Crest

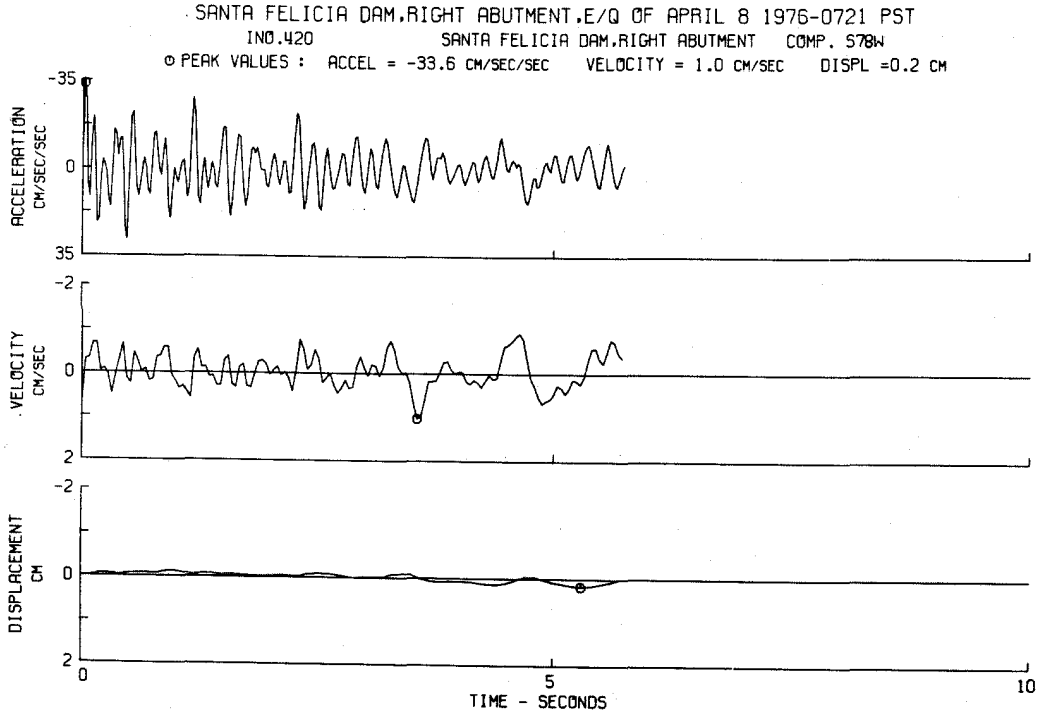

(b) Right Abutment

Fig. 14 Corrected accelerograms and computed velocities and displacements in the direction parallel to the dam axis.

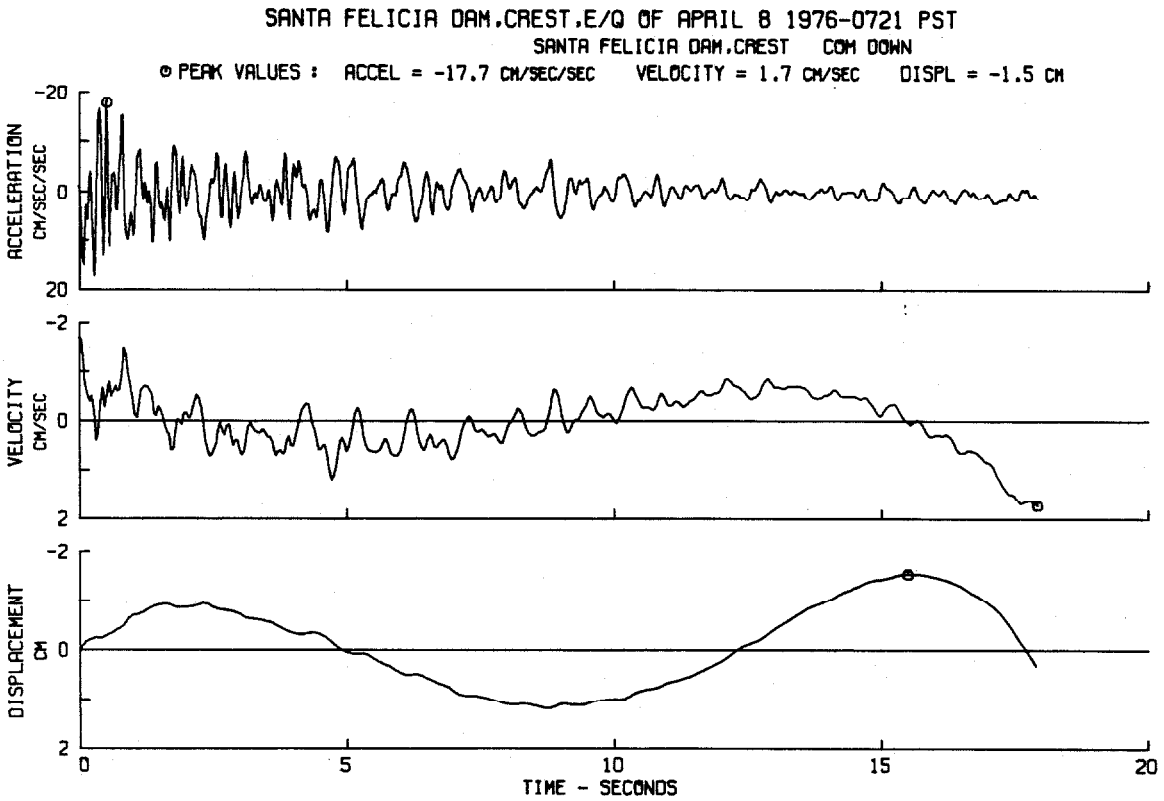

(a) Crest

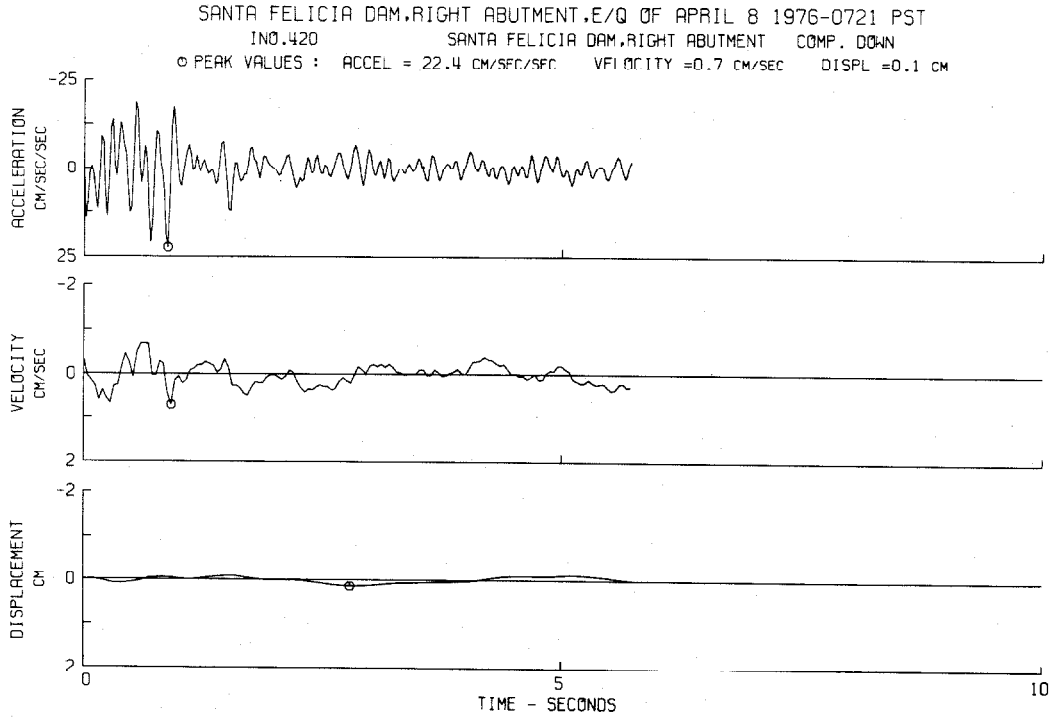

(b) Right Abutment

Fig. 15 Corrected accelerograms and computed velocities and displacements in the vertical direction

A-IV ANALYSES OF RECORDED MOTIONS

A-IV-1 Amplification Spectra

a - San Fernando Earthquake

The amplification spectra for the approximately 50 seconds of motion were computed by dividing the Fourier amplitude spectrum of the acceleration recorded at the dam crest by that recorded at the abutment for each component of motion, and then smoothing first with one pass and then with two passes of a Hanning Window ($\frac{1}{4}$, $\frac{1}{2}$, $\frac{1}{4}$ weights). Figures 16 through 24 show the Fourier amplitude spectra as well as the amplification spectra (with only one pass of smoothing) and the corresponding smoothed spectra (with two passes) for the two records of Santa Felicia Dam.

The amplification spectrum for the upstream/downstream direction (Fig. 18-a) shows a predominant single peak at 1.46 Hz, while the smoothed spectrum (Fig. 18-b) shows the peak at 1.44 Hz. This peak's amplitude is greater than twice that of the four next strongest peaks, occurring at 1.10, 1.83, 2.05 and 3.96 Hz. Several other small peaks are apparent in the spectrum.

The second horizontal component, parallel to the crest (the longitudinal component S78°W) shows two dominant peaks (in Fig. 21-b, at 1.35 and 4.88 Hz). However, this spectrum has several well-defined secondary peaks suggesting greater participation of the higher modes of vibration in this direction than in the upstream/downstream direction. More than eight of these peaks were higher than one-third of the amplitude of the main peak at 1.35 Hz.

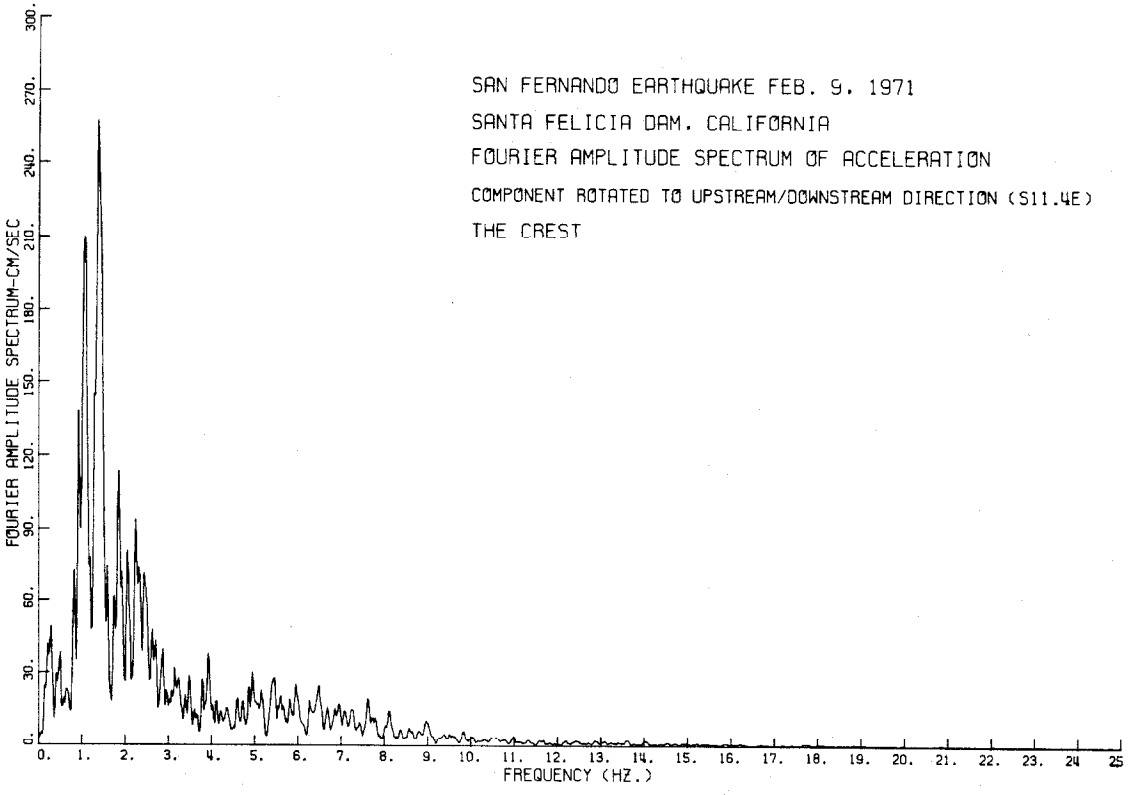

(a)

(Note: The ordinates of Fig. 16-b should be multiplied by a factor of 0.75)

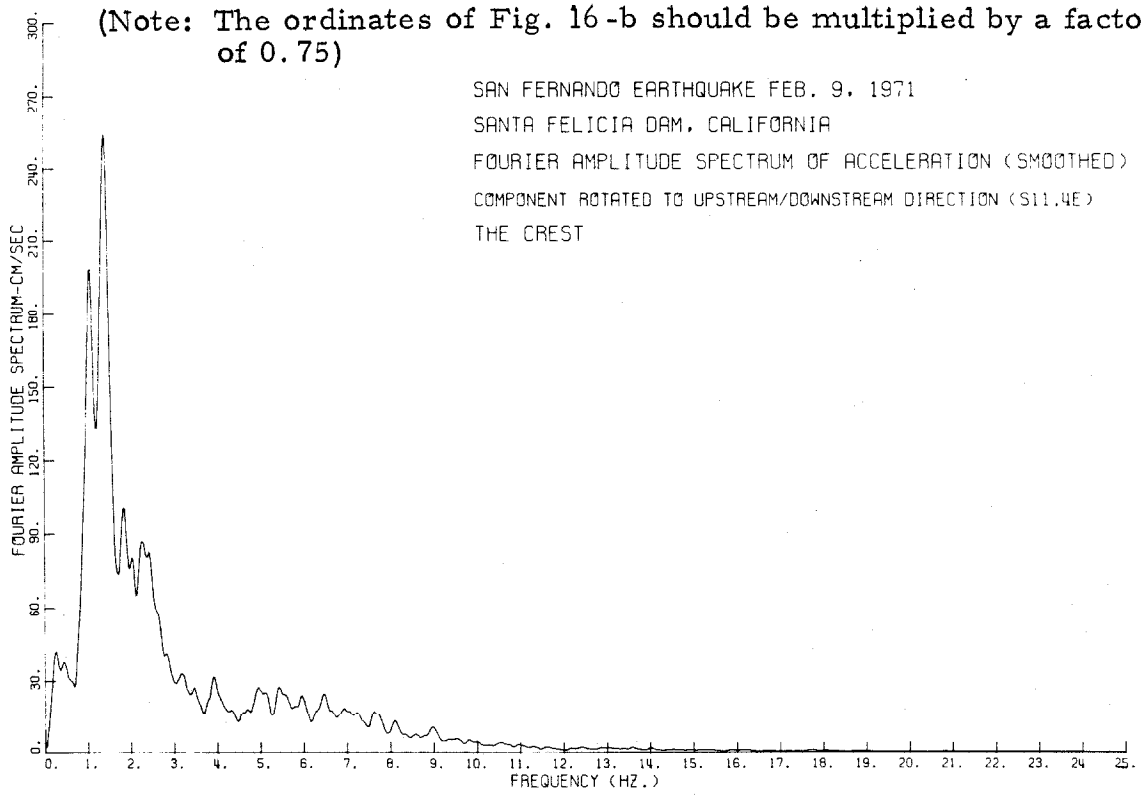

(b)

Fig. 16

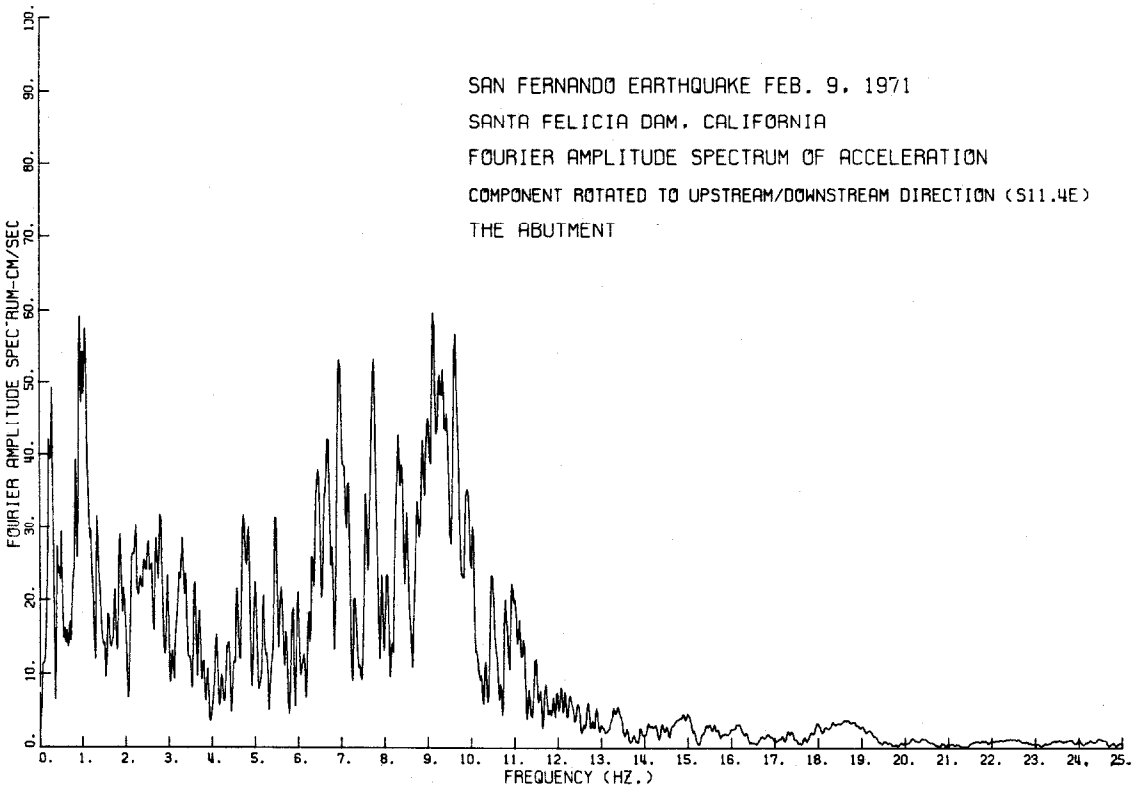

(a)

(Note: The ordinates of Fig. 17-b should be multiplied by a factor of 0.75)

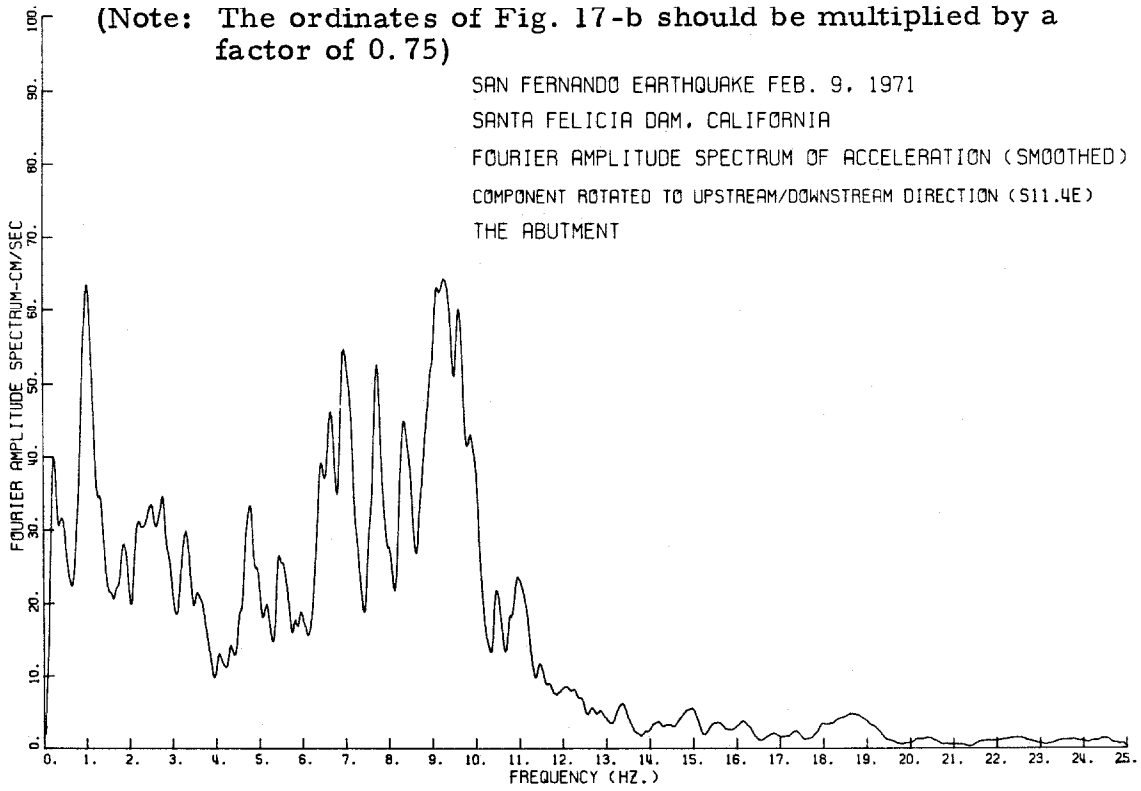

(b)

Fig. 17

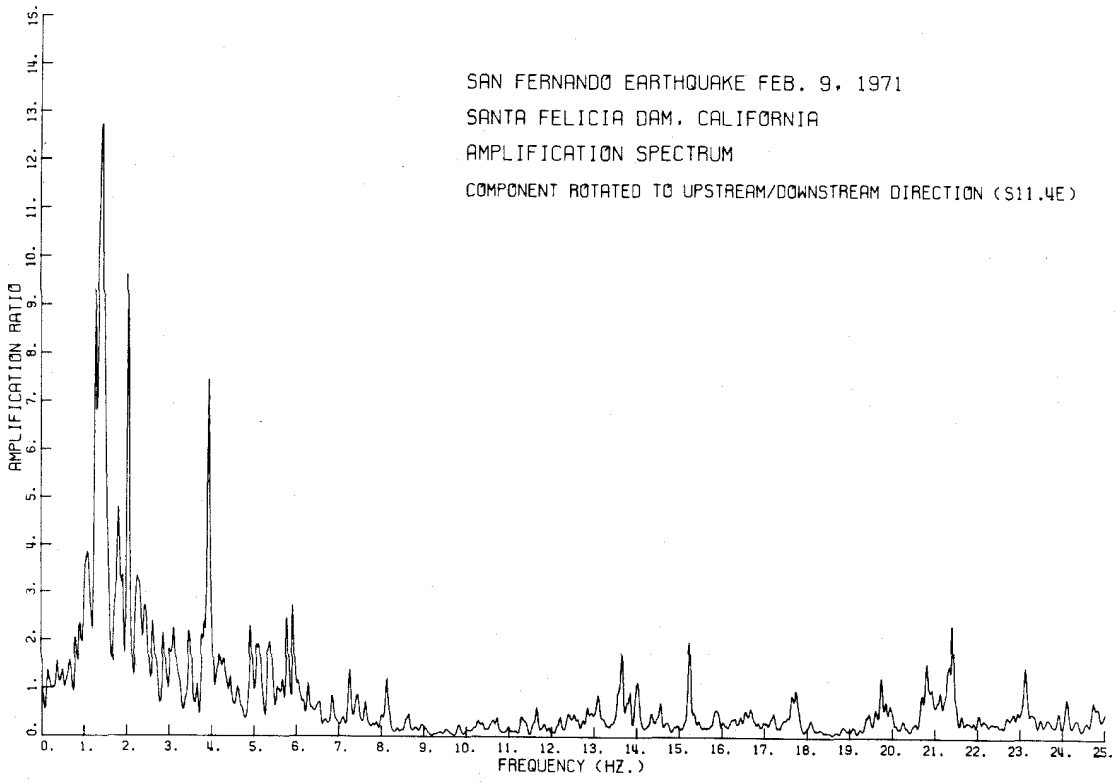

(a)

(Note: The ordinates of Fig. 18-b should be multiplied by a factor of $\frac{2}{3}$)

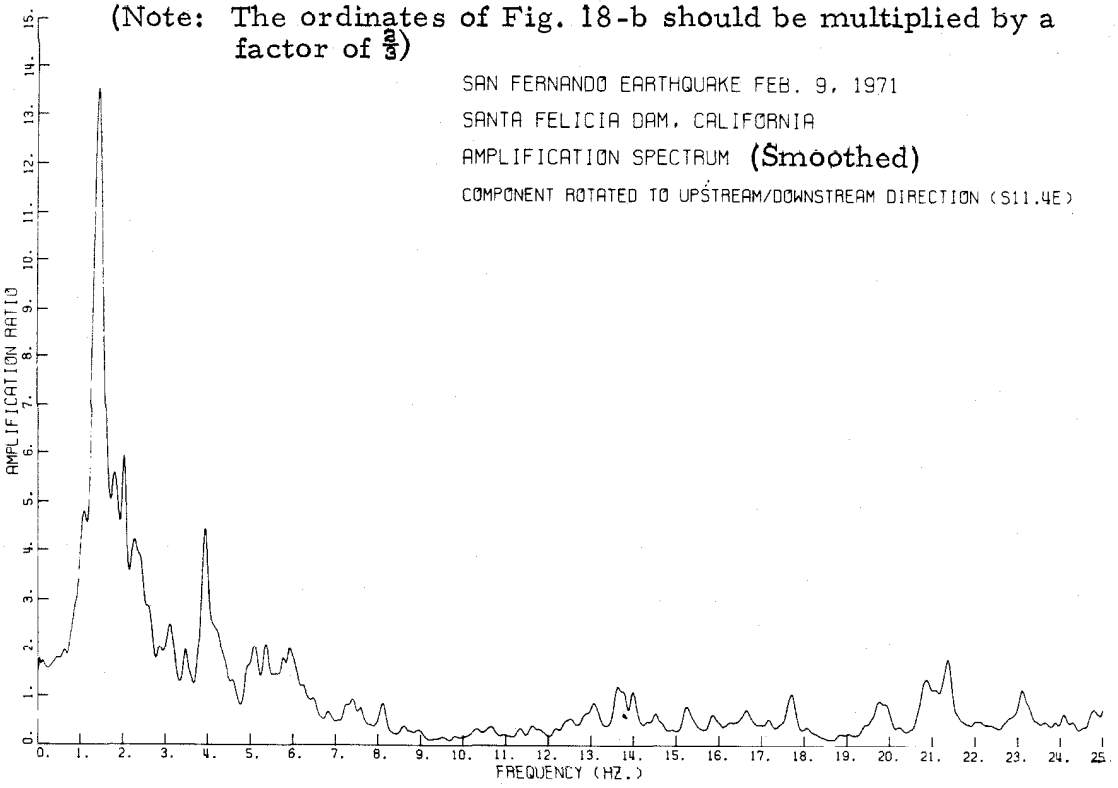

(b)

Fig. 18

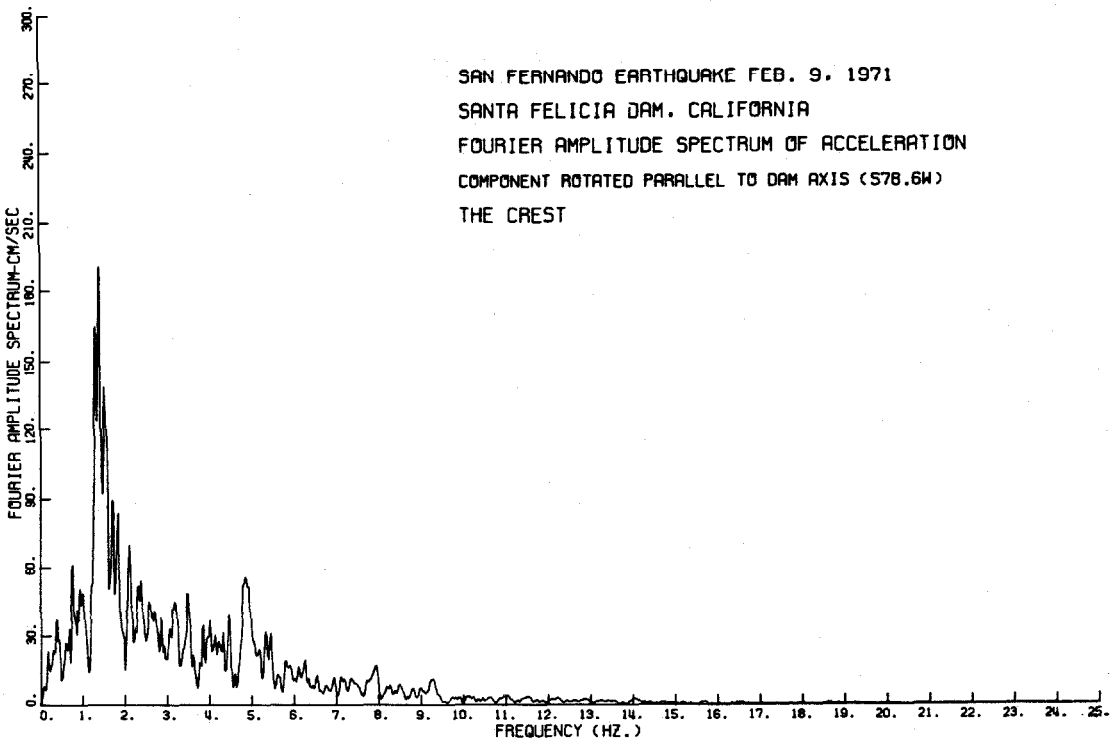

(a)

(Note: The ordinates of Fig. 19-b should be multiplied by a factor of 0.75)

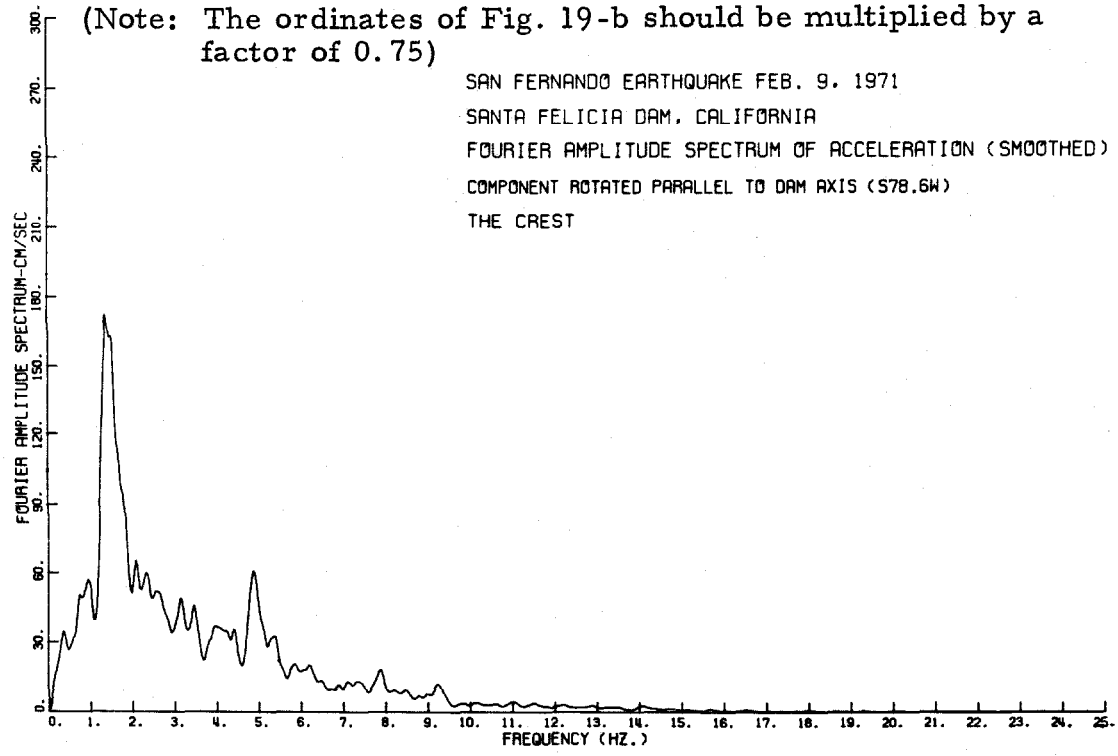

(b)

Fig. 19

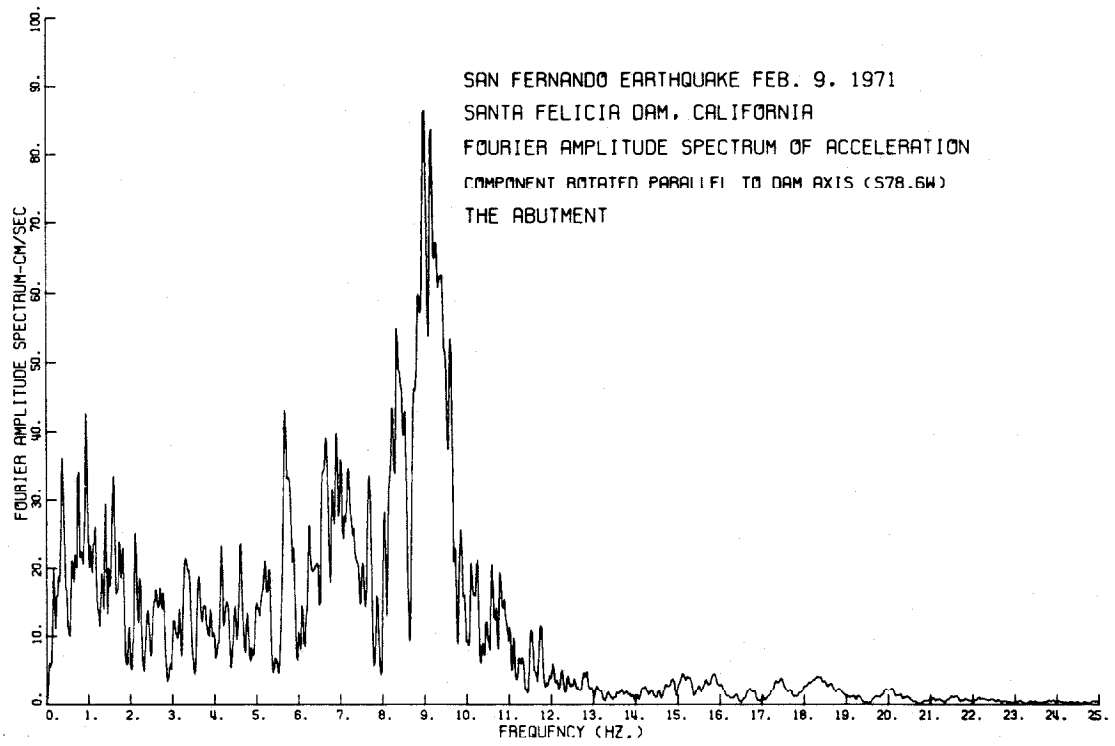

(a)

(Note: The ordinates of Fig. 20-b should be multiplied by a factor of 0.75)

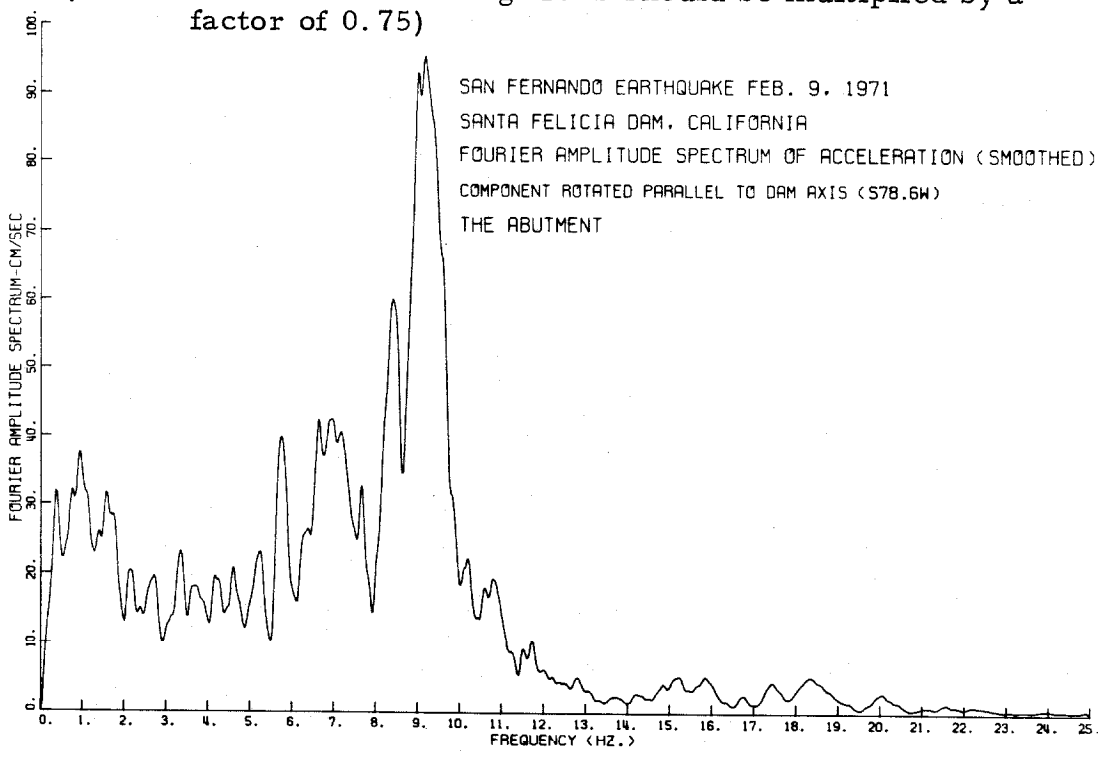

(b)

Fig. 20

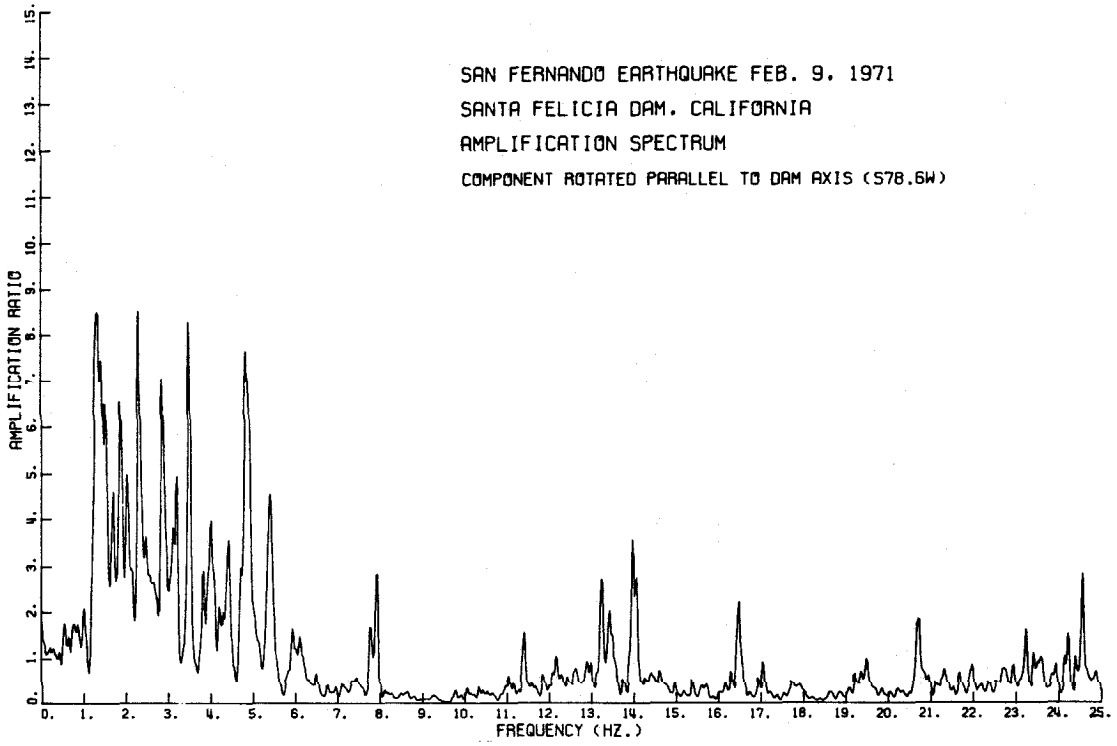

(a)

(Note: The ordinates of Fig. 21-b should be multiplied by a factor of $\frac{2}{3}$)

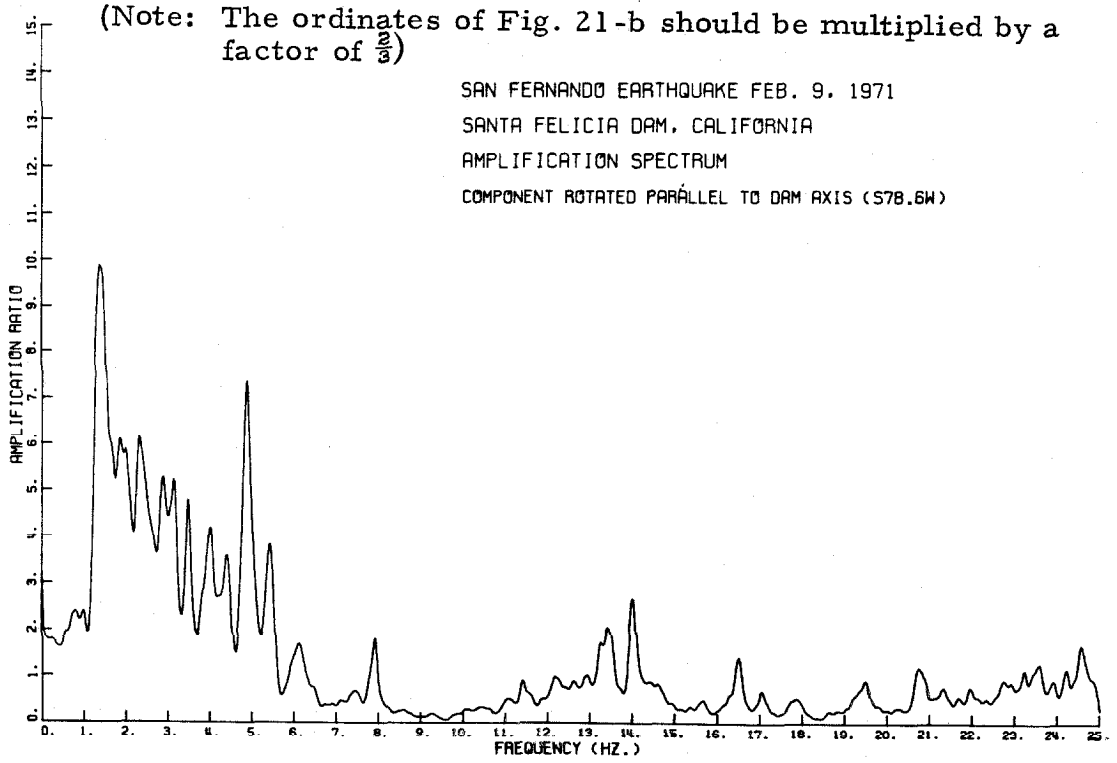

(b)

Fig. 21

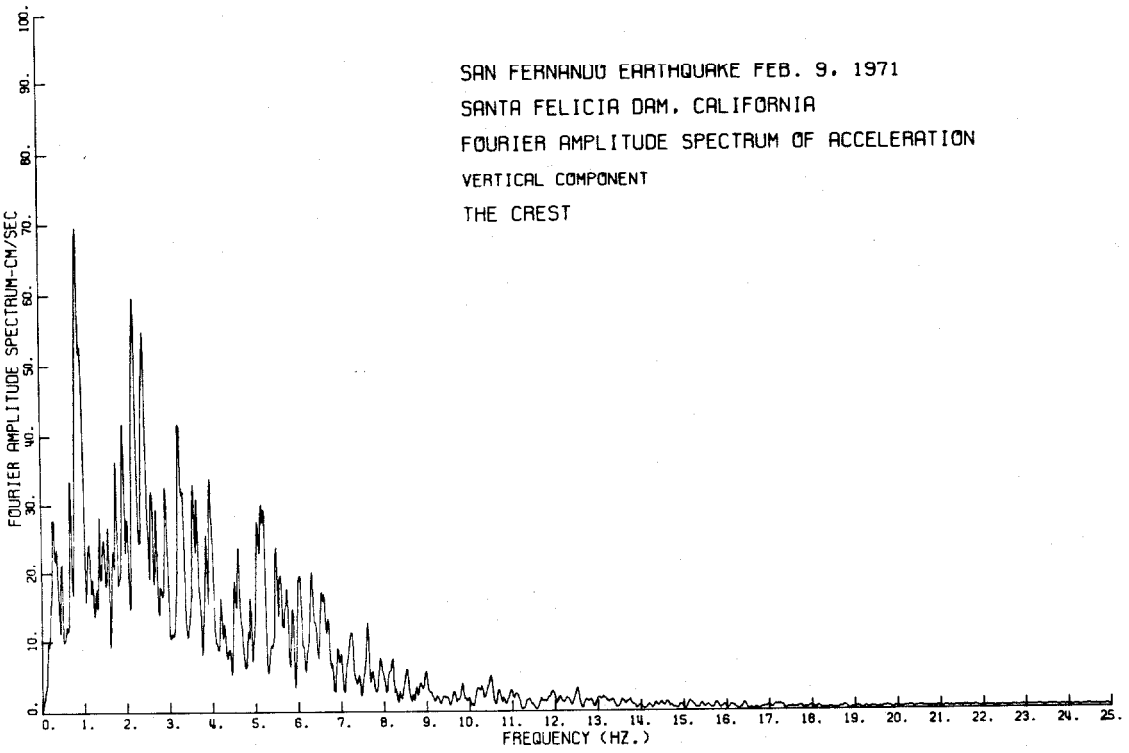

(a)

(Note: The ordinates of Fig. 22-b should be multiplied by a factor of 0.75)

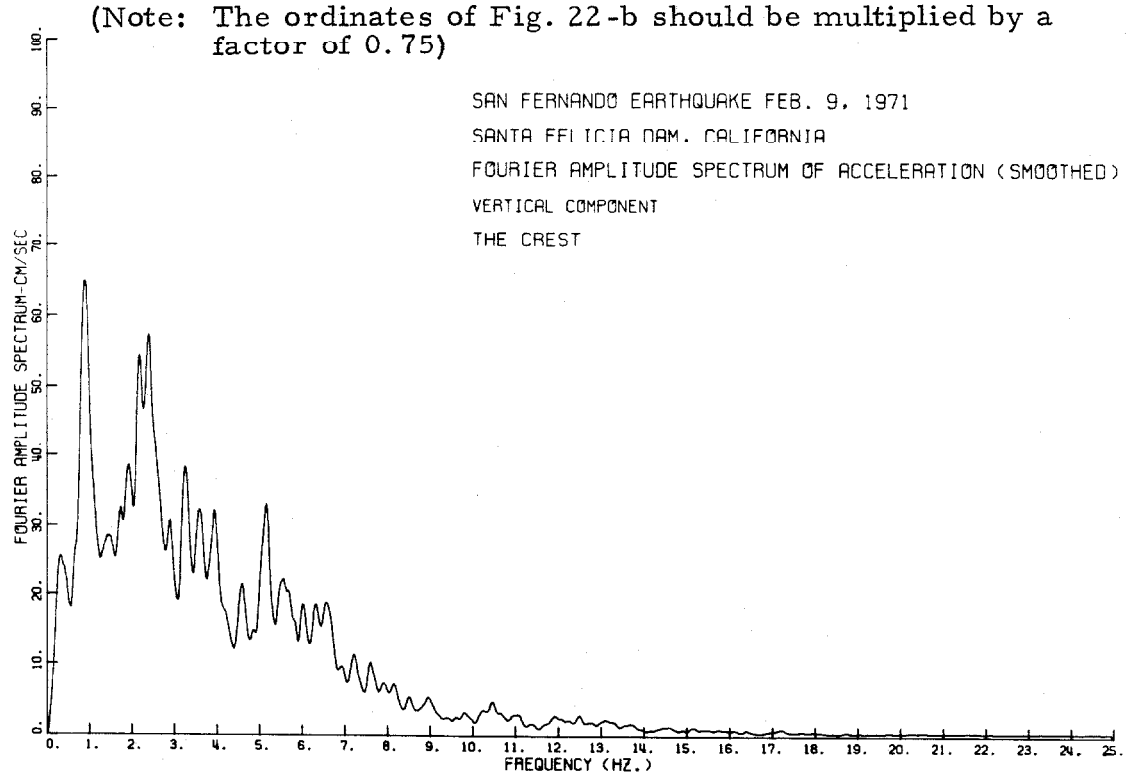

(b)

Fig. 22

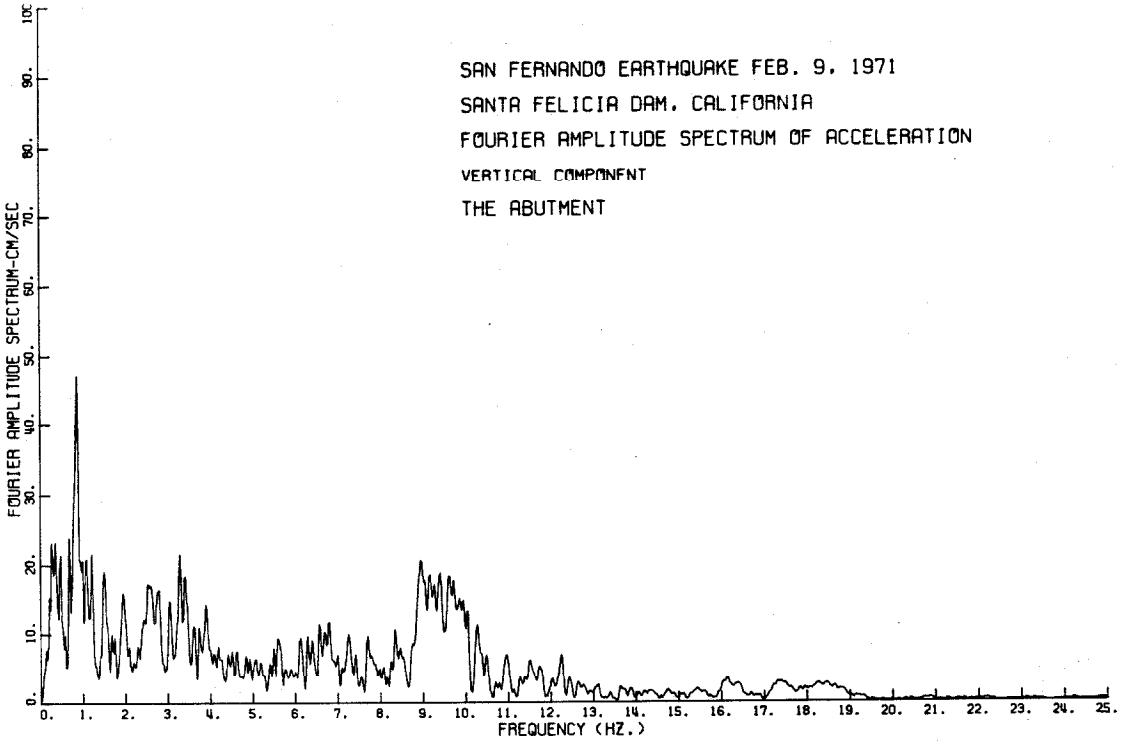

(a)

(Note: The ordinates of Fig. 23-b should be multiplied by a factor of 0.75)

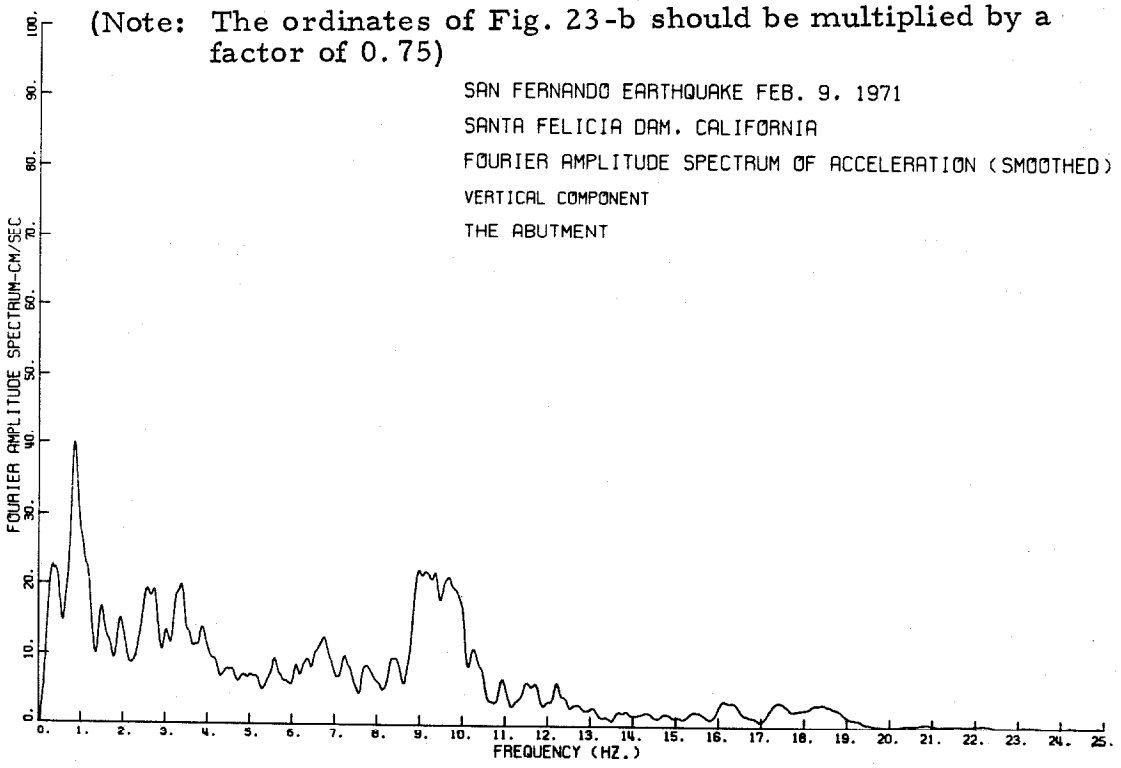

(b)

Fig. 23

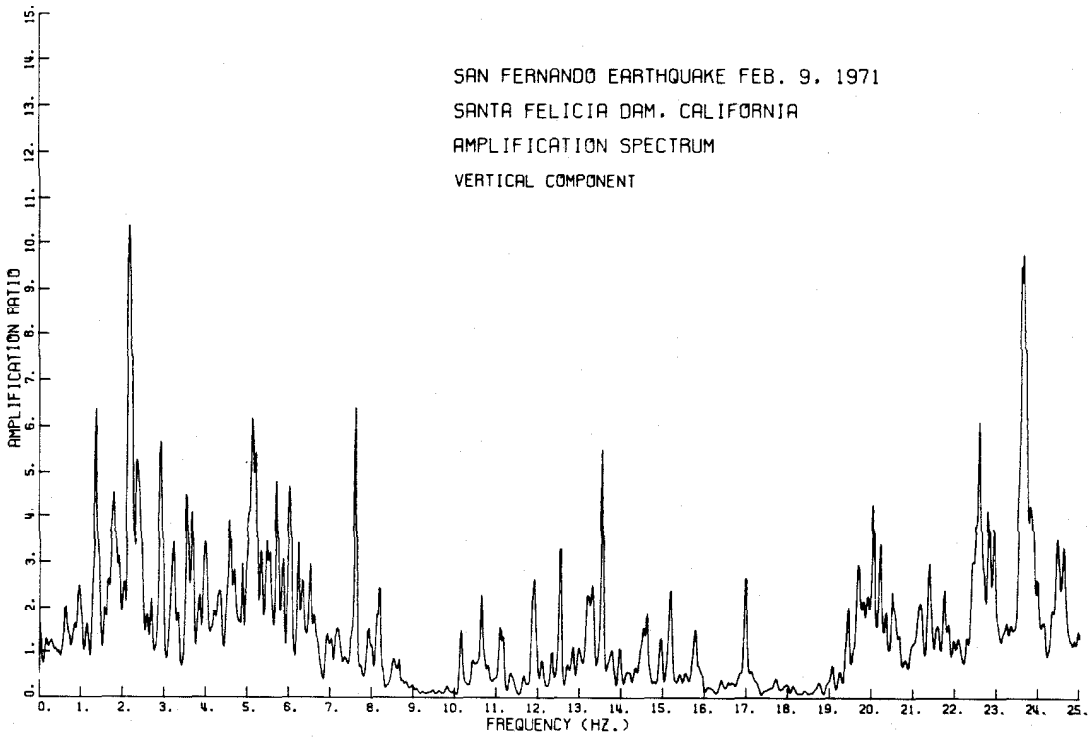

(a)

(Note: The ordinates of Fig. 24-b should be multiplied by a factor of $\frac{1}{3}$)

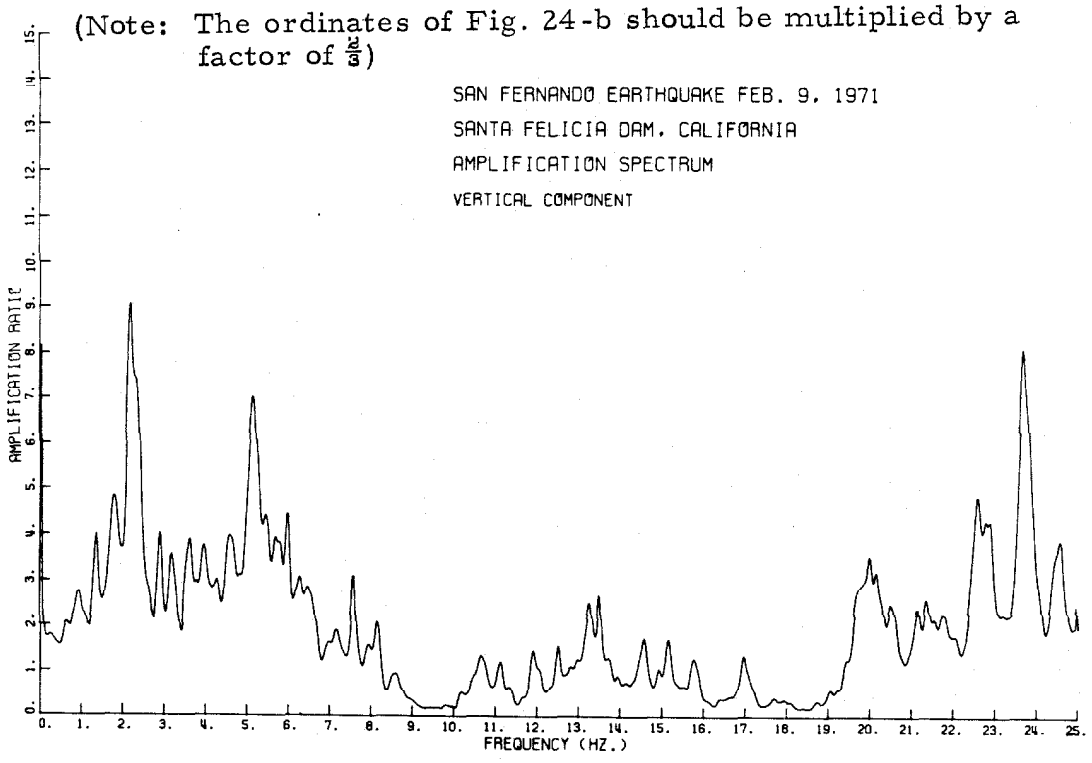

(b)

Fig. 24

The amplification spectrum of the vertical component (Fig. 24-b) shows two dominant peaks at about 2.20 and 5.15 Hz; it also has several well-defined secondary peaks. The high peaks in the frequency range 20 to 25 Hz in Fig. 24 do not look real, and they can be disregarded.

Finally, it is important to note the peaks in the Fourier amplitude spectra of the abutment records at about 10 Hz. These peaks were caused, as indicated previously, by the vibrations of the concrete standpipe on which the floor of the valve house rests. The strong-motion instrument was fixed on this floor rather than on firm ground.

b - The 1976 Southern California Earthquake

The Fourier amplitude spectra and the amplification spectra of the April 8, 1976 Southern California earthquake are shown in Figs. 25 through 29.

The amplification spectrum for the upstream/downstream direction (Fig. 26) again shows a dominant peak at 1.46 Hz; there is another high peak at 2.73 Hz, and several other smaller peaks occurred at 1.66, 1.86, 2.08, 2.25 and 3.81 Hz.

For the component parallel to the dam axis, shown in Fig. 29-a, there are several well-defined strong peaks occurring at 1.27, 1.66, 1.86, 3.22, 4.20, 5.57 and 6.93 Hz; these peaks have almost the same amount of participation in the response of the dam in that direction.

The vertical component (Fig. 29-b) shows one dominant peak at 2.25 Hz, in addition to several high secondary peaks at 0.98, 1.76, 3.03, 3.22, 4.10 and 6.64 Hz.

Tables 5, 6 and 7 contain the frequencies and relative heights of peaks in the three components' amplification spectra for the two earthquakes. They also show the effects of smoothing on both the frequencies and the amplitudes for the 1971 San Fernando earthquake. These tables further indicate that the two earthquakes have shaken the dam at essentially the same resonant frequencies.

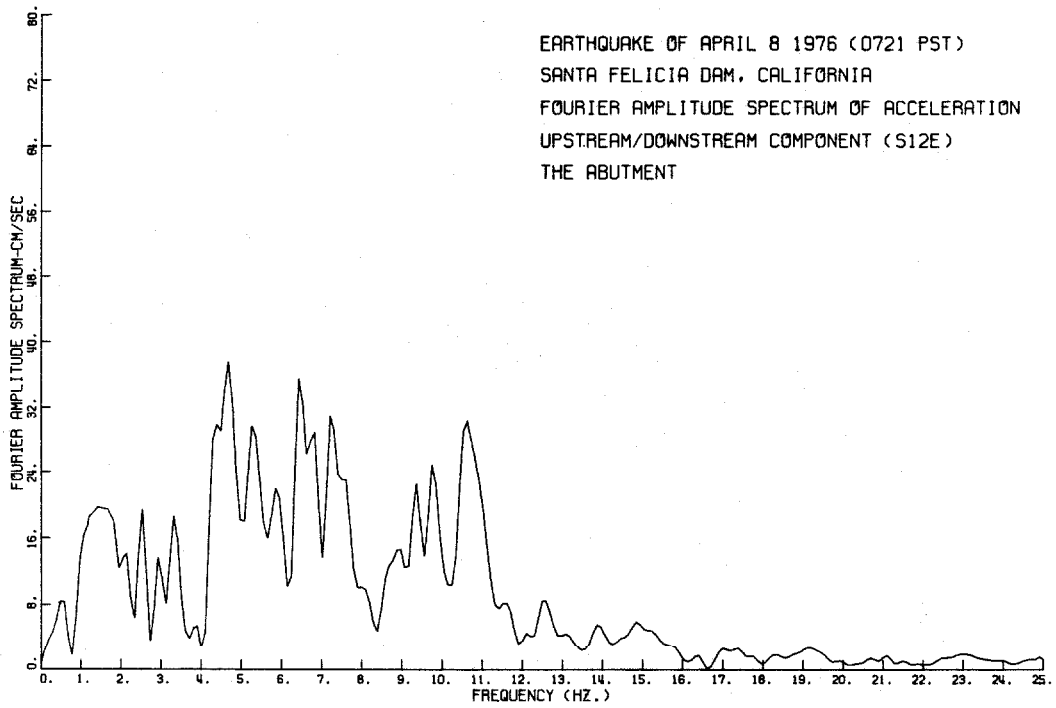
EARTHQUAKE OF APRIL 8 1976 (0721 PST)
SANTA FELICIA DAM, CALIFORNIA
FOURIER AMPLITUDE SPECTRUM OF ACCELERATION
UPSTREAM/DOWNSTREAM COMPONENT (S12E)
THE ABUTMENT
FOURIER AMPLITUDE SPECTRUM-CM/SEC
FREQUENCY (HZ.)

(a)

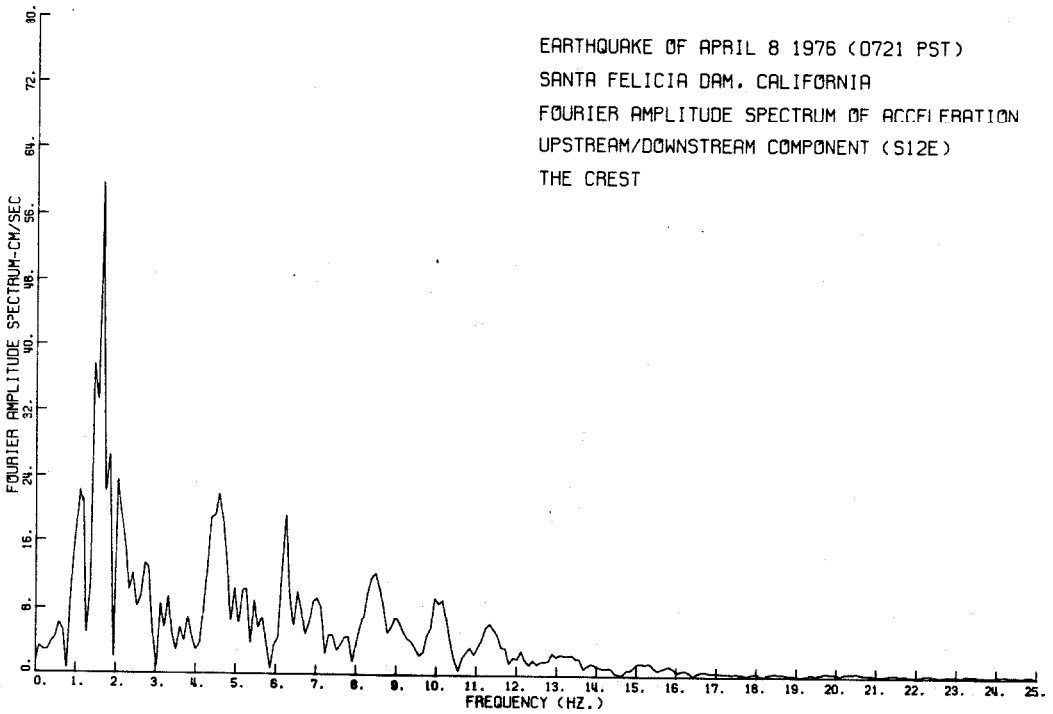
EARTHQUAKE OF APRIL 8 1976 (0721 PST)
SANTA FELICIA DAM, CALIFORNIA
FOURIER AMPLITUDE SPECTRUM OF ACCELERATION
UPSTREAM/DOWNSTREAM COMPONENT (S12E)
THE CREST
FOURIER AMPLITUDE SPECTRUM-CM/SEC
FREQUENCY (HZ.)

(b)

Fig. 25

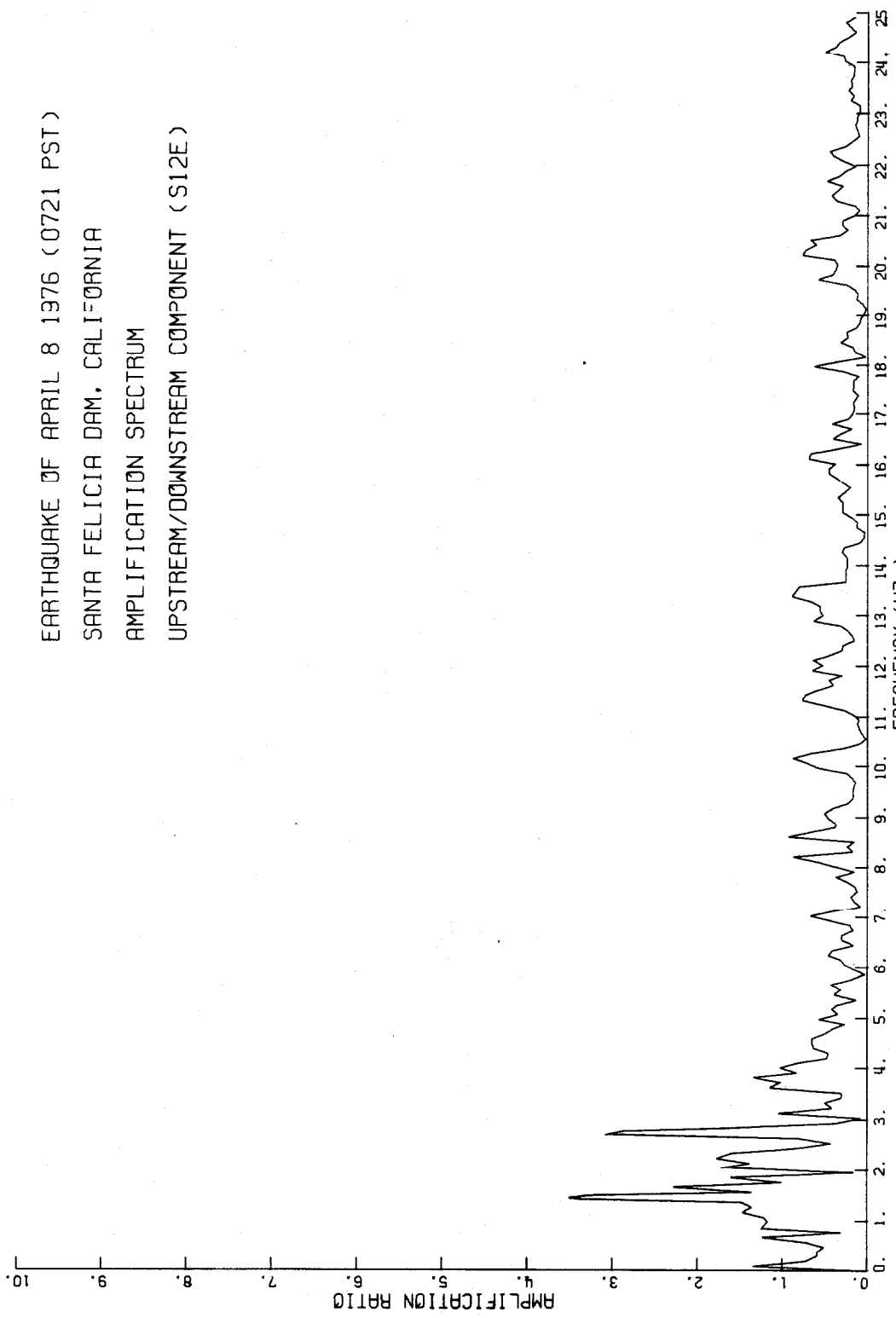
EARTHQUAKE OF APRIL 8 1976 (0721 PST)
SANTA FELICIA DAM, CALIFORNIA
AMPLIFICATION SPECTRUM
UPSTREAM/DOWNSTREAM COMPONENT (S12E)
AMPLIFICATION RATIO
0.
1.
2.
3.
4.
5.
6.
7.
8.
9.
10.
FREQUENCY (HZ.)
0.
1.
2.
3.
4.
5.
6.
7.
8.
9.
10.
11.
12.
13.
14.
15.
16.
17.
18.
19.
20.
21.
22.
23.
24.
25

Fig. 26

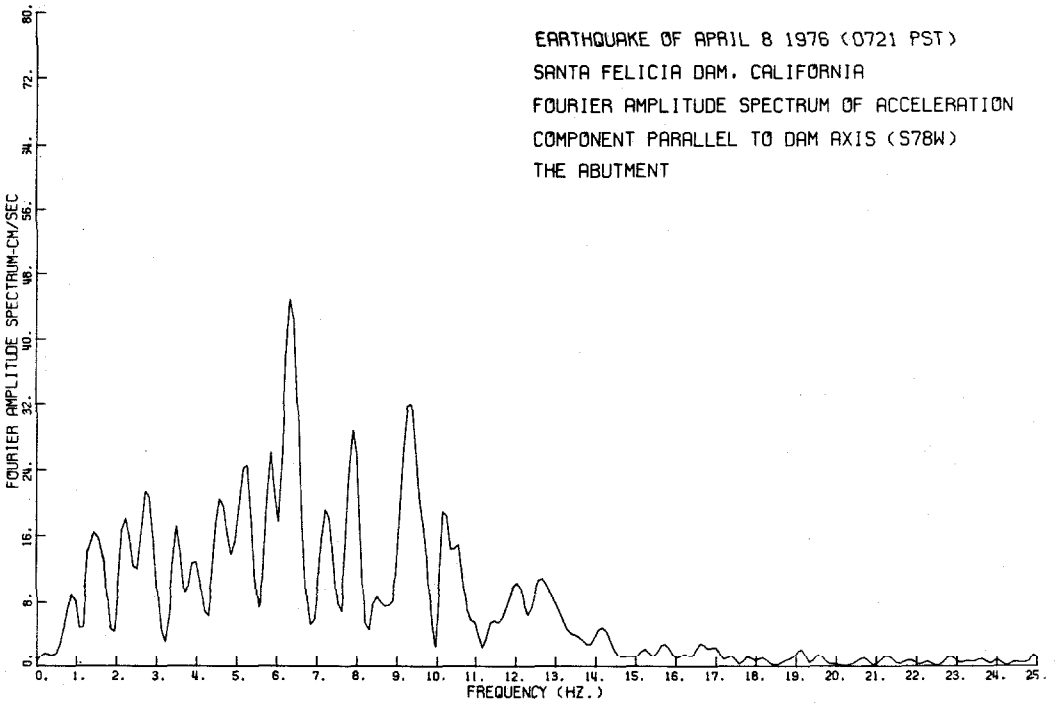
EARTHQUAKE OF APRIL 8 1976 (0721 PST)
SANTA FELICIA DAM, CALIFORNIA
FOURIER AMPLITUDE SPECTRUM OF ACCELERATION
COMPONENT PARALLEL TO DAM AXIS (S78W)
THE ABUTMENT
FOURIER AMPLITUDE SPECTRUM-CM/SEC
FREQUENCY (HZ.)

(a)

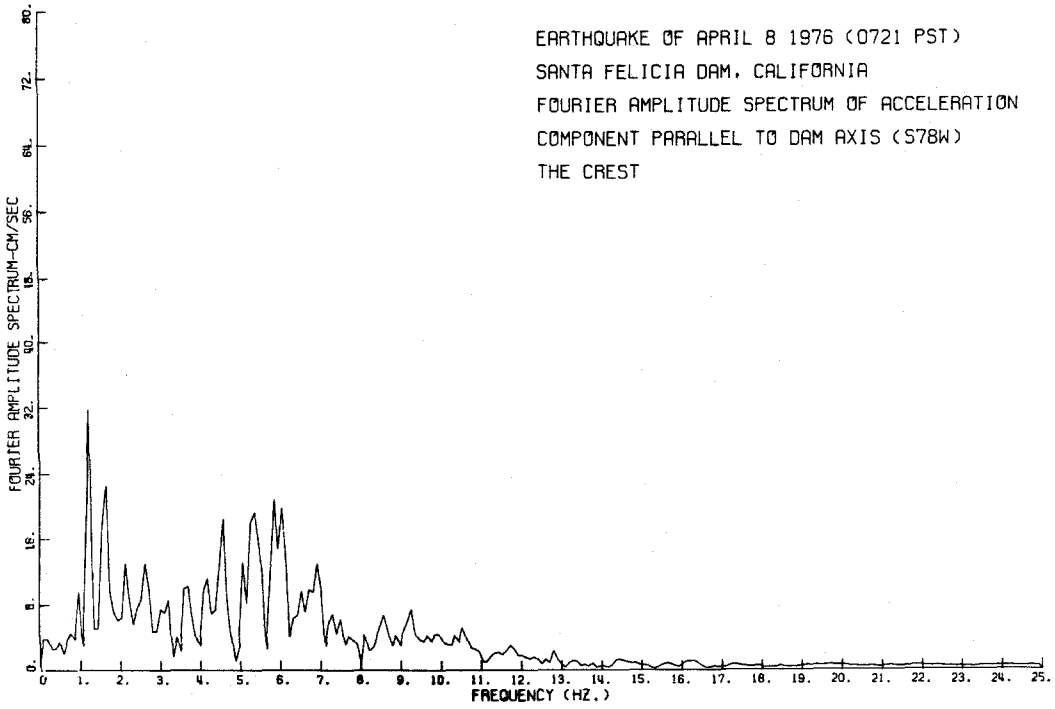
EARTHQUAKE OF APRIL 8 1976 (0721 PST)
SANTA FELICIA DAM, CALIFORNIA
FOURIER AMPLITUDE SPECTRUM OF ACCELERATION
COMPONENT PARALLEL TO DAM AXIS (S78W)
THE CREST
FOURIER AMPLITUDE SPECTRUM-CM/SEC
FREQUENCY (HZ.)

(b)

Fig. 27

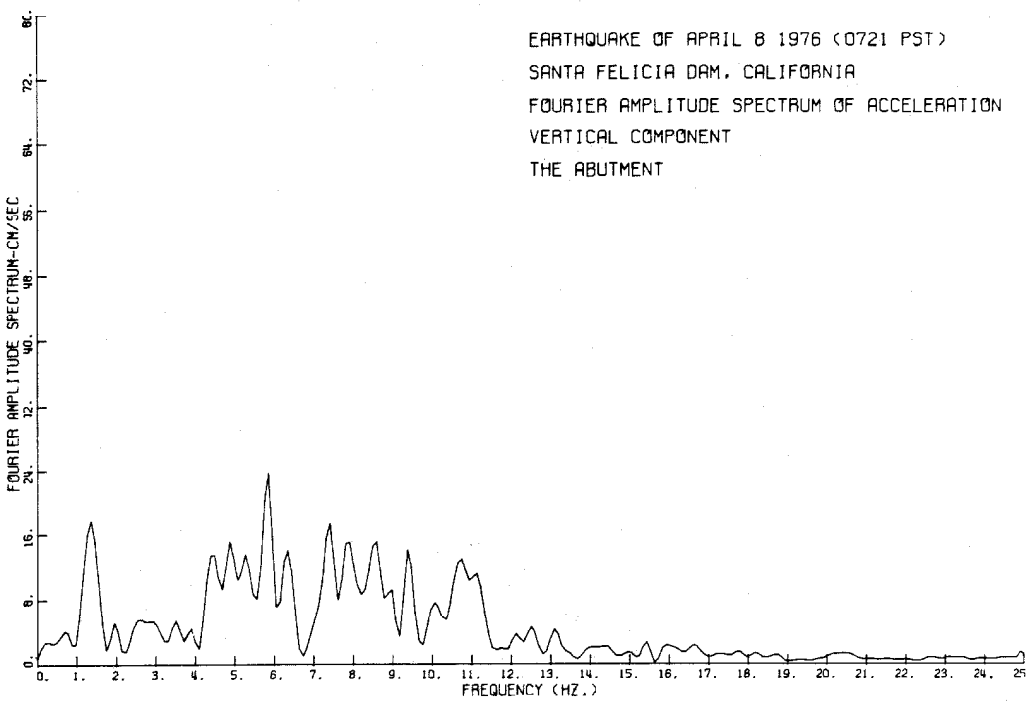
EARTHQUAKE OF APRIL 8 1976 (0721 PST)
SANTA FELICIA DAM, CALIFORNIA
FOURIER AMPLITUDE SPECTRUM OF ACCELERATION
VERTICAL COMPONENT
THE ABUTMENT
FOURIER AMPLITUDE SPECTRUN-CM/SEC
FREQUENCY (HZ.)

(a)

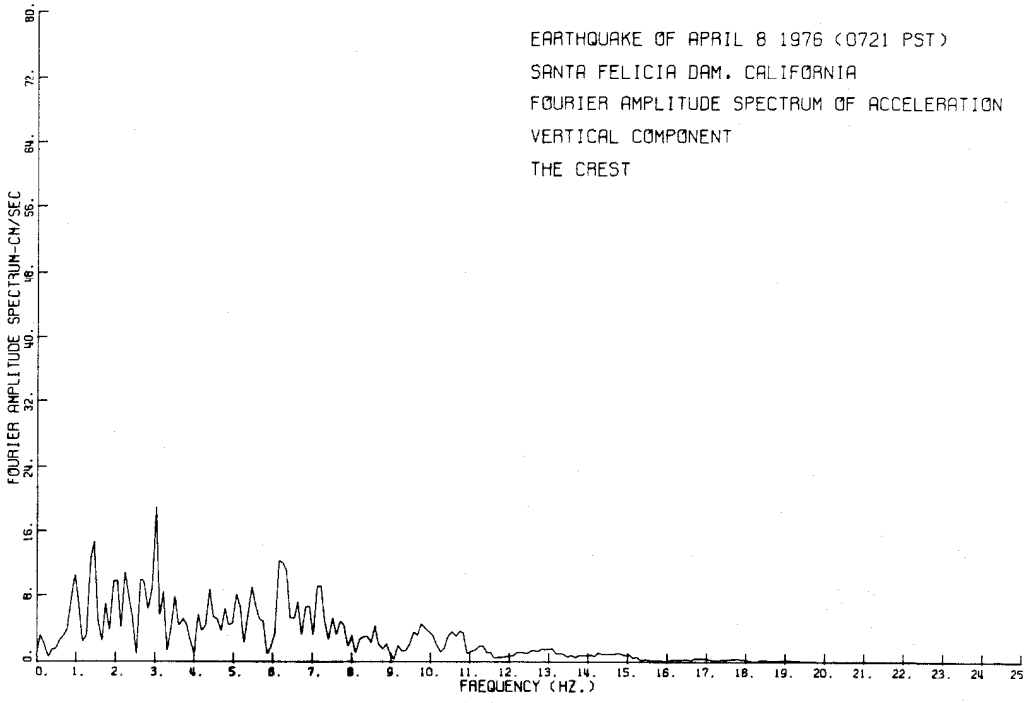
EARTHQUAKE OF APRIL 8 1976 (0721 PST)
SANTA FELICIA DAM, CALIFORNIA
FOURIER AMPLITUDE SPECTRUM OF ACCELERATION
VERTICAL COMPONENT
THE CREST
FOURIER AMPLITUDE SPECTRUN-CM/SEC
FREQUENCY (HZ.)

(b)

Fig. 28

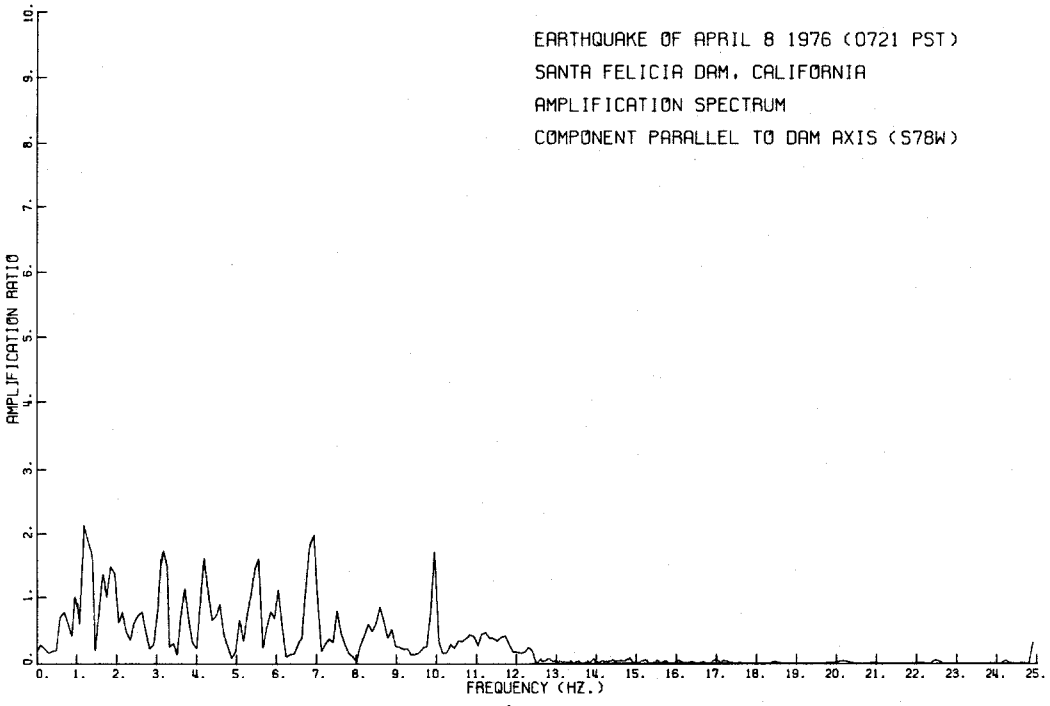
EARTHQUAKE OF APRIL 8 1976 (0721 PST)
SANTA FELICIA DAM, CALIFORNIA
AMPLIFICATION SPECTRUM
COMPONENT PARALLEL TO DAM AXIS (S78W)
AMPLIFICATION RATIO
FREQUENCY (HZ.)

(a)

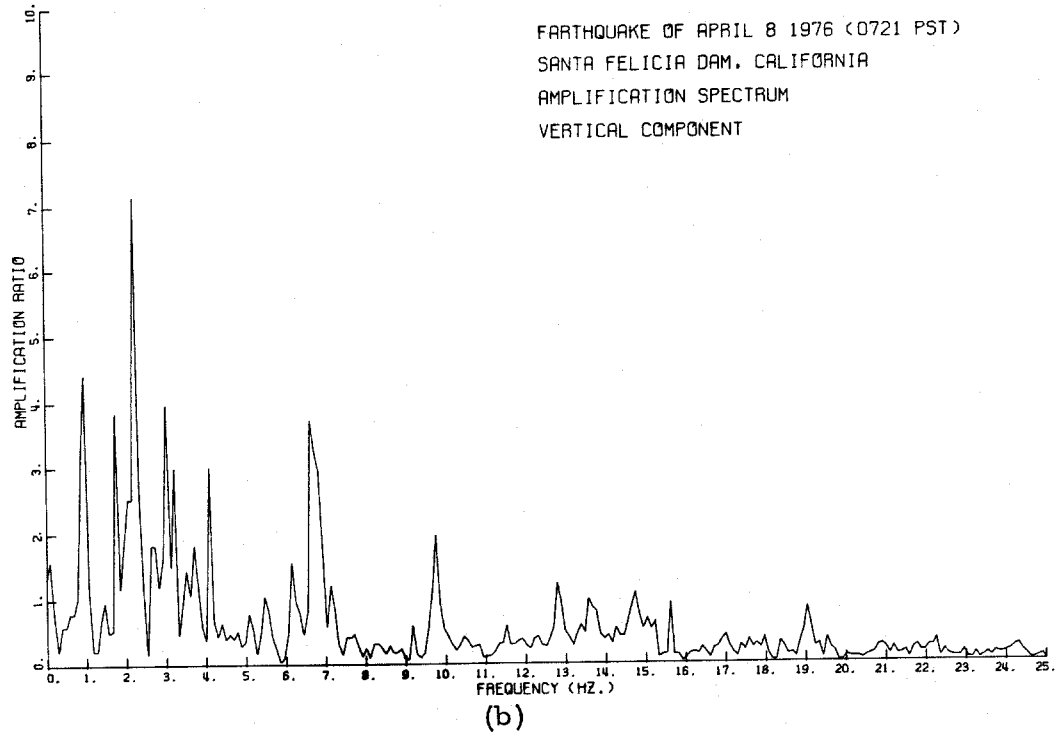
EARTHQUAKE OF APRIL 8 1976 (0721 PST)
SANTA FELICIA DAM, CALIFORNIA
AMPLIFICATION SPECTRUM
VERTICAL COMPONENT
AMPLIFICATION RATIO
FREQUENCY (HZ.)

(b)

Fig. 29

TABLE 5

Observed Natural Frequencies and Modal Participations
of the Santa Felicia Dam During San Fernando Earthquake
(1971) and Southern California Earthquake (1976)

Upstream/Downstream Component (S11.6°E)

San Fernando Earthquake, February 9, 1971						So. Cal. Earthquake April 8, 1976		
Amplification Spectrum			Smoothed Amplification Spectrum			Amplification Spectrum		
Frequency (Hz)	Amplification Ratio	Participation Factor	Frequency (Hz)	Amplification Ratio	Participation Factor	Frequency (Hz)	Amplification Ratio	Participation Factor
1.10	3.86	0.30	1.10	3.21	0.36	-	-	-
1.46	12.73	1.00	1.44	9.02	1.00	1.46	3.33	1.00
						1.66	2.29	0.69
1.83	4.80	0.38	1.81	3.72	0.41	1.86	1.61	0.48
2.05	9.62	0.76	2.03	3.94	0.44	2.08	1.73	0.52
2.27	3.36	0.26	2.27	2.83	0.31	2.25	1.78	0.53
2.47	2.73	0.21	2.47	1.88	0.21	-	-	-
2.88	2.15	0.17	2.88	1.36	0.15	2.73	3.05	0.92
3.13	2.25	0.18	3.10	2.25	0.25	3.13	1.05	0.32
3.49	2.20	0.17	3.47	1.31	0.14	3.61	1.16	0.35
3.96	7.46	0.59	3.93	2.97	0.33	3.81	1.35	0.41
4.27	1.61	0.13	4.25	1.45	0.16	4.00	1.03	0.31
4.93	2.31	0.18	4.90	1.07	0.12	-	-	-
5.08	1.92	0.15	5.08	1.36	0.15	-	-	-
5.40	1.96	0.15	5.32	1.39	0.15	-	-	-
5.93	2.72	0.21	5.93	1.32	0.15	-	-	-
7.25	1.39	0.11						
8.12	1.20	0.09	8.11	0.57	0.06	-	-	-

TABLE 6

Observed Natural Frequencies and Modal Participations
of the Santa Felicia Dam During San Fernando Earthquake
(1971) and Southern California Earthquake (1976)

Component Parallel to Dam Axis (S78.6°W)

San Fernando Earthquake, February 9, 1971						So. Cal. Earthquake April 8, 1976		
Amplification Spectrum			Smoothed Amplification Spectrum			Amplification Spectrum		
Frequency (Hz)	Amplification Ratio	Participation Factor	Frequency (Hz)	Amplification Ratio	Participation Factor	Frequency (Hz)	Amplification Ratio	Participation Factor
0.99	2.10	0.25	0.99	2.20	0.33	-	-	-
1.34	8.51	1.00	1.35	6.59	1.00	1.27	2.06	1.00
1.70	4.59	0.54	1.70	4.00	0.61	1.66	1.38	0.67
1.87	6.54	0.77	1.86	4.07	0.62	1.86	1.50	0.73
2.03	4.98	0.59	2.15	2.93	0.44	2.15	0.78	0.38
2.32	8.52	1.00	2.32	4.10	0.62	-	-	-
2.88	7.06	0.83	2.91	3.51	0.53	2.64	0.78	0.38
3.22	4.95	0.58	3.15	3.48	0.53	3.22	1.87	0.91
3.52	8.29	0.97	3.49	3.20	0.49	3.71	1.13	0.55
3.85	2.91	0.34	-	-	-	-	-	-
4.03	3.97	0.47	4.03	2.80	0.43	4.20	1.63	0.79
4.44	3.55	0.42	4.42	2.40	0.36	4.59	0.90	0.44
4.86	7.66	0.90	4.88	4.91	0.75	-	-	-
5.42	4.54	0.53	5.44	2.55	0.39	5.57	1.62	0.79
5.98	1.51	0.18	-	-	-	-	-	-
6.13	1.49	0.18	6.10	1.13	0.17	6.05	1.11	0.54
-	-	-	-	-	-	6.93	1.90	0.92
7.96	2.84	0.33	7.91	1.21	0.18	7.52	0.82	0.40
-	-	-	-	-	-	9.96	1.72	0.83

TABLE 7

Observed Natural Frequencies and Modal Participations
of the Santa Felicia Dam During San Fernando Earthquake
(1971) and Southern California Earthquake (1976)

Vertical Component

San Fernando Earthquake, February 9, 1971						So. Cal. Earthquake April 8, 1976		
Amplification Spectrum			Smoothed Amplification Spectrum			Amplification Spectrum		
Frequency (Hz)	Amplification Ratio	Participation Factor	Frequency (Hz)	Amplification Ratio	Participation Factor	Frequency (Hz)	Amplification Ratio	Participation Factor
0.63	2.02	0.19	-	-	-	-	-	-
0.95	2.49	0.24	.95	1.84	0.31	0.98	4.45	0.63
1.37	6.38	0.62	1.37	2.68	0.44	-	-	-
-	-	-	-	-	-	1.46	0.97	0.14
1.81	4.58	0.44	1.78	3.22	0.53	1.76	3.86	0.54
2.17	10.36	1.00	2.20	6.03	1.00	2.25	7.12	1.00
2.34	5.28	0.51	2.34	4.89	0.81	2.64	1.84	0.26
2.93	5.67	0.55	2.91	2.70	0.45	3.03	3.98	0.56
3.22	3.44	0.33	3.20	2.38	0.39	3.22	3.00	0.42
3.54	4.52	0.44	3.54	-		3.52	1.46	0.21
3.69	4.08	0.39	3.64	2.61	0.43	3.71	1.84	0.26
3.98	3.44	0.33	3.98	2.51	0.42	4.10	3.02	0.42
4.32	2.38	0.23	-	-	-	-	-	-
4.59	3.91	0.38	4.59	2.66	0.44	-	-	-
5.15	5.82	0.56	5.15	4.68	0.78	5.07	0.79	0.11
5.32	3.24	0.31	-	-	-	5.47	1.05	0.15
5.71	4.81	0.46	-	-	-	-	-	-
6.03	4.70	0.45	5.98	2.96	0.49	-	-	-
6.23	3.42	0.33	6.30	2.06	0.34	6.15	1.57	0.22
6.52	2.97	0.29	-	-	-	6.64	3.74	0.53
7.18	1.54	0.15	7.15	1.28	0.21	7.13	1.22	0.17
7.59	5.09	0.49	7.59	2.07	0.34	-	-	-
7.93	1.52	0.15	-	-	-	-	-	-
8.18	2.44	0.24	8.13	1.38	0.23	-	-	-

A-IV-2 Relative Acceleration, Velocity and Displacement

It is important to know the motion of the crest with respect to that of the abutment of the dam, as it will be employed later on. From the two recorded accelerograms of the 1971 San Fernando earthquake, the relative acceleration, velocity and displacement of the crest with respect to the abutment was obtained by taking the time differences of the two accelerograms (Table 3) into consideration.

Figures 30, 31 and 32 show the subtracted and corrected relative values of acceleration, velocity and displacement of the 1971 San Fernando earthquake; they all start at 3.34 seconds on the undistorted crest record of Fig. 6-b. The subtraction of the long-period ground displacement has not resulted in even comparatively smooth curves for relative displacement, as anticipated; instead, the relative displacement of the two horizontal components still includes even longer fluctuations with longer period of about 15 seconds; this could be due to a processing error in the digitizing of the accelerograms.

Comparing Figs. 9 and 31 (which are on different time scales), it is seen that for the upstream/downstream component, the relative velocity and displacement still show an apparent dominant period of about 0.7 seconds superimposed on long period fluctuations. Some possible contributions of the higher modes to the acceleration, velocity and displacement are still evident in these figures. Similarly, by comparing Figs. 11 and 31, one can see the response of the fundamental mode at period of about 0.75 seconds as well as contributions from the higher modes.

Since for the 1976 earthquake, the durations of the crest and abutment records are not the same, only part of the crest record is considered in calculating relative motion. And since the two recorded accelerograms have an accurate time correspondence, the relative velocity and displacement of the crest with respect to the abutment can be obtained by subtracting the calculated ground velocity and displacement from the record measured at the crest. The subtracted and corrected relative acceleration, velocity and displacement of only the upstream/downstream component are plotted in Fig. 33. The relative velocity curve shows the response of the predominant fundamental mode with apparent period of about 0.69 seconds as well as some contribution from higher modes.

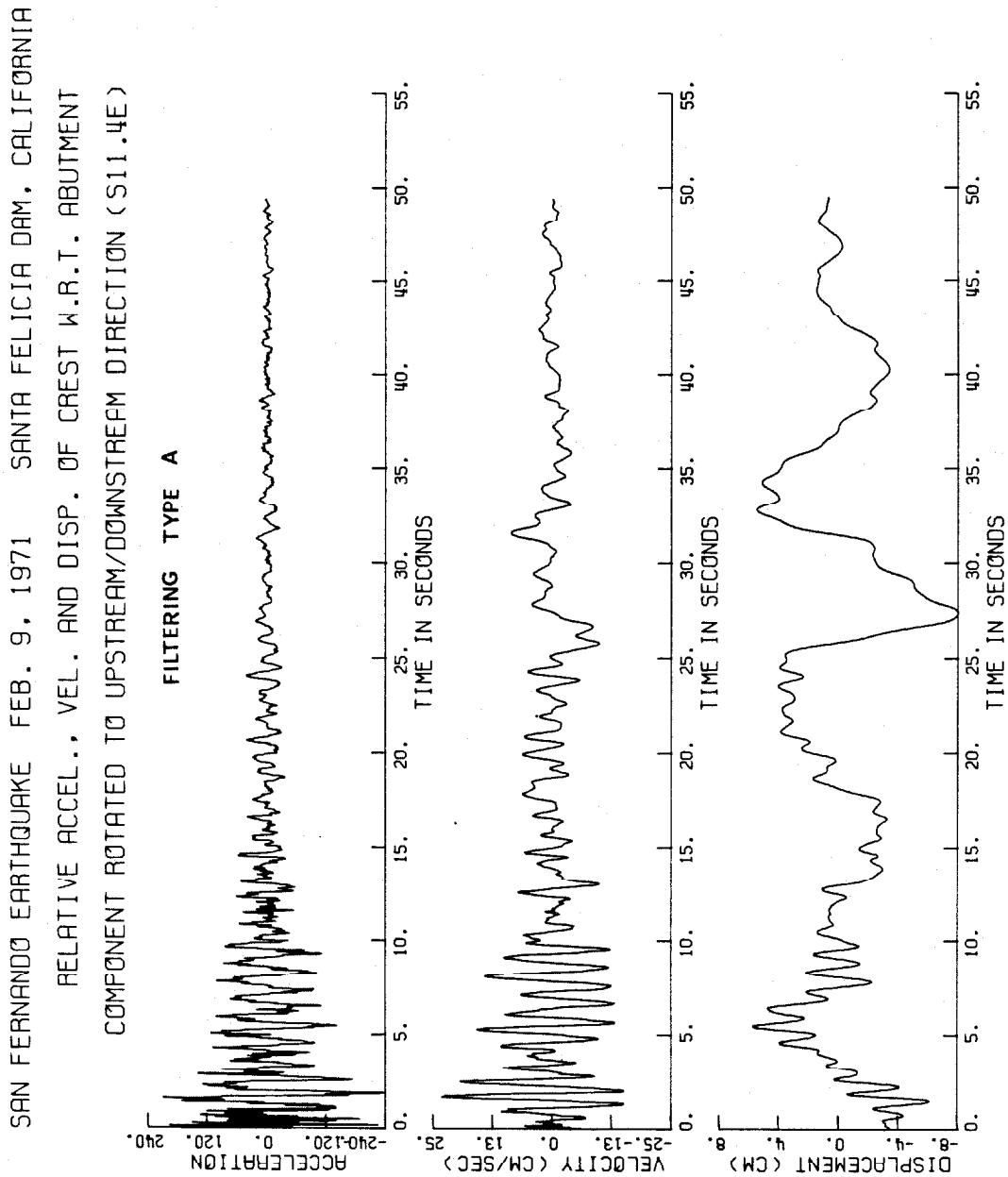
SAN FERNANDO EARTHQUAKE FEB. 9, 1971 SANTA FELICIA DAM, CALIFORNIA
RELATIVE ACCEL., VEL. AND DISP. OF CREST W.R.T. ABUTMENT
COMPONENT ROTATED TO UPSTREAM/DOWNSTREAM DIRECTION (S11.4E)
FILTERING TYPE A
ACCELERATION
-240. -120. 0. 120. 240.
VELOCITY (CM/SEC)
-25. -13. 0. 13. 25.
DISPLACEMENT (CM)
-8. -4. 0. 4. 8.
0. 5. 10. 15. 20. 25. 30. 35. 40. 45. 50. 55.
TIME IN SECONDS

Fig. 30

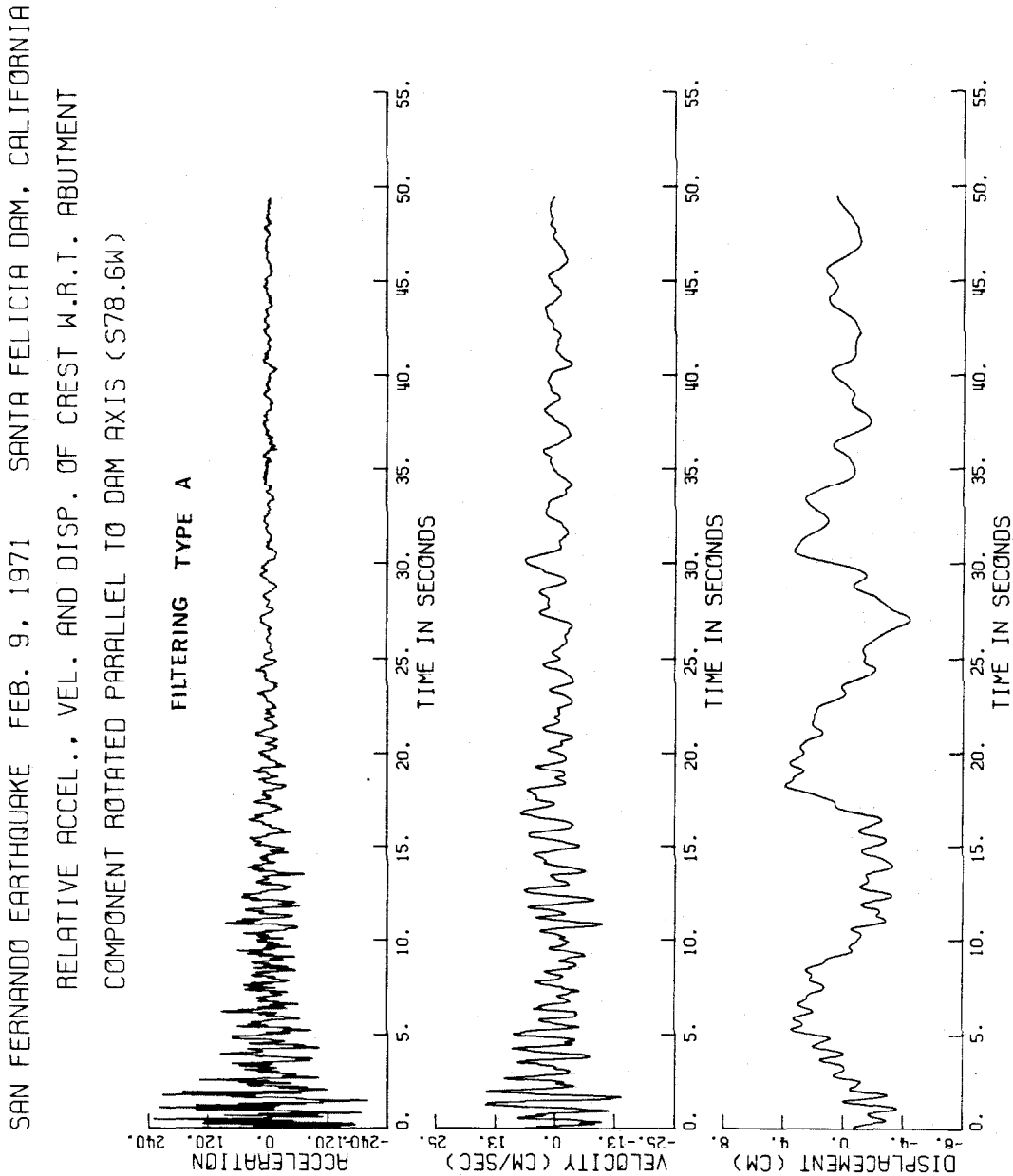
SAN FERNANDO EARTHQUAKE FEB. 9, 1971 SANTA FELICIA DAM, CALIFORNIA
RELATIVE ACCEL., VEL. AND DISP. OF CREST W.R.T. ABUTMENT
COMPONENT ROTATED PARALLEL TO DAM AXIS (S78.6W)
FILTERING TYPE A
ACCELERATION
VELOCITY (CM/SEC)
DISPLACEMENT (CM)
TIME IN SECONDS
0. 5. 10. 15. 20. 25. 30. 35. 40. 45. 50. 55.

Fig. 31

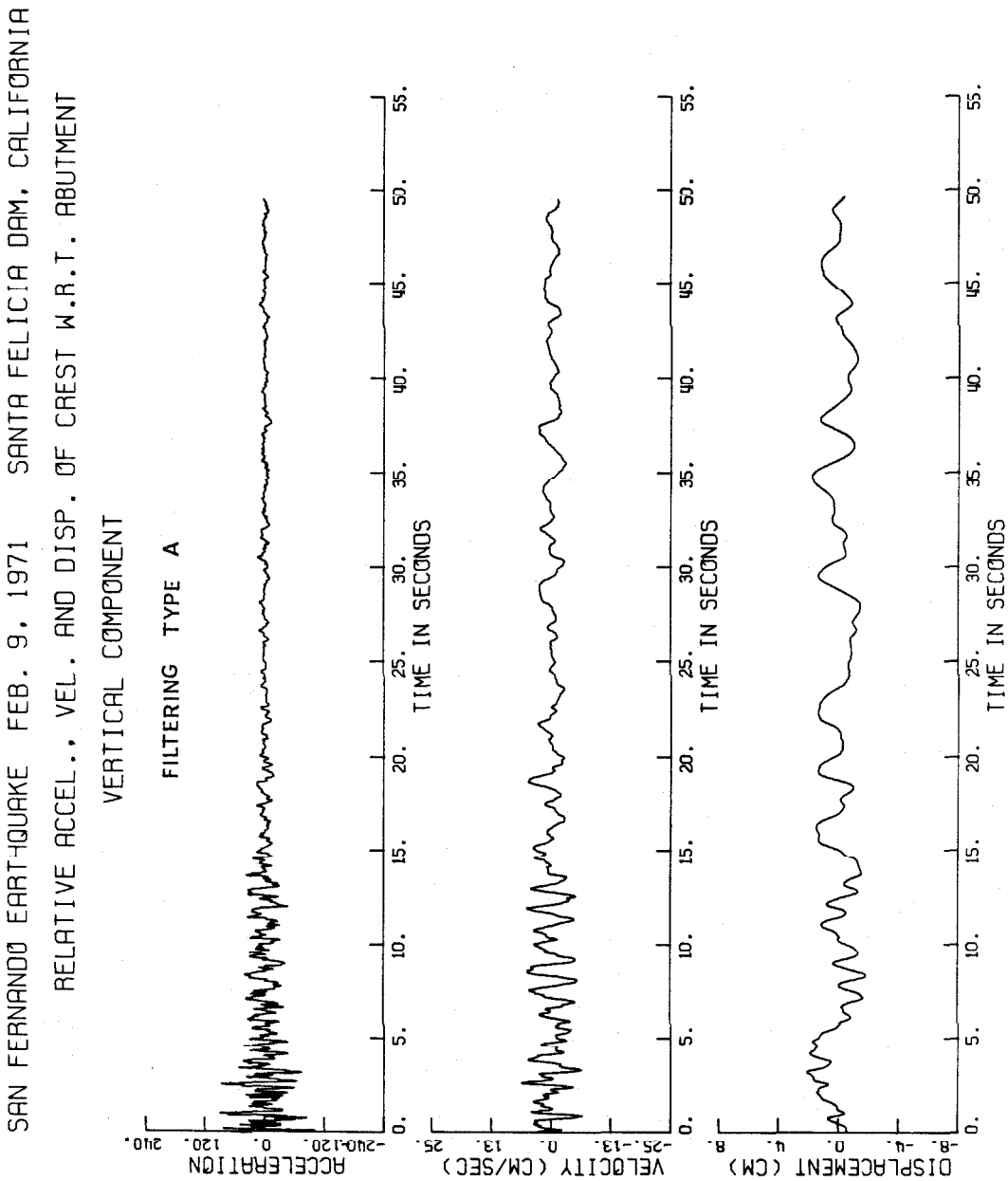
SAN FERNANDO EARTHQUAKE FEB. 9, 1971 SANTA FELICIA DAM, CALIFORNIA
RELATIVE ACCEL., VEL. AND DISP. OF CREST W.R.T. ABUTMENT
VERTICAL COMPONENT
FILTERING TYPE A
ACCELERATION
VELOCITY (CM/SEC)
DISPLACEMENT (CM)
TIME IN SECONDS

Fig. 32

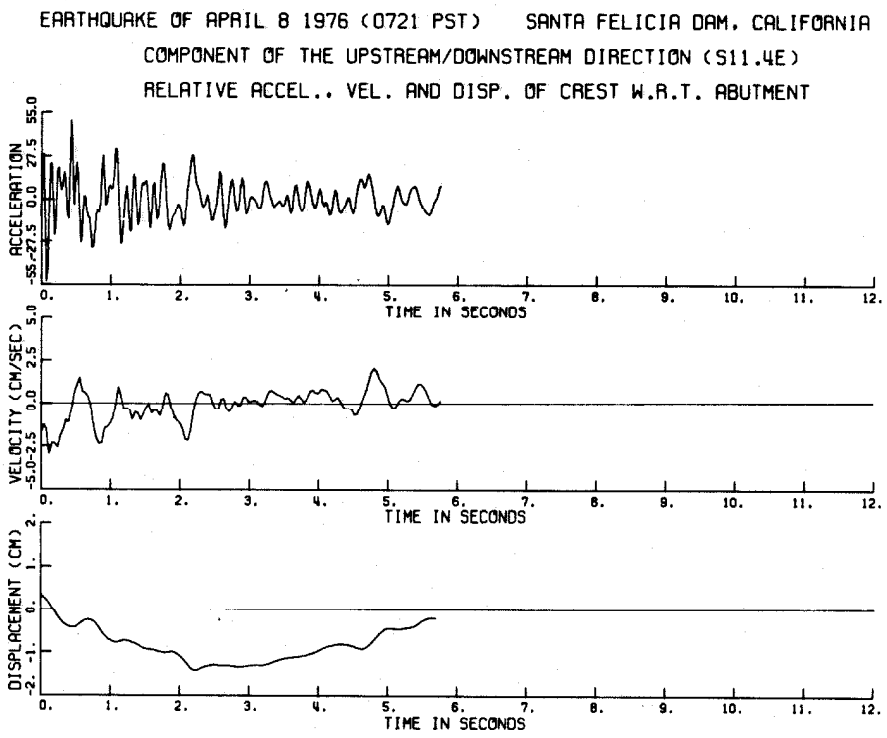
EARTHQUAKE OF APRIL 8 1976 (0721 PST) SANTA FELICIA DAM, CALIFORNIA
COMPONENT OF THE UPSTREAM/DOWNSTREAM DIRECTION (S11.4E)
RELATIVE ACCEL., VEL. AND DISP. OF CREST W.R.T. ABUTMENT
ACCELERATION
55.0
27.5
0.0
-27.5
-55.
0. 1. 2. 3. 4. 5. 6. 7. 8. 9. 10. 11. 12.
TIME IN SECONDS
VELOCITY (CM/SEC)
5.0
2.5
0.0
-2.5
-5.0
0. 1. 2. 3. 4. 5. 6. 7. 8. 9. 10. 11. 12.
TIME IN SECONDS
DISPLACEMENT (CM)
2.
1.
0.
-1.
-2.
0. 1. 2. 3. 4. 5. 6. 7. 8. 9. 10. 11. 12.
TIME IN SECONDS

Fig. 33

A-V FIELD WAVE-VELOCITY MEASUREMENTS

The most reliable method of determining values of the dam's material constants, such as elastic moduli and Poisson's ratio, is by measuring the velocities of shear and compression (or dilatation) waves through the material in situ.

Field wave-velocity measurements or seismic tests were carried out for Santa Felicia Dam with the following objectives:

1 - To check the order of magnitude of the suggested shear wave velocity (assumed constant throughout the dam) which was estimated from the observed resonant frequency of the amplification spectrum as well as from the use of the existing shear-beam theories, as mentioned later.

2 - To study the variation of the shear wave velocity at various depths in the dam, because the earth fill used for Santa Felicia Dam was cohesive in the core and cohesionless for the shell materials.

3 - To establish a representative and reliable mean value of the material constants for use in the earthquake response analyses.

4 - To compare shear modulus and consequently shear strain resulting from seismic tests with those resulting from the two earthquakes.

The wave-velocity measurements were made using the Bison Model 1570B Signal Enhancement Seismograph, a geophone and a sledge hammer, shown in Fig. 34. This equipment was generously made available by Kinemetrics, Inc., Pasadena, California.

The experimental procedures were carried out in the following manner:

1 - A line of hammer stations was used along both the crest and the upstream slope of the dam. First the crest was divided into three parts, each part (about 300 ft long) having a line of three hammer stations (about 100 ft apart) as shown in Fig. 35. Then the seismograph was placed at one end of each part, and the signals from the three hammer impact stations of that part were observed; the process was reversed at the other end. Second, the dam was struck twice with the sledge hammer at two different points on the upstream slope, and both the seismograph and the geophone were mounted on the downstream slope as shown in Fig. 36.

2 - The seismic signals were produced by the hammer impacts at the individual hammer stations. Then the signal travelled through the subsurface of the dam and caused minute vibrations of the geophone.

3 - The electrical output of the geophone was transmitted to the seismograph where it was amplified, digitized, and stored in electronic memory. Then the wave form was displayed on the viewing screen where the signal could be viewed for as long as desired, until erased, and where it also could be photographed.

4 - The travel time of the seismic wave through the dam between the hammer impact instant and any position on the wave form could be displayed digitally to three significant figures. Successive time measurements at increasing hammer distance can be interpreted in terms of subsurface structure and seismic velocities, as will be illustrated later.

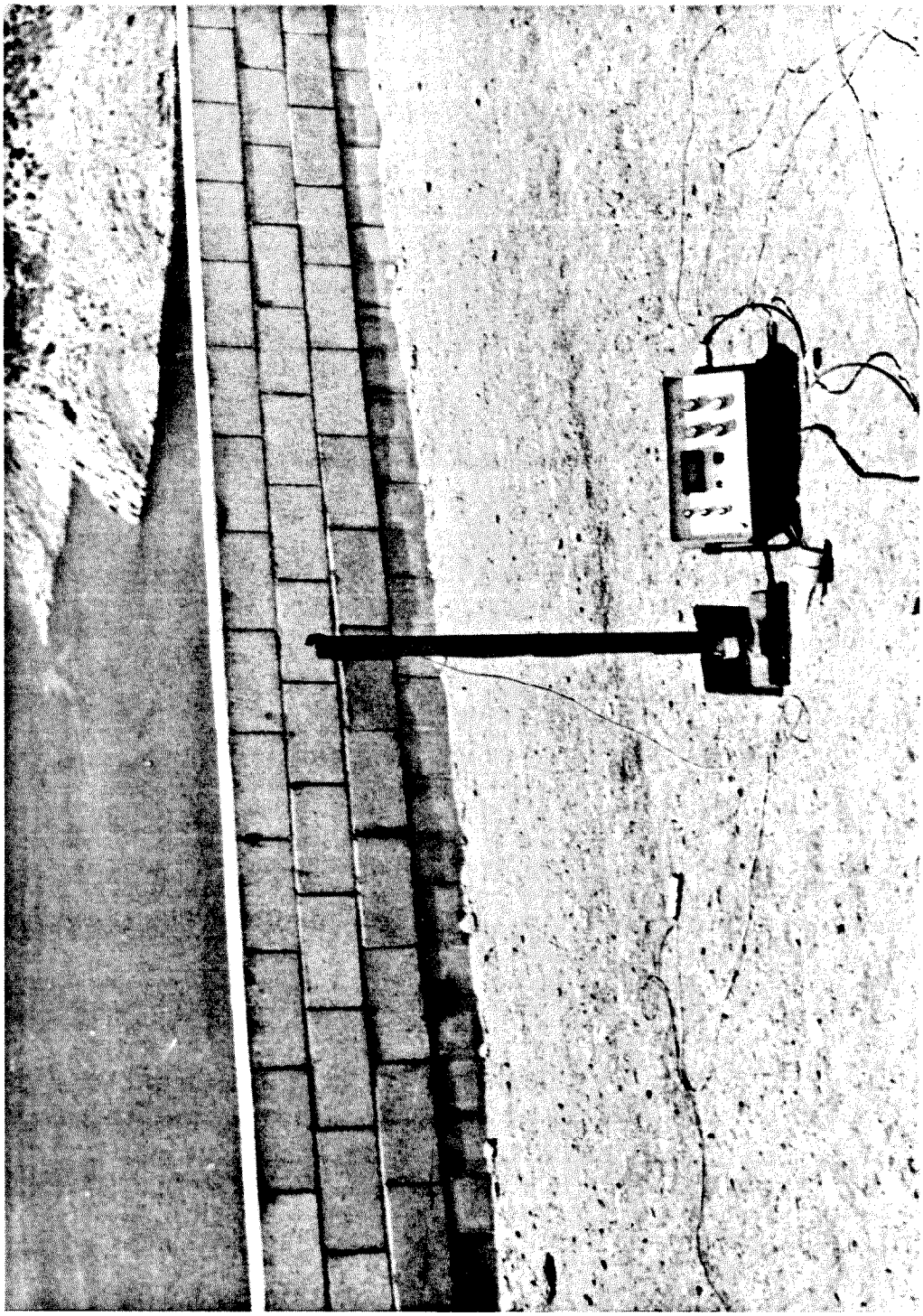

Fig. 34 The seismograph, geophone and the sledgehammer used in measuring wave velocities on and across Santa Felicia Dam

FIELD WAVE-VELOCITY MEASUREMENTS OF THE SANTA FELICIA DAM

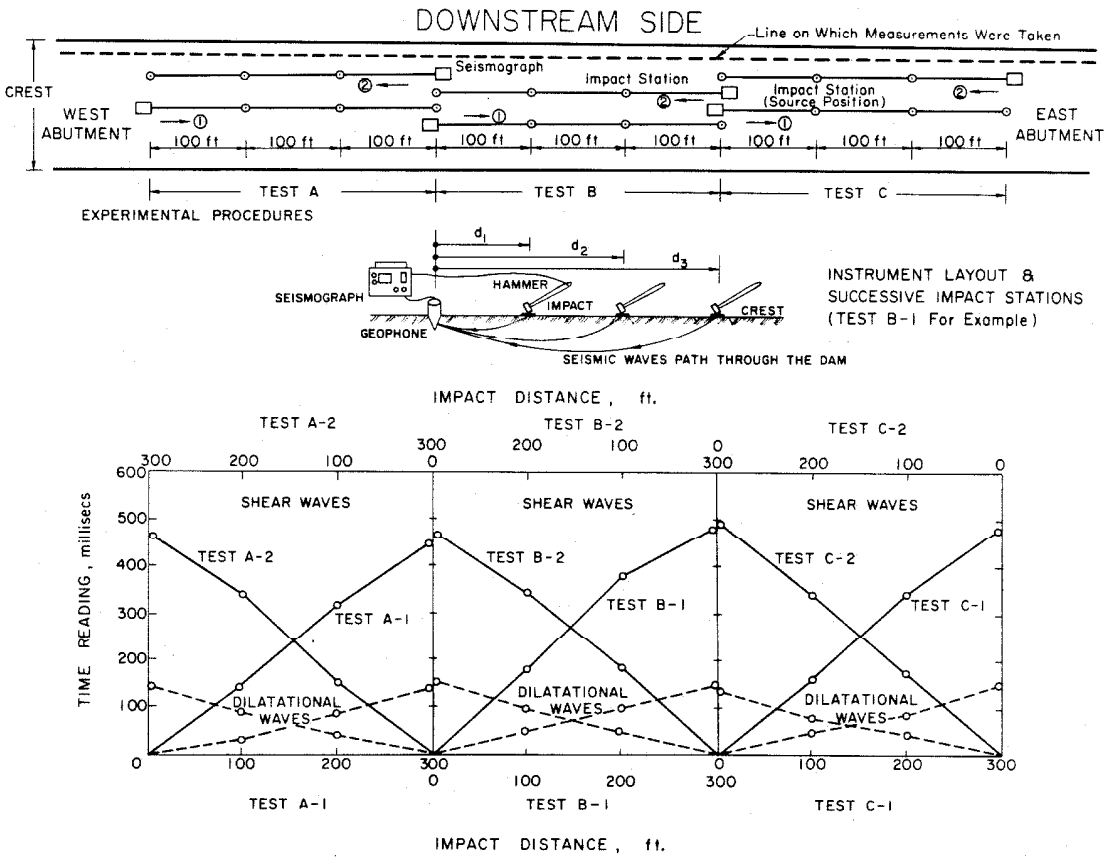

Fig. 35 The experimental set-up of the wave-velocity measurements and the field seismic graphs of the different tests

To enhance the signal at any hammer or impact station, the impact at this station was repeated so the in-phase signals, added together, reinforce each other and give a large total signal; signals which are randomly phased tend to cancel each other. The signals from any impact station always arrived at exactly the same time with respect to the impact instant (which initiated the process). Since the summed seismic signal at all times can be observed, it is possible to use one or two or three or as many impacts as necessary in order to bring out the true seismic signal.

The time intervals between the initiation of a seismic wave at the source and its arrival at the geophone, for both shear and compression waves, were instantaneously available. Figure 35 and Tables 8 and 9 show the field time readings for the arrival of the waves and the corresponding impact distance. The digital readout of time appears directly above the seismic wave form on the oscilloscope of the Bison apparatus, and by means of a visible marker on the wave form, the digital time reading can be referenced to any desired part of the signal such as the first motion or the first peak (or trough).

The seismograph does not tell what path the travelling wave has followed; this information can be obtained by means of seismic graphs (plots showing the field readings versus impact distance) such as those shown in Fig. 35. The seismic waves change in direction as the wave velocity increases with depth continuously or as they pass from one subsurface layer into the next; i.e., there is always refraction at the faces of discontinuity within the dam. In calculating shear wave velocities from the crest measurements, it was assumed

WAVE VELOCITY MEASUREMENTS ACROSS THE SANTA FELICIA DAM

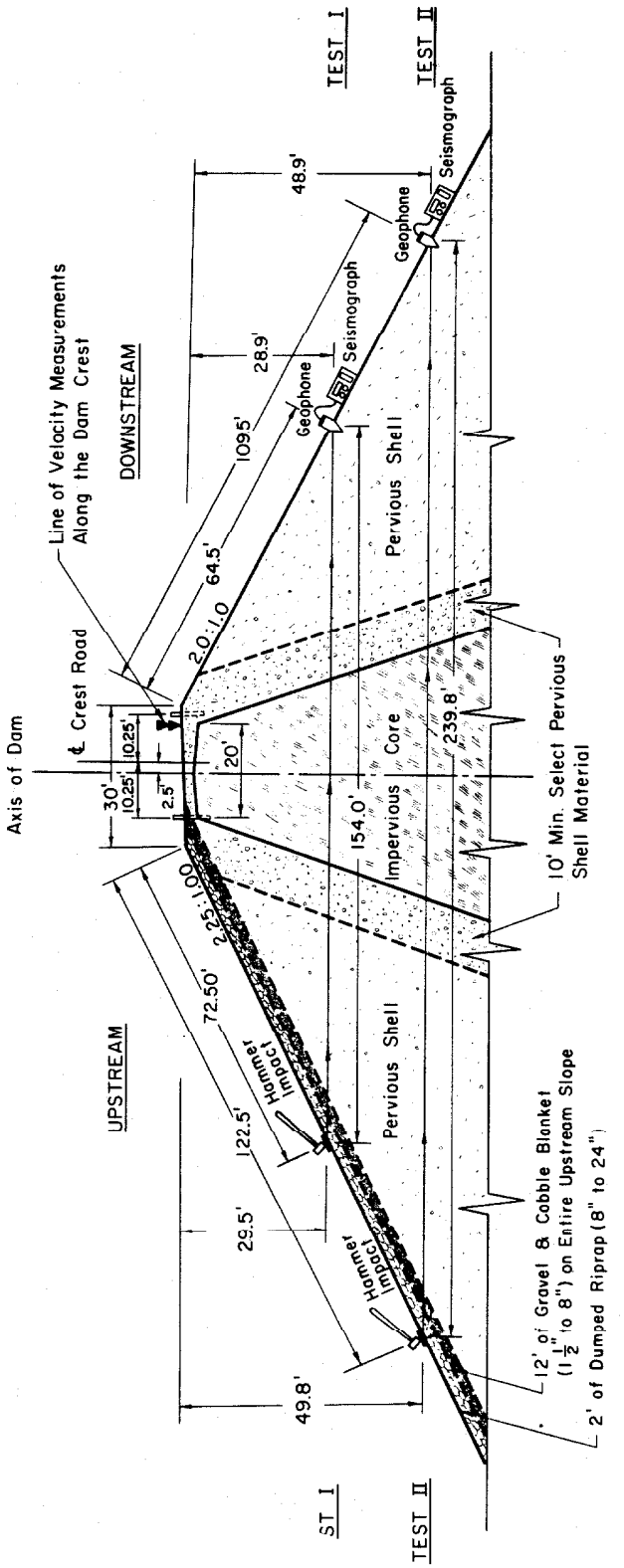

Fig. 36

that all seismic waves from the hammer blow and all seismic noise arrive at an angle, so that different points on the surface are reached at different times. The depth at which a test is conducted is closely related to the length of the seismic line. Assuming a ratio of 1:3 between these quantities, it was concluded that a 300-foot-long seismic line will detect soil within 100 feet of the surface. It was also assumed that the distance travelled by the wave is 1.2 times the impact distance. Thus, knowing the distance travelled and the time taken, the wave velocity could be computed at the suggested depth as shown by Table 8. For the wave velocity measurements taken across the dam cross section, data were taken by measuring on a horizontal path through the dam as shown in Fig. 36, extending from the downstream face to a point about 30 ft (and then 50 ft) vertically below the upstream edge of the crest. Approximately 30% of the length of the path traversed by the waves consisted of compacted fill, and 70% consisted of pervious fill; the computed wave velocities are shown in Table 9.

Poisson's ratio can be evaluated by using the two relations

$$\left(\frac{v_p}{v_s}\right)^2 = \frac{K}{G} + \frac{4}{3} , \qquad (1)$$

and

$$\frac{K}{G} = \frac{2}{3}\left[\frac{1+\nu}{1-2\nu}\right] , \qquad (2)$$

where K is the bulk modulus, v_p is the compression (or dilatational) wave velocity, v_s is the shear wave velocity and ν is Poisson's ratio. Table 9 and 10 show both the ratio K/G and Poisson's ratio ν for every test.

TAELE 8

Shear Wave and Compression Wave Velocities Measurements
of Santa Felicia Dam

(Measurements were taker along the crest of the dam)

Test No.	Impact Distance (ft)	Arrival Time T_s (m. s.)	Arrival Time T_p (m. s.)	Shear Wave Velocity (ft/sec)	Compression Wave Velocity (ft/sec)	Estimated Depth (ft)	Ratio $\frac{K}{G}$	Poisson's Ratio ν	Shear Modulus $G = v_s^2 \rho$ lb/ft^2
A-1	98	166	46	708.4	2556.5	32.7	11.69	0.46	2.0174×10^6
	202	305	89	897.8	2902.3	67.3	9.12	0.45	3.2403×10^6
	307	445	135	900.0	2739.1	102.3	7.93	0.44	3.2562×10^6
A-2	105	175	51	720.0	2470.6	35.0	10.44	0.45	2.0840×10^6
	209	335	99	780.0	2600.0	69.7	9.78	0.45	2.4458×10^6
	307	464	142	911.6	2734.9	102.3	7.67	0.44	3.3407×10^6
B-1	103	188	55	657.5	2247.3	34.3	10.35	0.45	1.7379×10^6
	206	377	101	654.0	2687.0	68.7	15.55	0.47	1.7194×10^6
	311	479	145	1235.3	2863.6	103.7	4.04	0.39	6.1344×10^6
B-2	105	178	53	707.9	2377.4	35.0	9.95	0.45	2.0145×10^6
	208	335	98	787.3	2746.7	69.3	10.84	0.46	2.4918×10^6
	311	460	140	988.8	2942.9	103.7	7.53	0.44	3.9305×10^6
C-1	105	167	49	754.5	2571.4	35.0	10.29	0.45	2.2885×10^6
	207	335	95	728.6	2660.9	69.0	12.01	0.46	2.1340×10^6
	308	479	142	841.7	2578.7	102.7	8.06	0.44	2.8480×10^6
C-2	101	165	47	734.6	2578.7	33.7	9.39	0.45	2.1693×10^6
	203	337	89	711.6	2914.3	67.7	15.44	0.47	2.0356×10^6
	308	485	133	851.4	2800.0	102.7	9.49	0.45	2.9140×10^6

TABLE 9

(Measurements were taken across the dam)

I	154.0	198	67	777.8	2298.5	29.5	7.40	0.44	2.4320×10^6
II	239.8	277	95	850.2	2524.3	49.8	7.49	0.44	2.9058×10^6

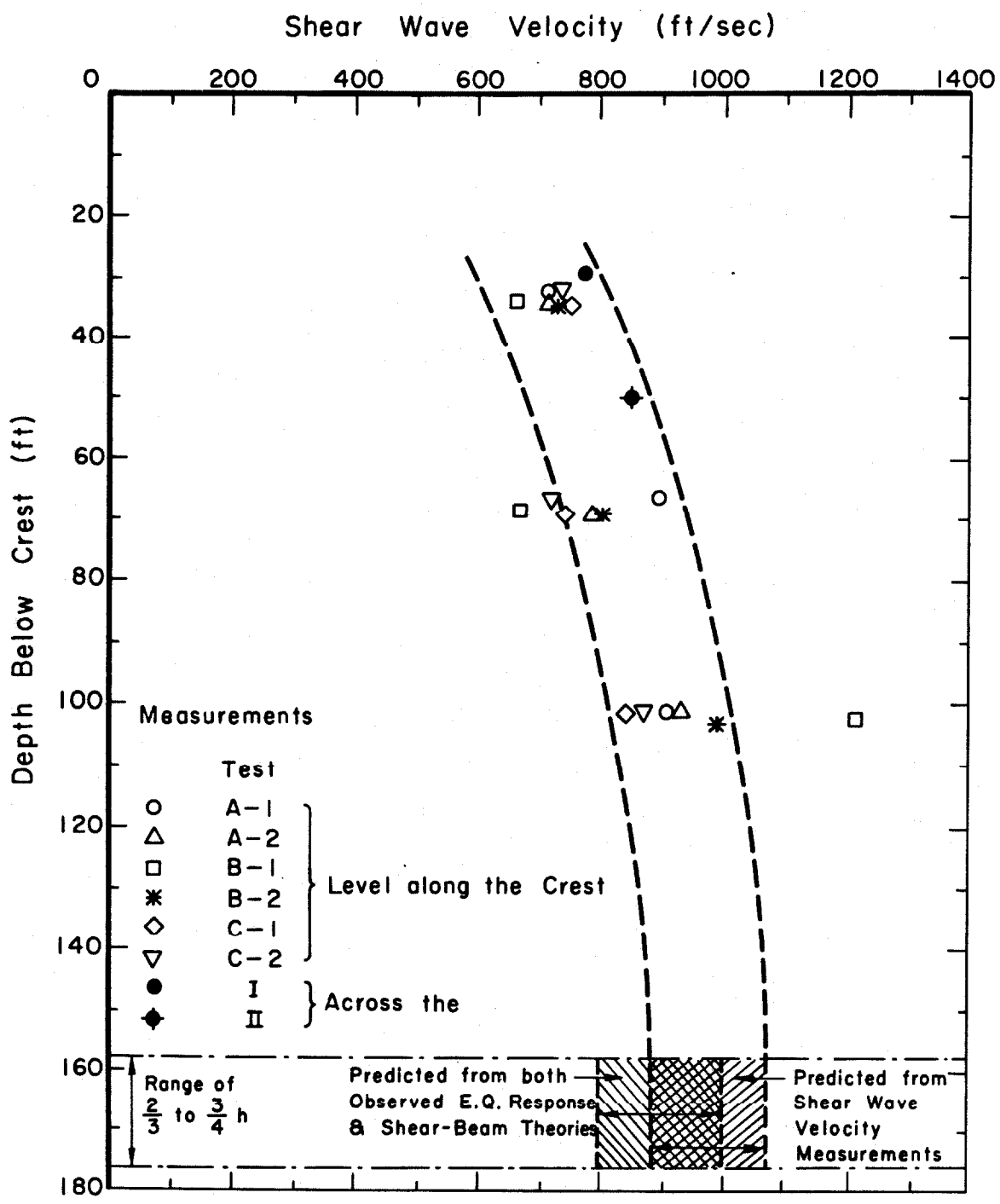
Shear Wave Velocity (ft/sec)
0
200
400
600
800
1000
1200
1400
Depth Below Crest (ft)
20
40
60
80
100
120
140
160
180
Measurements
Test
A-1
A-2
B-1
B-2
C-1
C-2
Level along the Crest
I
II
Across the
Range of 2/3 to 3/4 h
Predicted from both Observed E.Q. Response & Shear-Beam Theories
Predicted from Shear Wave Velocity Measurements

Fig. 37

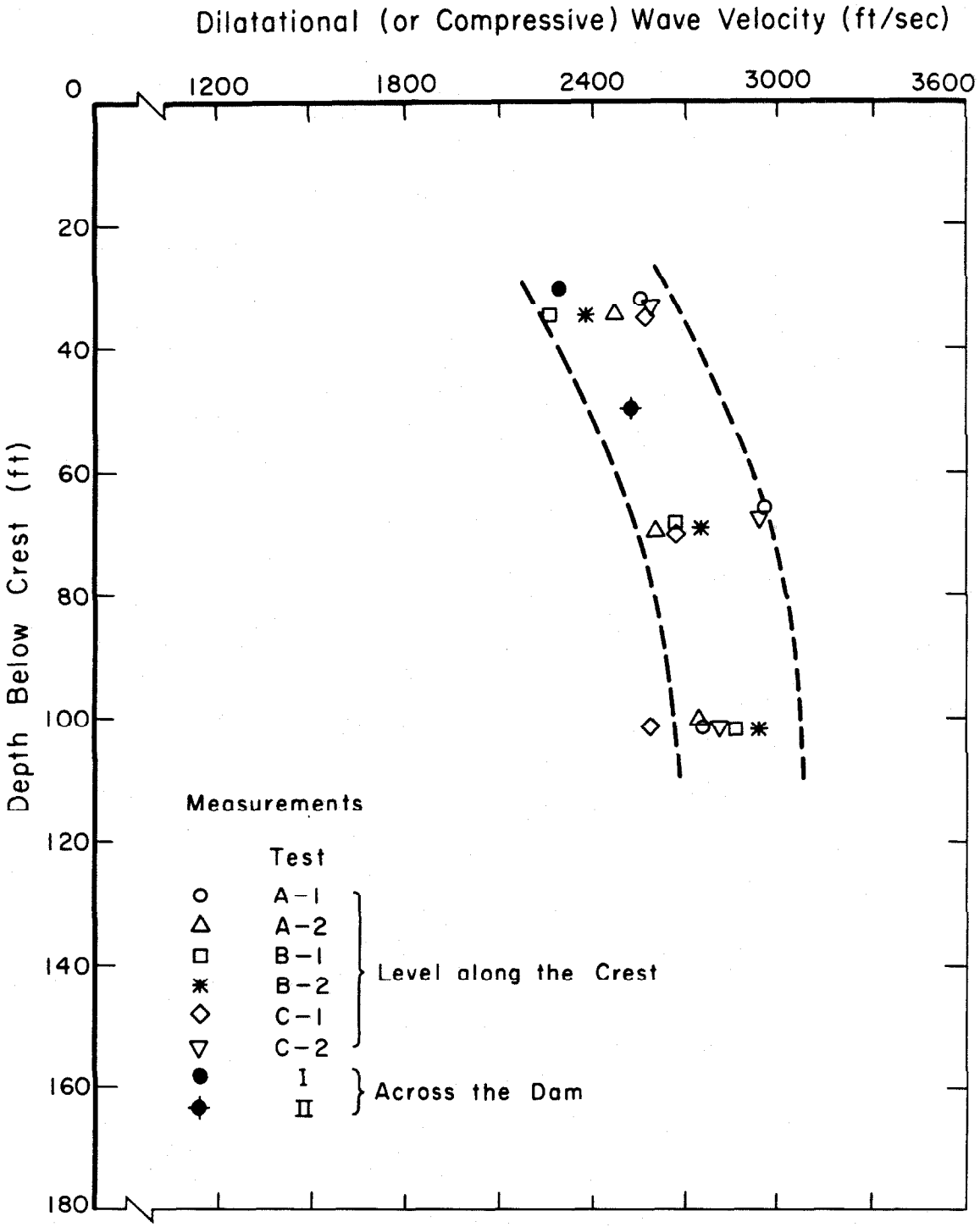
Dilatational (or Compressive) Wave Velocity (ft/sec)
0
1200
1800
2400
3000
3600
20
40
60
80
100
120
140
160
180
Depth Below Crest (ft)
Measurements
Test
A-1
A-2
B-1
B-2
C-1
C-2
Level along the Crest
I
II
Across the Dam

Fig. 38

Figure 37 shows the relationship between the measured shear wave velocity and the suggested depth at which this velocity is estimated, for the different tests; Fig. 39 shows the same relationship for the compression wave velocity. The area between the two dashed lines (in Figs. 38 and 39) is suggested for the region where data points are clustered. The extrapolated region is not necessarily representative of the dam materials. From the two figures the following observations can be made:

1 - The low value of v_s (or v_p) in the region close to the crest (at a depth of about 30 ft) and the relatively large increase of v_s (or v_p) below the crest, at a depth of about 100 ft, would seem to indicate that this dam consists of mainly cohesionless materials where the shear modulus varies with the confining pressure. It could also, however, be due to the variable nature of the fill material since the dam material consists of gravel, sand and silty clay. Thus, it can be assumed that the shear wave velocity is not constant throughout the dam.

2 - Due to the velocity variation throughout the dam, it was thought desirable to establish a mean value for use in dynamic response analyses and for use in comparing this mean value with the value computed from the amplification spectrum. Since measurements were not taken through the whole depth of the dam, it was decided to take the value of the velocity (in the extrapolated area) at a depth equal to ($\frac{2}{3}$ to $\frac{3}{4}$)h or at approximately 158 - 177 ft below the crest.

This gives a range of v_s between 870 ft/sec and about 1,070 ft/sec, as compared to the computed v_s of 850 ft/sec mentioned later. Thus, the value of v_s computed from the observed earthquake response was at least of the same order of magnitude as values determined from the wave velocity measurements. To obtain average values of v_s for the entire dam using seismic techniques, a comprehensive testing program would be necessary.

3 - As seen in Tables 8 and 9, the seismic tests give a mean value for Poisson's ratio ν of 0.45; this can be taken as representative of the dam material. This value is also in the same order of magnitude as that suggested by Martin (1965) for this type of dam.

4 - In any dynamic response analyses, shear-beam models with shear modulus varying with the depth (to be mentioned later) would be more appropriate than models with constant shear modulus to estimate dynamic shear strains and stresses. However, it would be interesting to compare results obtained by the two types of models.

It is worthwhile to compare values of shear modulus resulting from the measured shear wave velocity (assuming the density ρ is constant throughout the dam) with those values computed from the relation $G(y) = S_0(\gamma y/2)^{\frac{1}{3}}$ mentioned later. From the analysis in section B-II, a value of $v_{s0} = (S_0/\rho)^{\frac{1}{2}} = 195.0$ $(ft^{4/3}\ lb^{-1/6}\ sec^{-1})$ was obtained, leading to $S_0 = 0.1529 \times 10^6$; then by using $\gamma = 129.33$ lb/ft^3 one can have $G(y) = 0.6053 \times 10^6\ (y)^{\frac{1}{3}}$. This curve has been

plotted in Fig. 39 along with all the values of G from the different tests. It is difficult to determine the exact trend of the observed data points but they fit reasonably well with the curve $G(y) = S_0(\gamma y/2)^{\frac{1}{3}}$, especially at shallow depths, up to 90 ft, say beyond which there is deviation from the curve of G(y).

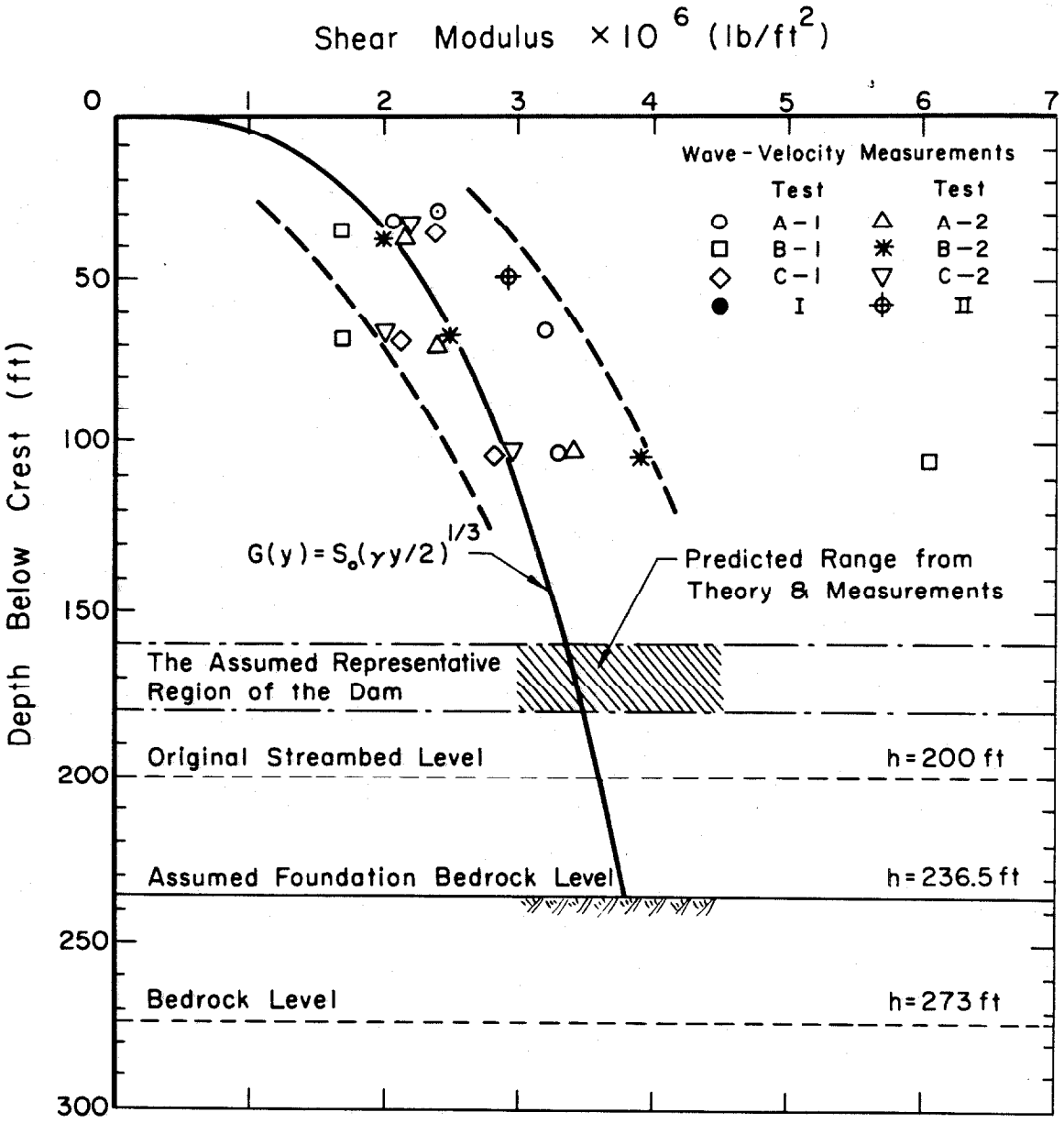
Shear Modulus $\times 10^6$ (lb/ft^2)
0
1
2
3
4
5
6
7
Depth Below Crest (ft)
50
100
150
200
250
300
Wave-Velocity Measurements
Test
Test
A-1
A-2
B-1
B-2
C-1
C-2
I
II
$G(y) = S_o(\gamma y/2)^{1/3}$
Predicted Range from Theory & Measurements
The Assumed Representative Region of the Dam
Original Streambed Level
h=200 ft
Assumed Foundation Bedrock Level
h=236.5 ft
Bedrock Level
h=273 ft

Fig. 39

B. ANALYSIS

B-I BASIS OF THE ANALYSIS

The idea of studying the nonlinear (or hysteretic) behavior of structures from their measured earthquake response was initiated by Iemura and Jennings (1973) when they attempted to find simple descriptions for the nonlinear response of a nine-story reinforced concrete building (Millikan Library of Caltech) during the San Fernando earthquake of 1971. In their study, the response of the fundamental mode of the building was treated as that of a single-degree-of-freedom hysteretic structure, and the dynamic force-deflection relation of this mode was recovered by plotting the measured values of absolute acceleration (recorded at the roof of the building) against the calculated values of relative displacement of the roof with respect to the base. The mathematics behind Iemura and Jennings' idea is based on the equation of motion of a single-degree-of-freedom system excited by an earthquake:

$$F(x,\dot{x}) = -M(\ddot{x} + \ddot{z}) \quad , \tag{3}$$

in which $F(x,\dot{x})$ represents the nonlinear restoring force due to relative velocity $\dot{x}$ and displacement x; M is the mass and $\ddot{z}$ is the ground acceleration as shown in Fig. 40-a. Using this relation, a preliminary version of the hysteretic response of the building was obtained by plotting the relative displacement $x(t)$ against the absolute acceleration $(\ddot{x}(t) + \ddot{z}(t))$.

From examination of the records of the dam's earthquake responses, in both the time and frequency domains, it was found that

the dam responded primarily in its fundamental mode in the upstream/downstream direction, although there was some vibration of the higher modes apparent in the response and in the amplification spectra. Consequently, the response in the fundamental mode of the dam in its upstream/downstream direction was treated as that of a single-degree-of-freedom hysteretic structure, in order to study the dam's nonlinear behavior. By applying Iemura-Jennings' basic idea, a preliminary version of the hysteretic response of the earth dam was obtained. From this, certain parameters such as equivalent soil moduli and damping factors can be estimated.

Because most soils, including earth dam fills, have curvilinear stress-strain relationships (Seed and Idriss, 1970) as shown in Fig. 41, the equivalent linear shear modulus is usually expressed as the secant modulus determined by the slope of the line joining the extreme points of the hysteresis loops, while the damping factor is proportional to the area inside the hysteresis loop. It is apparent that each of these properties will depend on the magnitude of the strain for which the hysteresis loop is determined, and thus both shear moduli and damping factors must be determined as functions of the induced strain in an earth dam or any soil specimen. As indicated by Fig. 41 for large dynamic strains, such as those which would occur in earth dams subjected to large earthquakes, the effective shear modulus would be less than that for the low amplitude vibrations, obtained in small earthquakes or in field tests, due to the nonlinear hysteretic behavior exhibited by the dam's materials.

It is the purpose of this investigation to provide some data on the dynamic shear moduli and damping factors for the Santa Felicia Dam

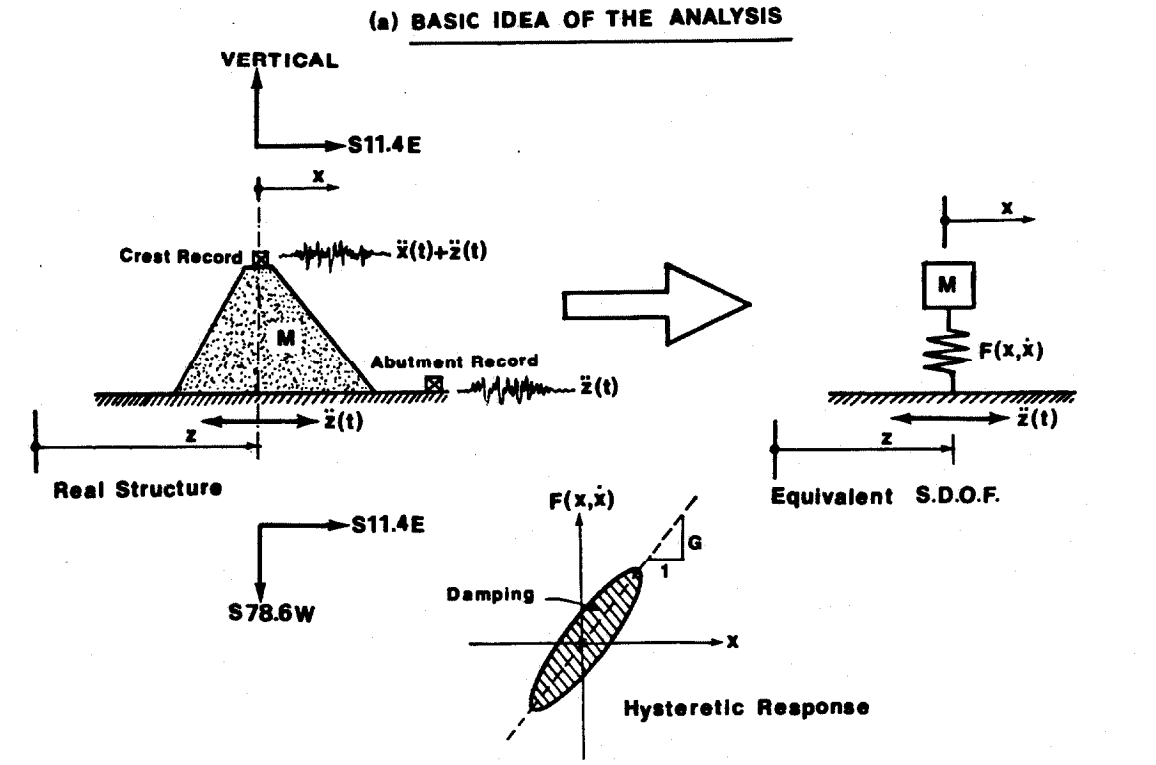
(a) BASIC IDEA OF THE ANALYSIS
VERTICAL
S11.4E
x
Crest Record
ẍ(t)+z̈(t)
M
Abutment Record
z̈(t)
z̈(t)
z
Real Structure
S11.4E
S78.6W
x
M
F(x,ẋ)
z̈(t)
z
Equivalent S.D.O.F.
F(x,ẋ)
G
1
Damping
x
Hysteretic Response

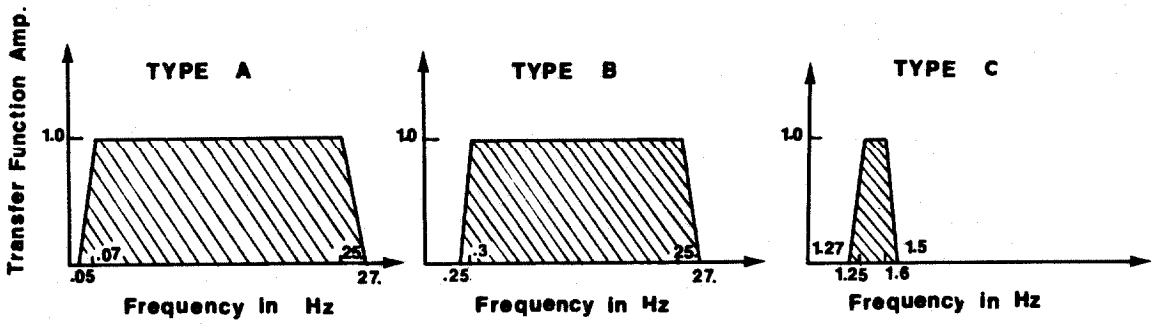
(b) DIFFERENT FILTERINGS
Transfer Function Amp.
TYPE A
1.0
.07
.25
.05
27.
Frequency in Hz
TYPE B
1.0
.3
.25
.25
27.
Frequency in Hz
TYPE C
1.0
1.27
1.5
1.25
1.6
Frequency in Hz

Fig. 40

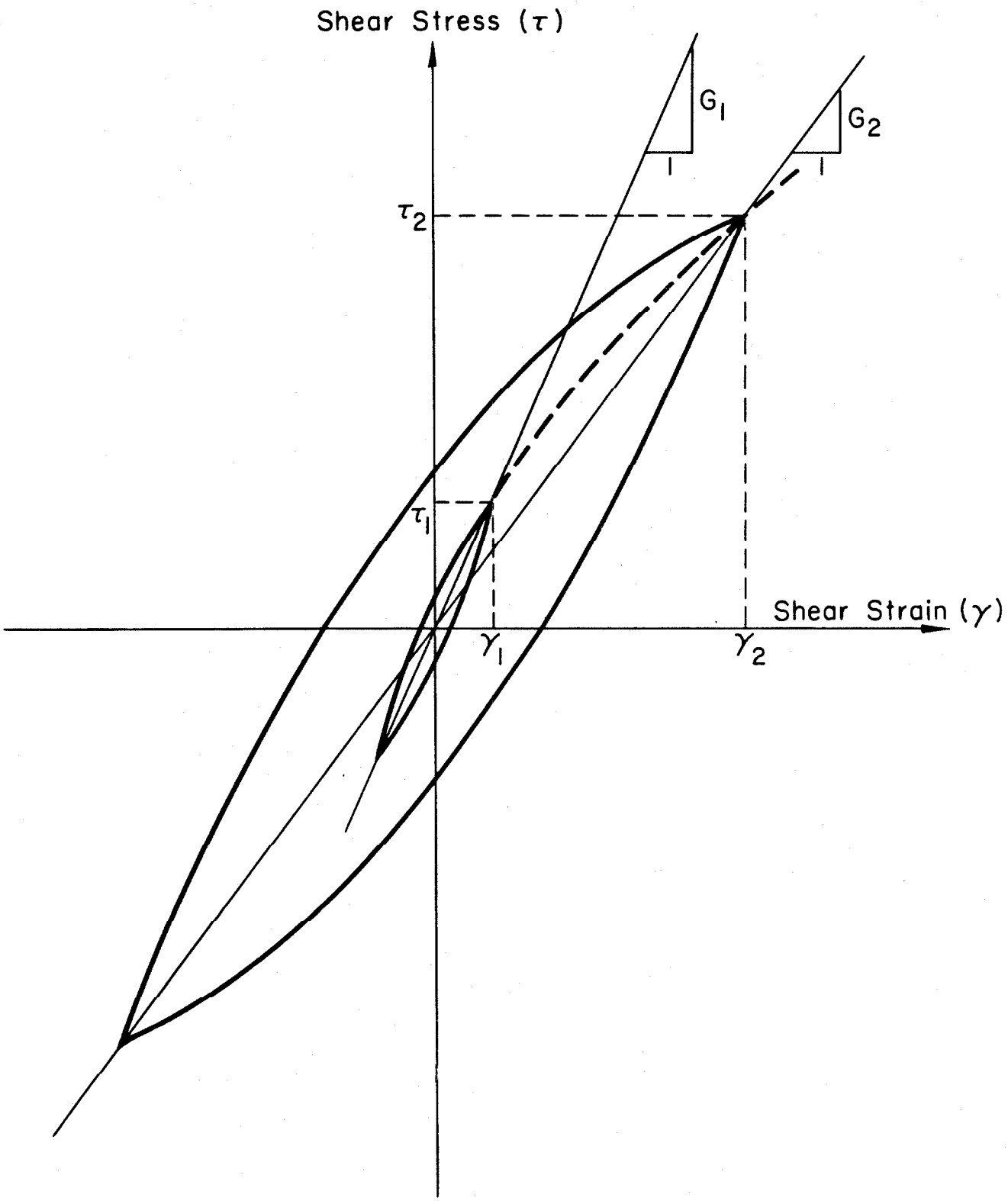

Fig. 41 Hysteretic stress-strain relationships at different strain amplitudes (after Seed and Idriss, 1970)

materials, from the earthquake observations; most available data to date have been developed for sands and saturated clays by means of laboratory tests.

B-II FREE VIBRATION ANALYSIS FOR EARTH DAMS

B-II-1 Obtaining Natural Frequencies and Modes of Vibration by Using Existing Shear-Beam Theories

Certain existing shear-beam theories are useful in obtaining a check on the order of magnitude of the resonant frequencies corresponding to peak values of the amplification spectrum curves and in estimating the shear wave velocity of the dam material. Use of these theories can establish a value for the shear wave velocity (assumed, as a first approximation, constant throughout the dam) from, for instance, the observed fundamental frequency. This estimated value of shear wave velocity can then be used to calculate other frequencies higher than the fundamental. Then a comparison between the values of resonant frequencies obtained from the earthquake observations and those computed by applying the existing theories, can be made. Actually, a visual inspection of the amplification spectra obtained from the two earthquakes reveals that the values of the resonant frequencies vary slightly from one earthquake to the other.

Earth dams are large three-dimensional structures constructed from inelastic and non-homogeneous materials. Consequently, the computation of natural frequencies and modes of vibration is extremely difficult, and as a result, existing theories and analyses of earth dams make many simplifying assumptions. The basic assumption in all these theories is that of horizontal shear deformation with shear stress uniformly distributed over horizontal planes. In this area, it is important to mention Mononobe, et. al., (1936), Hatanaka (1955), Ambraseys (1960), Minami (1960), Rashid (1961), Keightley (1963) and Martin (1965). These investigators and others have contributed

significantly to the development of the so-called shear-beam or "slice" theories of earth dams, for models ranging from an infinitely long beam with triangular cross-section resting on a rigid foundation, through a triangular elastic wedge in a rectangular canyon, and a truncated elastic wedge resting on an elastic foundation, to a case where the shear modulus varies with the depth of the dam. For the completeness of this report, a brief presentation of the results of some of these theories follows.

1 - The One-dimensional Shear-beam Theory (Infinite Length)

a - Constant Shear Modulus

Dams constructed of homogeneous compacted earth fill consisting of material which is cohesive in nature can, at first approximation, be assumed to have a constant shear modulus.

The equation of motion governing free vibration of an elastic wedge considered as a shear beam with depth h, infinite length and constant shear modulus, G, is given by

$$\frac{\partial^2 u}{\partial t^2} = \frac{G}{\rho}\left[\frac{\partial^2 u}{\partial y^2} + \frac{1}{y}\frac{\partial u}{\partial y}\right] , \qquad (3)$$

where u(y,t) is the displacement at depth y in the x-direction (see Fig. 42), and ρ is the mass density of the dam materials.

The natural frequencies and modes of vibration can be given by

$$\omega_n = \frac{\beta_n}{h}\sqrt{\frac{G}{\rho}} \quad , \quad n = 1, 2, 3, \ldots \ , \qquad (4)$$

$$Y_n(y) = J_0\left(\beta_n \frac{y}{h}\right) \quad , \quad n = 1, 2, 3, \ldots \ , \qquad (5)$$

where β_n, $n = 1, 2, 3, \ldots$, are the roots of the Bessel function of zero order of the first kind, $J_0(\beta_n)$, [e.g., $\beta_1 = 2.4048$, $\beta_2 = 5.5201$, $\beta_3 = 8.653$, etc.]. The constant $\sqrt{\frac{G}{\rho}}$ is equal to the velocity of shear wave propagation, v_s, within the dam. The modal participation factor is given by

$$P_n = \frac{\int_0^h Y_n(y)m(y)dy}{\int_0^h Y_n^2(y)m(y)dy} = \frac{2}{\beta_n J_1(\beta_n)} \quad , \quad n = 1, 2, 3, \ldots \tag{6}$$

where m(y) is the mass at depth y.

b - Shear Modulus Proportional to the Cube Root of the Depth

For earth dams consisting primarily of cohesionless materials, the analysis based on the assumption that $G(y) = S_0(\frac{\gamma y}{2})^{\frac{1}{3}}$ is more appropriate, for it has been shown that for such materials the dynamic shear modulus is approximately proportional to the cube root of the confining pressure (Richart, 1960). The parameter $v_{s0} = \sqrt{\frac{S_0}{\rho}}$, $(ft^{4/3}\ lb^{-1/6}\ sec^{-1})$, defines the elastic properties needed for dynamic analysis of the dam, as does v_s for the constant modulus case.

The equation of motion for this case, where G increases as the cube root of the depth, was derived by Rashid (1960); it can be shown to be

$$\frac{\partial^2 u}{\partial t^2} = \frac{S_0}{\rho}\left(\frac{\gamma y}{2}\right)^{\frac{1}{3}}\left[y^{\frac{1}{3}}\frac{\partial^2 u}{\partial y^2} + \frac{4}{3}y^{-\frac{1}{3}}\frac{\partial u}{\partial y}\right], \tag{7}$$

where γ is the density of the dam materials.

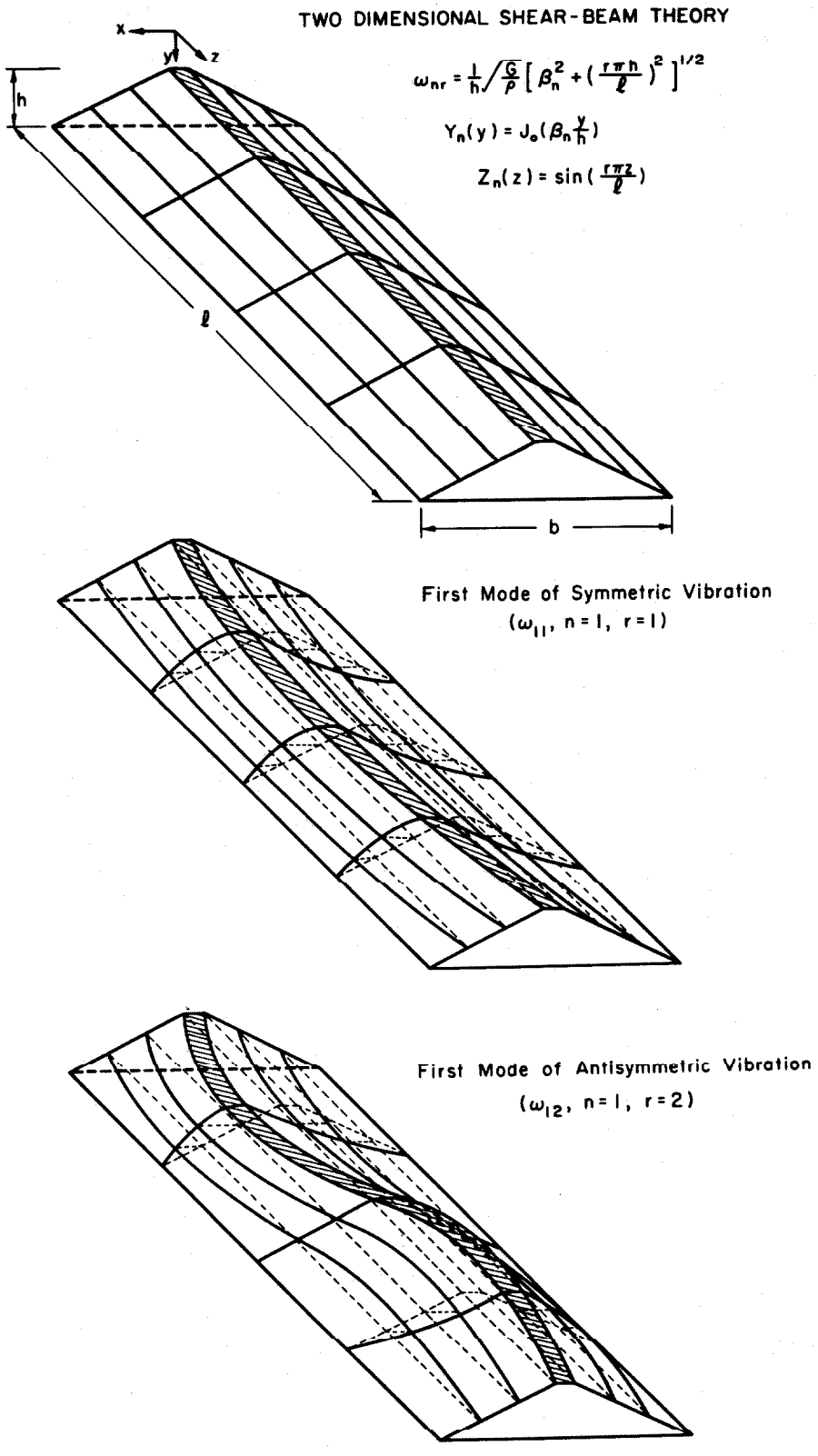
TWO DIMENSIONAL SHEAR-BEAM THEORY
$\omega_{nr} = \frac{1}{h}\sqrt{\frac{G}{\rho}}\left[\beta_n^2 + \left(\frac{r\pi h}{\ell}\right)^2\right]^{1/2}$
$Y_n(y) = J_o(\beta_n \frac{y}{h})$
$Z_n(z) = \sin\left(\frac{r\pi z}{\ell}\right)$
x
y
z
h
ℓ
b
First Mode of Symmetric Vibration
(ω_{11}, n = 1, r = 1)
First Mode of Antisymmetric Vibration
(ω_{12}, n = 1, r = 2)

Fig. 42

The natural frequencies and modes of vibration are given by

$$\omega_n = \frac{\alpha_n}{1.2h^{5/6}(2/\gamma)^{1/6}}\sqrt{\frac{S_0}{\rho}} \quad , \quad n = 1, 2, 3, \ldots \quad , \tag{8}$$

$$Y_n(y) = \left[\alpha_n(y/h)^{5/6}\right]^{-0.2} \cdot J_{0.2}\left[\alpha_n(y/h)^{5/6}\right] \quad , \quad n = 1, 2, 3, \ldots \quad , \tag{9}$$

where the values of α_n are given by the zero values of the Bessel function, $J_{0.2}(\alpha_n)$, [e.g., $\alpha_1 = 2.707$, $\alpha_2 = 5.83$, $\alpha_3 = 8.95$, etc.].

The modal participation factor is given by

$$P_n = \frac{\int_0^h Y_n(y)m(y)dy}{\int_0^h Y_n^2(y)m(y)dy} = \frac{2}{\alpha_n^{0.8} J_{1.2}(\alpha_n)} \quad , \quad n = 1, 2, 3, \ldots \quad . \tag{10}$$

2 - The Two-dimensional Shear-beam Theory (Finite Length)

In this case, the dam is assumed to be a triangular wedge in a rectangular canyon with finite length ℓ and a constant shear modulus G.

The equation of motion is given by (see Ref. 3)

$$\frac{\partial^2 u}{\partial t^2} = \frac{G}{\rho}\left[\frac{\partial^2 u}{\partial y^2} + \frac{\partial^2 u}{\partial z^2} + \frac{1}{y}\frac{\partial u}{\partial y}\right] \quad . \tag{11}$$

The natural frequencies and modes of vibration are given by

$$\omega_{nr} = \frac{v_s}{h}\left[\beta_n^2 + \left(\frac{r\pi h}{\ell}\right)^2\right]^{\frac{1}{2}} \quad , \quad n, r = 1, 2, 3, \ldots \quad , \tag{12}$$

$$\varphi_{nr}(y, z) = Y_n(y)\,Z_r(z) = J_0\left(\beta_n \frac{y}{h}\right)\sin\left(\frac{r\pi z}{\ell}\right) \quad , \quad n, r, = 1, 2, 3, \ldots \quad , \tag{13}$$

where the numerical values of β_n are the same as those for the one-dimensional case. Figure 42 shows the first symmetric and first antisymmetric mode shapes for the two-dimensional model of the dam. The modal participation factor is given by

$$P_{n,r} = \frac{\int_0^h \int_0^\ell Y_n(y)\, Z_r(z)\, m(y)\, dydz}{\int_0^h \int_0^\ell Y_n^2(y)\, Z_r^2(z)\, m(y)\, dydz} = \frac{8}{r\pi\beta_n J_1(\beta_n)} \quad , \quad n, r, = 1, 2, 3, \ldots \tag{14}$$

The results for the two-dimensional problem where the shear modulus G increases as the cube root of the depth, and for the Ambrasey's model of a truncated elastic wedge are very lengthy but can be found in Refs. 10 and 11.

B-II-2 Calculation of Natural Frequencies for Santa Felicia Dam

Inspection of the amplification spectrum curves obtained from the two earthquakes shows the fundamental frequency, f_1, in the upstream/downstream direction, to be about 1.45 Hz (or $\omega_1 = 2\pi f_1 = 9.11$ rad/sec).

1 - For the one-dimensional case with constant G, substituting values of h = 236.5 and of $\omega_1 = 9.11$ rad/sec, in Eq. 4, gives a value of $v_s = 895.98$ ft/sec. The depth of the dam h was taken to be the average value of the depth to the bed-rock level (273 ft) and the depth to the original streambed level (200 ft).

2 - For the one-dimensional case with G proportional to the cube root of the depth, the specific weight γ was assumed equal to 129.33 lb/ft^3, which is probably representative of most of the dam materials based on the average of the dry, moist

and saturated weight characteristics of both the core and shell materials of Table 1. Substituting values of $\gamma = 129.33$ lb/ft^3 ($\rho = \gamma/g = 4.02$ lb ft^{-4} sec^2), h = 236.5 ft and $\omega_1 = 9.11$ rad/sec in Eq. 8 gives a value of $v_{s0} = 191.35$ (ft$^{4/3}$ lb$^{-1/6}$ sec^{-1}).

3 - For the two-dimensional theory of a triangular wedge in a rectangular canyon, the trapezoidal canyon of Santa Felicia Dam (Fig. 3) is represented by an equivalent rectangle of length ℓ equal to the average of the crest length and the length of the base of the trapezoidal section, i.e., $\ell = 0.5\ (1275 + 450) = 912.5$ ft. Now substituting values of $f_{11} = 1.45$ Hz, $\ell = 912.5$ ft, h = 236.5 ft in Eq. 12 gives a value of $v_s = 848.66$ ft/sec. This is fairly close to, but still lower than, the value obtained by the one-dimensional theory, with G being constant.

4 - Setting $f_{11} = 1.45$ Hz in Ambrasey's truncated, finite-length shear wedge model results in a shear wave velocity, v_s, of 850.23 ft/sec. This is very close to the value obtained from the two-dimensional shear beam theory.

5 - Martin (1965) has indicated that the fundamental mode of vibration is generally the predominant mode controlling the response of an earth dam, and hence it is of interest to observe the variation of fundamental period over the range of shear wave velocities appropriate for earth dams. He suggested the curves of Fig. 43 which show the variation of fundamental period for earth dams of varying heights for both the one-dimensional theory and the two-dimensional

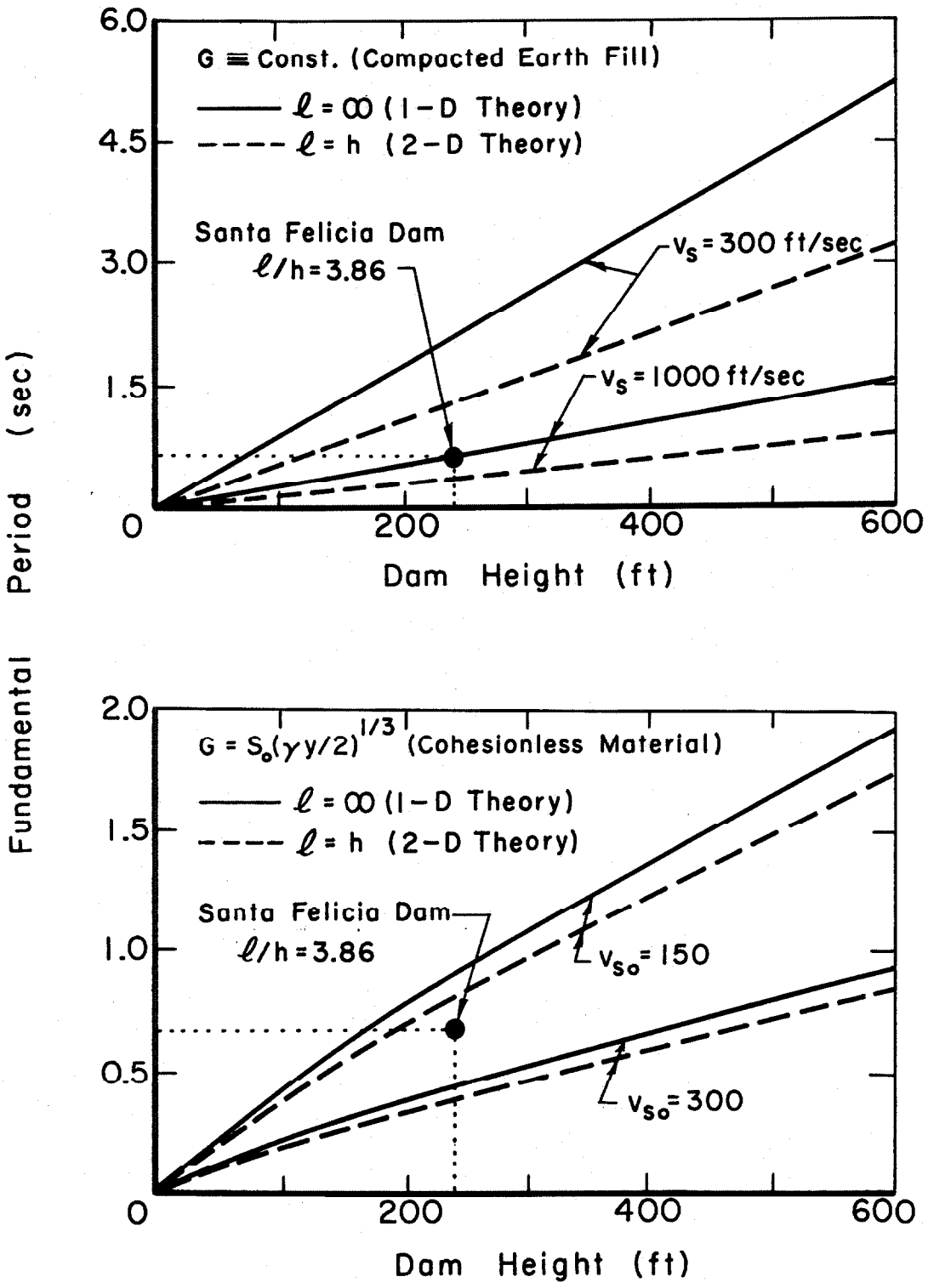

Fig. 43 Variation of fundamental period with dam height and material properties (after Martin, 1965)

theory, the latter being applied to the particular case of a rectangular canyon where the dam height equals the canyon width. It is seen, from Fig. 43, that dams constructed of cohesionless material [$G = S_0(\gamma y/2)^{\frac{1}{3}}$] have lower periods of vibration than dams of the same height constructed from compacted cohesive earth-fill (G = constant). For a dam with a height of 236.5' and a natural period of vibration of 0.69 seconds (f_1 = 1.45 Hz), Martin's curves (Fig. 43) give the following:

a - $v_s \simeq$ 1000 ft/sec ($\ell = \infty$, one-dimensional theory)

b - $v_s \simeq$ 800 ft/sec (ℓ = h, two-dimensional theory)

c - $v_{s0} \simeq 210$ ($ft^{4/3}$ $lb^{-1/6}$ sec^{-1}) ($\ell = \infty$, one-dimensional theory)

d - $v_{20} \simeq 180$ ($ft^{4/3}$ $lb^{-1/6}$ sec^{-1}) (ℓ = h, two-dimensional theory)

6 - Martin (1965) also shows that for well-graded alluvial materials with some binder, and compacted gravelly clays, the values of the shear wave velocity can vary between 800 and 1200 ft/sec; since the Santa Felicia Dam material in general consists of a gravelly, sandy, silty clay (typical of well graded alluvial material), and since the dam was constructed using modern compaction methods and controls Martin's suggested range of shear velocity is in reasonable agreement with the previously calculated values of v_s for the dam.

As the earth fill used for Santa Felicia Dam was cohesive in nature for the core materials and cohesionless for the shell materials,

it was decided to study both the case where G is constant and the case where G varies with the depth. For constant G in a dam of $\ell/h = 3.86$, a value of $v_s = 850$ ft/sec is taken to be a reasonable value for computing the natural frequencies of the dam. Shear wave velocity measurements at the dam (Section A-V) show that there is a velocity variation as the depth changes, but a mean value of $v_s \simeq 850$ ft/sec would be appropriate for use in the dynamic analyses even though it is not necessarily representative of the entire dam. For the case where G is not constant, a value of $v_{s0} = 195$ $(ft^{4/3}\ lb^{-1/6}\ sec^{-1})$ would be reasonable for use in computing the natural frequencies of the dam.

Substituting values of $v_s = 850$ ft/sec and $v_{s0} = 195$ $(ft^{4/3}\ lb^{-1/6}\ sec^{-1})$ in the frequency equations of the existing shear-beam theories gives the natural frequencies of the dam. Table 10 illustrates a comparison between the observed resonant and modal participations and estimated values computed by using the shear-beam theories. From this table the following observations can be drawn:

1 - For Santa Felicia Dam, which has the ratio $\ell/h = 3.86$, the error in the value for the fundamental frequency of vibration obtained by the two-dimensional theory as compared to the value obtained by the one-dimensional theory (with constant shear modulus) is less than 5%. Both Hatanaka (1955) and Rashid (1961) have shown, for the case of a dam in a rectangular canyon, that when the ratio ℓ/h is greater than 4 this error in the fundamental frequency is less than 5%.

TABLE 10

Comparison Between Observed Resonant Frequencies and Modal Participations and Those Computed by the Existing Shear Beam Theories

Observations						Theoretical Analyses													
San Fernando Earthquake, 1971				So. California Earthquake, 1976		Two-dimensional Theories								One-dimensional Theories					
Amplification Spectrum		Smoothed Amplification Spectrum		Amplification Spectrum		Triangular Elastic Wedge (Eq. 8)				Ambraseys' Model (Truncated Elastic Wedge)				Constant Shear Modulus (Eq. 2)				Variable Shear Modulus (Eq. 5)			
								Participation Factor				Participation Factor						Participation Factor			
Freq Hz	Particip Factor	Freq Hz	Particip Factor	Freq Hz	Particip Factor	Mode n,r	Freq $f_{n,r}$ (Hz)	$P_{n,r}$	$P_{n,r}/P_{1,1}$	Mode n,r	Freq $f_{n,r}$ (Hz)	$P_{n,r}$	$P_n/P_{1,1}$	Mode n	Freq f_n (Hz)	P_n	P_n/P_1	Mode n	Freq f_n (Hz)	P_r	P_n/P_1
1.10	0.30	1.10	0.36	-	-	-	-	-	-	-	-	-	-								
1.46	1.00	1.44	1.00	1.46	1.00	1,1	1.45	2.04	1.00	1,1	1.45	2.04	1.00	1	1.38	1.60	1.00	1	1.46	1.34	1.00
-	-	-	-	1.66	0.59	-	-	-	-	-	-	-	-								
1.83	0.38	1.81	0.41	1.86	0.48	1,2	1.66	1.02	0.50	1,2	1.67	1.02	0.50								
2.05	0.76	2.03	0.44	2.08	0.52	1,3	1.96	0.68	0.33	1,3	1.95	0.68	0.33								
2.27	0.26	2.27	0.31	2.25	0.53	1.4	2.32	0.51	0.25	1,4	2.32	0.51	0.25								
2.47	0.21	-	-	-	-																
2.88	0.17	2.88	0.15	2.73	0.92	1,5	2.70	0.41	0.20	1,5	2.71	0.41	0.20								
3.13	0.18	3.10	0.25	3.13	0.32	1,6	3.11	0.34	0.17	1,6	3.11	0.34	0.17								
						2,1	3.19	1.35	0.66	2,1	3.21	1.35	0.66	2	3.16	1.06	0.66	2	3.18	1.47	0.80
3.49	0.17	3.47	0.14	3.61	0.35	2,2	3.29	0.68	0.33	2,2	3.33	0.68	0.66								
						2,3	3.45	0.45	0.22	2,3	3.48	0.45	0.22								
						1,7	3.54	0.29	0.14	1,7	3.54	0.29	0.14								
3.96	0.59	3.93	0.33	3.81	0.41	2,4	3.67	0.34	0.17	2,4	3.68	0.34	0.17								
						2,5	3.92	0.27	0.13	2,5	3.96	0.27	0.13								
						1,8	3.97	0.26	0.13	1,8	3.97	0.26	0.13								
4.27	0.13	4.25	-	4.00	0.31	2,6	4.22	0.23	0.11	2,6	4.25	0.23	0.11								
						1,9	4.41	0.23	0.11	1,9	4.41	0.23	0.11								
						2,7	4.54	0.19	0.09	2,7	4.54	0.19	0.09								
4.93	0.18	4.90	-	-	-	1,10	4.86	0.20	0.10	1,10	4.87	0.20	0.10								
						2,8	4.88	0.17	0.08	2,8	4.90	0.17	0.08								
5.08	0.15	5.08	0.15	-	-	3,1	4.97	1.09	0.53	3,1	5.14	1.10	0.54	3	4.95	0.85	0.53	3	4.89	1.30	0.70
5.40	0.15	5.32	0.15	-	-	2,9	5.25	0.15	0.07	2,9	5.28	0.15	0.07								
5.93	0.21	5.93	0.15			2,10	5.63	0.14	0.07	2,10	5.64	0.14	0.07								

2 - The one-dimensional theory with shear modulus proportional to the cube root of the dam depth gives approximately the same fundamental frequency as does the two-dimensional theory with constant shear modulus.

3 - The two one-dimensional theories are not good in evaluating natural frequencies higher than the fundamental frequency. Actually, ω_n (or f_n) in the one-dimensional theory corresponds to ω_{nr} (or f_{nr}) with $r = 1$ in the two-dimensional theory.

4 - In general, values of the observed resonant frequencies vary slightly from those predicted by the theoretical analyses as seen from Table 10, but overall, it is fair to say that the correspondence between observation and analysis is good over the entire frequency range evaluated.

B-III HYSTERETIC RESPONSE OF THE FUNDAMENTAL MODE IN THE UPSTREAM/DOWNSTREAM DIRECTION

A preliminary version of the hysteretic response of Santa Felicia Dam was obtained by plotting the measured and corrected values of acceleration (recorded during the San Fernando earthquake of 1971), shown in Fig. 9, against the calculated values of relative displacement, shown in Fig. 30, using the actual time difference between the crest and abutment records. The time dependence of the hysteretic behavior of the dam for the first 20 seconds of the corrected record is shown in Fig. 44; each trajectory is plotted every 0.02 seconds and each loop is plotted every second. It is important to note that the corrected acceleration (and consequently the calculated displacement) was wide band-pass filtered using an Ormsby digital filter with cut-off frequencies of 0.07 and 25 Hz and roll-off termination frequencies of 0.05 and 27 Hz as shown in Fig. 40-b. This is standard filtering at Caltech; in this report this filtering is designated by "filtering type A".

It was anticipated that a reasonable estimate of the first-mode hysteresis of the dam, during the first 20 seconds of the response, would be obtained, because the first mode of the vibration predominates at this time. However, the first portion of the response (0 to 20 secs) showed marked fluctuations along the badly tangled trajectory of the supposed first-mode hysteresis. This fluctuation and tangling was thought to be the result of the non-negligible contributions of the higher modes of vibration of the dam, as well as of long-period human digitization errors.

To obtain reasonable hysteresis loops and to remove the long-period component ($f << 1.45$ Hz) that is superimposed on the response,

SAN FERNANDO EARTHQUAKE FEB. 9, 1971
SANTA FELICIA DAM, CALIFORNIA.
COMPONENT ROTATED TO UPSTREAM/DOWNSTREAM DIRECTION (S11.4E)
HYSTERETIC RESPONSE FILTERING TYPE A

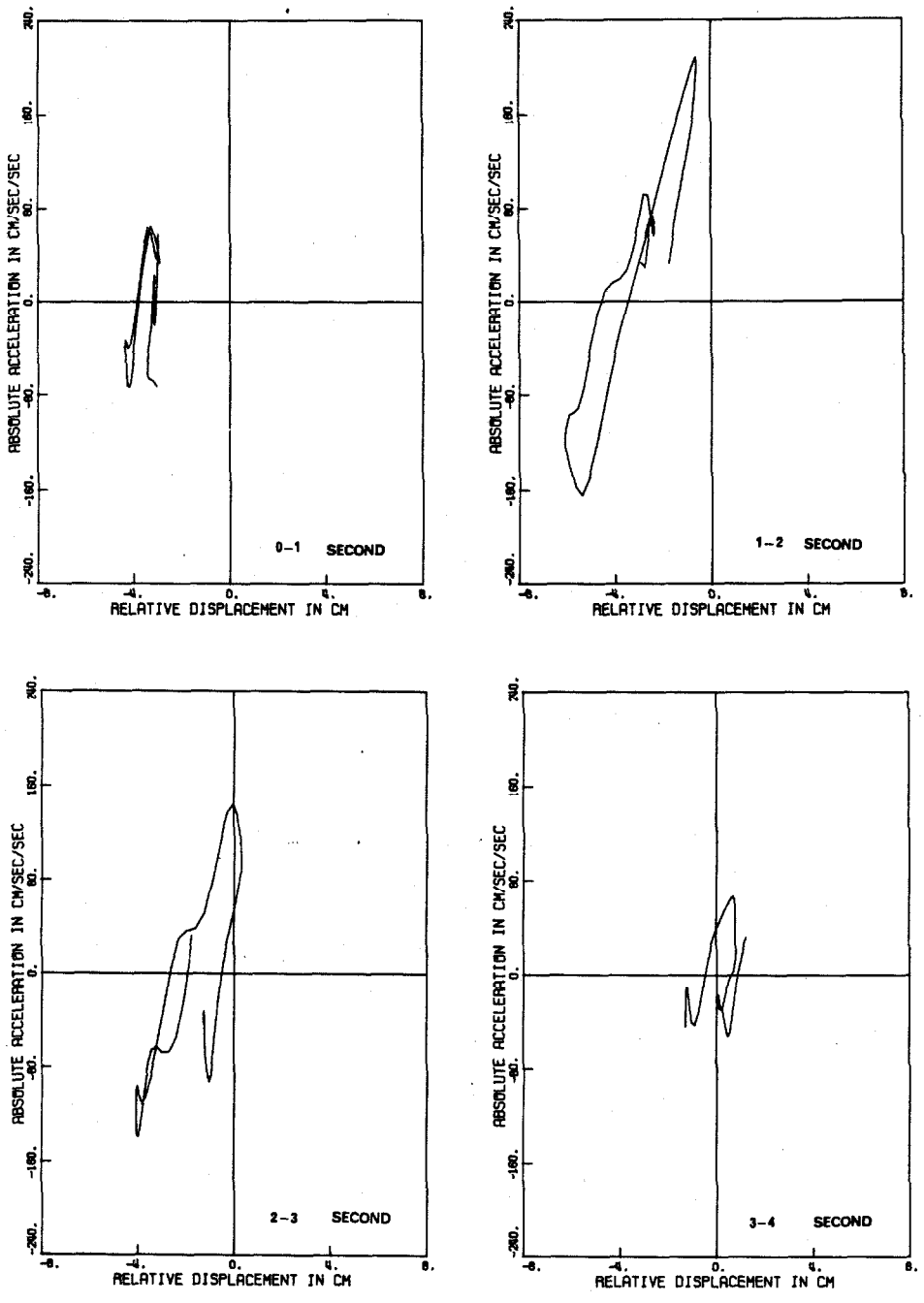

Fig. 44-a

SAN FERNANDO EARTHQUAKE FEB. 9, 1971
SANTA FELICIA DAM, CALIFORNIA,
COMPONENT ROTATED TO UPSTREAM/DOWNSTREAM DIRECTION (S11.4E)
HYSTERETIC RESPONSE FILTERING TYPE A

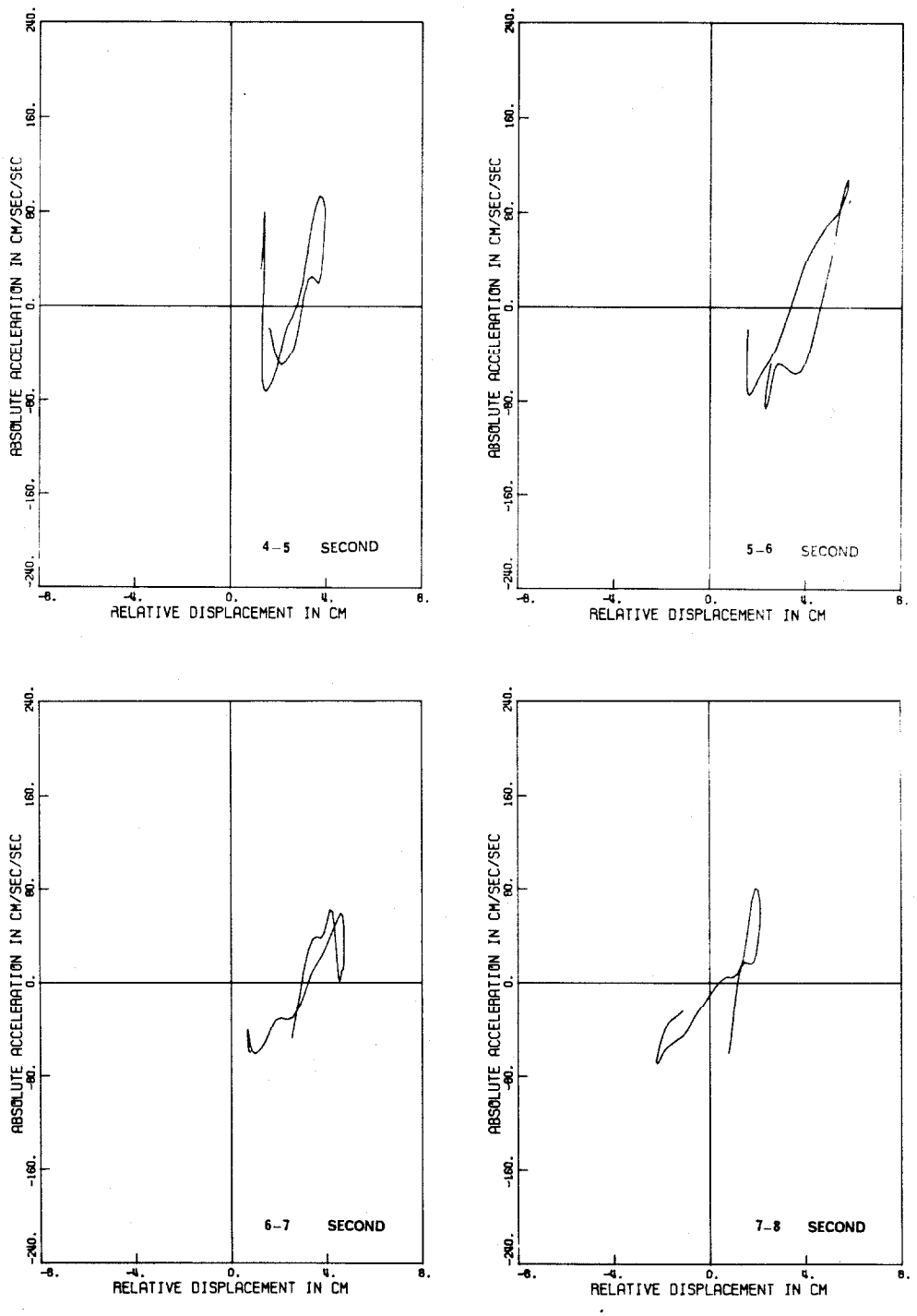

Fig. 44-b

· SANTA FELICIA DAM, CALIFORNIA.

COMPONENT ROTATED TO UPSTREAM/DOWNSTREAM DIRECTION (S11.4E)

HYSTERETIC RESPONSE FILTERING TYPE A

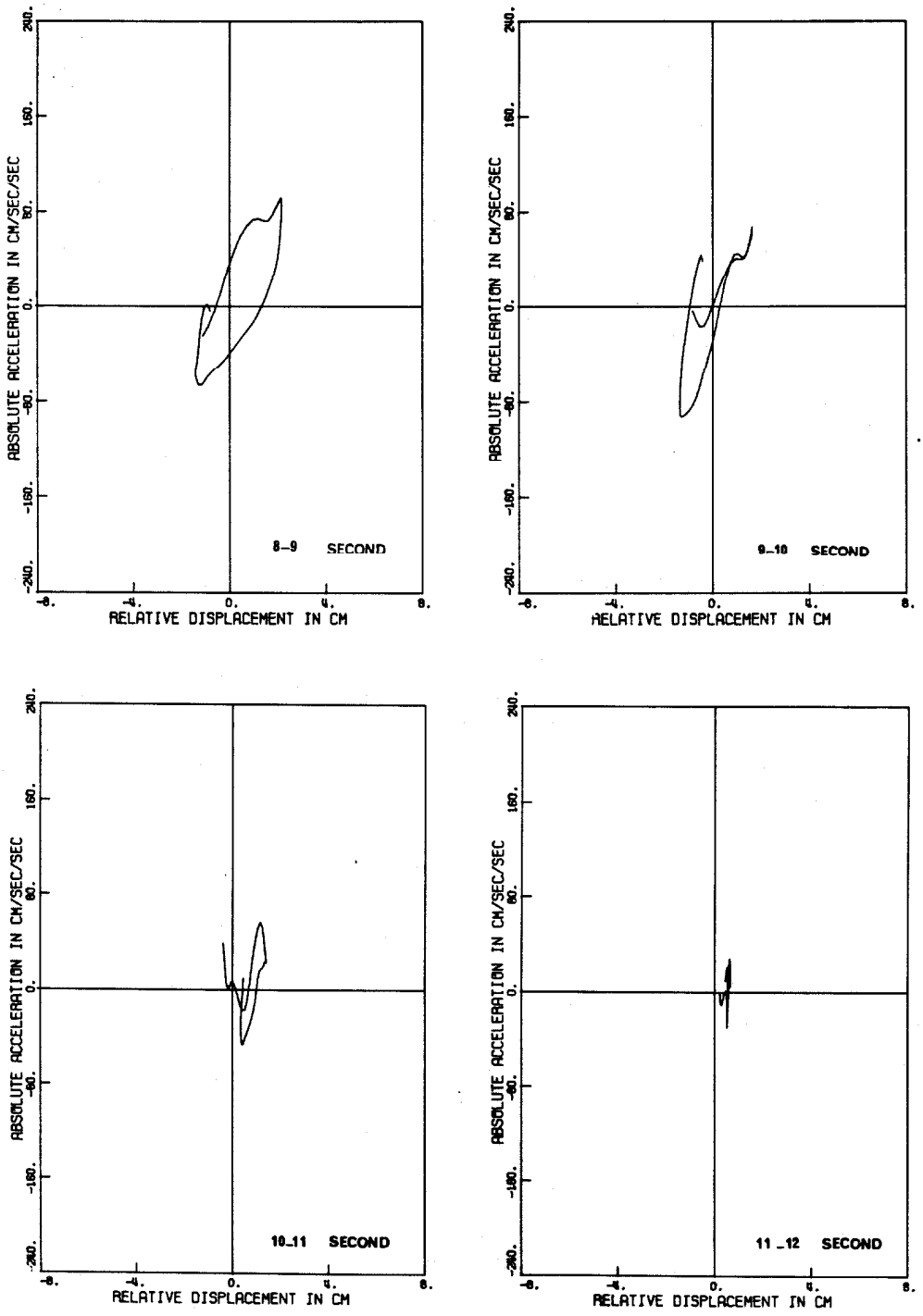

Fig. 44-c

SAN FERNANDO EARTHQUAKE FEB. 9, 1971

SANTA FELICIA DAM, CALIFORNIA.

COMPONENT ROTATED TO UPSTREAM/DOWNSTREAM DIRECTION (S11.4E)

HYSTERETIC RESPONSE FILTERING TYPE A

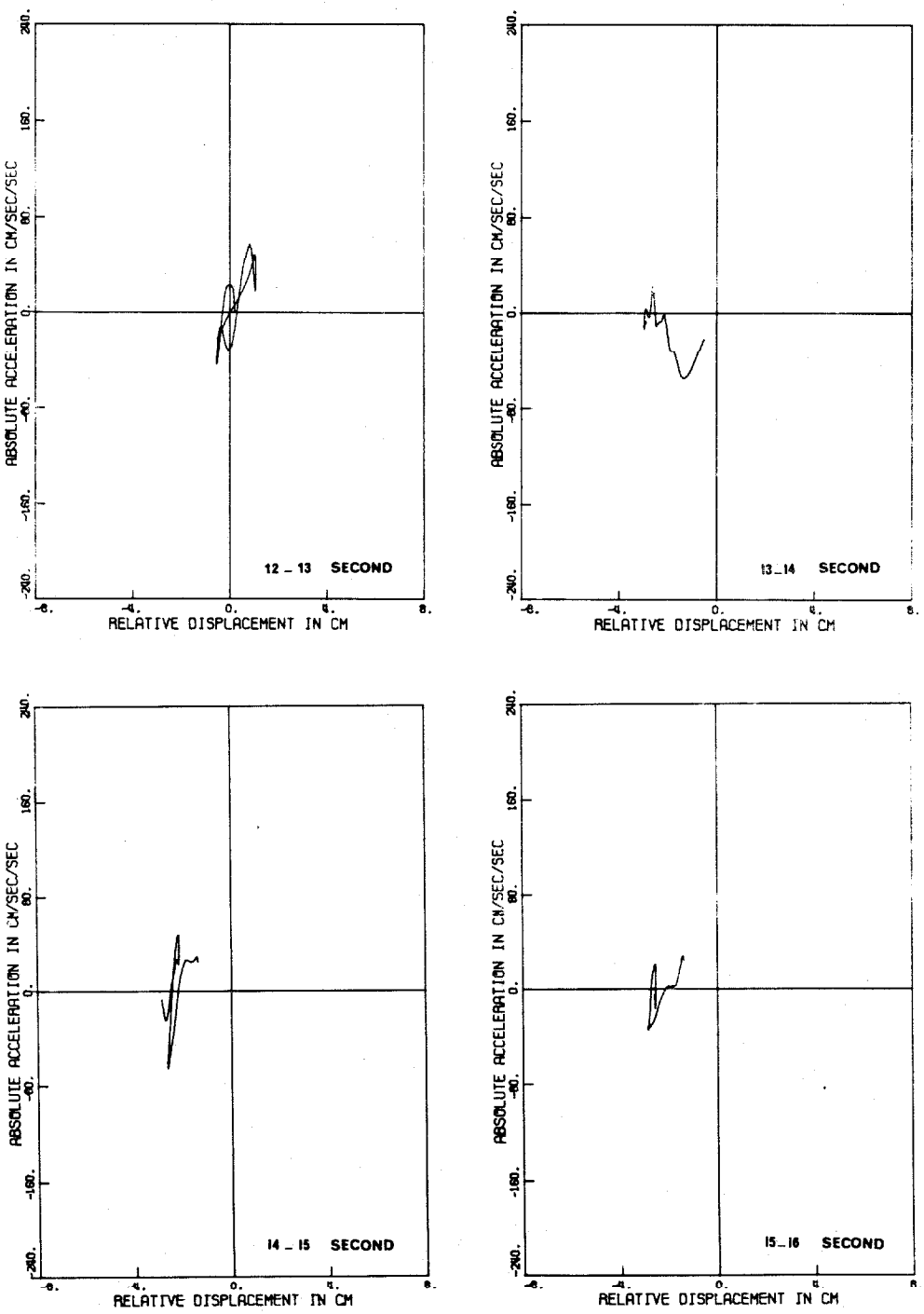

Fig. 44-d

SAN FERNANDO EARTHQUAKE FEB. 9, 1971
SANTA FELICIA DAM, CALIFORNIA.
COMPONENT ROTATED TO UPSTREAM/DOWNSTREAM DIRECTION (S11.4E)
HYSTERETIC RESPONSE FILTERING TYPE A

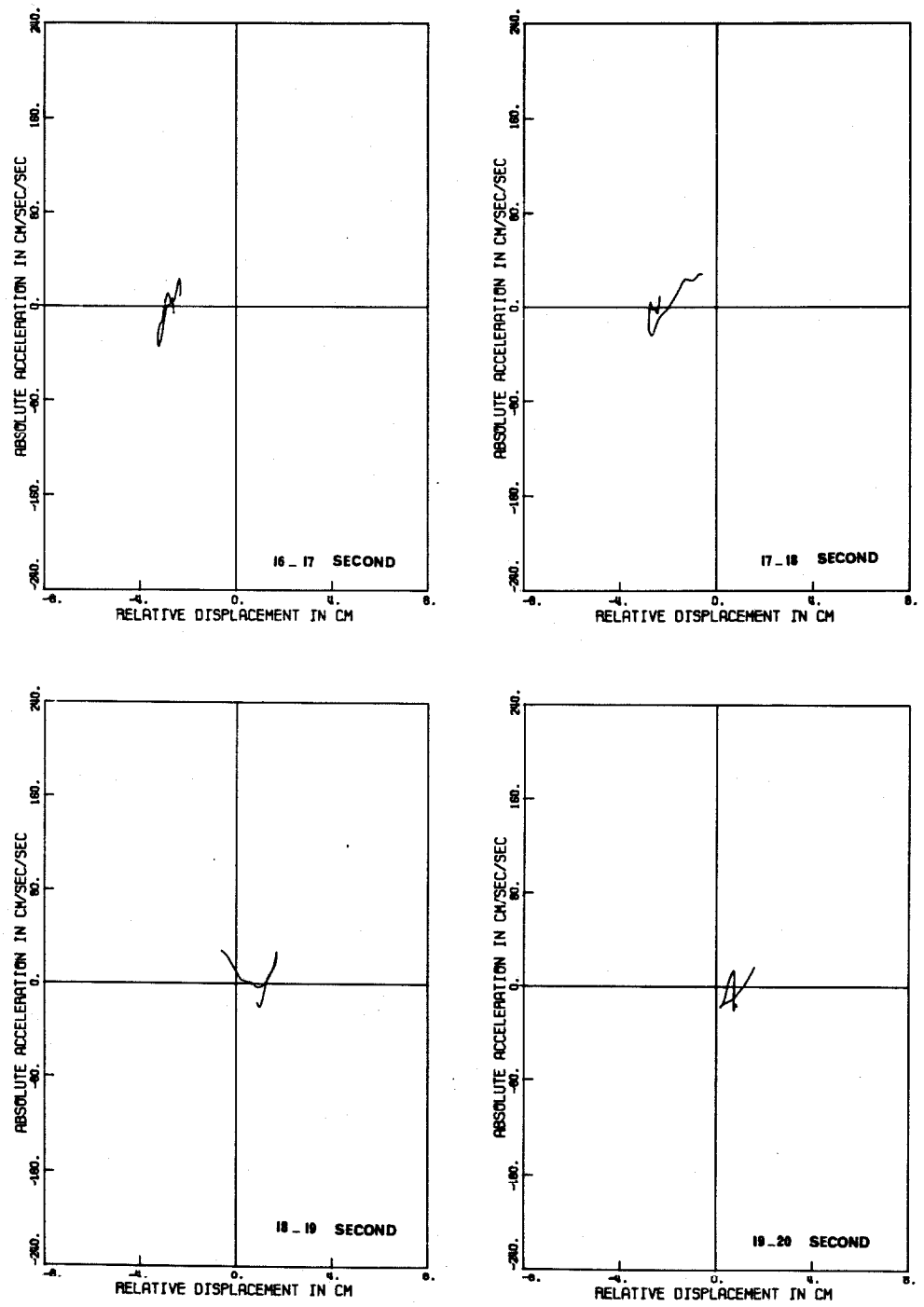

Fig. 44-e

the data was again band-pass filtered using an Ormsby filter with cut-off frequencies of 0.3 and 25 Hz and roll-off termination frequencies of 0.25 and 27 Hz, as shown in Fig. 40-b. By doing so, the long-period fluctuations (equal to or larger than 4 secs) were eliminated from the absolute acceleration record, and then the relative velocity and displacement were calculated. Figures 45 and 46 show the time history of the newly filtered data; this filtering is designated "type B" (Fig. 40-b). From comparison of these newly filtered curves with the absolute acceleration of the standard filtering type A shown in Fig. 9 and the relative velocity and displacement in Fig. 30, it can be seen that the long-period fluctuations have been greatly diminished, but not completely eliminated, especially in the region from about 10 secs to the end of the records. The first portion (6 to 20 secs) of the absolute acceleration (crest record of Fig. 45-a) still shows some contributions of the higher modes while the same portion of the calculated relative displacement (Fig. 46) still exhibits long-period fluctuations with period about 3 to 4 seconds.

The time-dependence of the hysteretic response of the dam, for filtering type B, is shown in Fig. 47. The hysteresis loops are noticeably smoother when compared to the earlier hysteretic response obtained by filtering type A (Fig. 44), but they are still very tangled, in particular in the figures of the period from 9 to 20 seconds (Figs. 47-c, d and e). Thus, the hysteresis diagrams again showed marked fluctuations along the trajectory of the supposed first-mode hysteresis loops because of the non-negligible contributions of the higher modes of vibration. These fluctuations make estimation of the

slope of each loop very difficult as well as estimation of the area inside the loop -- the two parameters necessary to estimate the equivalent shear modulus and the equivalent viscous damping.

Finally, very narrow band-pass filtering was used in the expectation of obtaining good hysteresis loops. Because of the assumption of a single-degree-of-freedom response, the effect of the second mode of vibration was eliminated as well as any higher modes that may have participated in the response. Thus, a narrow band-pass filtering around 1.45 Hz (the natural frequency of the dam in the upstream/downstream direction) was applied to the abutment and crest records in order to produce reasonable loops. This had cut-off frequencies at 1.27 and 1.50 Hz and roll-off termination frequencies of 1.25 and 1.60 Hz (Fig. 40-b). The filtered acceleration records and the calculated velocities and displacements are shown in Figs. 48 and 49, which can be compared with the accelerations, velocities and displacements resulting from both filtering type A and type B of Figs. 9, 10, 30, 45 and 46. From this comparison, it is apparent that the response of the higher modes and the long-period fluctuations ($\geq$ 4 seconds) have been eliminated.

Using the results shown in Figs. 48-a and 49, the relationship between the first mode's absolute acceleration, which is proportional to the nonlinear restoring force (Eq. 3), and the relative displacement was plotted every 0.02 secs and is given in Fig. 50.

It was particularly unfortunate that the first 3 to 3.5 secs of the abutment record were lost due to double exposure because this part of the record would have provided very useful information on the small amplitude motion of the dam at the beginning of the earthquake.

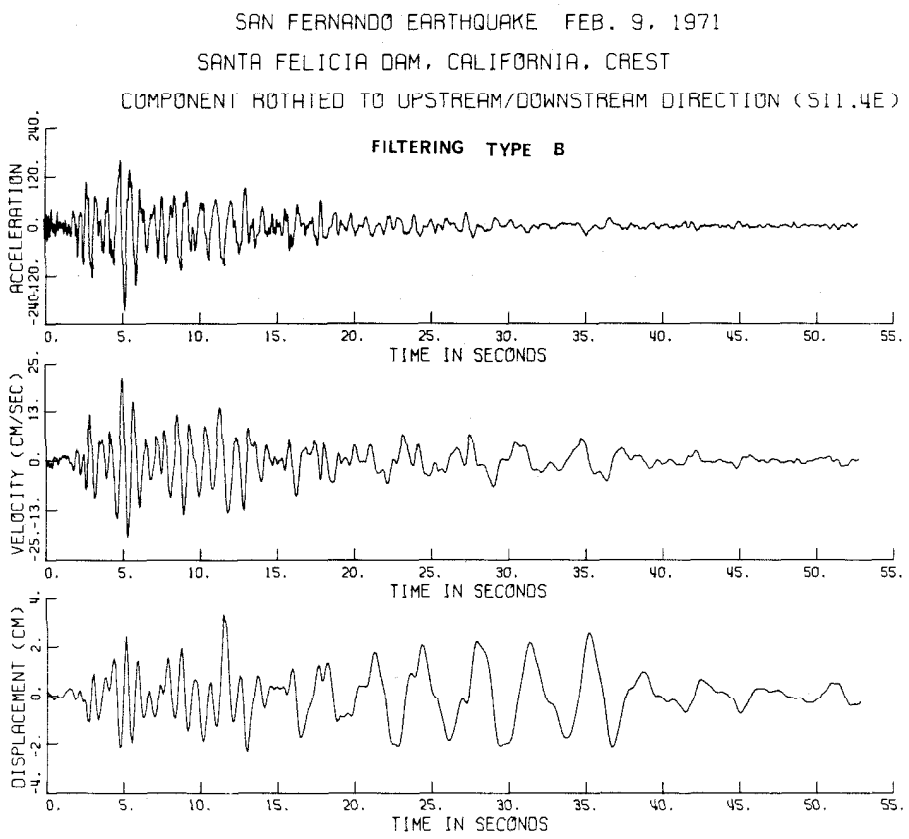
SAN FERNANDO EARTHQUAKE FEB. 9, 1971
SANTA FELICIA DAM, CALIFORNIA, CREST
COMPONENT ROTATED TO UPSTREAM/DOWNSTREAM DIRECTION (S11.4E)
FILTERING TYPE B
ACCELERATION
VELOCITY (CM/SEC)
DISPLACEMENT (CM)
TIME IN SECONDS

(a)

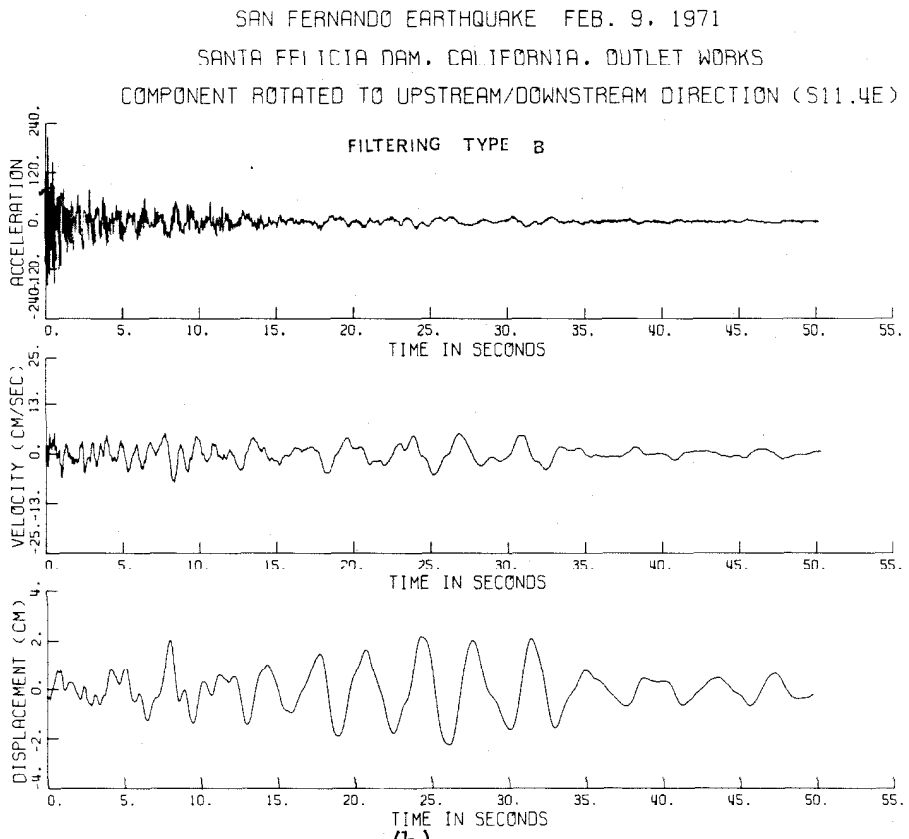
SAN FERNANDO EARTHQUAKE FEB. 9, 1971
SANTA FELICIA DAM, CALIFORNIA, OUTLET WORKS
COMPONENT ROTATED TO UPSTREAM/DOWNSTREAM DIRECTION (S11.4E)
FILTERING TYPE B
ACCELERATION
VELOCITY (CM/SEC)
DISPLACEMENT (CM)
TIME IN SECONDS

(b)

Fig. 45

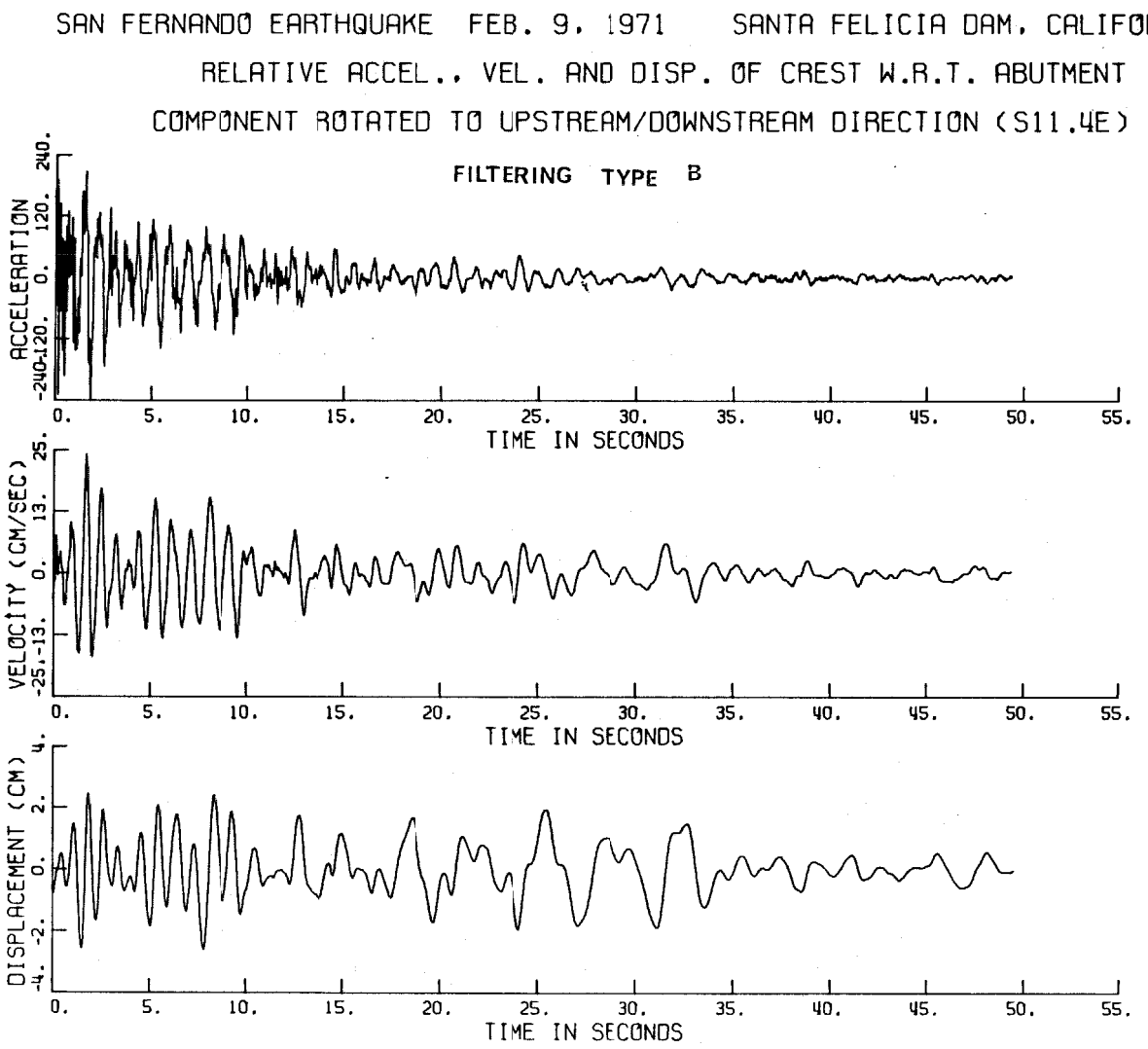
SAN FERNANDO EARTHQUAKE FEB. 9, 1971 SANTA FELICIA DAM, CALIFORNIA
RELATIVE ACCEL., VEL. AND DISP. OF CREST W.R.T. ABUTMENT
COMPONENT ROTATED TO UPSTREAM/DOWNSTREAM DIRECTION (S11.4E)
FILTERING TYPE B
ACCELERATION
-240. -120. 0. 120. 240.
VELOCITY (CM/SEC)
-25. -13. 0. 13. 25.
DISPLACEMENT (CM)
-4. -2. 0. 2. 4.
0. 5. 10. 15. 20. 25. 30. 35. 40. 45. 50. 55.
TIME IN SECONDS

Fig. 46

SAN FERNANDO EARTHQUAKE FEB. 9, 1971
SANTA FELICIA DAM, CALIFORNIA.
COMPONENT ROTATED TO UPSTREAM/DOWNSTREAM DIRECTION (S11.4E)
HYSTERETIC RESPONSE FILTERING TYPE B

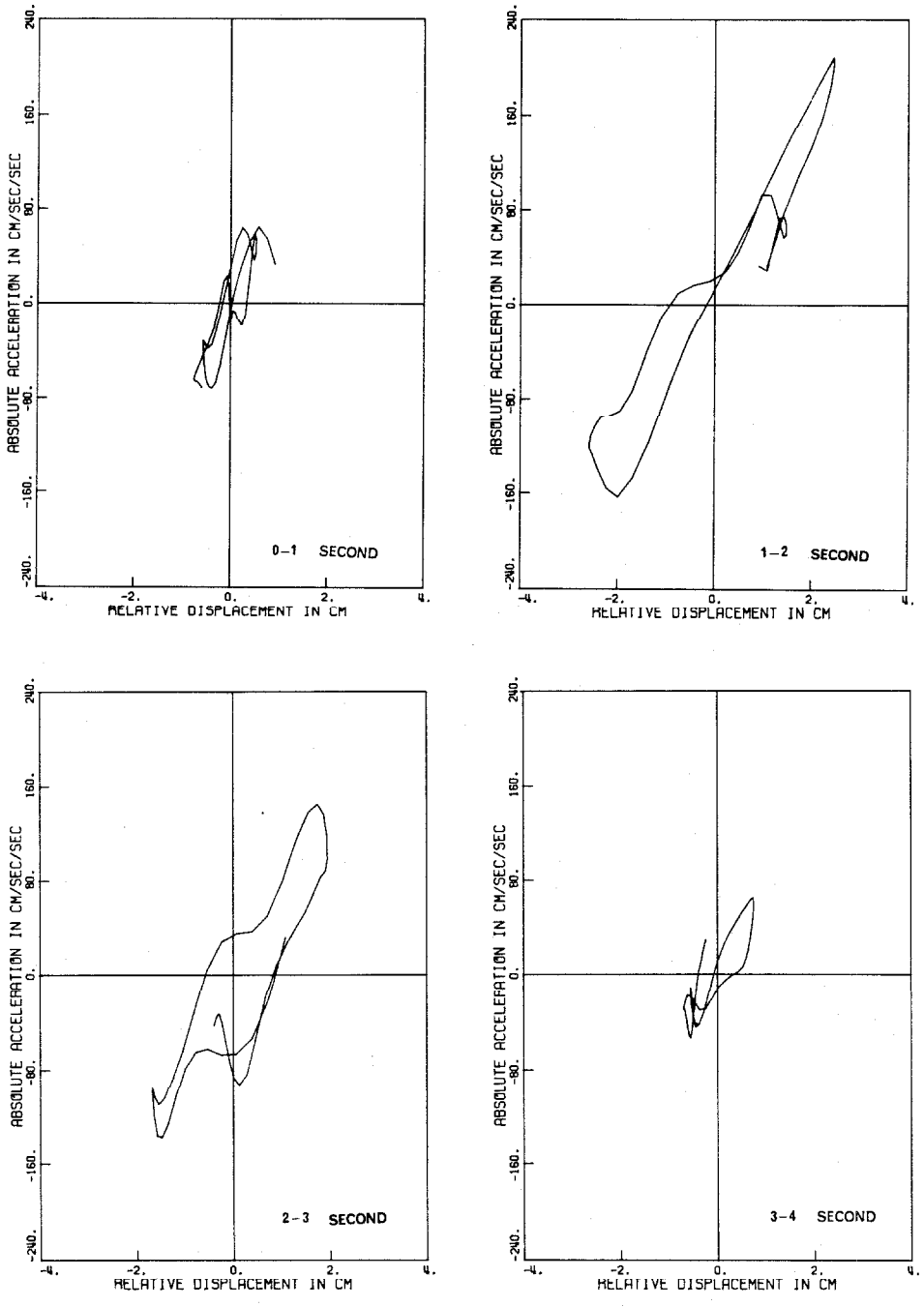

Fig. 47-a

SAN FERNANDO EARTHQUAKE FEB. 9. 1971
SANTA FELICIA DAM. CALIFORNIA.
COMPONENT ROTATED TO UPSTREAM/DOWNSTREAM DIRECTION (S11.4E)
HYSTERETIC RESPONSE FILTERING TYPE B

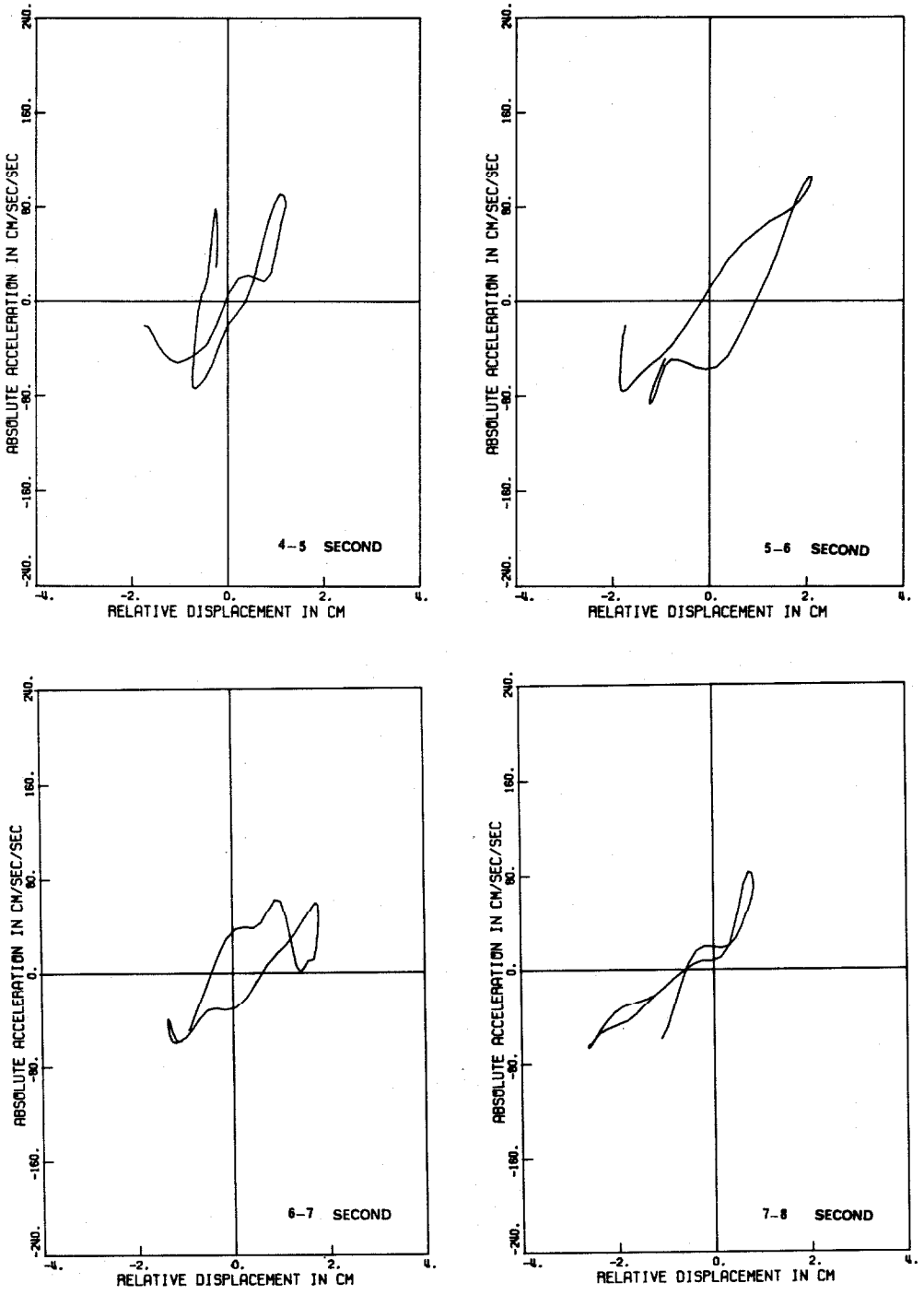

Fig. 47-b

SAN FERNANDO EARTHQUAKE FEB. 9, 1971
SANTA FELICIA DAM, CALIFORNIA.
COMPONENT ROTATED TO UPSTREAM/DOWNSTREAM DIRECTION (S11.4E)

HYSTERETIC RESPONSE **FILTERING TYPE B**

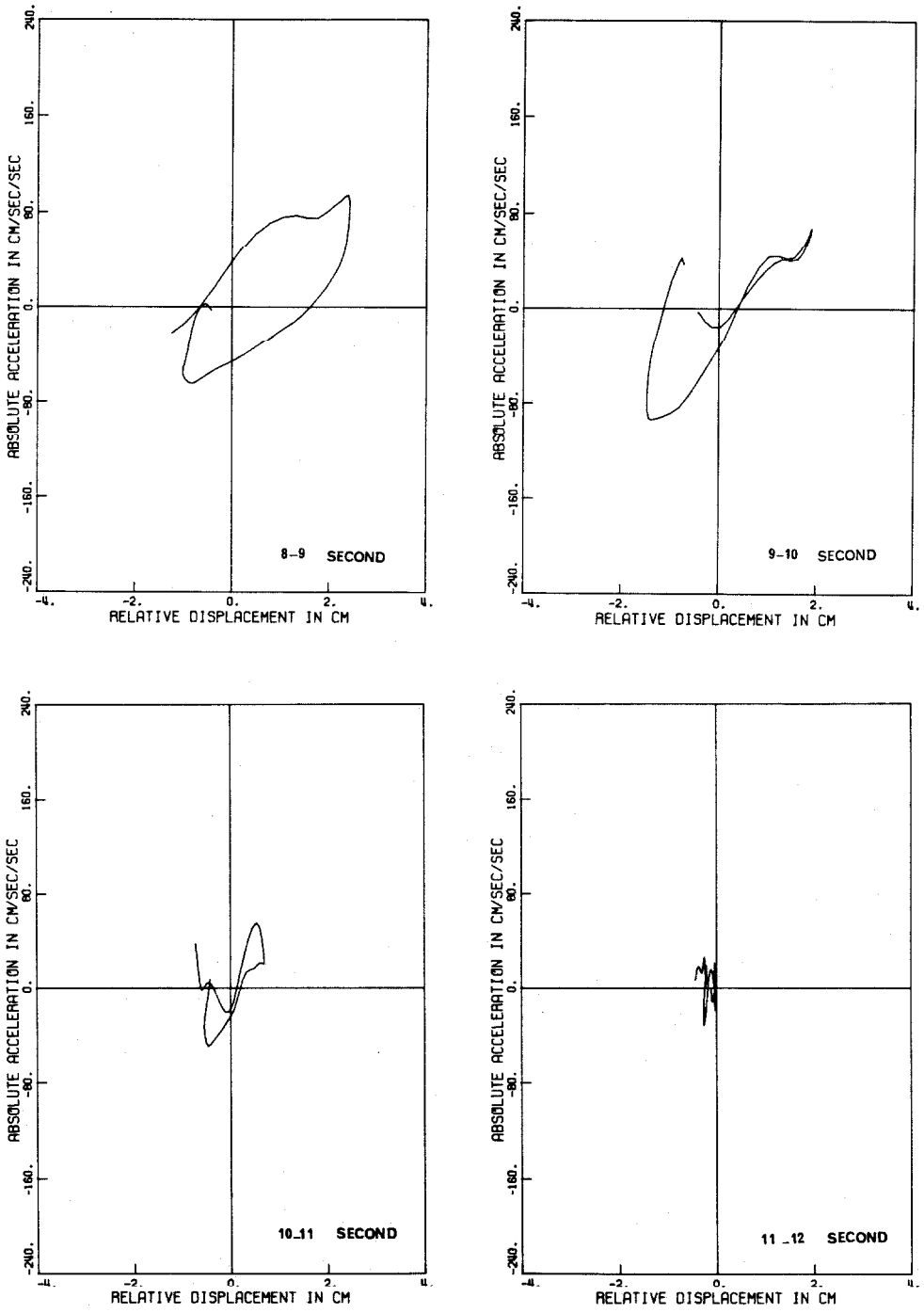

Fig. 47-c

SAN FERNANDO EARTHQUAKE FEB. 9, 1971
SANTA FELICIA DAM, CALIFORNIA.
COMPONENT ROTATED TO UPSTREAM/DOWNSTREAM DIRECTION (S11.4E)

HYSTERETIC RESPONSE **FILTERING TYPE B**

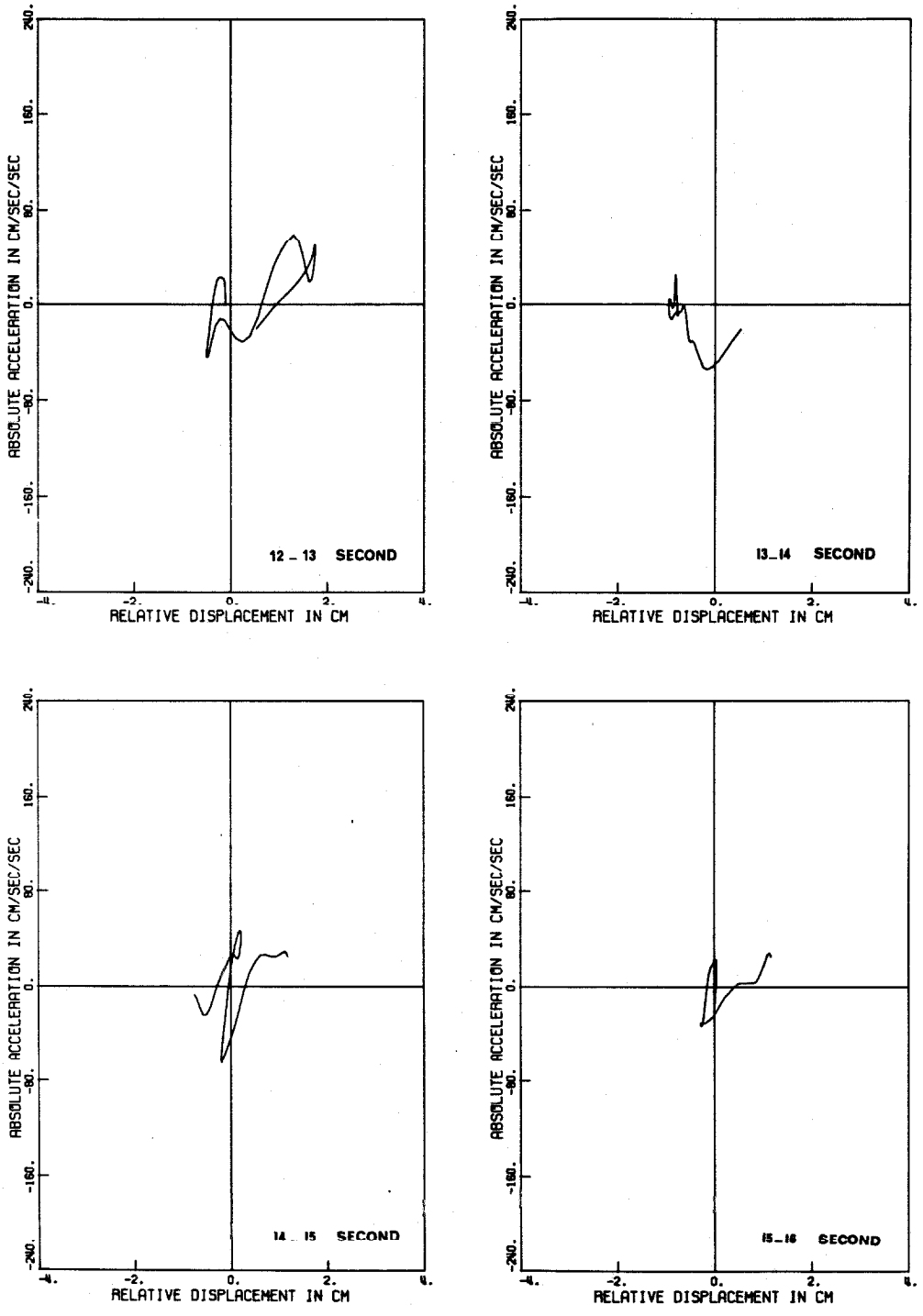

Fig. 47-d

SAN FERNANDO EARTHQUAKE FEB. 9, 1971
SANTA FELICIA DAM. CALIFORNIA.
COMPONENT ROTATED TO UPSTREAM/DOWNSTREAM DIRECTION (S11.4E)
HYSTERETIC RESPONSE FILTERING TYPE B

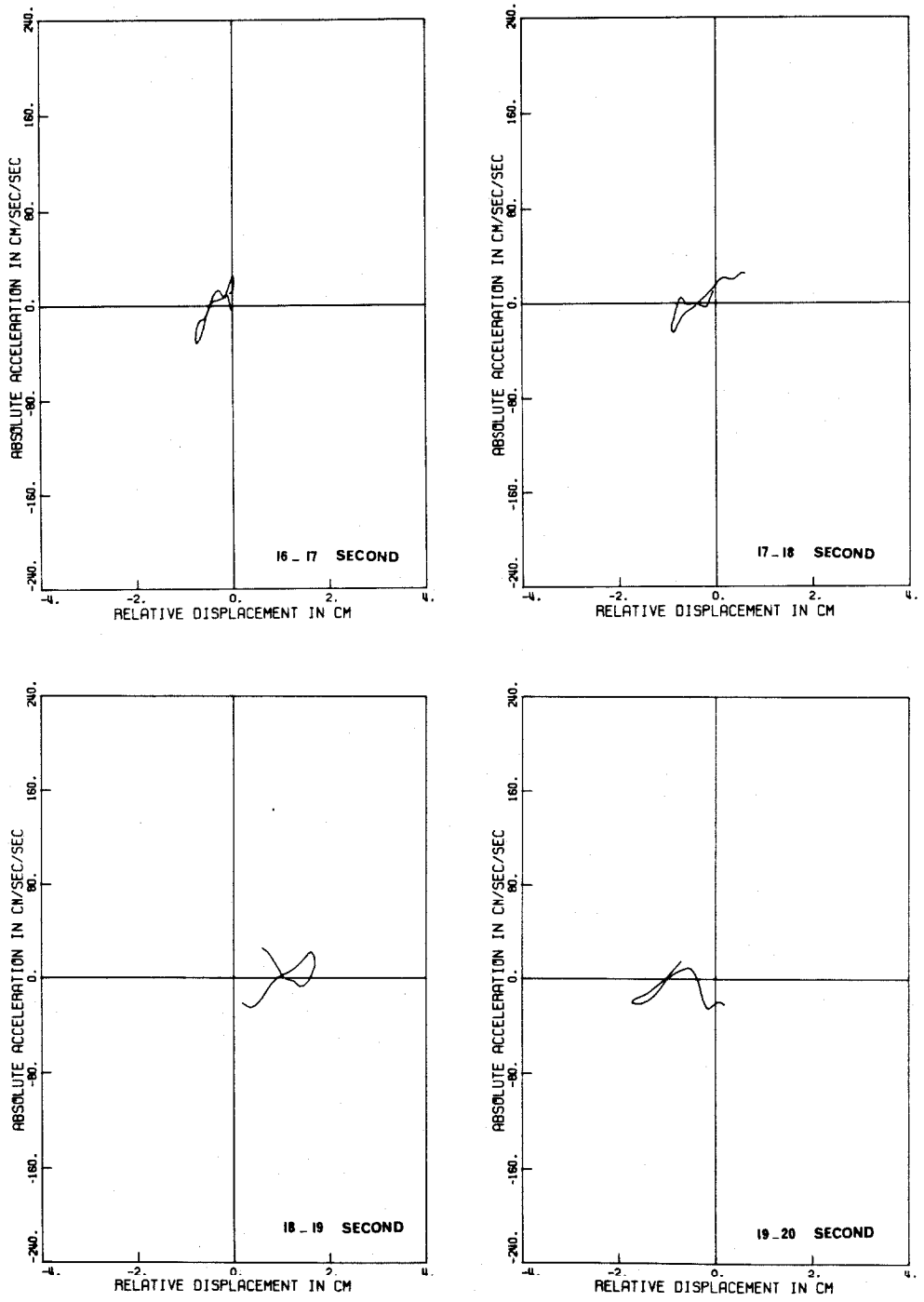

Fig. 47-e

From the calculated relative displacement curve (Fig. 49) for filtering type C, it can be seen that the level of vibration during the first 20 seconds can be divided into four regions. The first region, from about 0 to 6 secs, has relatively high amplitudes. The second and third regions include the parts from about 6 to 10 secs, and from 16 to 20 secs, respectively, and both contain relatively small amplitudes. Finally, the fourth region is from about 10 to 16 secs with intermediate amplitudes.

The plots of Figs. 50-a and b which are all to the same scales show high amplitude hysteresis loops due to the high response levels. At the beginning of the corrected response, from 0 to 6 secs (which does not include the first 3 to 3.5 secs of the crest record), the slopes of the hysteresis loops of the dam are quite clear; however, the areas of the first three loops (from 0 to 3 secs) are not easy to estimate. The first four loops have essentially the same slope while the next two loops (from 4 to 6 secs), which have smaller amplitudes, have larger slopes. Also, the areas of the fourth, fifth and sixth loops are larger than those of the first two loops. The slopes of the hysteresis loops are steep from 5 to 10 secs (as shown in Figs. 50-b and c) as compared to those from 0 to 5 secs (Figs. 50-a and b). Generally, from 6 to 10 secs the hysteretic properties of the dam are not clear because of the small amplitudes in this part and because of the high-frequency contribution in the absolute acceleration of Fig. 48-a. From 10 to 16 secs the slopes of the smoother hysteresis loops (Fig. 50-c and d) decrease compared with those from 6 to 10 secs, and the areas of the loops are clearer and smaller. Figures 50-c, d and e show the response from 16 to 20 secs and

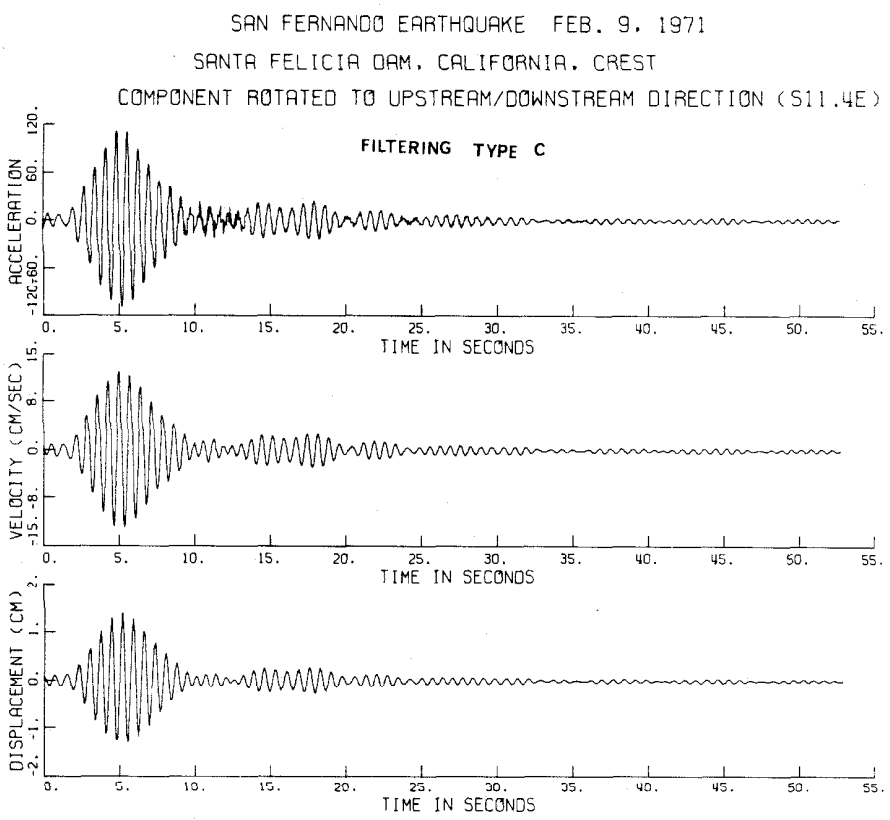
SAN FERNANDO EARTHQUAKE FEB. 9, 1971
SANTA FELICIA DAM, CALIFORNIA, CREST
COMPONENT ROTATED TO UPSTREAM/DOWNSTREAM DIRECTION (S11.4E)
FILTERING TYPE C
ACCELERATION
VELOCITY (CM/SEC)
DISPLACEMENT (CM)
TIME IN SECONDS

(a)

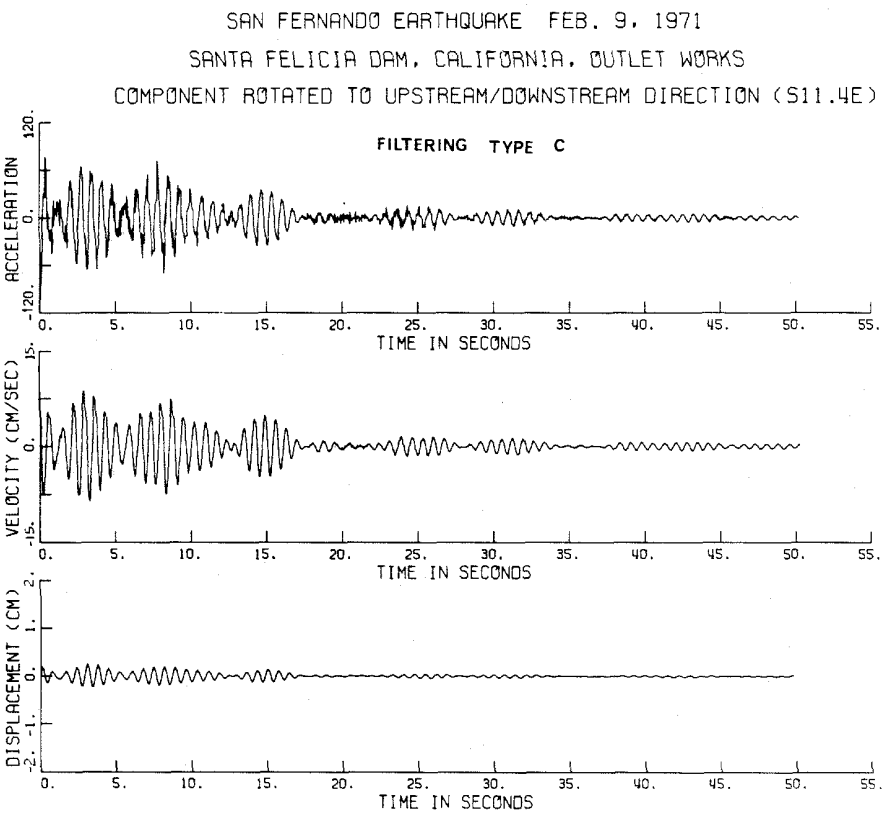
SAN FERNANDO EARTHQUAKE FEB. 9, 1971
SANTA FELICIA DAM, CALIFORNIA, OUTLET WORKS
COMPONENT ROTATED TO UPSTREAM/DOWNSTREAM DIRECTION (S11.4E)
FILTERING TYPE C
ACCELERATION
VELOCITY (CM/SEC)
DISPLACEMENT (CM)
TIME IN SECONDS

(b)

Fig. 48

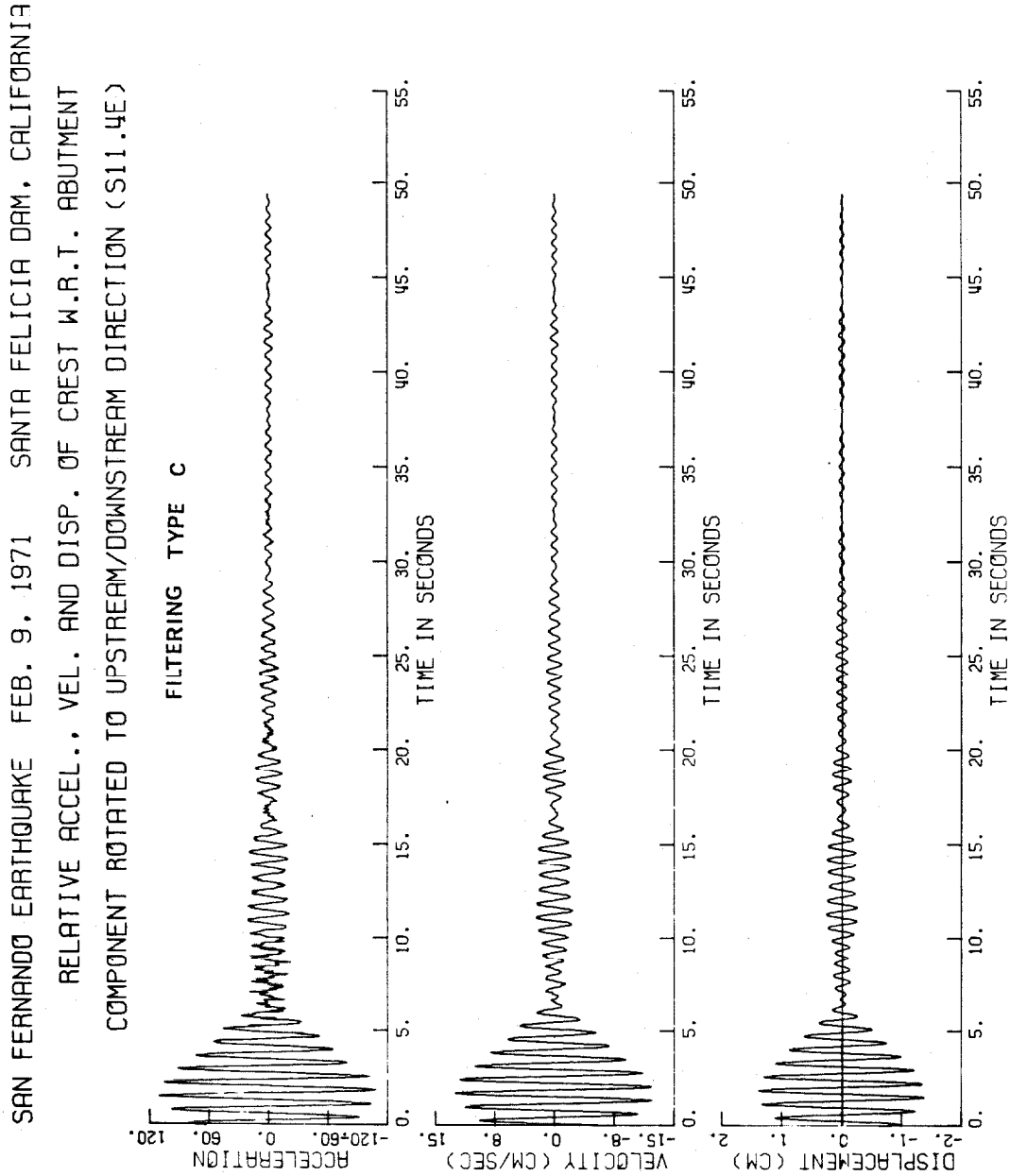
SAN FERNANDO EARTHQUAKE FEB. 9, 1971 SANTA FELICIA DAM, CALIFORNIA
RELATIVE ACCEL., VEL. AND DISP. OF CREST W.R.T. ABUTMENT
COMPONENT ROTATED TO UPSTREAM/DOWNSTREAM DIRECTION (S11.4E)
FILTERING TYPE C
ACCELERATION
VELOCITY (CM/SEC)
DISPLACEMENT (CM)
TIME IN SECONDS

Fig. 49

demonstrate that there are sudden changes in the restoring force due to the small response level; the slopes are relatively steeper than those from 10 to 16 secs. In addition, the areas of the hysteresis loops during the period from 16 to 20 secs have clearly become smaller than those for 10 to 16 secs or 6 to 10 secs. In addition, this portion of the response (from 16 to 20 secs) shows that the dam continued to exhibit a stiffer restoring force the smaller the response levels became, with a relatively smaller energy dissipation capacity, than during the earlier small response level from 6 to 10 secs. However, if the small response levels of the dam at the beginning of the earthquake are taken into consideration, then there is a possibility that the high amplitude response (from 0 to 6 secs) caused degradation of the stiffness of the dam. Then, the low level response from 6 to 10 secs increased the stiffness of the dam again, and this was followed by a reduction of the stiffness caused by the moderate amplitudes between 10 and 16 secs. Finally, the remaining portion of small amplitudes from 16 to 20 secs again caused the stiffness to increase considerably. It is readily apparent that the slope of the hysteresis loop and the area inside the loop are dependent on the magnitude of the response level for which the hysteresis loop is determined; i.e., both shear moduli and damping factors must be determined as functions of the induced strain in the dam.

Close examination of all the hysteresis loops reveals some short-period fluctuations along the supposed first-mode hysteresis loops which are thought to be the result of small errors in the calculation. Other possibilities include an incorrect time difference between the crest and abutment records or a small error in phase that might

have been introduced because of the application of the digital filter subroutine to the records.

Finally, the accelerations recorded at the abutment and crest of Santa Felicia Dam in the upstream/downstream direction during the small earthquake of April 8, 1976 were narrow band-pass filtered (filtering type C), and the velocities and displacements were calculated. Figures 51 and 52 show the filtered and calculated motions as well as the relative motion of the crest with respect to the abutment. The first-mode hysteretic response of the dam during the first 6 seconds of the crest record is shown in Fig. 53. The scales of Fig. 53 are all the same but are different from those of Fig. 50. Close examination of the absolute filtered acceleration (the crest record in Fig. 51-a), shows that the acceleration record started with a relatively high peak; this initial peak caused distortion of the first hysteresis loop (from 0 to 1 sec) of Fig. 53-a. The appearance of this peak at the very beginning of the record is actually a result of the accuracy of the digital filter calculation, because by comparing Fig. 51-a with Fig. 13 which has the corrected crest acceleration (filtering type A or the standard Caltech filtering), it can be seen that the absolute acceleration started at zero and then peaked abruptly. Thus the digital filter used in the analyses could cause small errors in phase between the crest and abutment records, in addition to small errors in the calculation. Also, in the filtered absolute acceleration there is some high-frequency motion superimposed on the smoothed curve from 0 to 2 secs; this could also be due to errors resulting from the application of the digital filter. In general, the slopes of the hysteresis loops resulting from the 1976

SAN FERNANDO EARTHQUAKE FEB. 9, 1971
SANTA FELICIA DAM, CALIFORNIA,
COMPONENT ROTATED TO UPSTREAM/DOWNSTREAM DIRECTION (S11.4E)

HYSTERETIC RESPONSE **FILTERING TYPE C**

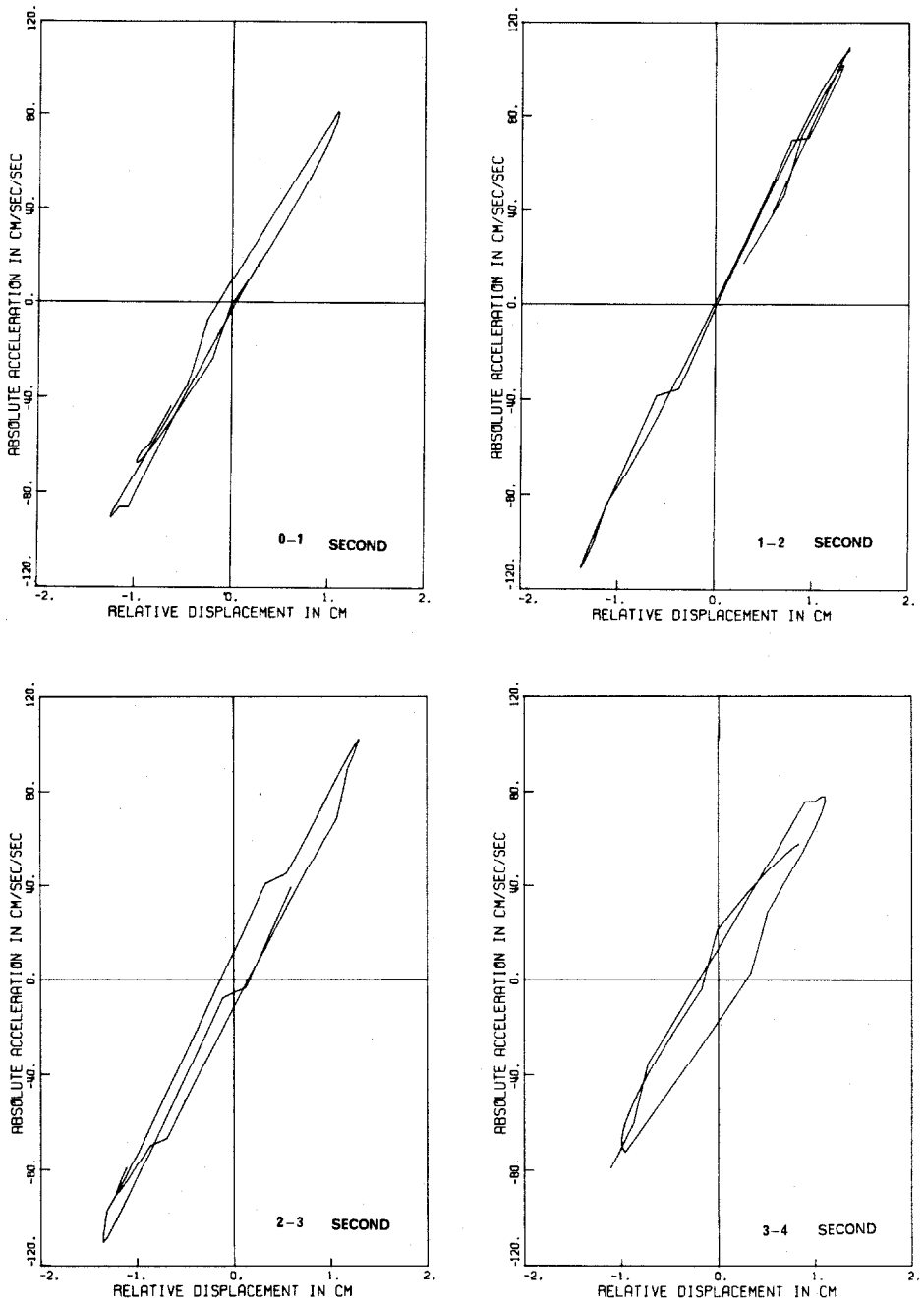

Fig. 50-a

SAN FERNANDO EARTHQUAKE FEB. 9, 1971
SANTA FELICIA DAM, CALIFORNIA,
COMPONENT ROTATED TO UPSTREAM/DOWNSTREAM DIRECTION (S11.4E)
HYSTERETIC RESPONSE FILTERING TYPE C

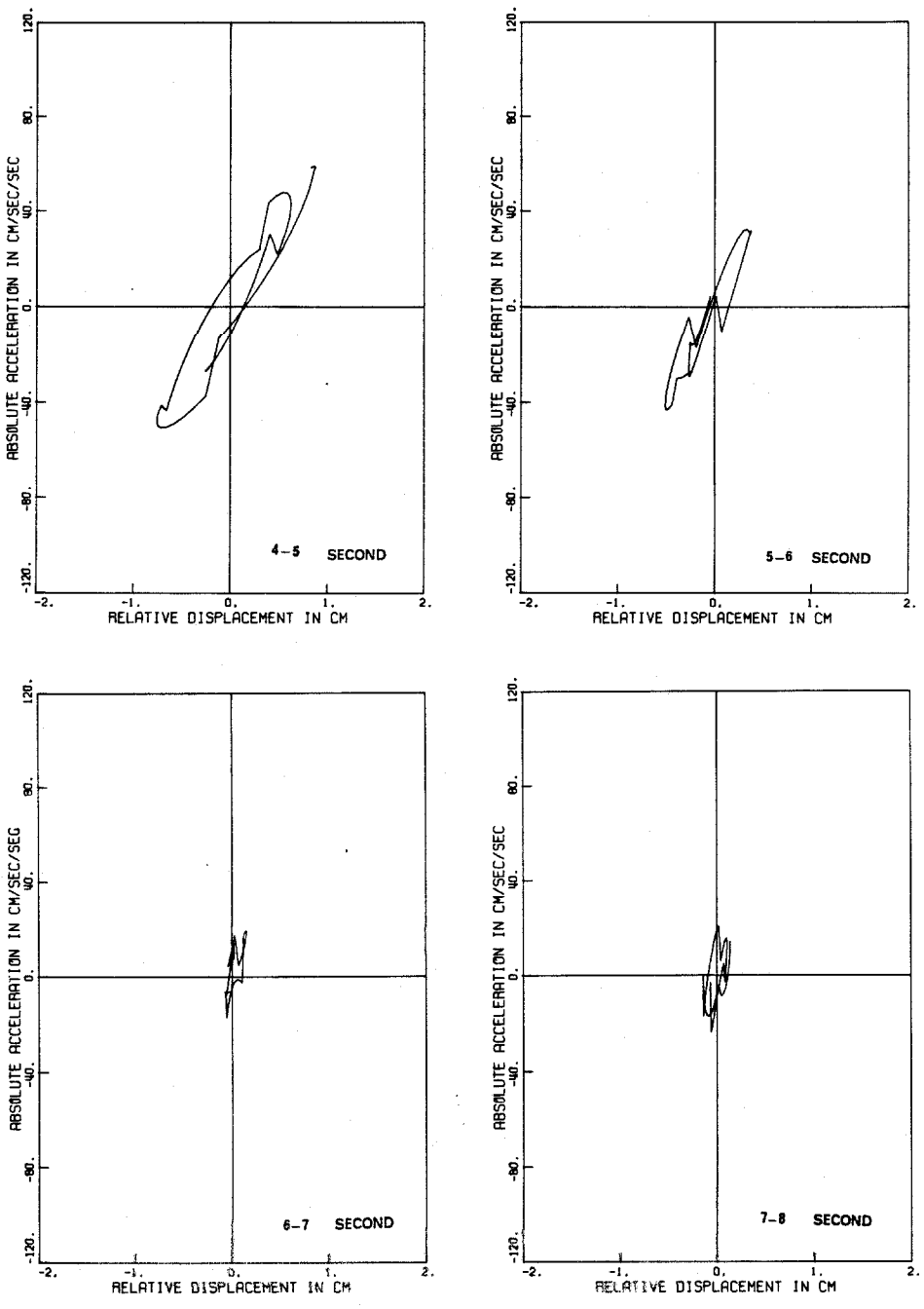

Fig. 50-b

SAN FERNANDO EARTHQUAKE FEB. 9, 1971
SANTA FELICIA DAM, CALIFORNIA.
COMPONENT ROTATED TO UPSTREAM/DOWNSTREAM DIRECTION (S11.4E)
HYSTERETIC RESPONSE FILTERING TYPE C

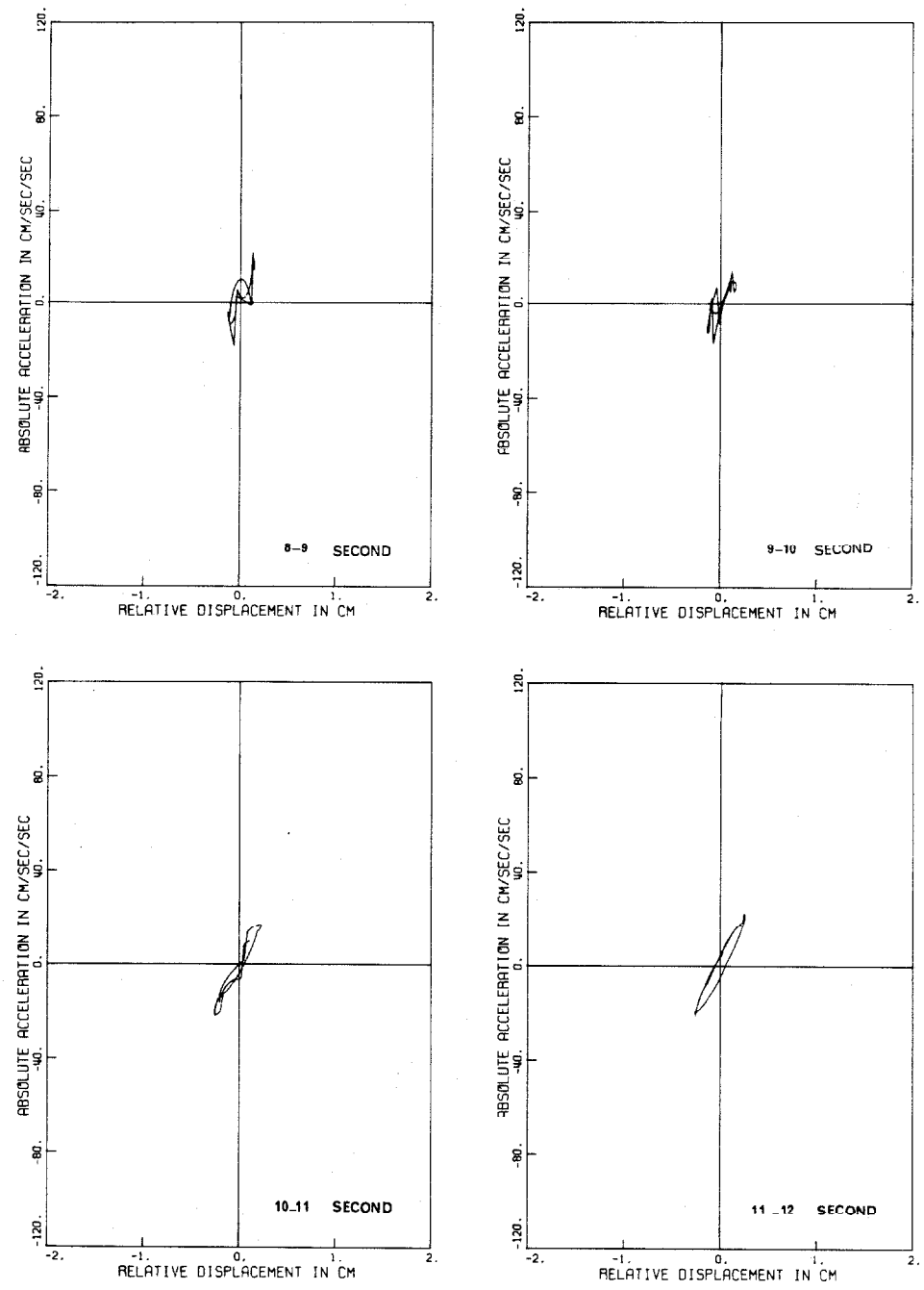

Fig. 50-c

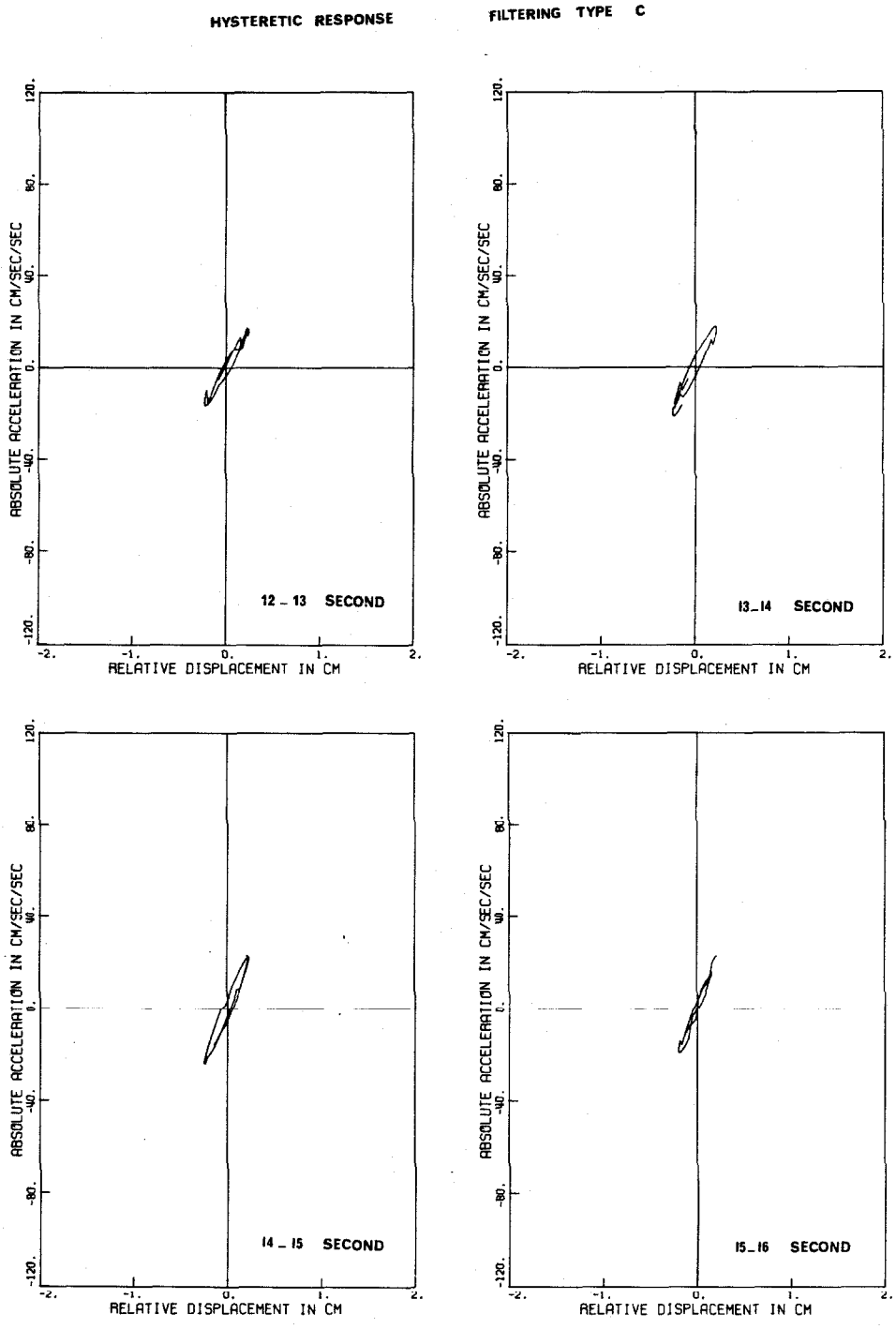
SAN FERNANDO EARTHQUAKE FEB. 9, 1971
SANTA FELICIA DAM, CALIFORNIA.
COMPONENT ROTATED TO UPSTREAM/DOWNSTREAM DIRECTION (S11.4E)
HYSTERETIC RESPONSE
FILTERING TYPE C
ABSOLUTE ACCELERATION IN CM/SEC/SEC
RELATIVE DISPLACEMENT IN CM
12 - 13 SECOND
13-14 SECOND
14 - 15 SECOND
15-16 SECOND

Fig. 50-d

SAN FERNANDO EARTHQUAKE FEB. 9, 1971
SANTA FELICIA DAM, CALIFORNIA.
COMPONENT ROTATED TO UPSTREAM/DOWNSTREAM DIRECTION (S11.4E)
HYSTERETIC RESPONSE FILTERING TYPE C

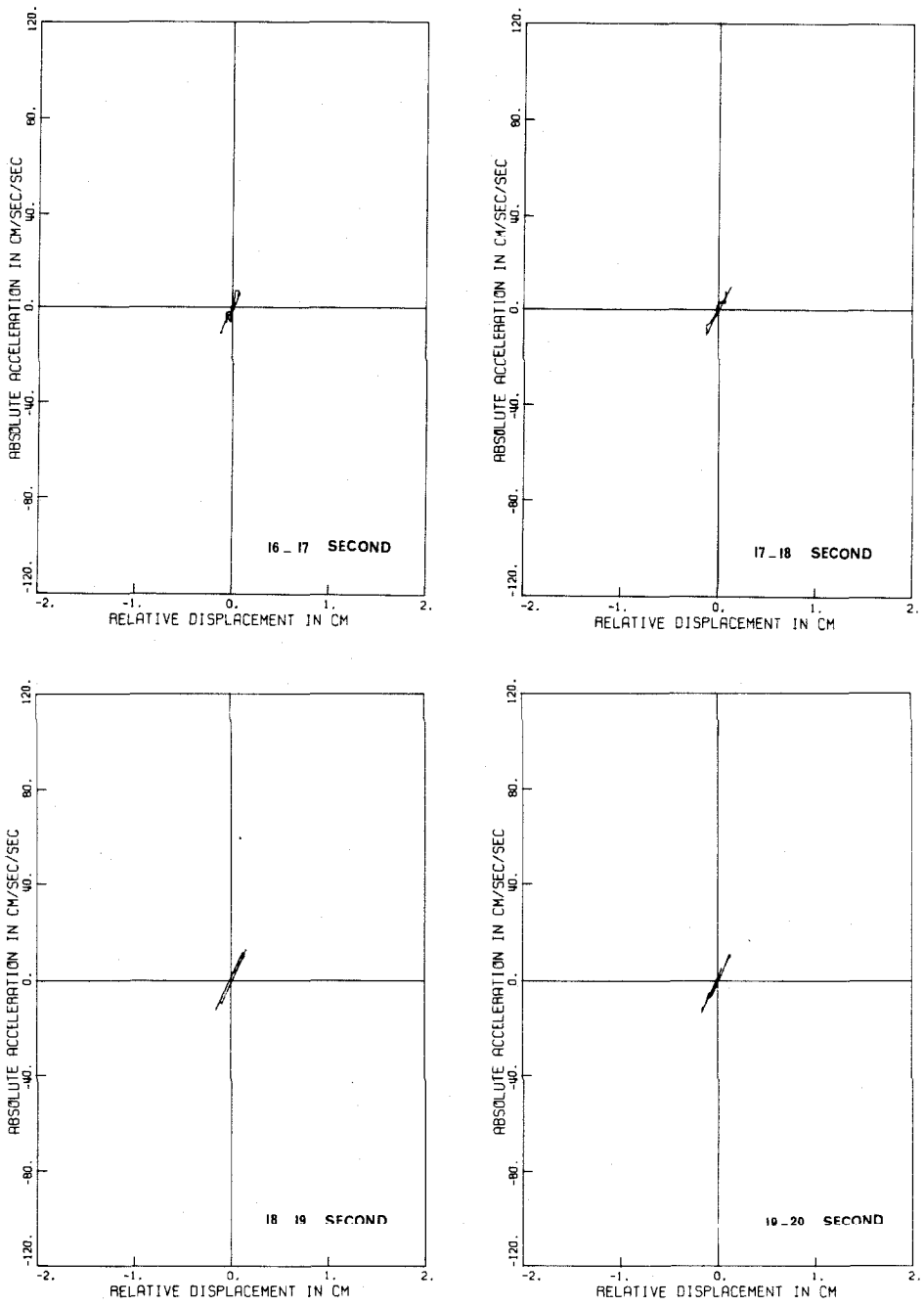

Fig. 50-e

earthquake are steeper than those resulting from the small amplitude motion of the 1971 earthquake; for instance, the slopes resulting from the first four loops (from 0 to 4 secs) in Fig. 53-a are 130, 105, 140 and 135/sec^2 compared with the slopes resulting from the last four loops (from 16 to 20 secs) in Fig. 50-e which have the values 80, 68, 63 and 69/sec^2. In addition, for the 1976 earthquake, the loops with relatively small amplitude have steeper slopes than those with relatively high amplitude; for example the two loops from 2 to 3 secs and from 3 to 4 secs (small amplitudes) are steeper than the loop from 1 to 2 secs (relatively large amplitude).

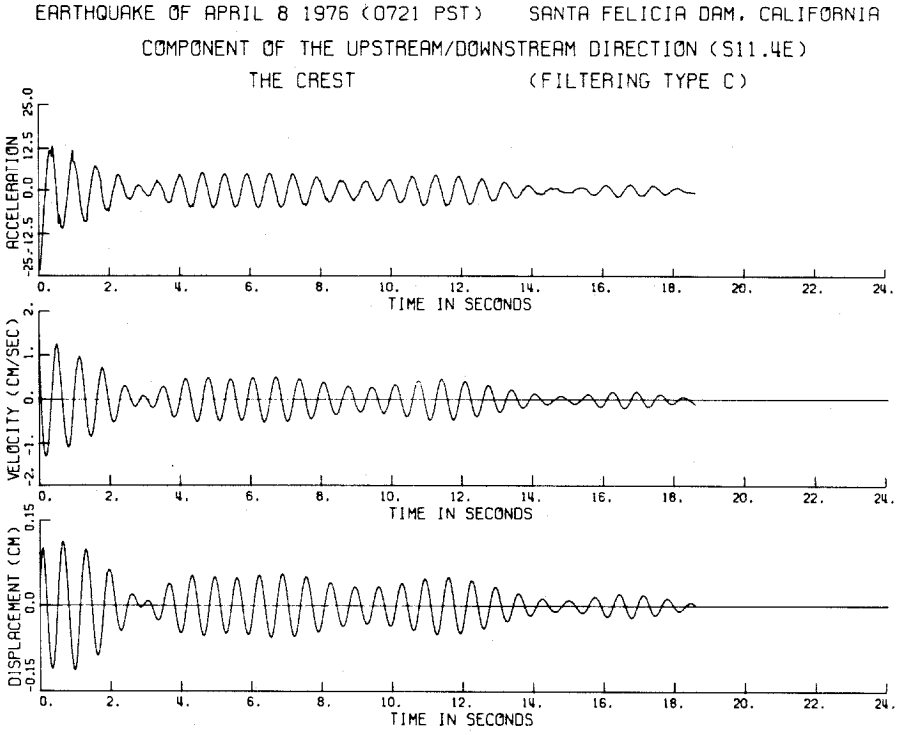
EARTHQUAKE OF APRIL 8 1976 (0721 PST) SANTA FELICIA DAM, CALIFORNIA
COMPONENT OF THE UPSTREAM/DOWNSTREAM DIRECTION (S11.4E)
THE CREST (FILTERING TYPE C)
ACCELERATION
VELOCITY (CM/SEC)
DISPLACEMENT (CM)
TIME IN SECONDS

(a)

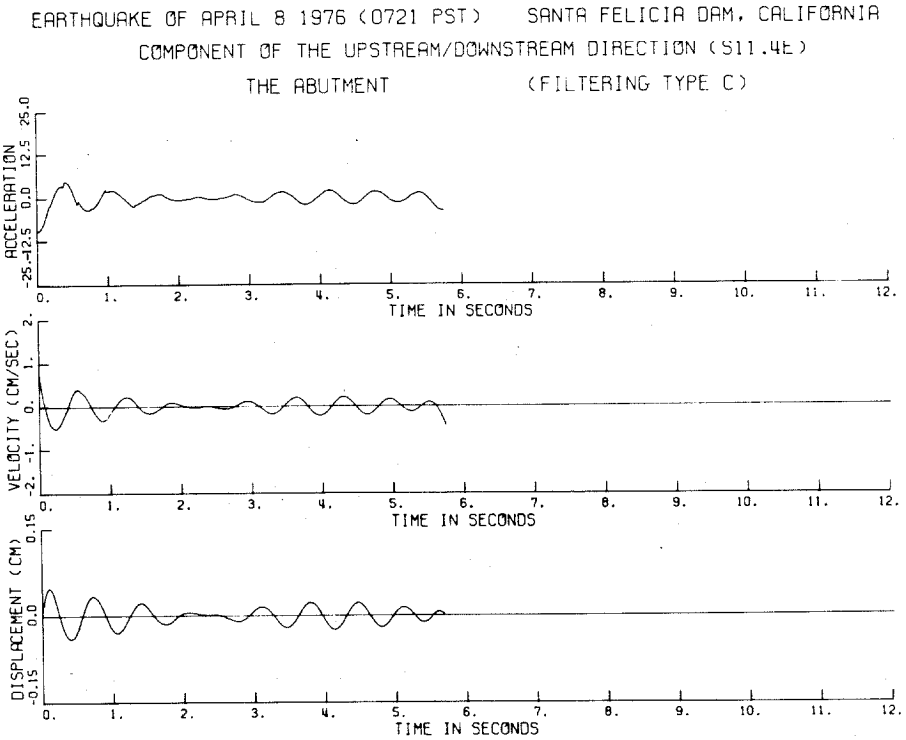
EARTHQUAKE OF APRIL 8 1976 (0721 PST) SANTA FELICIA DAM, CALIFORNIA
COMPONENT OF THE UPSTREAM/DOWNSTREAM DIRECTION (S11.4E)
THE ABUTMENT (FILTERING TYPE C)
ACCELERATION
VELOCITY (CM/SEC)
DISPLACEMENT (CM)
TIME IN SECONDS

(b)

Fig. 51

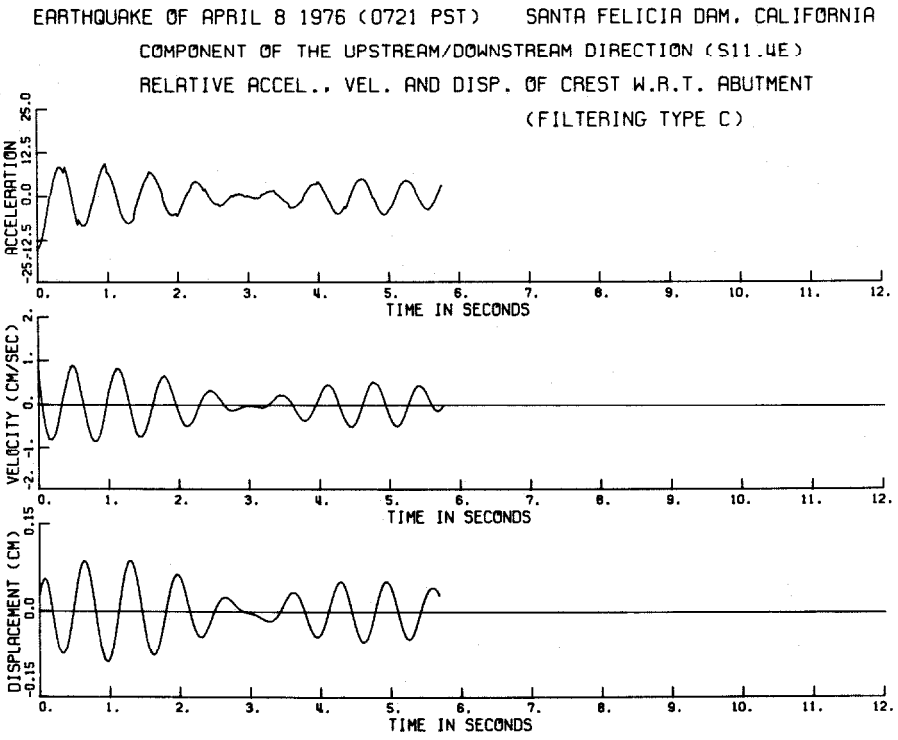
EARTHQUAKE OF APRIL 8 1976 (0721 PST) SANTA FELICIA DAM, CALIFORNIA
COMPONENT OF THE UPSTREAM/DOWNSTREAM DIRECTION (S11.4E)
RELATIVE ACCEL., VEL. AND DISP. OF CREST W.R.T. ABUTMENT
(FILTERING TYPE C)
ACCELERATION
25.0
12.5
0.0
-12.5
-25.
0. 1. 2. 3. 4. 5. 6. 7. 8. 9. 10. 11. 12.
TIME IN SECONDS
VELOCITY (CM/SEC)
2.
1.
0.
-1.
-2.
0. 1. 2. 3. 4. 5. 6. 7. 8. 9. 10. 11. 12.
TIME IN SECONDS
DISPLACEMENT (CM)
0.15
0.0
-0.15
0. 1. 2. 3. 4. 5. 6. 7. 8. 9. 10. 11. 12.
TIME IN SECONDS

Fig. 52

EARTHQUAKE OF APRIL 8 1976 (0721 PST) SANTA FELICIA DAM, CALIFORNIA
COMPONENT OF THE UPSTREAM/DOWNSTREAM DIRECTION (S11.4E)
HYSTERETIC RESPONSE FILTERING TYPE C

ACCELEROGRAM IS BAND-PASS FILTERED BETWEEN 1.25 AND 1.60 HZ.

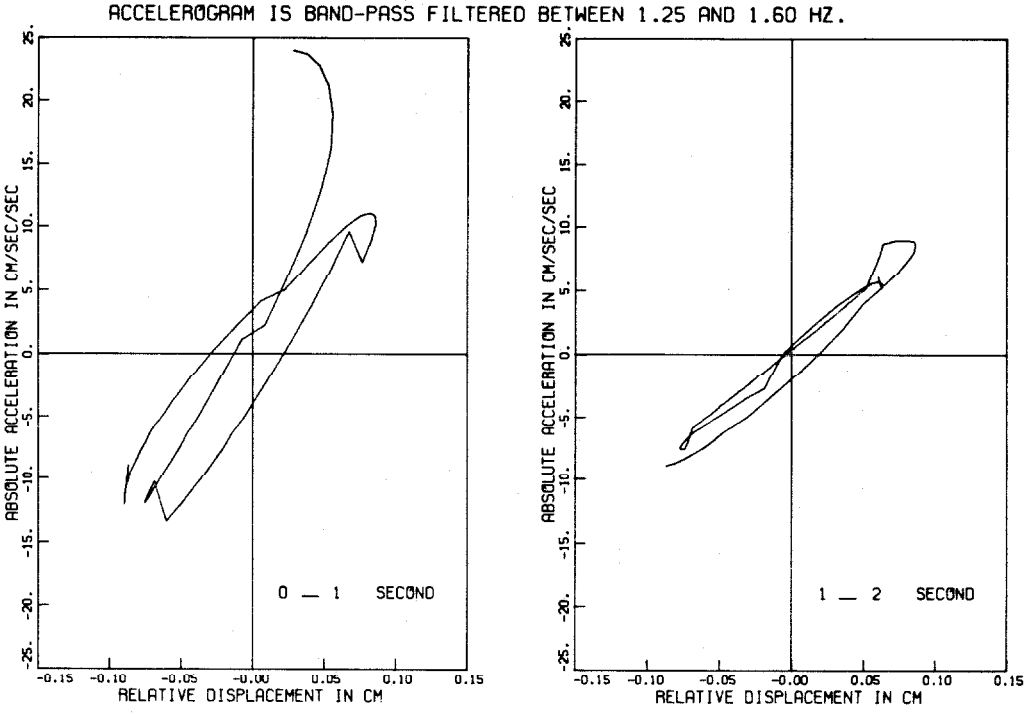

ACCELEROGRAM IS BAND-PASS FILTERED BETWEEN 1.25 AND 1.60 HZ.

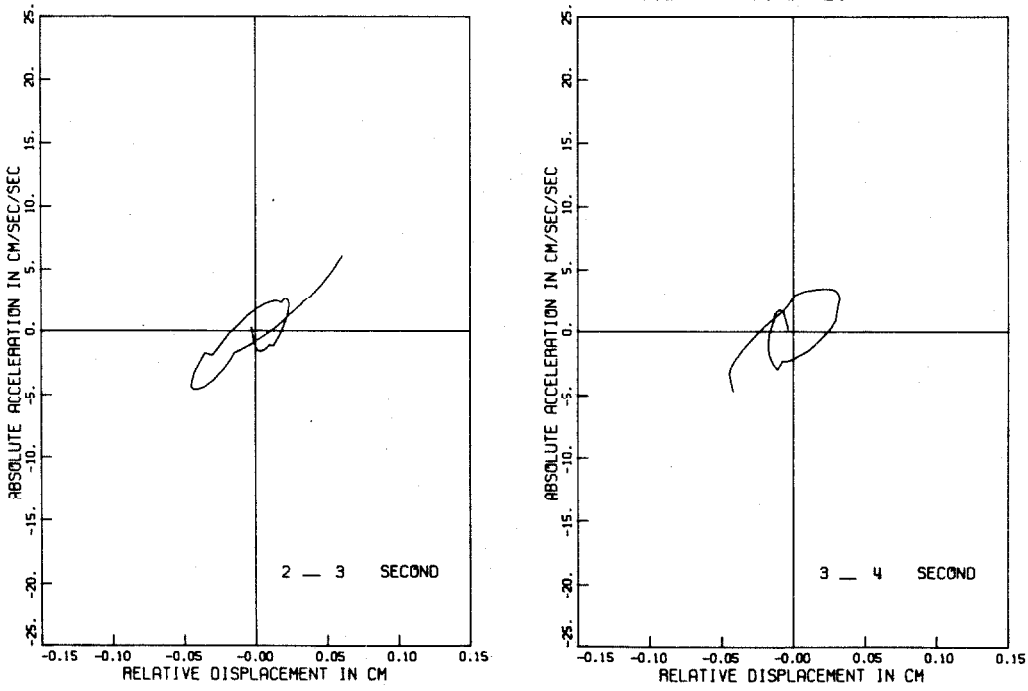

Fig. 53-a

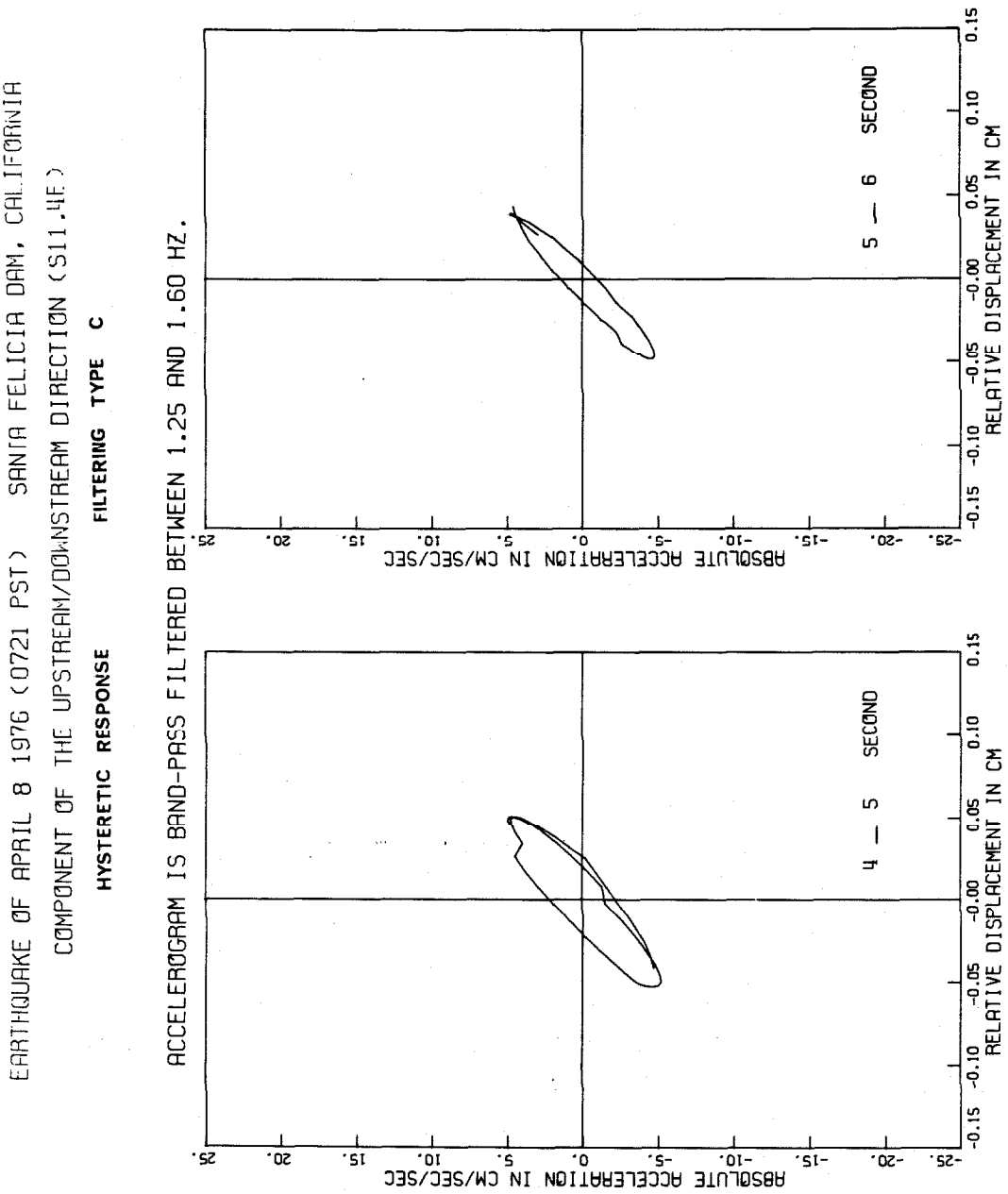
EARTHQUAKE OF APRIL 8 1976 (0721 PST) SANTA FELICIA DAM, CALIFORNIA
COMPONENT OF THE UPSTREAM/DOWNSTREAM DIRECTION (S11.4E)
HYSTERETIC RESPONSE
FILTERING TYPE C
ACCELEROGRAM IS BAND-PASS FILTERED BETWEEN 1.25 AND 1.60 HZ.
ABSOLUTE ACCELERATION IN CM/SEC/SEC
RELATIVE DISPLACEMENT IN CM
4 — 5 SECOND
5 — 6 SECOND

Fig. 53-b

B-IV DYNAMIC SHEAR MODULI OF THE DAM MATERIAL

B-IV-1 Dynamic Response Analysis for Earth Dams

It is the purpose of this study to: (1) provide data on the dynamic shear moduli and damping factors for earth dam materials, from earthquake response observations; (2) correlate this data with that obtained for sands and saturated clays; most of the data available to date have been developed only from laboratory tests on sands and saturated clays. Thus, the heart of the investigation is to find values for the average shear modulus and equivalent viscous damping from the force-displacement plots or hysteresis loops, previously obtained. The slope and area of a hysteresis loop can be related to the shear modulus and equivalent viscous damping factor through a model of the dam's response, e.g., the one-dimensional or two-dimensional shear-beam models or a finite-element model.

In evaluating the earthquake response of the dam, the one-dimensional shear-beam model with shear modulus varying with depth is used to estimate dynamic shear strains and stresses. It is also interesting to examine results obtained from the two-dimensional model with constant shear modulus. Thus, using the two existing elastic-response theories, a method is outlined whereby the shear stresses and shear strains can be determined as functions of the maximum absolute acceleration and maximum relative displacement, respectively, for each hysteresis loop, and consequently the shear moduli can be evaluated. As is well known, the internal stresses generated at a point in a dam by the internal resistance to the ground motion, are a function of the absolute acceleration at that point.

The absolute acceleration at any instant is determined by the dynamic response of the dam to the earthquake, which in turn is a function of the energy absorbing capacity, and the mass and stiffness characteristics of the dam.

Although the assumption of elastic behavior during earthquakes is not strictly correct for earth dams, it provides a basis for establishing the natural frequencies of the dam, as seen before, and in addition it gives at least a qualitative picture of the dynamic response characteristics of the dam. To enable a better understanding of the outlines and implications of dynamic response, the two-dimensional shear-beam response theory is presented for the case of a finite elastic wedge having a constant shear modulus. The analogous results (or expressions) for the case where the shear modulus varies with the cube root of the depth are also briefly presented.

a - Earthquake Response of the Two-dimensional Shear-beam Theory

To evaluate the magnitude and distribution of the modal shear strains and stresses, the equation of motion (assuming constant shear modulus and zero damping) of the dam subjected to ground motion $u_g(t)$, can be written as

$$m(y)\frac{\partial^2 u}{\partial t^2} - \alpha G\left(y\frac{\partial^2 u}{\partial y^2} + y\frac{\partial^2 u}{\partial z^2} + \frac{\partial u}{\partial y}\right) = -m(y)\ddot{u}_g(t) \quad , \qquad (15)$$

where $m(y)$ is the mass at a depth y ($= \rho \alpha y$), $\ddot{u}_g(t)$ is the ground acceleration, and $u(y, z, t)$ is the horizontal displacement relative to the base of the dam.

Using the generalized coordinates and the principle of mode superposition, one can write

$$u(y,z,t) = \sum_{n=1}^{\infty} \sum_{r=1}^{\infty} Y_n(y)\, Z_r(z)\, T_{nr}(t) \quad , \tag{16}$$

where, the subscripts n and r refer to the $(n,r)^{th}$ mode of vibration.

Substituting in Eq. 15 and using the orthogonality properties of the mode shapes gives

$$\ddot{T}_{nr}(t) + \omega_{nr}^2\, T_{nr}(t) = -\frac{W_{nr}}{M_{nr}}\, \ddot{u}_g(t) \quad , \qquad n,r = 1,2,3,\ldots \quad , \tag{17}$$

where M_{nr} is the generalized mass; it is given by

$$M_{nr} = \int_0^h \int_0^\ell Y_n^2(y)\, Z_r^2(z)\, m(y)\, dydz = \frac{\alpha \rho \ell h^2}{4}\, J_1^2(\beta_n) \quad . \tag{18}$$

$W_{nr}\ddot{u}_g(t)$ is the effective earthquake force for the $(n,r)^{th}$ mode with

$$W_{nr} = \int_0^h \int_0^\ell Y_n(y)\, Z_r(z)\, m(y)\, dydz = \frac{2\,\alpha \rho \ell h^2}{r\pi \beta_n}\, J_1(\beta_n) \quad . \tag{19}$$

Because only the symmetrical modes can contribute to the response in the case of a uniformly distributed ground motion, values of r are limited to odd integers, i.e., r = 1, 3, 5, 7, ... etc.

Now Eq. 17 can be written as

$$\ddot{T}_{nr}(t) + \omega_{nr}^2\, T_{nr}(t) = \frac{-8}{r\pi \beta_n J_1(\beta_n)}\, \ddot{u}_g(t) \qquad n = 1,2,3,\ldots, \; r = 1,3,5,\ldots \quad . \tag{20}$$

The solution of Eq. 20 can be obtained using the Duhamel integral, as

$$T_{nr}(t) = \frac{8}{r\pi \beta_n \omega_{nr} J_1(\beta_n)} \left[\int_0^t \ddot{u}_g(t)\, \sin \omega_{nr}(t-\tau)\, d\tau \right], \quad n=1,2,3,\ldots, \; r=1,3,5,\ldots \tag{21}$$

For the maximum value of Eq. 21, one can get

$$T_{nr}(t)\Big|_{max} = \frac{8}{r\pi\beta_n\omega_{nr}J_1(\beta_n)} S_v \ , \qquad (22)$$

where S_v is the maximum value of the quantity between the two brackets of Eq. 21; it is the ordinate of the velocity spectrum of the ground motion, corresponding to the natural frequency of the $(n, r)^{th}$ mode.

The damped solution is similar but with

$$T_{dnr}(t) = \frac{8}{r\pi\beta_n\omega_{dnr}J_1(\beta_n)}\left[\int_0^t \ddot{u}_g(t)\, e^{-\lambda_{nr}\omega_{nr}(t-\tau)} \sin \omega_{dnr}(t-\tau)d\tau\right] \ , \qquad (23)$$

where $\lambda_{nr} = \frac{c}{2\rho\omega_{nr}}$ is the damping factor for the $(n, r)^{th}$ mode, and $\omega_{dnr} = \omega_{nr}[1 - \lambda_{nr}]^{\frac{1}{2}}$ is the damped natural frequency [$\omega_{dnr} \simeq \omega_{nr}$ for $\lambda < 0.2$].

From Eq. 23, one can obtain

$$T_{dnr}(t)\Big|_{max} = \frac{8}{r\pi\beta_n\omega_{dnr}J_1(\beta_n)} S_{dv} \ , \qquad (24)$$

where S_{dv} is now the ordinate of the velocity spectrum calculated from the damping factor λ_{nr} of the $(n, r)^{th}$ mode and corresponding to the damped natural frequency ω_{dnr}.

Using mode superposition and the modes of vibration of Eq. 13, the response of the dam to the earthquake can be written as

$$u(y, z, t) = \sum_{n=1}^{\infty} \sum_{r=1, 3, 5}^{\infty} J_0\left(\beta_n \frac{y}{h}\right) \sin\left(\frac{r\pi z}{\ell}\right) \frac{8\, V_{nr}(t)}{r\pi\beta_n\omega_{nr}J_1(\beta_n)} \ , \qquad (25)$$

where the function $V_{nr}(t)$ is equal to the quantity between the two brackets in Eq. 21 (or for the damped case, $V_{dnr}(t)$ is equal to the quantity between the two brackets in Eq. 23).

The magnitude and distribution of shear strains in the $(n, r)^{th}$ mode, along the y-axis, are given by

$$\gamma_{nr}(y, z, t) = \frac{\partial y_{nr}(y, z, t)}{\partial y} = \frac{8V_{nr}(t)}{r\pi h\, \omega_{nr} J_1(\beta_n)} J_1\left(\beta_n \frac{y}{h}\right) \sin\left(\frac{\pi r z}{\ell}\right) . \tag{26}$$

Therefore, multiplying numerator and denominator by ω_{nr} and substituting for

$$\omega_{nr}^2 = \frac{v_s^2}{h}\left[\beta_n^2 + \left(\frac{r\pi h}{\ell}\right)^2\right] ,$$

one can obtain

$$\gamma_{nr} = \frac{\partial u_{nr}}{\partial y} = \left\{\frac{8J_1\left(\beta_n \frac{y}{h}\right) \sin\left(\frac{r\pi z}{\ell}\right)}{\pi\left[\beta_n^2 + \left(\frac{r\pi h}{\ell}\right)^2\right] J_1(\beta_n)}\right\} \frac{h\omega_{nr}}{v_s^2} V_{nr}(t) , \tag{27}$$

or

$$\gamma_{nr} = \frac{\partial u_{nr}}{\partial y} = \Phi_{nr}(y, z) \frac{h\omega_{nr}}{v_s^2} V_{nr}(t) , \tag{28}$$

where the function $\Phi_{nr}(y, z)$ is defined through Eq. 27; it expresses the modal participation and distribution of shear strain.

The maximum shear strain associated with each mode is given by

$$\gamma_{nr}\Big|_{max} = \frac{\partial u_{nr}}{\partial y}\Big|_{max} = \Phi_{nr}(y, z) \frac{hS_a}{v_s^2} , \tag{29}$$

where $S_a = \omega_{nr} V_{nr}(t)\Big|_{max} = \omega_{nr} S_v$ and is the ordinate of the calculated acceleration spectrum.

At the central region of the dam ($z \simeq \frac{\ell}{2}$) one can write

$$\gamma_{nr}\Big|_{z\simeq\frac{\ell}{2}} = \Phi_{nr}(y,z)\Big|_{z\simeq\frac{\ell}{2}} \frac{h\omega_{nr}}{v_s^2} V_{nr}(t) \quad . \tag{30}$$

Since this investigation of the earthquake response is focused only on the first mode, where n=1, r=1 and $\beta_1 = 2.4048$, then Eqs. 29 and 30 give

$$\gamma_{11}\Big|_{max} = \Phi_{11}(y) \frac{hS_a}{v_s^2} \tag{31}$$

at the central region.

It is important to note that the ratio between the maximum shear strain calculated by using the one-dimensional theory (Martin, 1965) and that calculated by using the above two-dimensional theory, for $\ell/h = 3.86$, is equal to 1.14 for the first mode. Figure 54-a shows a comparison between the modal participation factor $\Phi_{11}(y)$ derived from the above two-dimensional theory and that derived by Martin from the one-dimensional theory. The maximum shear strain associated with the first mode occurs at about 0.70 to 0.75 the depth of the dam (measured from the crest).

The corresponding modal shear stresses are given by

$$\tau_{nr}(y,z,t) = G \frac{\delta u_{nr}(y,z,t)}{\delta y} \quad ,$$

and

$$\tau_{nr}(y,z,t)\Big|_{max} = \Phi_{nr}(y,z)\, \rho h S_a \quad . \tag{32}$$

It follows that the modal participation and distribution function for the shear stress are expressed by the function $\Phi_{nr}(y)$ as in the case of the shear strain.

At the central region of the dam ($z \simeq \frac{\ell}{2}$) and for the first mode (n=1, r=1), Eq. 32 becomes

$$\tau_{11}\Big|_{max} = \Phi_{11}(y)\,\rho\,h\,S_a \quad . \tag{33}$$

Since it was assumed that each hysteresis loop is a response of a single-degree-of-freedom oscillator, and in order to get a qualitative picture of the dynamic shear stress from the force-displacement plot, the value of S_a in Eq. 33 is assumed to be the maximum absolute acceleration for each hysteresis loop. Thus, the maximum absolute acceleration can be translated into an equivalent shear stress. Similarly, since for small values of damping, $S_a = \omega_{11}^2 S_d$ (for the first mode) where S_d is the ordinate of the calculated displacement spectrum, Eq. 31 can be written in terms of the maximum relative displacement:

$$\gamma_{11}\Big|_{max} = \Phi_{11}(y)\,\frac{h\omega_{11}^2}{v_s^2}\,S_d \quad . \tag{34}$$

The assumption that S_d is equal to the maximum relative displacement is again made here.

b - <u>Earthquake Response of the One-dimensional Shear-beam Theory $\left[G = S_0\left(\frac{\gamma y}{2}\right)^{\frac{1}{3}}\right]$</u>

Analogous to the development of the previous equations expressing dynamic shear strains and stresses, it can be shown that the magnitude

and distribution of shear strains in the n^{th} mode is given by (Rashid, 1961 and Martin, 1965)

$$\gamma_n(y,t) = \frac{\partial u_n(y,t)}{\partial y} = \frac{2.4h\, J_{1.2}\left(\alpha_n\left(\frac{y}{h}\right)^{5/6}\right)}{v_{s0}^2\left(\frac{\gamma h}{2}\right)^{\frac{1}{3}}\alpha_n^2\, J_{1.2}(\alpha_n)}\left(\frac{y}{h}\right)^{-\frac{1}{3}}\omega_n V_n(t) \quad . \tag{35}$$

Equation 35 can also be written as

$$\gamma_n = \frac{\Psi_n(y)\,\omega_n V_n(t)}{v_{s0}^2\left(\frac{\gamma h}{2}\right)^{\frac{1}{3}}} \quad , \tag{36}$$

or

$$\gamma_n\Big|_{max} = \Psi_n(y)\,\frac{hS_a}{v_{s0}^2\left(\frac{\gamma h}{2}\right)^{\frac{1}{3}}} \quad . \tag{37}$$

In this case the analogous function $\Psi_n(y)$ expressing the modal participation and distribution of shear strain is expressed through Eq. 35.

Thus, for the first mode and in terms of the maximum relative hysteretic displacement, Eq. 37 can now be written as

$$\gamma_1\Big|_{max} = \Psi_1(y)\,\frac{h\,\omega_1^2}{v_{so}^2\left(\frac{\gamma h}{2}\right)^{\frac{1}{3}}}\,S_d \quad . \tag{38}$$

The modal shear stress is given by

$$\tau_n = S_0\left(\frac{\gamma y}{2}\right)^{\frac{1}{3}}\frac{\partial u_n}{\partial y} = \frac{2.4\rho h\, J_{1.2}\left(\alpha_n\left(\frac{y}{h}\right)^{5/6}\right)\omega_n V_n(t)}{\alpha_n^2\, J_{1.2}(\alpha_n)} \quad . \tag{39}$$

or

$$\tau_n(y,t) = \tilde{\Psi}_n(y)\,\rho h\,\omega_n V_n(t) \quad , \tag{40}$$

where $\tilde{\Psi}_n(y)$ expresses the distribution and participation of shear stress.

The maximum distribution of shear stress associated with each mode is hence given by

$$\tau_n\Big|_{max} = \tilde{\Psi}_n(y)\,\rho h S_a \quad , \tag{41}$$

and for the first mode

$$\tau_1\Big|_{max} = \tilde{\Psi}_1(y)\,\rho h S_a \quad . \tag{42}$$

Figure 54-b shows the modal participation factors $\Psi_1(y)$ and $\tilde{\Psi}_1(y)$ for the first mode.

c - Shear Modulus

For the two-dimensional shear-beam theory the shear modulus can be obtained by dividing the expression for shear stress (Eq. 33) by the expression for shear strain (Eq. 34) as follows

$$G = \frac{\tau_{11}}{\gamma_{11}} = \frac{\rho v_s^2}{\omega_{11}^2}\,\frac{S_a}{S_d} \simeq \rho\left(\frac{v_s}{\omega_{11}}\right)^2 \frac{(\ddot{x} + \ddot{u}_g)_{max}}{x_{max}} \quad , \tag{43}$$

where $(\ddot{x} + \ddot{u}_g)_{max}$ is the maximum absolute acceleration of each hysteretic loop and x_{max} is the maximum relative displacement of the same loop. Thus, the shear modulus G for each loop can be expressed by the slope of the loop.

As is well known, for the single-degree-of-freedom oscillator responding essentially in the linear range, one can write

$$\omega^2 = \frac{k}{m} = \frac{(\ddot{x} + \ddot{u}_g)_{max}}{x_{max}} \tag{44}$$

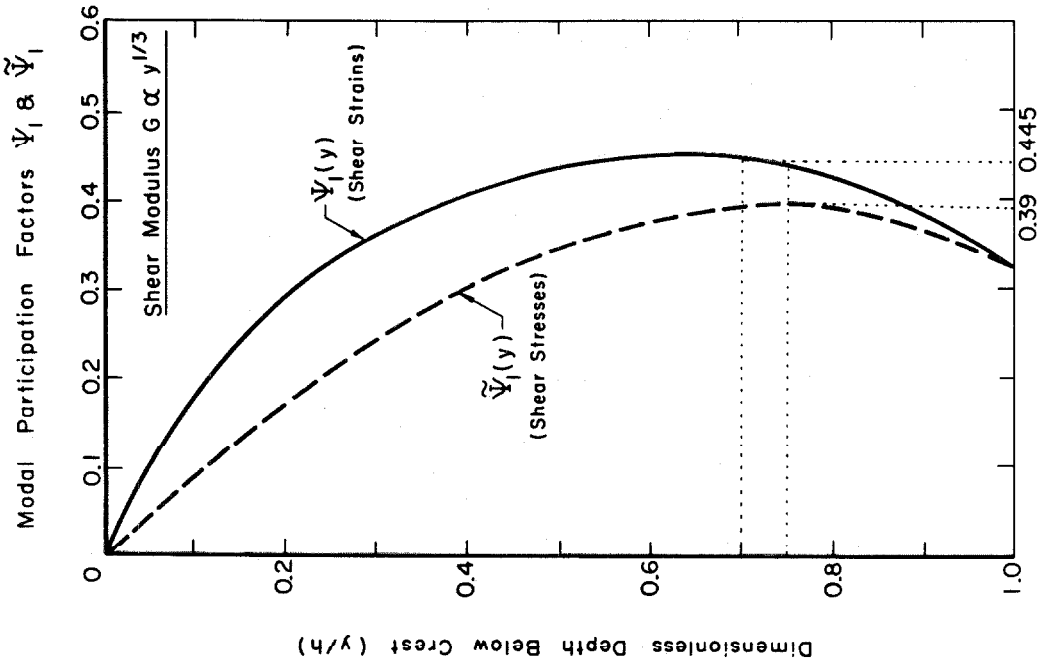

Fig. 54-b Modal participation factor for the first mode (one-dimensional theory with $G\alpha y^{\frac{1}{3}}$) (After Martin, 1965)

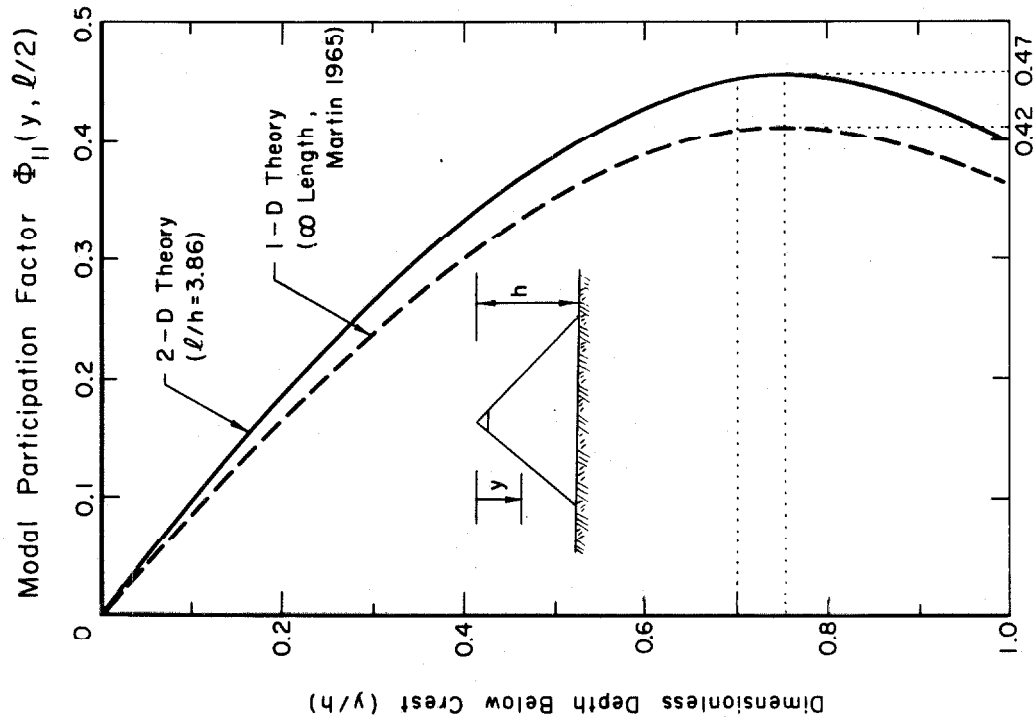

Fig. 54-a Modal participation factor for the first mode (central region of the dam)

where k and m are the stiffness and mass of the oscillator, respectively. Now using this expression for ω^2 and the expression for the natural frequency (Eq. 4) obtained by the one-dimensional theory with constant G, the following relation can be derived

$$G = \frac{\rho h^2 \omega_1^2}{\beta_1^2} = \frac{\rho h^2}{\beta_1^2} \frac{(\ddot{x} + \ddot{u}_g)_{max}}{x_{max}} = \rho\left(\frac{v_s}{\omega_1}\right)^2 \frac{(\ddot{x} + \ddot{u}_g)_{max}}{x_{max}} \qquad (45)$$

which is identical to Eq. 43; however ω_1 is slightly different from ω_{11} for the two-dimensional case (it mainly depends on the ratio ℓ/h).

For the one-dimensional shear-beam theory (with $G \alpha y^{\frac{1}{3}}$), the shear modulus can be obtained by dividing Eq. 42 by Eq. 38 to obtain

$$G = \frac{\tau_1}{\gamma_1} = \frac{\tilde{\Psi}_1(y)}{\Psi(y)} \frac{\rho v_{so}^2 \left(\frac{\gamma h}{2}\right)^{\frac{1}{3}}}{\omega_1^2} \frac{S_a}{S_d} \; ; \qquad (46)$$

again $\frac{S_a}{S_d}$ can be approximated by $\frac{(\ddot{x} + \ddot{u}_g)_{max}}{x_{max}}$.

B-IV-2 Calculation of the Dynamic Shear Moduli of Santa Felicia Dam

The earthquake response of Santa Felicia Dam was studied using Eqs. 31 and 33 for the two-dimensional theory and Eqs. 38 and 42 for the one-dimensional theory. The determination of the material properties for use in elastic response analyses and consequently the evaluation of the dynamic shear strains and stresses were determined as follows:

1 - For the dry, moist and saturated weight characteristics of both the core and the shell materials (Table 1), the average specific weight for use in response analysis is

$$\gamma_{average} = \frac{1}{6}[114+131+134+125+131++141] = 129.33 \text{ lb/ft}^3$$

which gives an average mass density $\rho_{average}$ of 4.02 lb . sec^2/ft^4.

2 - From Figs. 54-a,b one can see that the maximum shear strain (or stress) occurs at about 0.70 to 0.75 the height of the dam, where the value of the modal participation factor Φ_{11} is equal to 0.47. Therefore for h = 236.5 ft, the maximum shear stress at any time t (Eq. 33) is given by

$$\tau_{11}(t)\Big|_{max} = 0.47 \times 4.02 \times 236.5 \times S_a = 437.3\,(\ddot{x} + \ddot{u}_g)_{max} \text{ lb/ft}^2 \quad , \tag{47}$$

where $(\ddot{x}+\ddot{u}_g)_{max}$ is in ft/sec^2 .

3 - The fundamental frequency has already been shown to be $1.45 \times 2\pi = 9.11$ rad/sec. Since the value of the shear wave velocity v_s resulting from both the earthquake response and the two-dimensional theory is 848.66 ft/sec, and since wave-velocity measurements predicted a range from v_s = 870 ft/sec to v_s = 1,070 ft/sec at a depth equal to (0.7 to 0.75)h, therefore one can use the value of v_s = 850 ft/sec as a representative shear wave velocity of the dam for the analysis. Thus, the maximum shear strain from the two-dimensional theory (Eq. 31), at any time t, is expressed as

$$\gamma_{11}(t)_{max} = \frac{0.47 \times 236.5 \times (9.11)^2}{(850)^2} x_{max} = 0.0125 x_{max} \quad . \tag{48}$$

where x_{max} is in ft.

4 - For the one-dimensional theory with $G(y) = S_0\left(\frac{\gamma y}{2}\right)^{\frac{1}{3}}$, the maximum shear stress occurs at about (0.7 to 0.75)h where the modal participation factor $\tilde{\Psi}$, equals 0.39 (Fig. 54-b). Thus, the maximum shear stress (Eq. 42) is

$$\tau_1(t)_{max} = 0.39 \times 4.02 \times 236.5(\ddot{x} + \ddot{u}_g)_{max} = 370.78(\ddot{x} + \ddot{u}_g)_{max} \quad lb/ft^2 \quad ; \tag{49}$$

i.e., the maximum shear stress resulting from the two-dimensional theory with constant G (Eq. 47) is 1.18 times greater than that from the one-dimensional theory with varying G (Eq. 49).

5 - From Fig. 54-b the maximum shear strain occurs at $y \simeq$ (0.7 to 0.75)h, where $\Psi_1 = 0.445$. Using $v_{s0} = 195$, the shear strain at any time t is expressed as

$$\gamma_1(t)\Big|_{max} = \frac{0.445 \times 236.5 \times (9.11)^2}{(195)^2 (0.5 \times 129.3 \times 236.5)^{\frac{1}{3}}} = 0.0098 x_{max} \quad ; \tag{50}$$

where x_{max} is in ft.

i.e., the shear strain resulting from the two-dimensional theory (with constant G) is 1.28 times greater than the value resulting from the one-dimensional theory (with G not constant).

6 - The equivalent shear modulus for each hysteresis loop can be obtained by using either Eqs. 43 and 46 or Eqs. 47, 48 and Eqs. 49, 50. From Eq. 43, the shear modulus can be expressed as

$$G = 34996.70 \frac{(\ddot{x} + \ddot{u}_g)_{max}}{x_{max}} \text{ lb/ft}^2 \text{ for the two-dimensional case.}$$

Similarly, from Eq. 46, one has

$$G = 37951.11 \frac{(\ddot{x} + \ddot{u}_g)_{max}}{x_{max}} \text{ lb/ft}^2 \text{ for the one-dimensional}$$

theory with varying G; i.e., for Santa Felicia Dam the shear modulus resulting from the one-dimensional theory with varying G is 1.08 greater than that value from the two dimensional theory with constant G.

Tables 11 and 12 show the estimated stresses and strains and the corresponding shear moduli evaluated from the hysteretic response of the two earthquakes.

The relationship between the estimated shear modulus and the earthquake-induced strain may be illustrated by the results shown on the semi-log plots of Fig. 55 for the one-dimensional model and by the results in Fig. 56 for the two-dimensional model. It is apparent that the equivalent shear modulus depends on the magnitude of the strain for which the hysteresis loop is determined. The results of Fig. 55 cover a range of shear strain from 10^{-3} percent to 5×10^{-2} percent while the results of Fig. 56 cover a range of shear strain from 10^{-3} percent to 6×10^{-2} percent, which are relatively reasonable bands. While there is considerable scattering of the data in the two figures, most of the results of this analysis fall within the dashed lines in Figs. 55 and 56, that is, within $\pm$ 50% of the average values shown by the solid line in these figures. Thus the average values

are likely to provide reasonable estimates of the shear modulus for the soil of the dam.

At higher strains, additional data on modulus values is needed; however approximate values for use in some types of response analyses can be estimated by the suggested extrapolation of the data at low strain. A close approximation of the modulus versus shear strain relationship can be obtained by determining the modulus at a very low strain level, perhaps by forced vibration tests or by wave propagation methods in the field, as indicated by Figs. 55 and 56, where the predicted range of the shear modulus determined by both the wave-velocity measurements and the relation $G = S_0(\gamma y/2)^{\frac{1}{3}}$, (Fig. 41), for Santa Felicia Dam, is shown.

TABLE 11

Estimated Shear Strains and Stresses and the Corresponding Shear Moduli By the Two-dimensional Shear-beam Theory (With Constant G)

a - San Fernando Earthquake of February 9, 1971

Cycle No.	Time Secs	Max. Accel. $(\ddot{x} + \ddot{u}_g)_{max}$ (cm/sec^2)		Max. Disp. x_{max} (cm)		Average $(\ddot{x} + \ddot{u}_g)_{max}$ (cm/sec^2)	Average x_{max} cm	Slope $\frac{(\ddot{x} + \ddot{u}_g)_{max}}{x_{max}}$ /sec^2	Equivalent Stress lb/ft^2	Equivalent Strain Percent	Equivalent Shear Modulus lb/ft^2
		+ve	-ve	+ve	-ve						
1	0- 1	82.0	90.	1.10	1.20	86.0	1.15	74.78	1236.64	4.72×10^{-2}	2.62×10^6
2	1- 2	108.0	110.	1.30	1.35	109.0	1.33	81.95	1564.15	5.45×10^{-2}	2.87×10^6
3	2- 3	100.0	110.	1.29	1.31	105.0	1.30	80.77	1508.39	5.33×10^{-2}	2.83×10^6
4	3- 4	78.0	72.	1.10	1.00	75.0	1.05	71.43	1077.50	4.31×10^{-2}	2.50×10^6
5	4- 5	48.0	48.	0.67	0.71	48.0	0.69	69.57	690.52	2.83×10^{-2}	2.44×10^6
6	5- 6	32.0	43.	0.36	0.50	37.5	0.43	87.21	538.56	1.76×10^{-2}	3.06×10^6
7	6- 7	18.0	18.	0.16	0.16	18.0	0.16	112.50	260.04	0.66×10^{-2}	3.94×10^6
8	7- 8	20.0	20.	0.15	0.15	20.0	0.15	133.33	289.54	0.62×10^{-2}	4.67×10^6
9	8- 9	22.0	19.	0.15	0.13	20.5	0.14	146.43	287.28	0.56×10^{-2}	5.13×10^6
10	9-10	13.5	16.	0.11	0.13	14.8	0.12	122.92	211.19	0.49×10^{-2}	4.31×10^6
11	10-11	16.0	22.	0.20	0.22	19.0	0.21	90.48	272.62	0.86×10^{-2}	3.17×10^6
12	11-12	22.0	21.	0.22	0.24	21.5	0.23	93.48	308.32	0.94×10^{-2}	3.28×10^6
13	12-13	17.0	16.	0.25	0.22	16.5	0.24	68.75	236.18	0.98×10^{-2}	2.41×10^6
14	13-14	17.0	21.	0.21	0.25	19.0	0.23	82.61	272.60	0.94×10^{-2}	2.90×10^6
15	14-15	23.0	24.	0.28	0.21	23.0	0.25	94.00	339.90	1.03×10^{-2}	3.30×10^6
16	15-16	23.0	19.	0.20	0.20	21.0	0.20	105.00	301.76	0.82×10^{-2}	3.68×10^6
17	16-17	8.0	11.	0.08	0.11	9.5	0.10	95.00	136.53	0.41×10^{-2}	3.33×10^6
18	17-18	11.0	11.	0.11	0.11	11.0	0.11	100.00	143.91	0.41×10^{-2}	3.51×10^6
19	18-19	12.0	13.	0.18	0.17	12.5	0.18	69.44	179.82	0.74×10^{-2}	2.43×10^6
20	19-20	10.0	12.	0.15	0.17	11.0	0.16	68.75	159.06	0.66×10^{-2}	2.41×10^6

b - Southern California Earthquake of April 8, 1976

1	0- 1	11.0	12.5	0.085	0.085	11.75	0.085	138.24	168.70	0.35×10^{-2}	4.82×10^6
2	1- 2	8.0	9.0	0.085	0.075	8.50	0.080	106.25	122.43	0.33×10^{-2}	3.71×10^6
3	2- 3	5.0	4.5	0.045	0.045	4.75	0.045	105.56	66.24	0.18×10^{-2}	3.68×10^6
4	3- 4	3.5	4.0	0.030	0.030	3.75	0.030	125.00	52.32	0.12×10^{-2}	4.36×10^6
5	4- 5	5.0	5.0	0.050	0.050	5.00	0.050	100.00	73.29	0.21×10^{-2}	3.49×10^6
6	5- 6	4.5	5.0	0.040	0.045	4.75	0.043	110.47	69.30	0.18×10^{-2}	3.85×10^6

TABLE 12

Estimated Shear Strains and Stresses and the Corresponding Shear Moduli By the One-dimensional Shear-beam Theory (with $G(y) = S_0(\gamma y/2)^{\frac{1}{3}}$

a - San Fernando Earthquake of February 9, 1971

Cycle No.	Time Secs	$(\ddot{x} + \ddot{u}_g)_{max}$ cm/sec^2	x_{max} cm	Slope $\frac{(\ddot{x} + \ddot{u}_g)_{max}}{x}$ /sec^2	Equivalent Stress lb/ft^2	Equivalent Strain Percent	Equivalent Shear Modulus lb/ft^2
1	0- 1	86.0	1.15	74.78	1041.44	3.68×10^{-2}	2.83×10^6
2	1- 2	109.0	1.33	81.95	1317.50	4.15×10^{-2}	3.10×10^6
3	2- 3	105.0	1.30	80.77	1272.96	4.16×10^{-2}	3.06×10^6
4	3- 4	75.0	1.05	71.43	907.20	3.36×10^{-2}	2.70×10^6
5	4- 5	48.0	0.69	69.57	583.44	2.21×10^{-2}	2.64×10^6
6	5- 6	37.5	0.43	87.21	452.10	1.37×10^{-2}	3.30×10^6
7	6- 7	18.0	0.16	112.50	217.26	0.51×10^{-2}	4.26×10^6
8	7- 8	20.0	0.15	133.33	241.92	0.48×10^{-2}	5.04×10^6
9	8- 9	20.5	0.14	146.43	243.76	0.44×10^{-2}	5.54×10^6
10	9-10	14.8	0.12	122.92	176.70	0.38×10^{-2}	4.65×10^6
11	10-11	19.0	0.21	90.48	229.14	0.67×10^{-2}	3.42×10^6
12	11-12	21.5	0.23	93.48	258.42	0.73×10^{-2}	3.54×10^6
13	12-13	16.5	0.24	68.75	197.60	0.76×10^{-2}	2.60×10^6
14	13-14	19.0	0.23	82.61	228.49	0.73×10^{-2}	3.13×10^6
15	14-15	23.0	0.25	94.00	284.80	0.80×10^{-2}	3.56×10^6
16	15-16	21.0	0.20	105.00	254.08	0.64×10^{-2}	3.97×10^6
17	16-17	9.5	0.10	95.00	115.20	0.32×10^{-2}	3.60×10^6
18	17-18	11.0	0.11	100.00	121.28	0.32×10^{-2}	3.79×10^6
19	18-19	12.5	0.18	69.44	151.96	0.58×10^{-2}	2.62×10^6
20	19-20	11.0	0.16	68.75	132.60	0.51×10^{-2}	2.60×10^6

b - Southern California Earthquake of April 8, 1976

1	0- 1	11.75	0.085	138.24	140.67	0.27×10^{-2}	5.21×10^6
2	1- 2	8.50	0.080	106.25	104.26	0.26×10^{-2}	4.01×10^6
3	2- 3	4.75	0.045	105.56	55.58	0.14×10^{-2}	3.97×10^6
4	3- 4	3.75	0.030	125.00	42.39	0.09×10^{-2}	4.71×10^6
5	4- 5	5.00	0.050	100.00	60.32	0.16×10^{-2}	3.77×10^6
6	5- 6	4.75	0.043	110.47	58.24	0.14×10^{-2}	4.16×10^6

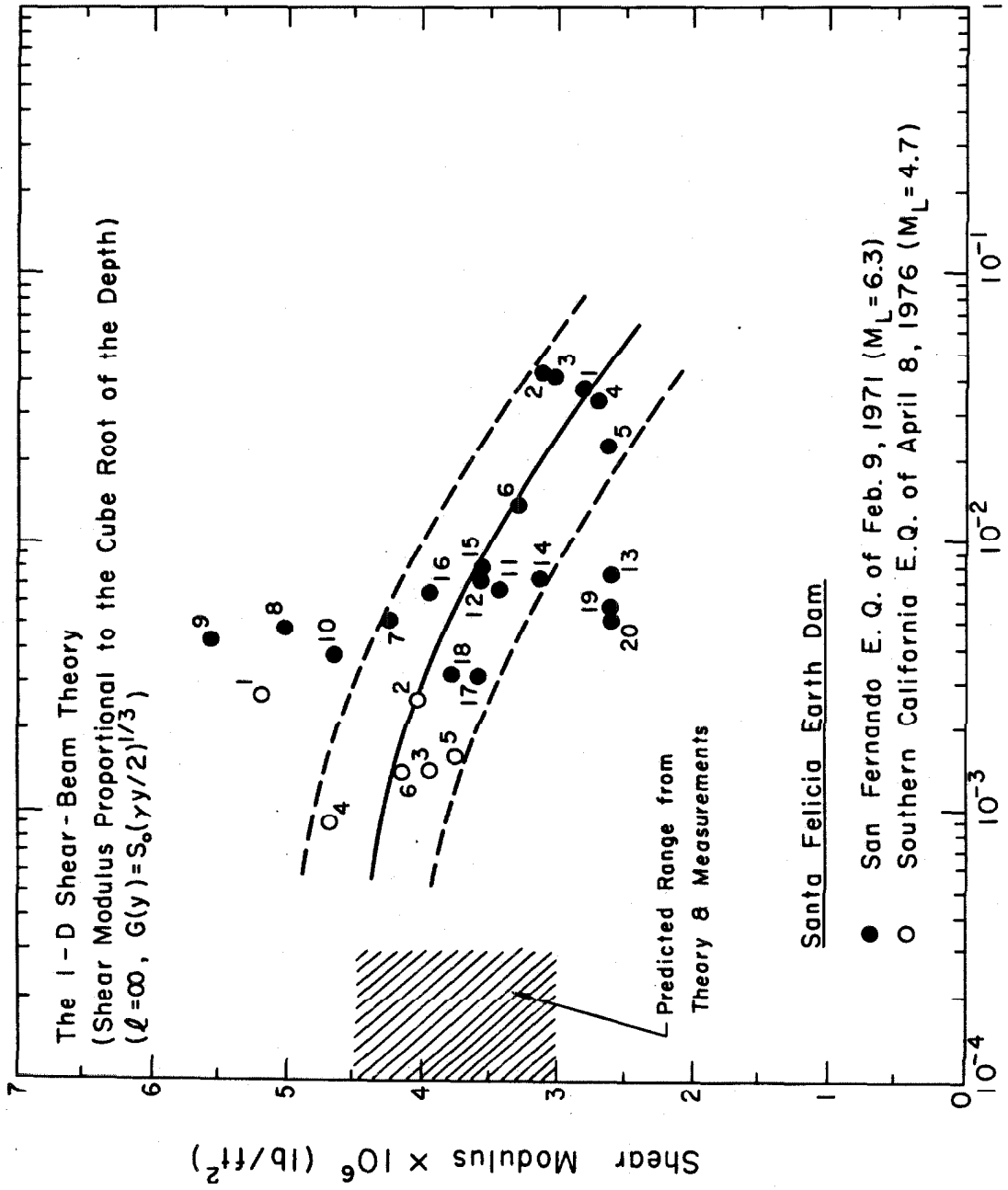
The 1-D Shear-Beam Theory
(Shear Modulus Proportional to the Cube Root of the Depth)
($\ell=\infty$, $G(y)=S_o(y/2)^{1/3}$)
Predicted Range from
Theory & Measurements
Santa Felicia Earth Dam
● San Fernando E.Q. of Feb. 9, 1971 (M_L=6.3)
○ Southern California E.Q. of April 8, 1976 (M_L=4.7)
Shear Modulus x 10^6 (lb/ft^2)
Shear Strain (percent)
0
1
2
3
4
5
6
7
10^{-4}
10^{-3}
10^{-2}
10^{-1}

Fig. 55

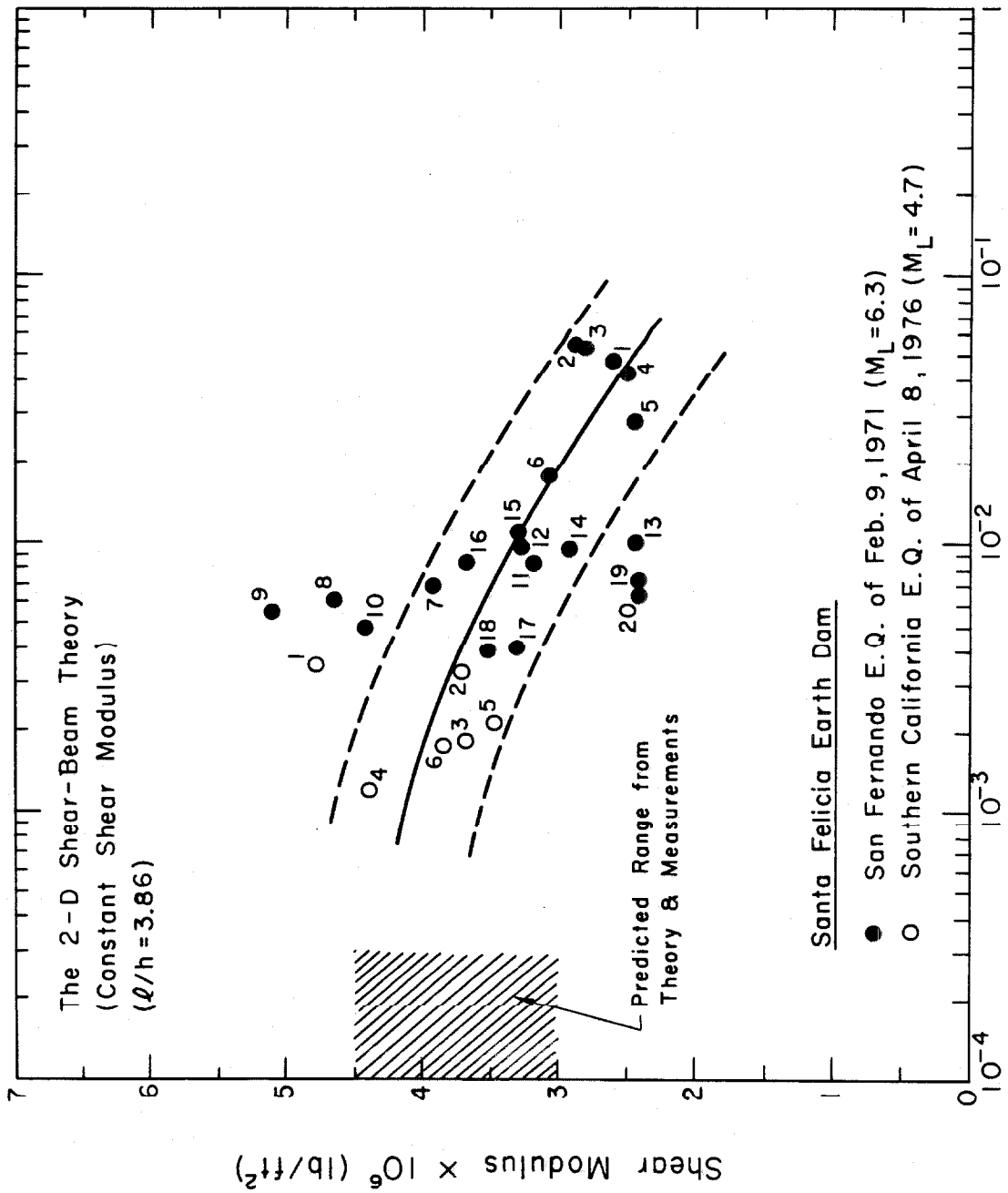
The 2-D Shear-Beam Theory
(Constant Shear Modulus)
(ℓ/h = 3.86)
Predicted Range from
Theory & Measurements
Santa Felicia Earth Dam
● San Fernando E.Q. of Feb. 9, 1971 (M_L = 6.3)
○ Southern California E.Q. of April 8, 1976 (M_L = 4.7)
Shear Modulus × 10^6 (lb/ft^2)
Shear Strain (percent)
0
1
2
3
4
5
6
7
10^-4
10^-3
10^-2
10^-1
1

Fig. 56

B-V EQUIVALENT VISCOUS DAMPING FACTORS OF THE DAM MATERIAL

Although the damping mechanism present in the gravelly soil of the dam is probably non-viscous in nature, it is of interest to estimate values of the equivalent viscous damping factors. The concept of equivalent viscous damping was introduced by Jacobsen (1930), the equivalent viscous damping forces dissipating the same amount of energy as the true damping forces. The concept is often used to evaluate the damping characteristics of non-viscous materials.

By considering a typical observed force-displacement cycle, or a hysteretic loop as shown in Fig. 57, the total dissipated work per cycle, ΔW, is represented by the area of the hysteresis loop ABDEA. Assuming that the non-linearity is due to damping, and that the restoring force is represented by the linear line EOB, the area OBC + OEF represents the work capacity, W, per cycle. Now, by considering the theoretical counterparts of ΔW and W for a viscously damped system, and equating the ratio of $\Delta W/W$ for both systems, it can be shown that the equivalent viscous damping factor η_{eq} for the non-viscous system (for small values of η_{eq}) is given by

$$\eta_{eq} = \frac{1}{2\pi} \frac{\Delta W}{W} \quad . \tag{51}$$

Values of η_{eq} determined from the observed hysteresis loops (filtering type C) are shown in Table 13. For some loops, like those measured at low amplitudes of vibration, the loop's area could not be determined with reasonable accuracy. The relationship between the estimated damping factor, from the area of each hysteresis loop, and the corresponding shear strain amplitude is shown in Fig. 58.

There is considerable scatter of the data for damping factors (particularly loop Nos. 1, 2, 3, 7, 8 and 10). However, approximate upper and lower bound relationships are shown by dashed lines, and a representative average relationship for all of the data is shown by the solid line. This average relationship can provide a basis for evaluating the relationship between the damping ratio and the strain for this earth dam for which limited data is available. So the probable damping ratios at other strains can also be closely approximated by the extrapolated solid line.

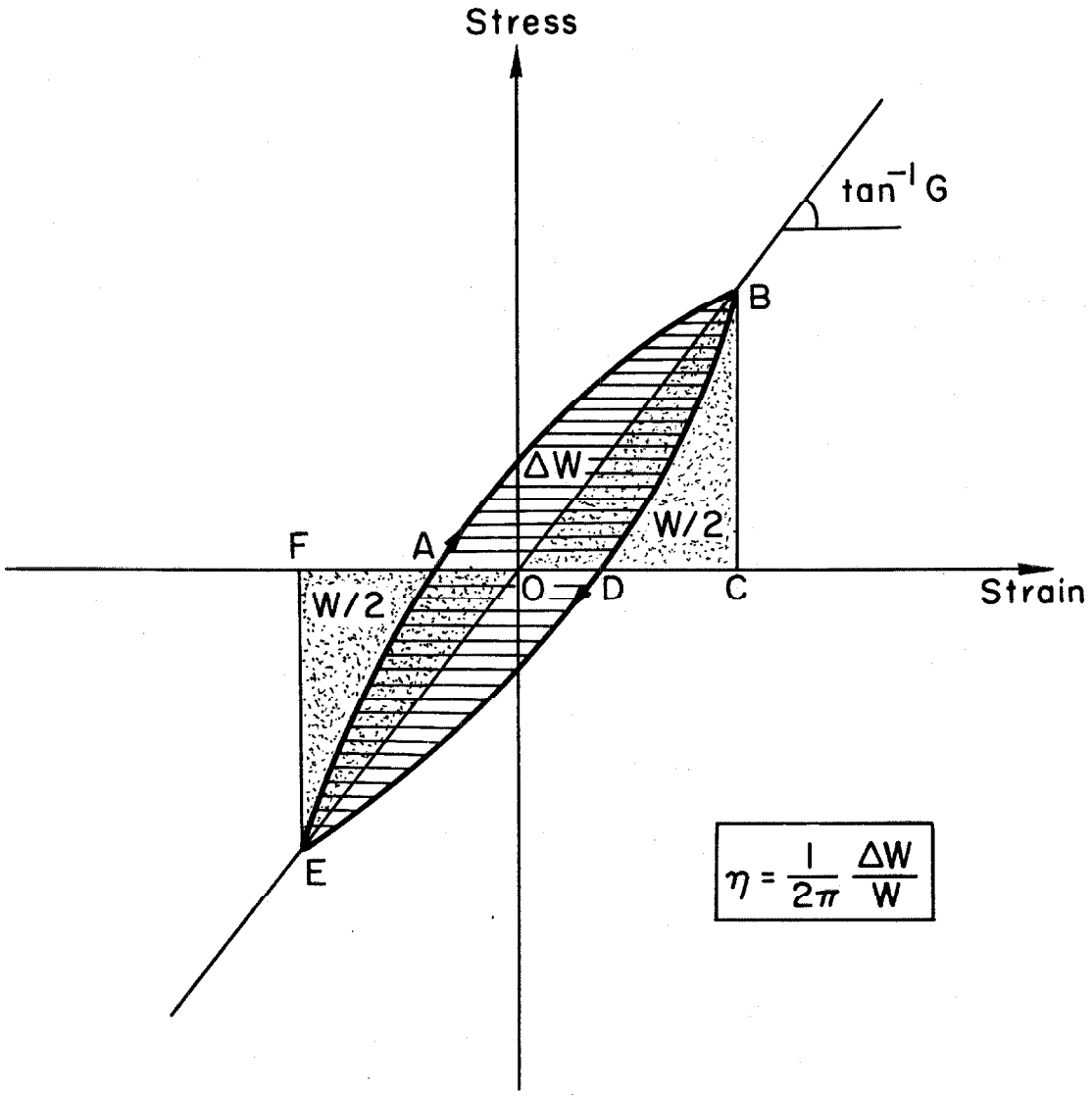

Fig. 57 Hysteretic damping factor η for equivalent viscous damping

TABLE 13

Equivalent Viscous Damping Factors (From Hysteresis Loops)

a - San Fernando Earthquake of February 9, 1971

No.	Time Seconds	ΔW	W	Damping Factor (Percent) $\eta = \frac{1}{2\pi}\frac{\Delta W}{W}$
1	0- 1	687.0	1520.5	7.2
2	1- 2	735.0	2250.0	5.2
3	2- 3	825.0	2186.0	6.0
4	3- 4	1036.0	1236.0	13.3
5	4- 5	585.0	596.0	15.7
6	5- 6	259.0	269.0	15.3
7	6- 7	45.0	42.0	17.1
8	7- 8	49.5	52.0	15.2
9	8- 9	42.0	53.5	12.5
10	9-10	36.0	38.0	15.1
11	10-11	64.0	74.0	13.8
12	11-12	66.0	81.0	13.0
13	12-13	42.0	61.0	11.0
14	13-14	53.0	72.0	11.7
15	14-15	63.0	89.0	11.3
16	15-16	41.0	66.0	9.9
17	16-17	9.5	15.0	10.1
18	17-18	12.0	21.0	9.1
19	18-19	13.5	30.8	7.0
20	19-20	13.0	29.0	7.1

b - Southern California Earthquake of April 8, 1976

1	0-1	1092.7	904.5	1.9
2	1-2	536.9	607.5	1.4
3	2-3	251.2	158.8	2.5
4	3-4	301.4	100.0	4.8
5	4-5	397.2	206.0	3.0
6	5-6	177.0	156.0	1.8

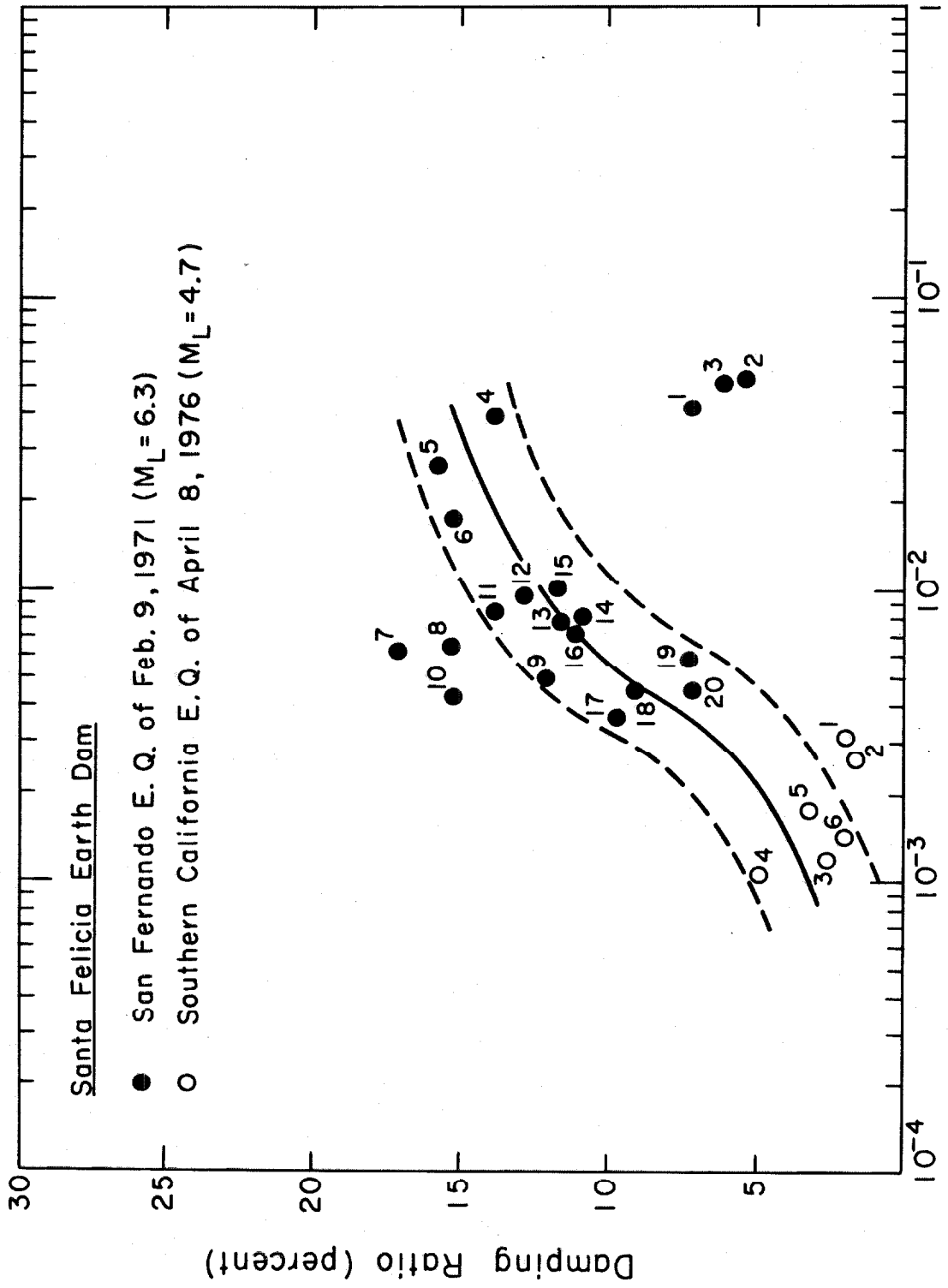
Santa Felicia Earth Dam
San Fernando E. Q. of Feb. 9, 1971 (M_L=6.3)
Southern California E.Q. of April 8, 1976 (M_L=4.7)
Damping Ratio (percent)
Shear Strain (percent)
30
25
20
15
10
5
10^{-4}
10^{-3}
10^{-2}
10^{-1}
1
.04
.05
.06
.03
.02
.01

Fig. 58

C. EVALUATION

C-I COMPARISON BETWEEN THE OBTAINED RESULTS AND PREVIOUSLY AVAILABLE DATA

In a comprehensive survey Seed and Idriss (1970) summarized, in a convenient form, the available data from laboratory and field tests concerning the dynamic shear moduli and damping factors for sands and saturated clays. In their study they suggested that the primary factors affecting shear moduli and damping factors are: strain amplitude, effective mean principal stress, void ratio, number of cycles of loading and degree of saturation for cohesive soils. They indicated that all investigations have shown that modulus values for sands are strongly influenced by the confining pressure, the strain amplitude and the void ratio (or relative density) but not significantly by variations in grain size characteristics. In general, the shear modulus, G, and confining pressure, σ'_m, are related by the relation

$$G = 1000 k_2 (\sigma'_m)^{\frac{1}{2}} , \qquad (52)$$

so that the influence of void ratio and strain amplitude can be expressed through their influence on the parameter k_2. Thus for practical purposes, values of k_2 may be considered to be determined mainly by the void ratio or relative density and the strain amplitude of the motion. A number of investigations, using different laboratory testing procedures, have presented data on the relationships between these factors. Figure B-1 in Appendix B shows the results of an investigation which illustrates the relationship between the factor k_2 and strain at a relative density of about 0.75%. Each investigator

who contributed to the results in Fig. B-1 used a different range for the effective confining pressures. A representative average relationship, which was suggested by Seed and Idriss, for all of the test data is shown by the solid line. This average relationship may well provide values of k_2 with sufficient accuracy for many practical purposes. Other relationships have been obtained and are summarized for different relative densities. Thus a close approximation to the modulus versus shear strain relationship for any sand can be obtained by determining the modulus at a very low strain level, say by wave propagation methods in the field, and then reducing this value for other strain levels in accordance with obtained results similar to the approximate curve of Fig. B-1.

For gravelly soils it is extremely difficult to perform any lab investigation because of the large diameter of the test specimens required. However, Seed and Idriss (1970) summarized the results of a very limited number of moduli determinations for gravelly soils, based on in-situ shear wave velocity measurements; Fig. B-2 (Appendix B) shows these results. From Fig. B-2 it may be seen that at small strain levels, modulus values are between 1.25 and 2.5 times greater than those for dense sands. Seed and Idriss suggested that at higher strains, the moduli for gravelly soils decrease in a manner similar to that for sands. Thus by applying the moduli reducing factors of the data obtained for sands to the limited data shown by solid circular points in Fig. B-2, they estimated variations in shear moduli with strain as shown in Fig. B-2. From this, approximate values for use in some types of response analyses can be estimated by the procedure shown in Fig. B-2.

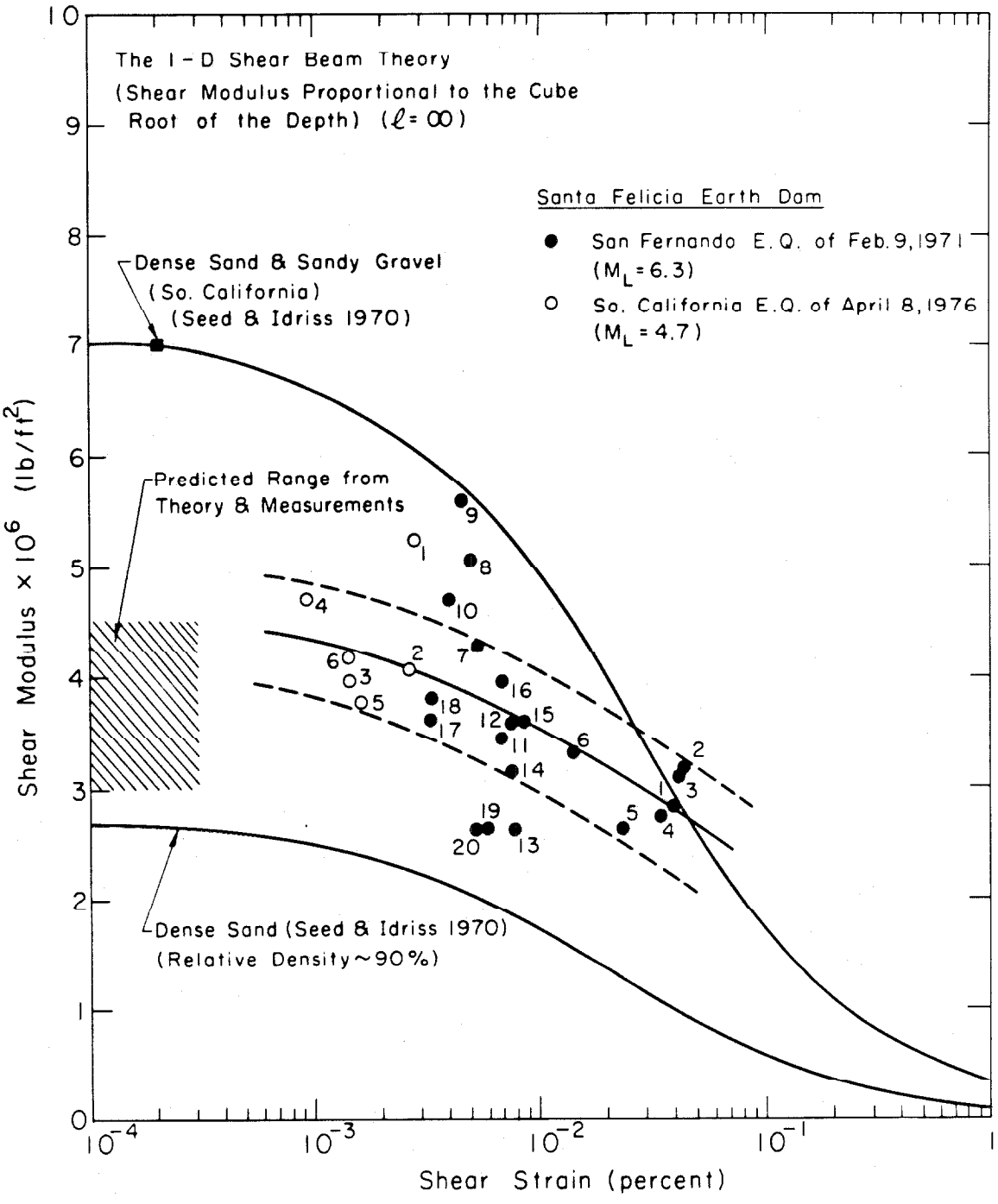
The 1-D Shear Beam Theory
(Shear Modulus Proportional to the Cube Root of the Depth) (ℓ = ∞)
Santa Felicia Earth Dam
San Fernando E.Q. of Feb. 9, 1971 (M_L = 6.3)
So. California E.Q. of April 8, 1976 (M_L = 4.7)
Dense Sand & Sandy Gravel (So. California) (Seed & Idriss 1970)
Predicted Range from Theory & Measurements
Dense Sand (Seed & Idriss 1970) (Relative Density ~ 90%)
Shear Modulus × 10^6 (lb/ft^2)
Shear Strain (percent)

Fig. 59

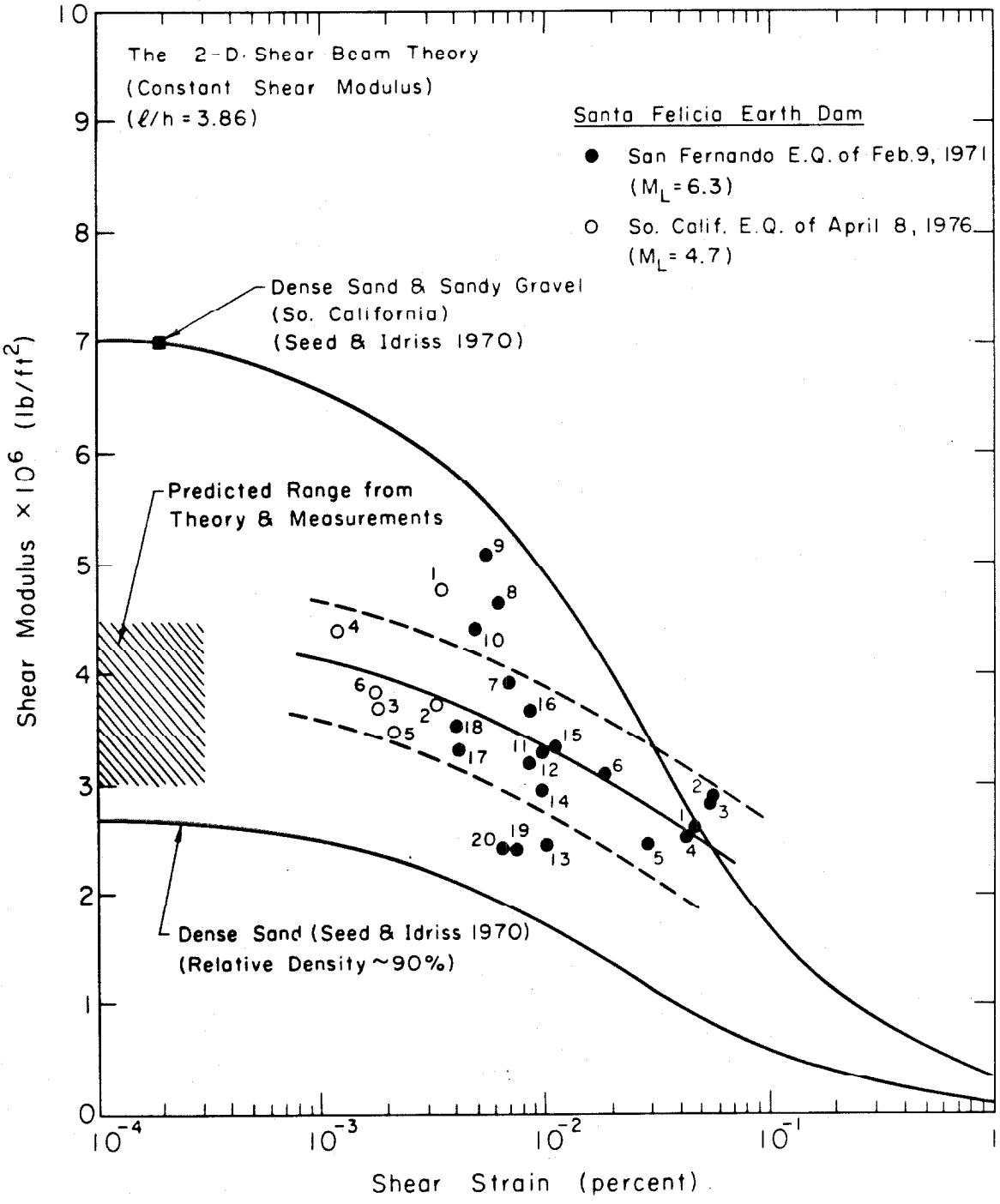
The 2-D Shear Beam Theory
(Constant Shear Modulus)
(ℓ/h = 3.86)
Santa Felicia Earth Dam
San Fernando E.Q. of Feb.9, 1971
(M_L = 6.3)
So. Calif. E.Q. of April 8, 1976
(M_L = 4.7)
Dense Sand & Sandy Gravel
(So. California)
(Seed & Idriss 1970)
Predicted Range from
Theory & Measurements
Dense Sand (Seed & Idriss 1970)
(Relative Density ~90%)
Shear Modulus ×10^6 (lb/ft^2)
Shear Strain (percent)

Fig. 60

To compare the results obtained in this investigation from the two earthquake observations, one has to know either the confining pressure at a depth of 0.75h (below the crest) of the dam or to translate the values of k_2 in Fig. B-2 (or B-1) to values of shear modulus G. The data points obtained by Seed (1968) in Fig. B-1 (the solid circular points) were based on a confining pressure of 2,000 psf; thus by substituting this pressure into Eq. 52, the k_2 value can be expressed in terms of G. Therefore, an estimate of the relationship between the shear modulus G and shear strain γ can be obtained for the two Figures B-1 and B-2.

The results of this investigation, obtained by using both the one- and two-dimensional models, are shown (in Figs. 59 and 60) on the same plot with the results suggested by Seed and Idriss for the Southern California gravelly soils (dense sand and sandy gravel) at a depth of 175 ft. At lower and medium strains, it seems that the two results lie in a region halfway between the curve suggested for dense sand and sandy gravel and the curve suggested for dense sand only (of relative density ~ 90%). At higher strains it seems likely that the shear moduli obtained in this investigation for gravelly soils of the dam decrease in a manner dissimilar to that suggested by Seed and Idriss (which was based on results for dense sands).

For the damping factors, Seed and Idriss (1970) indicated that the main factor affecting the relationship between damping ratio and shear strain is the vertical confining pressure. However, the effect of variations in pressure is very small compared with the effect of shear strain, and an average damping ratio versus shear strain relationship determined for an effective vertical stress of 2,000 - 3,000 psf

would appear to be adequate for many practical purposes as indicated by Seed and Idriss. Results of previous investigations of damping ratios for saturated clays and sands are presented in Fig. B-3 and B-4 (Appendix B). Approximate upper and lower bound relationships between damping ratio and shear strain are shown by the dashed lines, and a representative average relationship for all of the test data is shown by the solid line. This average relationship provides a basis for evaluating the relationship between damping ratio and strain for any particular clay or sand.

Additional data on damping ratios for gravelly soils is badly needed as acknowledged by Seed and Idriss who nonetheless suggested that gravelly soils' damping factor is approximately the same as that for sandy materials. A comparison between the results of this investigation and those shown in Fig. B-3 and B-4 is shown in Fig. 61. It is apparent that damping ratios for gravelly soils are somewhat different from those for sands, contrary to Seed and Idriss. Clearly, more data on these dynamic characteristics is required, particularly for very low and very high strain levels. In general, however, it is believed that the data presented here will broaden the understanding of soil properties for earthquake dynamic analyses of earth dams.

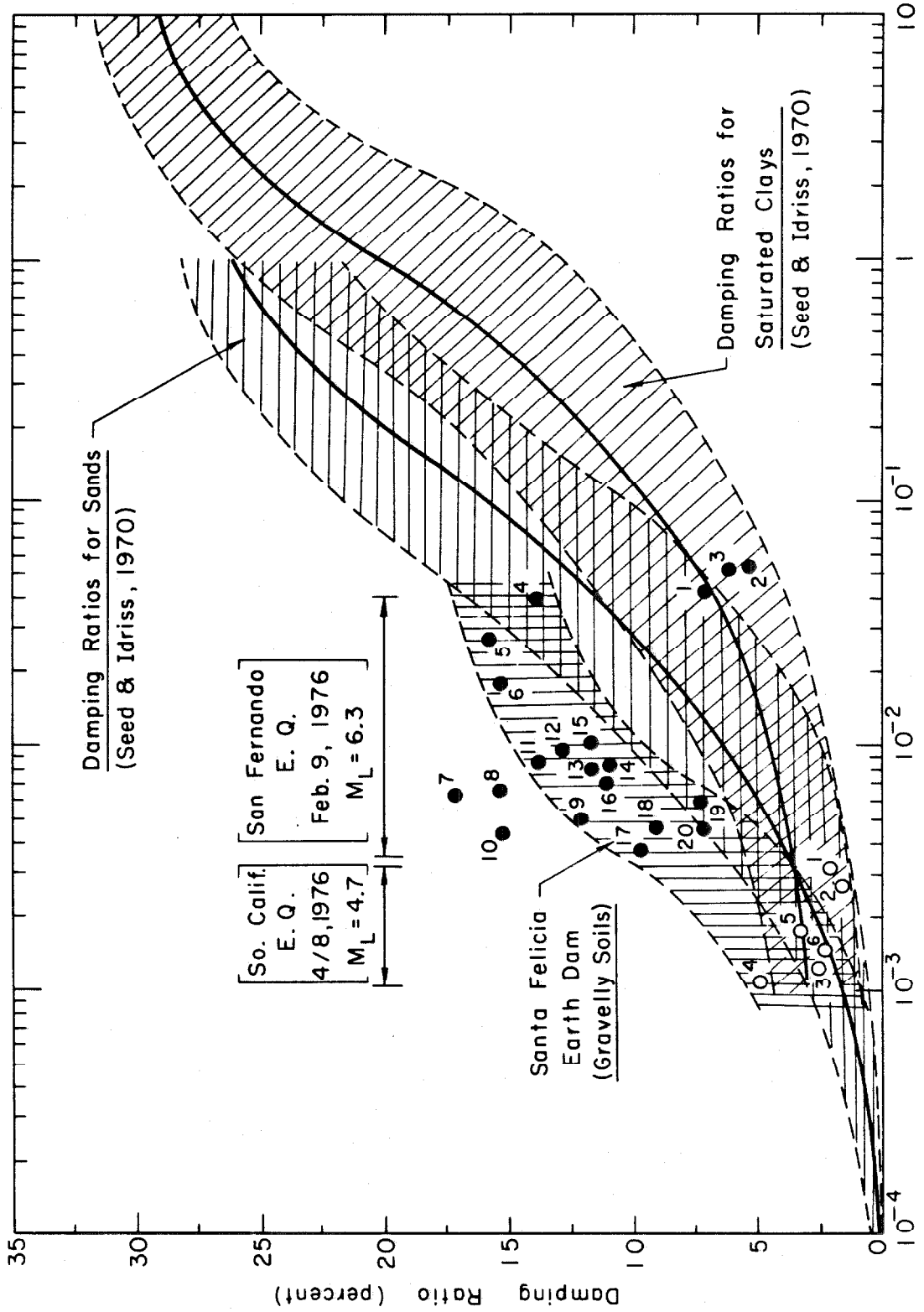
Damping Ratios for Sands
(Seed & Idriss, 1970)
Damping Ratios for
Saturated Clays
(Seed & Idriss, 1970)
[So. Calif. E. Q. 4/8, 1976 M_L = 4.7]
[San Fernando E. Q. Feb. 9, 1976 M_L = 6.3]
Santa Felicia
Earth Dam
(Gravelly Soils)
Damping Ratio (percent)
Shear Strain (percent)
0
5
10
15
20
25
30
35
10^-4
10^-3
10^-2
10^-1
1
10

Fig. 61

CONCLUSIONS

The analyses and the results presented in this investigation lead to the following conclusions concerning the seismic behavior of an earth dam:

1 - Since an earthquake is an occurrence that can never be exactly repeated, it is recommended that not less than four strong-motion accelerographs be installed on and around major dams. Two of these should be located to record earthquake motions at the base and two to measure dam response. The purpose of requiring two instruments is to provide backup to obtain useful information in the event of instrument malfunction (Bolt and Hudson, 1975) such as the double exposure situation which occurred during the 1971 San Fernando earthquake at Santa Felicia Dam.

2 - Amplification spectra are good criteria to indicate the natural frequencies of the structure and to estimate the relative contribution of different modes.

3 - A visual inspection of the amplification spectra obtained from the 1971 San Fernando and the 1976 Southern California earthquakes revealed that the values of the resonant or natural frequencies vary slightly from one earthquake to the other.

4 - The amplification spectra also showed that the dam responded primarily in its fundamental mode in the upstream/downstream direction. The peak amplification ratio of horizontal acceleration at the dam crest to that of the

base is 1:13 for the large earthquake, and 1:4 for the small earthquake, in a normal direction to the dam axis; i.e., the rate of amplification in that direction increases with the intensity of earthquake shaking over this range of intensity.

5 - The other two directional components indicate similar amplification patterns, but they are lacking pronounced single peaks.

6 - Very narrow band-pass filtering, around the fundamental frequency, is needed to obtain a good hysteresis loop, if the dam is treated as a single-degree-of-freedom hysteretic oscillator.

7 - The comparison of the computed natural frequencies using existing shear-beam theories, with those obtained from observed records shows that these dynamic characteristics can be evaluated by the existing theories.

8 - Although the assumption of elastic behavior during earthquakes is not strictly correct for earth dams, it provides a basis for establishing the natural frequencies of the dam, and it gives at least a qualitative picture of the dynamic response characteristics of the dam. Therefore, the earthquake response of a massive structure, such as an earth dam, can be approximated by using the existing elastic-response theories.

9 - The shear modulus and the damping factor obtained from the hysteresis loop depend on the magnitude of the strain for which the hysteresis loop is determined.

10 - Data obtained from the wave-velocity measurements of the dam materials indicated that the dam consists of mainly cohesionless materials where the shear modulus varies with the confining pressure (or the depth below the crest).

11 - Damping effect increases with the intensity of vibration.

12 - Estimation of shear moduli and damping factors of the dam materials is possible from the earthquake records of the dam.

13 - From the comparison between the obtained results and previously available data for dense sand, it seems that at lower and medium strain levels, the two results for the shear modulus correlate very well; however at the higher strains, the shear moduli obtained in this investigation for the gravelly materials of the dam decrease in a manner dissimilar to that suggested by Seed and Idriss (1970) for sand. The comparison also shows that the damping ratios for gravelly soils are somewhat higher than those obtained for sands.

14 - Finally, the data presented here are likely to provide reasonable estimates of the shear moduli and damping factors for the gravelly materials of Santa Felicia Dam.

REFERENCES

1 - Price, W. P., Jr., "Technical Record of Design and Construction, Santa Felicia Dam", United Water Conservation District of Ventura County, California, Santa Paula, California (1956). [Caltech Earthquake Engineering Library Call No. 3.2.2b PR 1956].

2 - Correspondence between Professor George Housner of the California Institute of Technology and the United Water Conservation District of Ventura County, California [Caltech Earthquake Engineering Library Call No. 10.1.8a].

3 - Martin, G.R., "The Response of Earth Dams to Earthquakes", Ph.D. Theses, 1965, Civil Engineering Department, University of California, Berkeley.

4 - Seed, H.B. and Idriss, I.M. (1970), "Soil Moduli and Damping Factors for Dynamic Response Analyses", Report No. EERC 70-10, December, College of Engineering, University of California, Berkeley.

5 - Hudson, D.E., Editor, "Strong-Motion Instrumental Data on the San Fernando Earthquake of Feb. 9, 1971, Earthquake Engineering Research Laboratory, California Institute of Technology, Sept. 1971.

6 - "Strong-Motion Earthquake Accelerograms, Corrected Accelerograms and Integrated Ground Velocity and Displacement Curves, Vol. II, Part E," Earthquake Engineering Research Laboratory Report EERL 73-50, California Institute of Technology, 1973.

7 - "Seismic Engineering Program Report", April-June 1976, Geological Survey Circular 736-B, U.S. Department of the Interior, 1976.

8 - Mononobe, N., Takata, A., and Matumura, M. (1936), "Seismic Stability of the Earth Dam", Second Congress on Large Dams, Washington, 1936, Vol. IV, pp. 435-442.

9 - Hatanaka, M. (1955), "Fundamental Considerations on the Earthquake Resistant Properties of the Earth Dam", Disaster Prevention Research Institute, Kyoto University, Bulletin No. 11, Dec. 1955.

10 - Ambraseys, N.N. (1960a), "On the Seismic Behavior of Earth Dams", Proceedings of the Second World Conference on Earthquake Engineering, Japan, 1960, Vol. I, pp. 331-354.

11 - Ambraseys, N.N. (1960b), "On the Shear Response of a Two Dimensional Wedge Subjected to an Arbitrary Disturbance", Bulletin of the Seismological Society of America, Vol. 50, Jan. 1960, pp. 45-56.

12 - Minami, I., (1960), "A Consideration of Earthquake Proof Design Methods for Earth Dams", Proceedings of the Second World Conference on Earthquake Engineering, Japan, 1960, Vol. III, pp. 1061-1074.

13 - Rashid, Y.R. (1961), "Dynamic Response of Earth Dams to Earthquakes", Graduate Student Research Report, University of California, Berkeley, 1961.

14 - Keightley, W.O. (1964), "A Dynamic Investigation of Bouquet Canyon Dam", Earthquake Engineering Research Laboratory, California Institute of Technology, Sept. 1964.

15 - Jacobsen, L.S., "Steady Forced Vibration as Influenced by Damping", Transaction A.S.C.E. APM-52-15, 1930.

16 - Seed, H.B. and Idriss, I.M., "Influence of Soil Conditions on Ground Motions During Earthquakes", Proceedings ASCE, Journal of Soil Mechanics and Foundations Division, SM1, Jan. 1969, pp. 99-137.

17 - Kawakami, F. and Asada, A., "Earthquake Response of an Earth Dam", The Technology Reports of the Tohoku University, Vol. 32 (1967) No.2, June 1967, pp. 247-174.

18 - Iemura, H. and Jennings, P.C., "Hysteretic Reponse of a Nine-Story Reinforced Concrete Building During the San Fernando Earthquake", Earthquake Engineering Research Laboratory, Report No. EERL 73-07, California Institute of Technology, Oct. 1973.

19 - Mori, Y. and Kawakami, F., "Dynamic Properties of the Ainono Earth Dam and Ushino Rock-Fill Dam", Transactions of JSCE, Vol. 7, 1975, pp. 122-123.

20 - Bolt, B.A. and Hudson, D.E., "Seismic Instrumentation of Dams", ASCE, Journal of the Geotechnical Engineering Division, Nov. 1975, pp. 1095-1104.

21 - Morrison, P., Maley, R., Brady, G. and Prcella, R., "Earthquake Recordings on or Near Dams", Report, USCOLD Committee on Earthquakes, Printed at California Institute of Technology, Pasadena, November 1977.

D. APPENDICES

APPENDIX A

Standard Data Processing of the Southern California Earthquake of April 8, 1976

Santa Felicia Dam (Ventura County, California)

This appendix contains the computed plots of:

1 - Volume I which contains the uncorrected digitized accelerograms,
2 - Volume III which contains the response spectrum curves with linear and three-way logarithmic plots,
3 - Volume IV which contains Fourier amplitude spectra with linear and logarithmic plots.

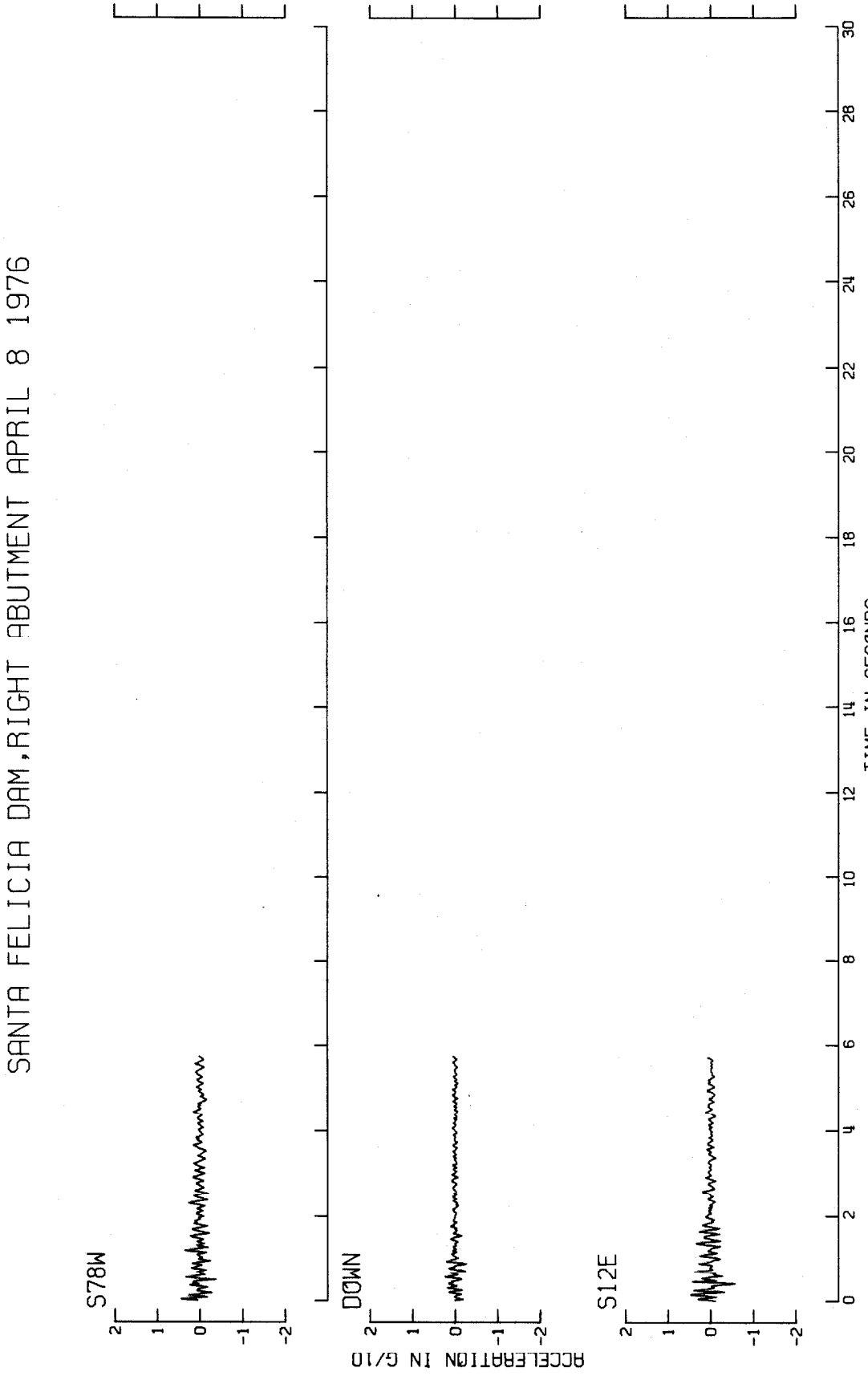
SANTA FELICIA DAM, RIGHT ABUTMENT APRIL 8 1976
S78W
DOWN
S12E
ACCELERATION IN G/10
TIME IN SECONDS
2
1
0
-1
-2
0
2
4
6
8
10
12
14
16
18
20
22
24
26
28
30

Fig. A-1

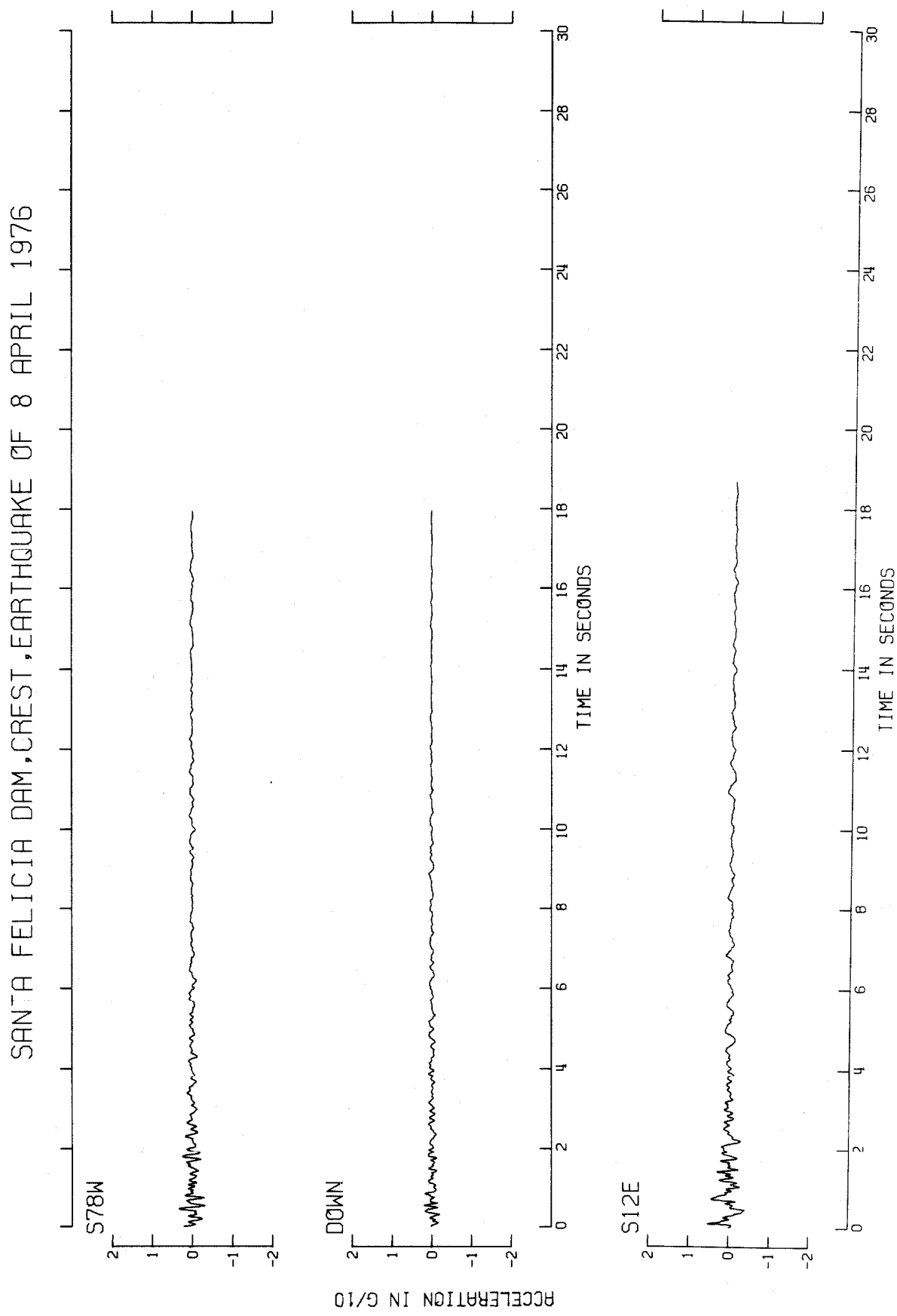
SANTA FELICIA DAM, CREST, EARTHQUAKE OF 8 APRIL 1976
S78W
DOWN
S12E
ACCELERATION IN G/10
TIME IN SECONDS
TIME IN SECONDS

Fig. A-2

RESPONSE SPECTRUM

SANTA FELICIA DAM,CREST,E/Q OF APRIL 8 1976-0721 PST

SANTA FELICIA DAM,CREST COMP S12E

DAMPING VALUES ARE 0, 2, 5, 10 AND 20 PERCENT OF CRITICAL

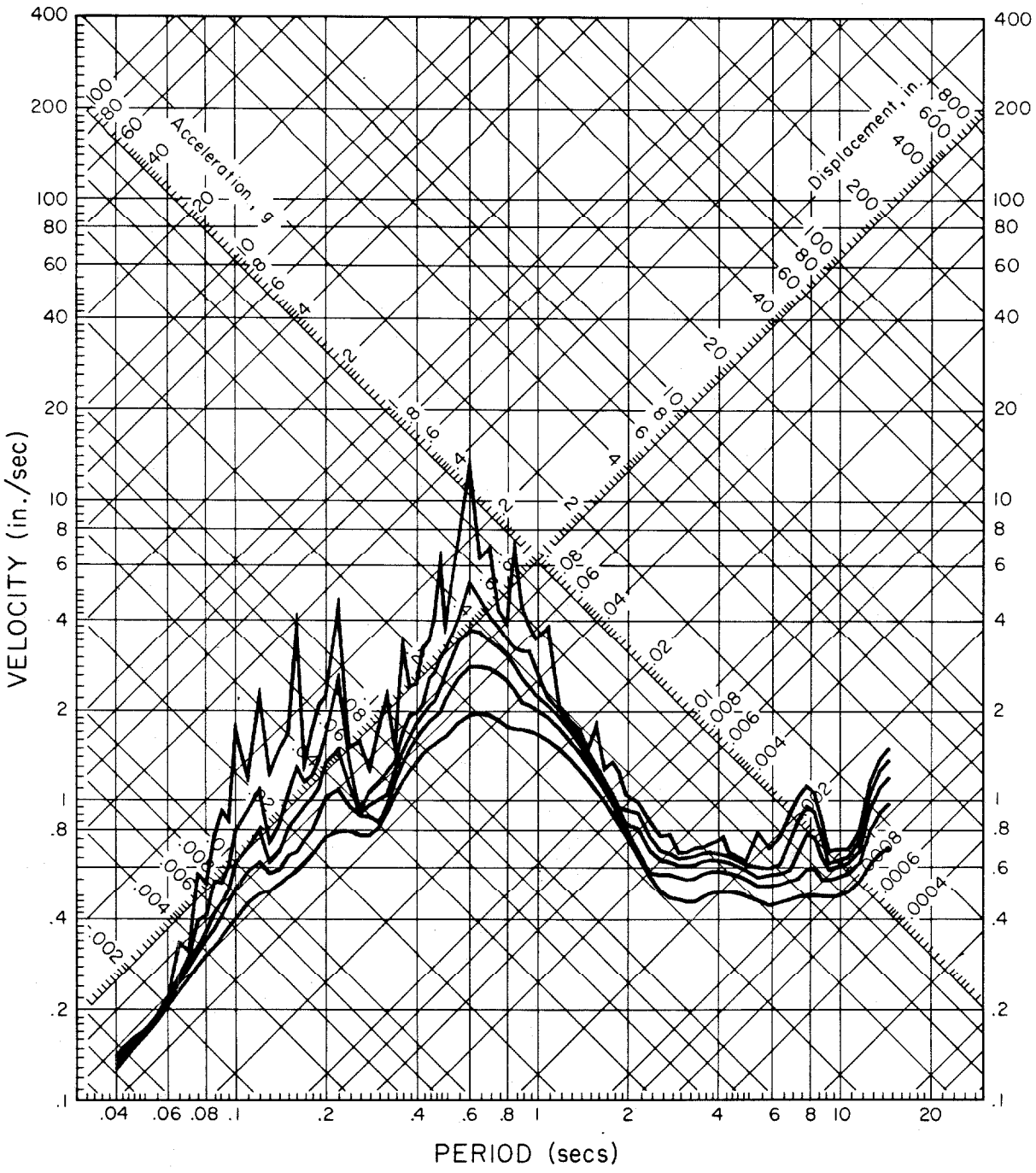

Fig. A-3

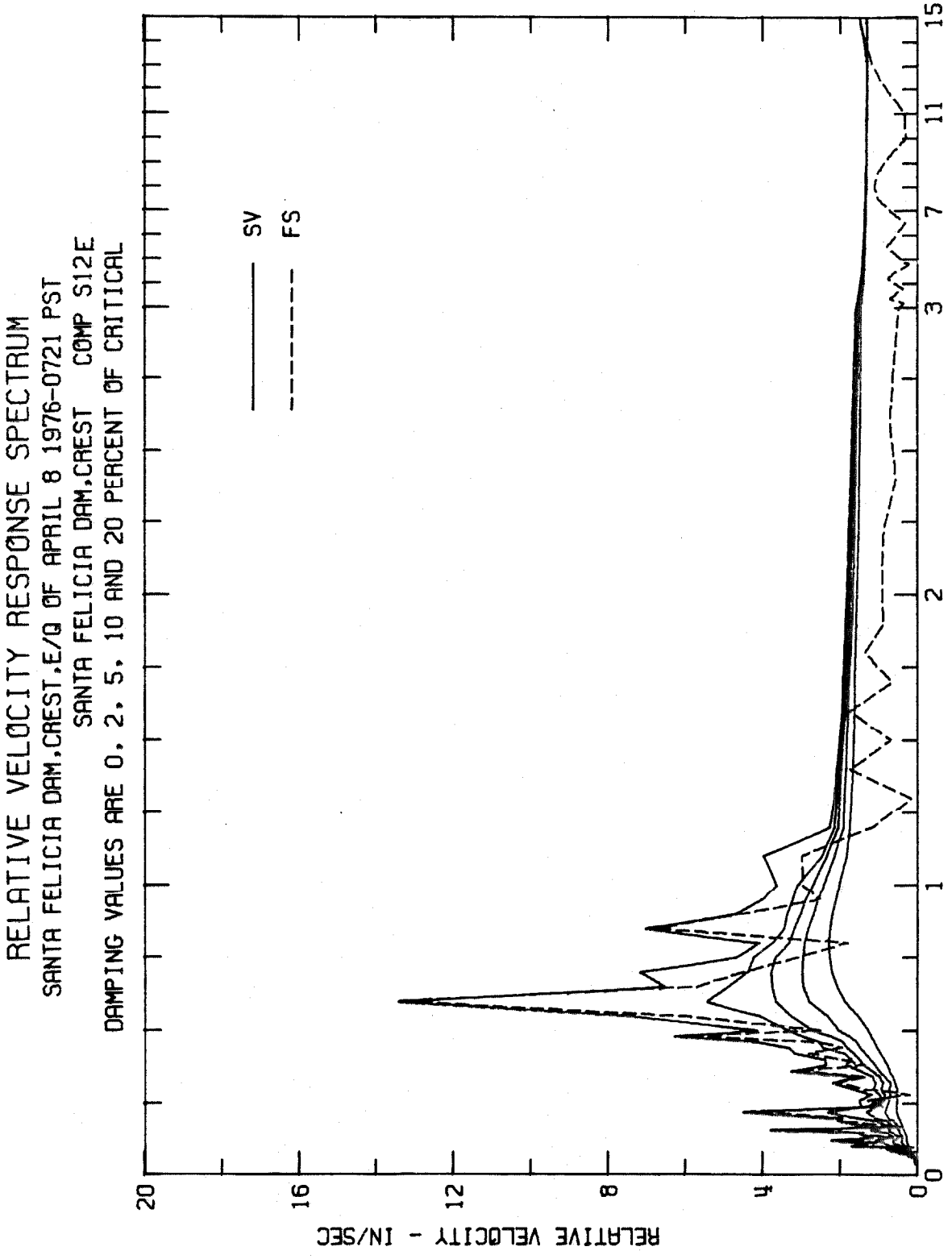
RELATIVE VELOCITY RESPONSE SPECTRUM
SANTA FELICIA DAM,CREST,E/Q OF APRIL 8 1976-0721 PST
SANTA FELICIA DAM,CREST COMP S12E
DAMPING VALUES ARE 0, 2, 5, 10 AND 20 PERCENT OF CRITICAL
SV
FS
RELATIVE VELOCITY - IN/SEC
PERIOD - SECONDS
0
4
8
12
16
20
1
2
3
7
11
15

Fig. A-4

RESPONSE SPECTRUM

SANTA FELICIA DAM.CREST,E/Q OF APRIL 8 1976-0721 PST

SANTA FELICIA DAM.CREST COM S78W

DAMPING VALUES ARE 0, 2, 5, 10 AND 20 PERCENT OF CRITICAL

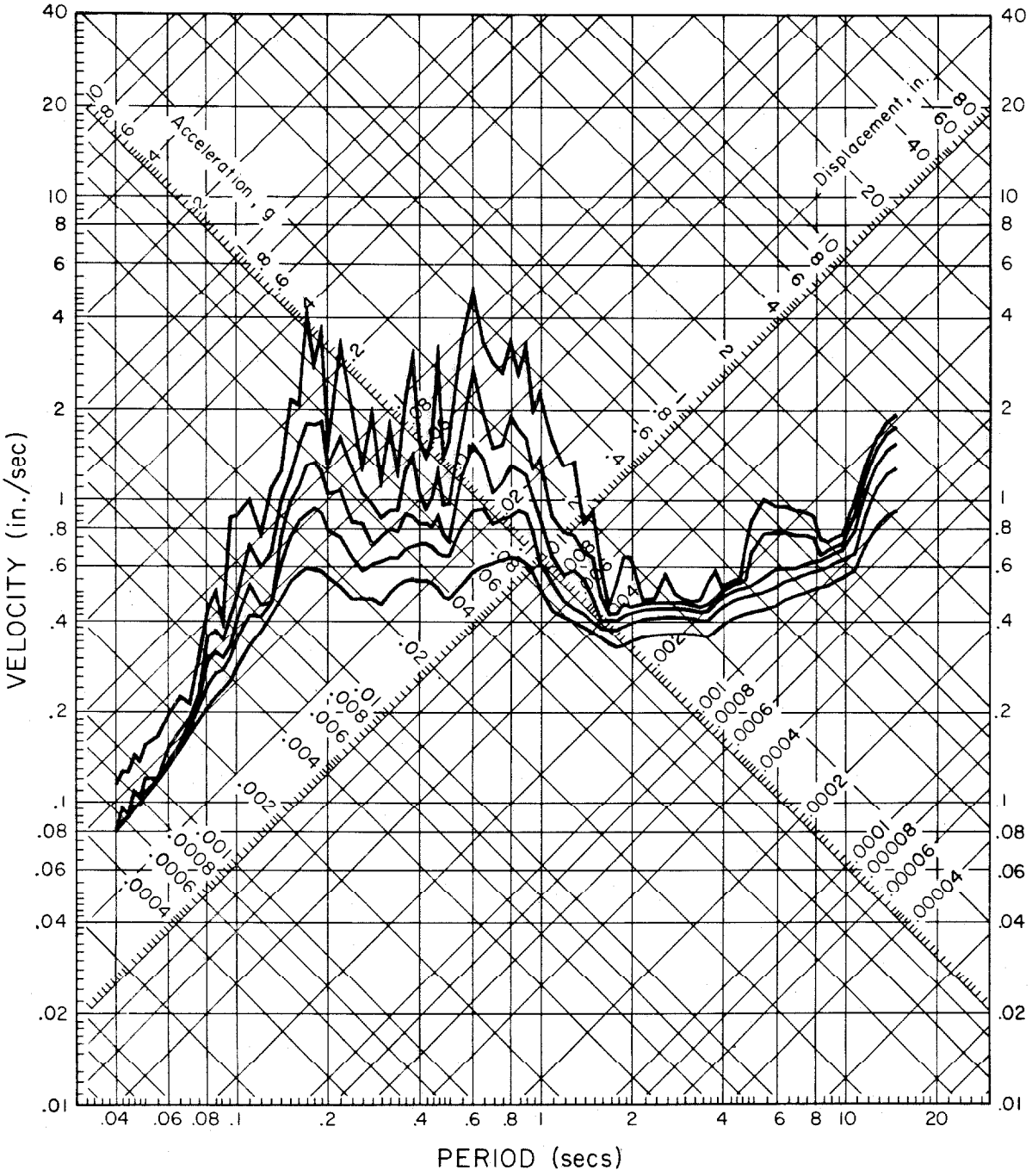

Fig. A-5

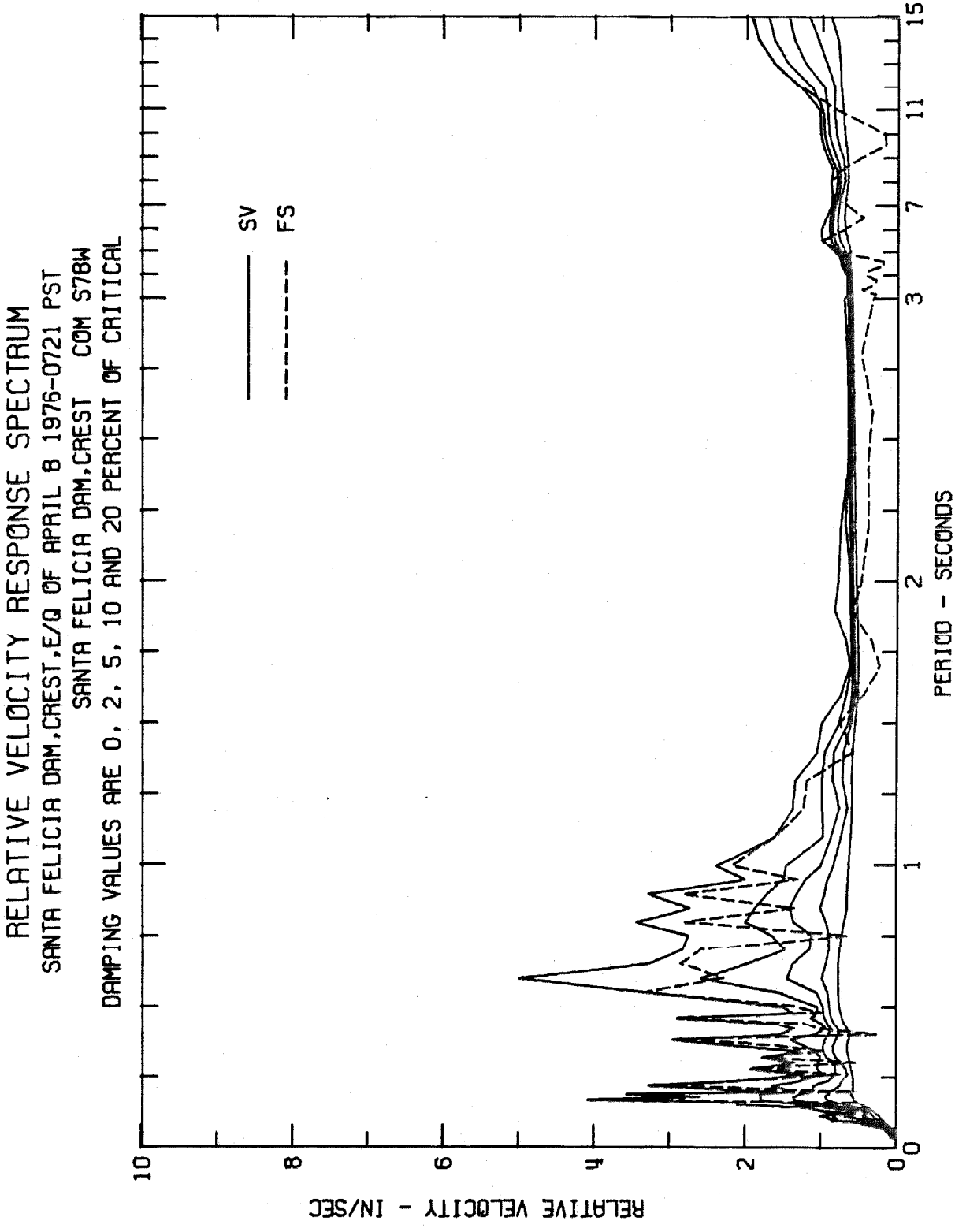
RELATIVE VELOCITY RESPONSE SPECTRUM
SANTA FELICIA DAM,CREST,E/Q OF APRIL 8 1976-0721 PST
SANTA FELICIA DAM,CREST COM S78W
DAMPING VALUES ARE 0, 2, 5, 10 AND 20 PERCENT OF CRITICAL
SV
FS
RELATIVE VELOCITY - IN/SEC
PERIOD - SECONDS
0
2
4
6
8
10
1
3
7
11
15

Fig. A-6

RESPONSE SPECTRUM

SANTA FELICIA DAM.CREST.E/Q OF APRIL 8 1976-0721 PST

SANTA FELICIA DAM.CREST COM DOWN

DAMPING VALUES ARE 0, 2, 5, 10 AND 20 PERCENT OF CRITICAL

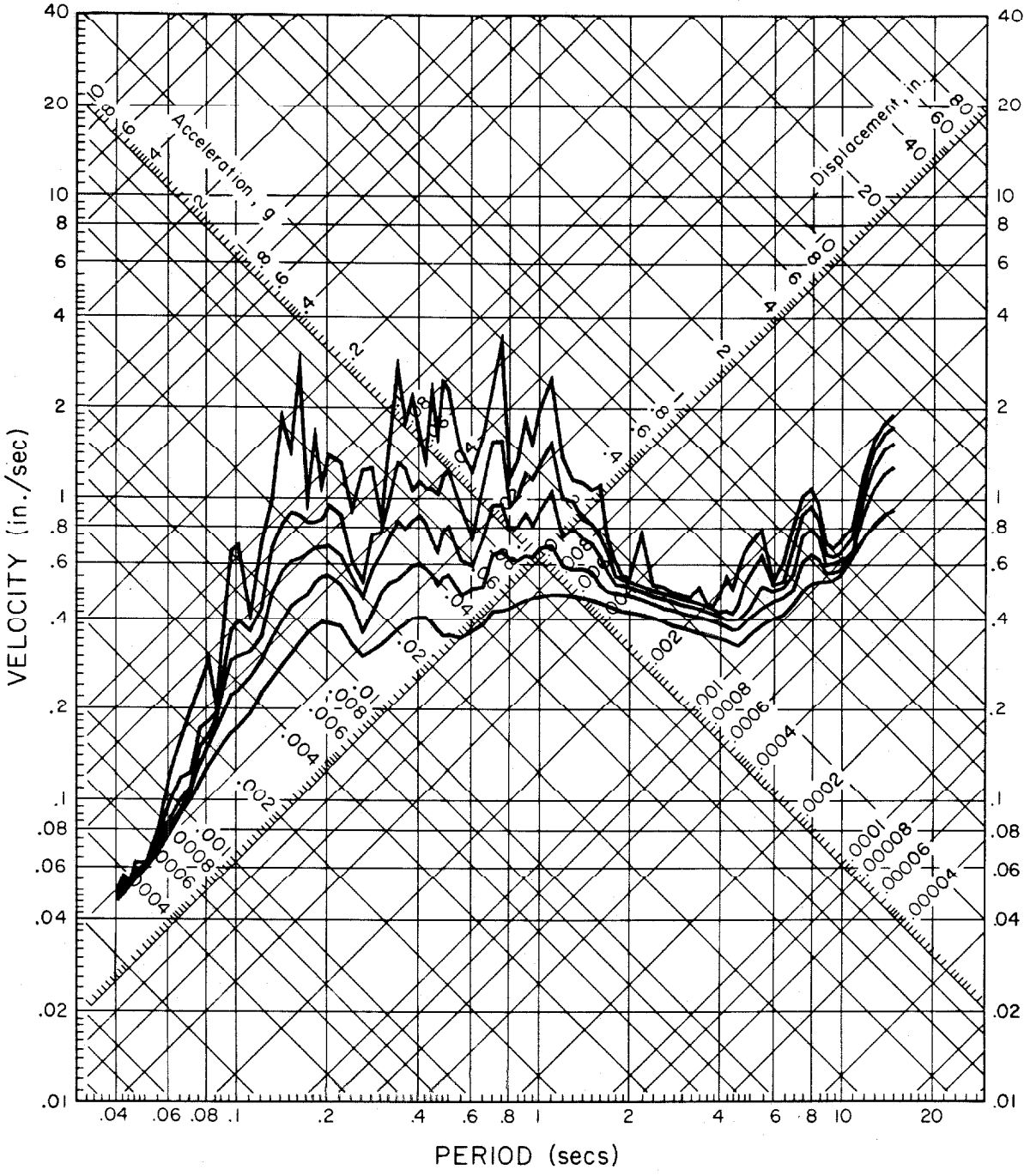

Fig. A-7

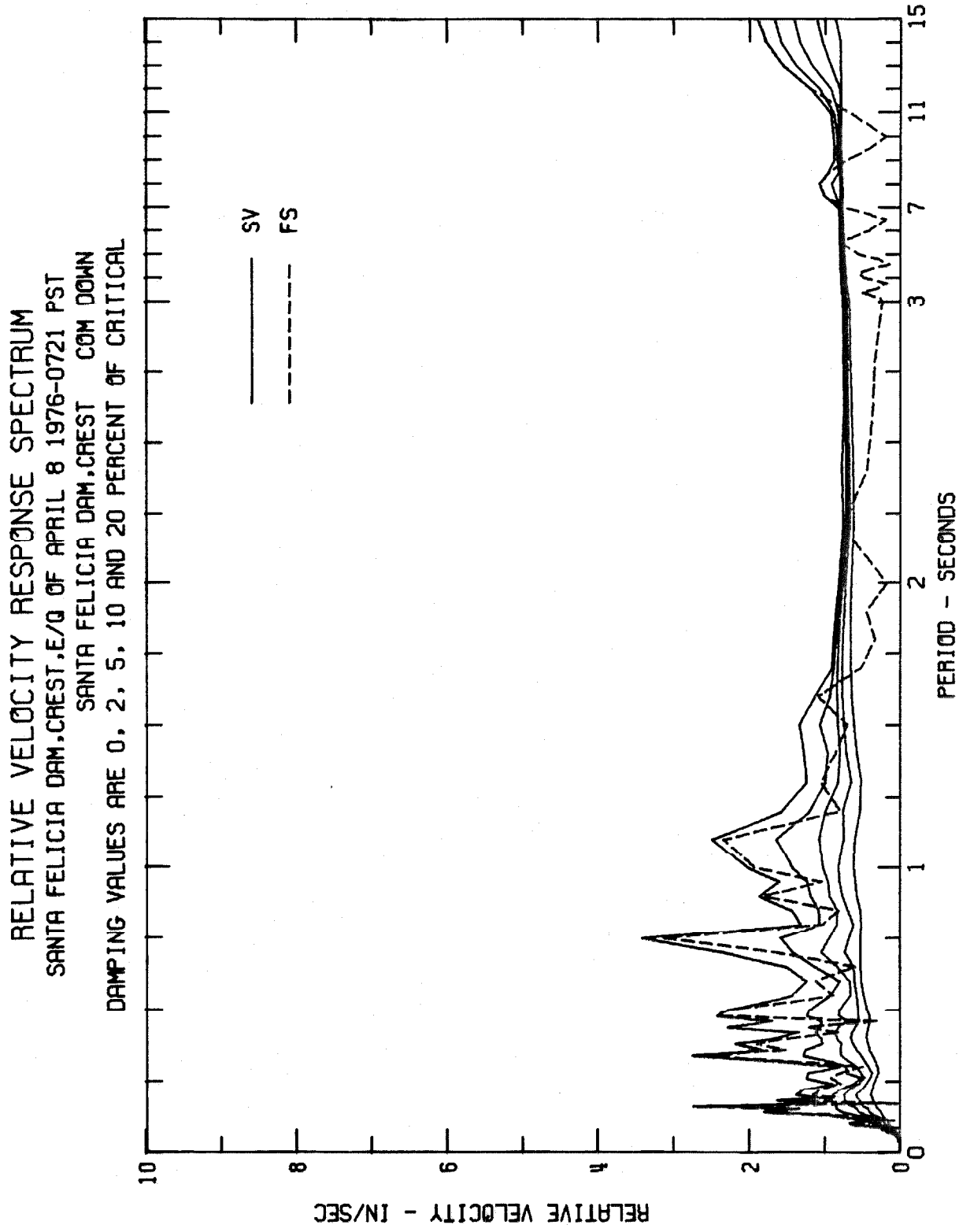
RELATIVE VELOCITY RESPONSE SPECTRUM
SANTA FELICIA DAM,CREST,E/Q OF APRIL 8 1976-0721 PST
SANTA FELICIA DAM,CREST COM DOWN
DAMPING VALUES ARE 0, 2, 5, 10 AND 20 PERCENT OF CRITICAL
SV
FS
RELATIVE VELOCITY - IN/SEC
PERIOD - SECONDS
0
2
4
6
8
10
1
3
7
11
15

Fig. A-8

RESPONSE SPECTRUM

SANTA FELICIA DAM,RIGHT ABUTMENT,E/Q OF APRIL 8 1976-0721 PST

SANTA FELICIA DAM,RIGHT ABUTMENT COMP. S12E

DAMPING VALUES ARE 0, 2, 5, 10 AND 20 PERCENT OF CRITICAL

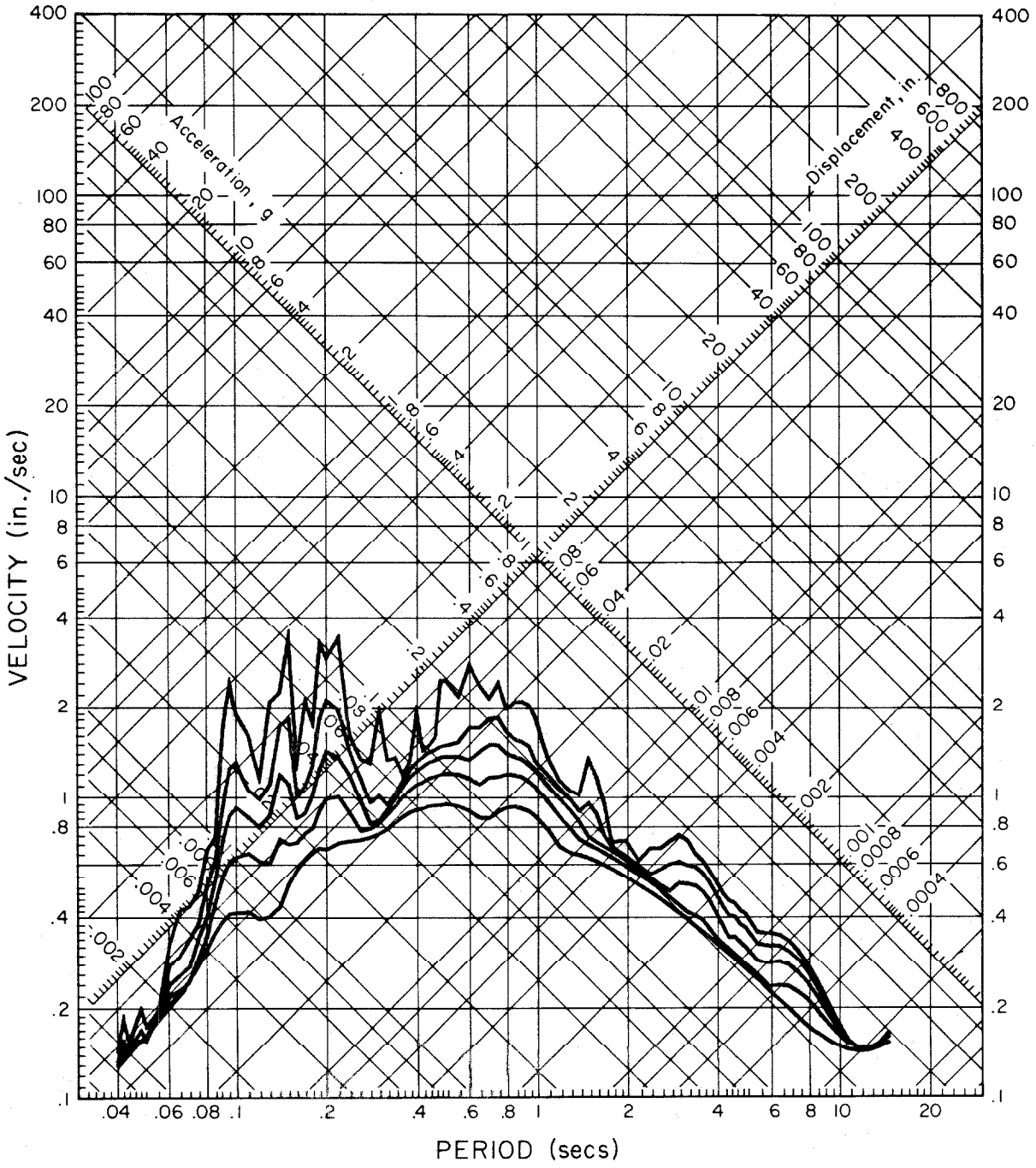

Fig. A-9

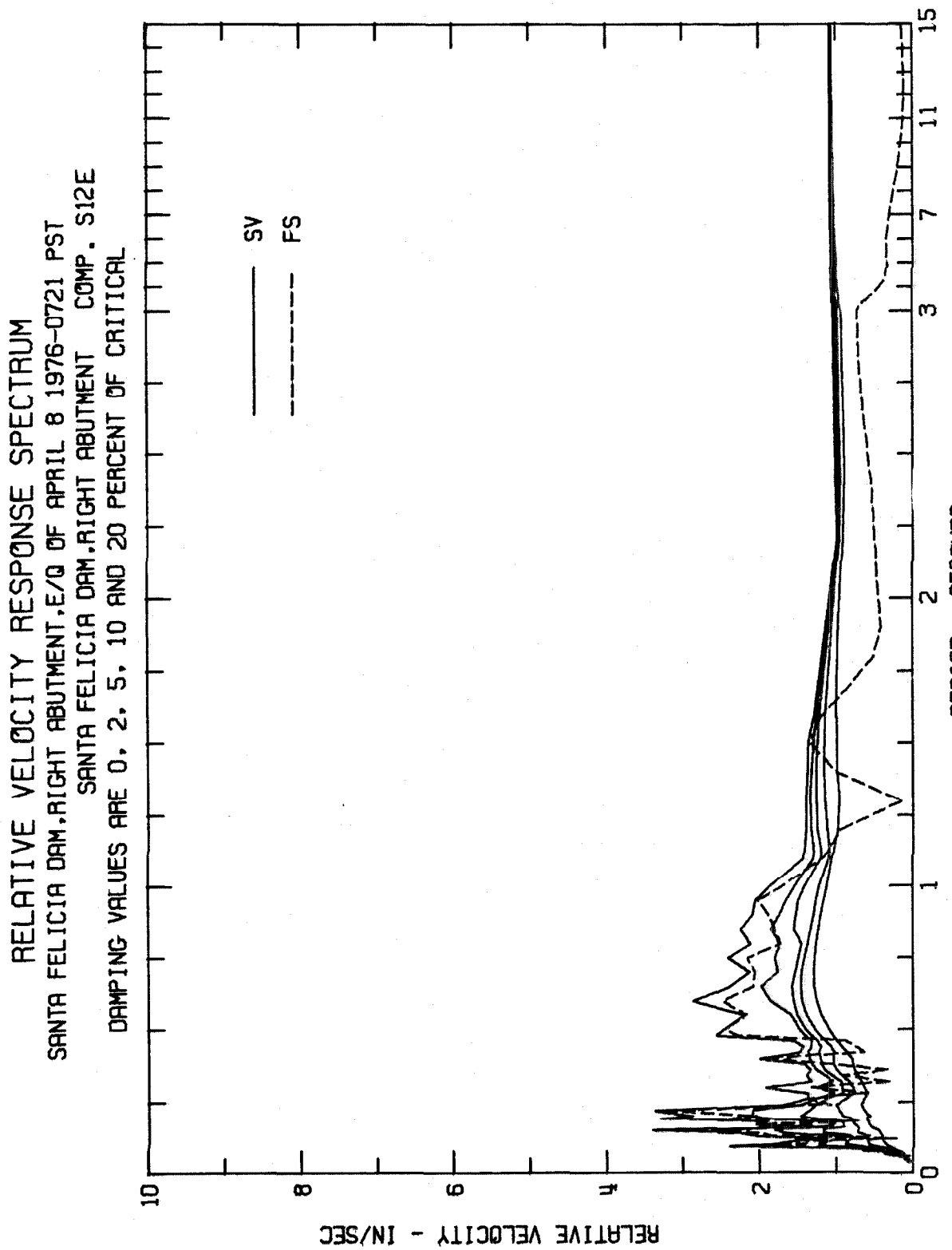
RELATIVE VELOCITY RESPONSE SPECTRUM
SANTA FELICIA DAM,RIGHT ABUTMENT,E/Q OF APRIL 8 1976-0721 PST
SANTA FELICIA DAM,RIGHT ABUTMENT COMP. S12E
DAMPING VALUES ARE 0, 2, 5, 10 AND 20 PERCENT OF CRITICAL
SV
FS
RELATIVE VELOCITY - IN/SEC
PERIOD - SECONDS
0
2
4
6
8
10
1
3
7
11
15

Fig. A-10

RESPONSE SPECTRUM

SANTA FELICIA DAM.RIGHT ABUTMENT.E/Q OF APRIL 8 1976-0721 PST

SANTA FELICIA DAM.RIGHT ABUTMENT COMP. S78W

DAMPING VALUES ARE 0, 2, 5, 10 AND 20 PERCENT OF CRITICAL

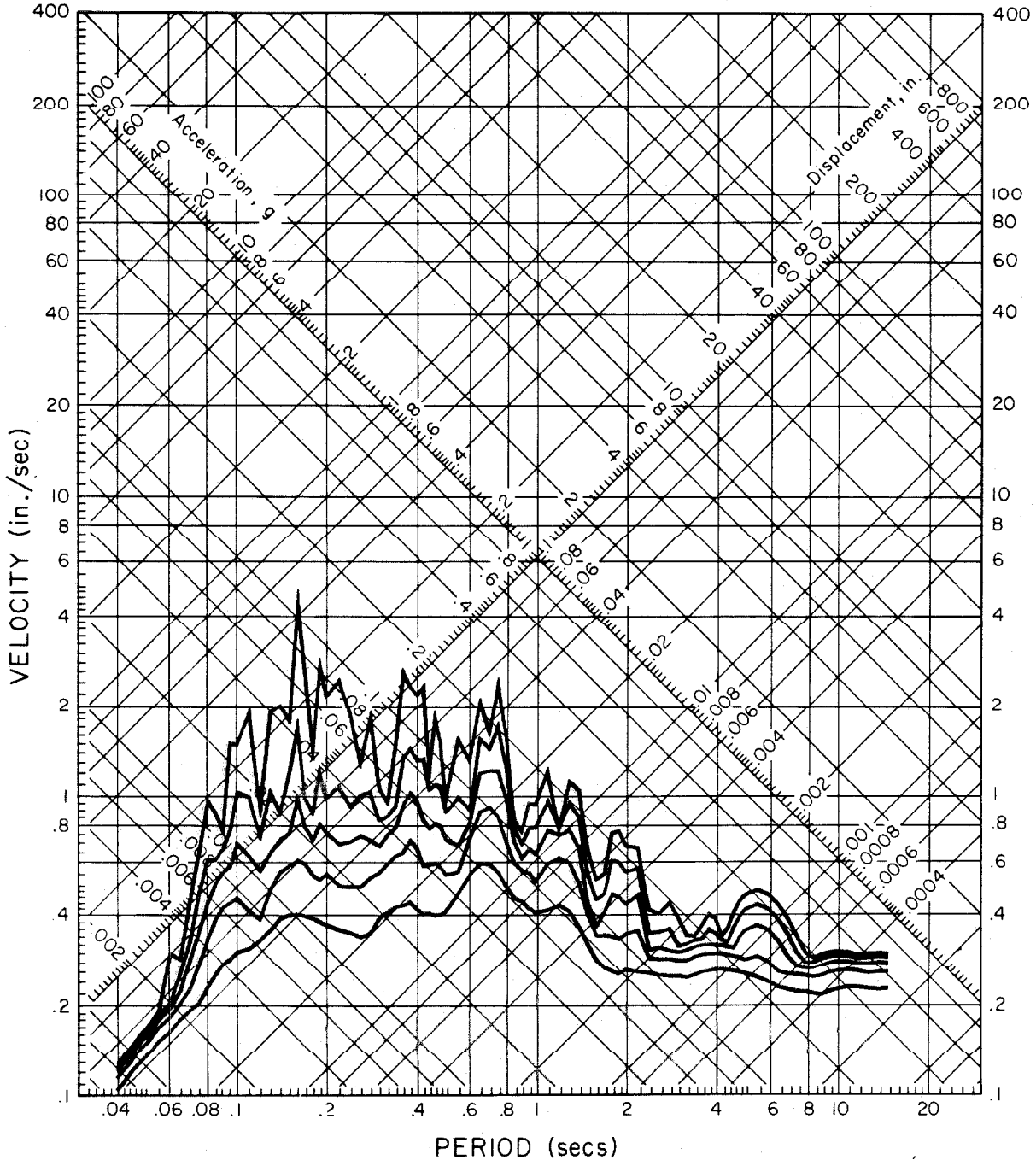

Fig. A-11

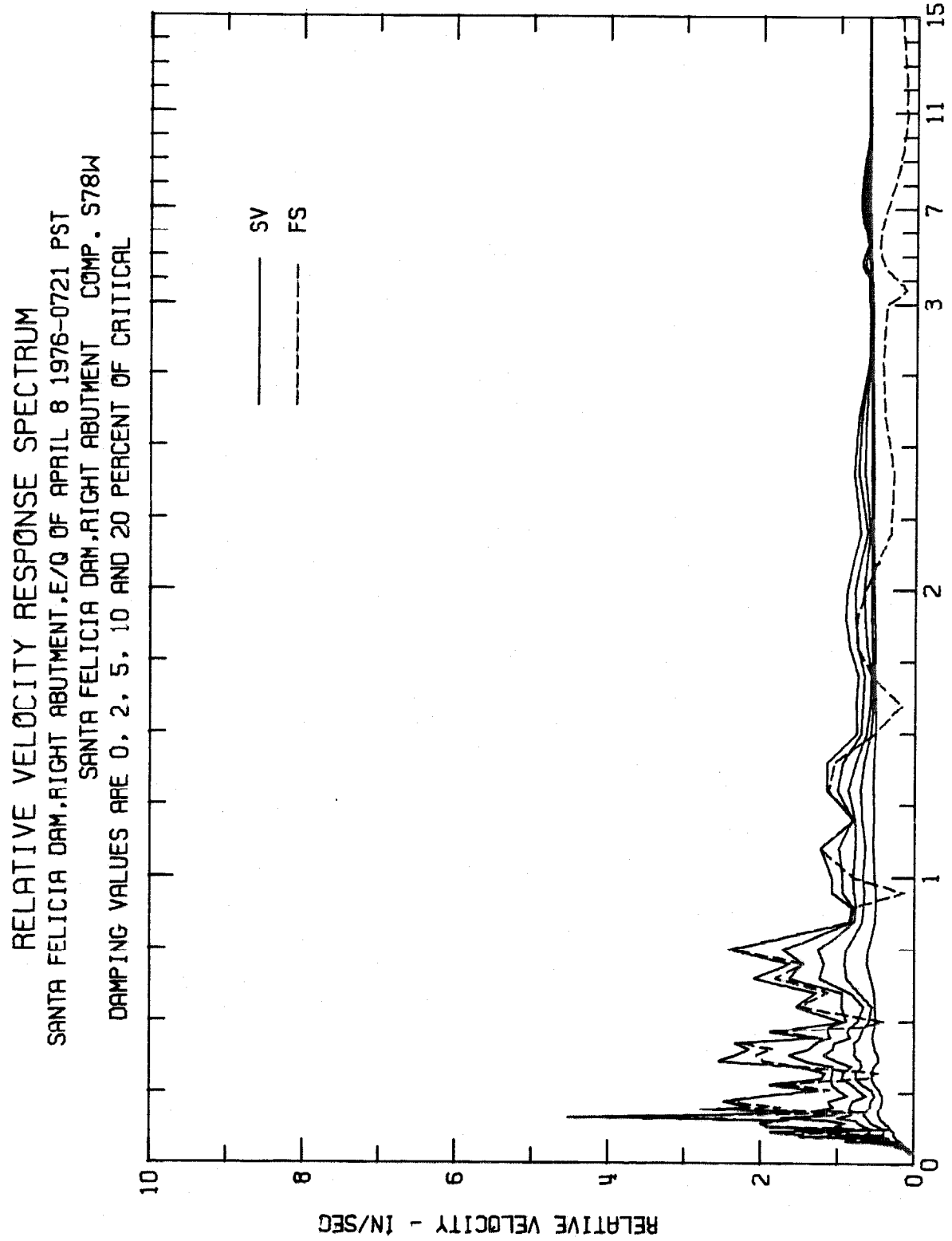
RELATIVE VELOCITY RESPONSE SPECTRUM
SANTA FELICIA DAM,RIGHT ABUTMENT,E/Q OF APRIL 8 1976-0721 PST
SANTA FELICIA DAM,RIGHT ABUTMENT COMP. S78W
DAMPING VALUES ARE 0, 2, 5, 10 AND 20 PERCENT OF CRITICAL
SV
FS
RELATIVE VELOCITY - IN/SEC
PERIOD - SECONDS
0
2
4
6
8
10
1
3
7
11
15

Fig. A-12

RESPONSE SPECTRUM

SANTA FELICIA DAM,RIGHT ABUTMENT,E/Q OF APRIL 8 1976-0721 PST

SANTA FELICIA DAM,RIGHT ABUTMENT COMP. DOWN

DAMPING VALUES ARE 0, 2, 5, 10 AND 20 PERCENT OF CRITICAL

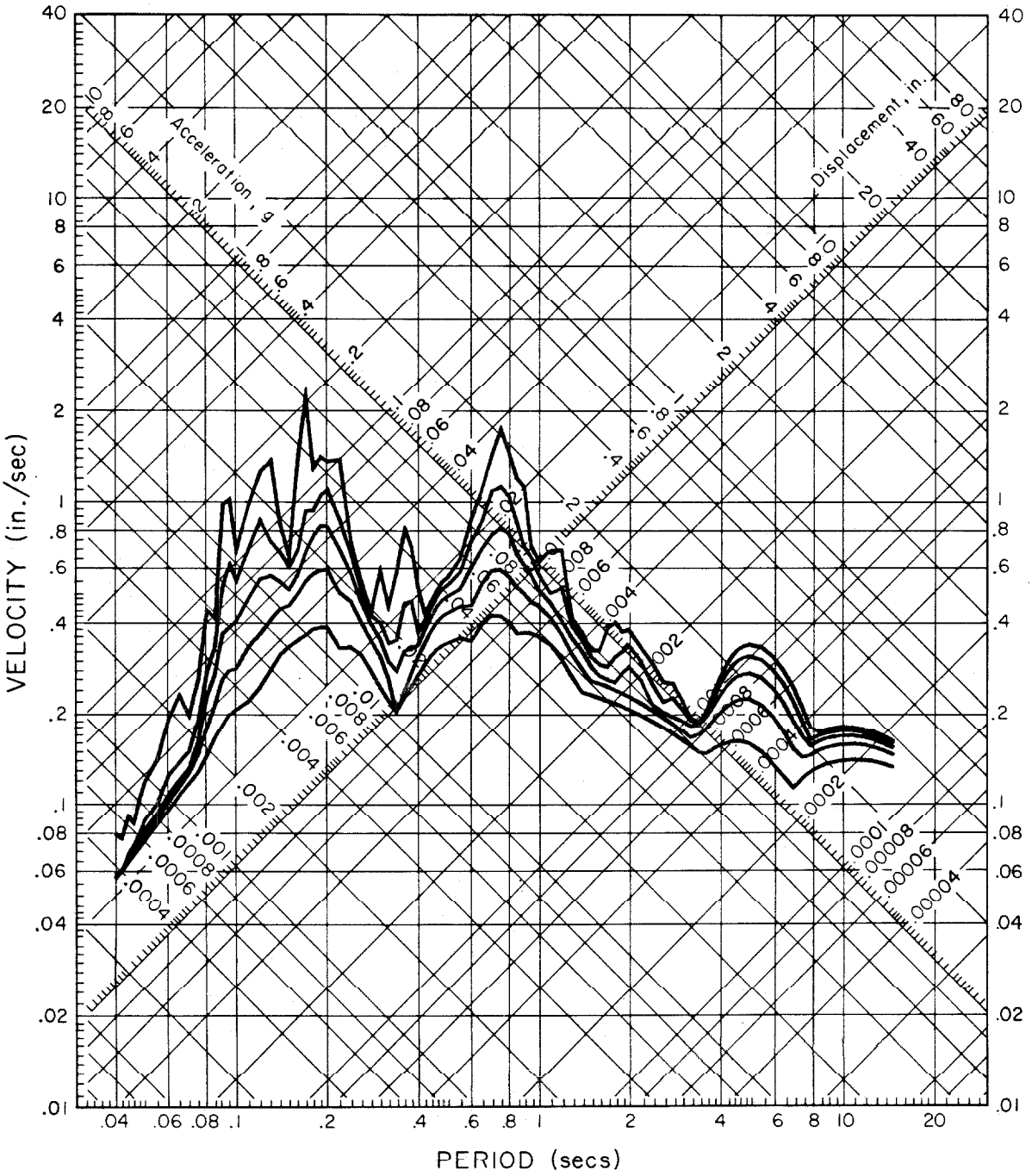

Fig. A-13

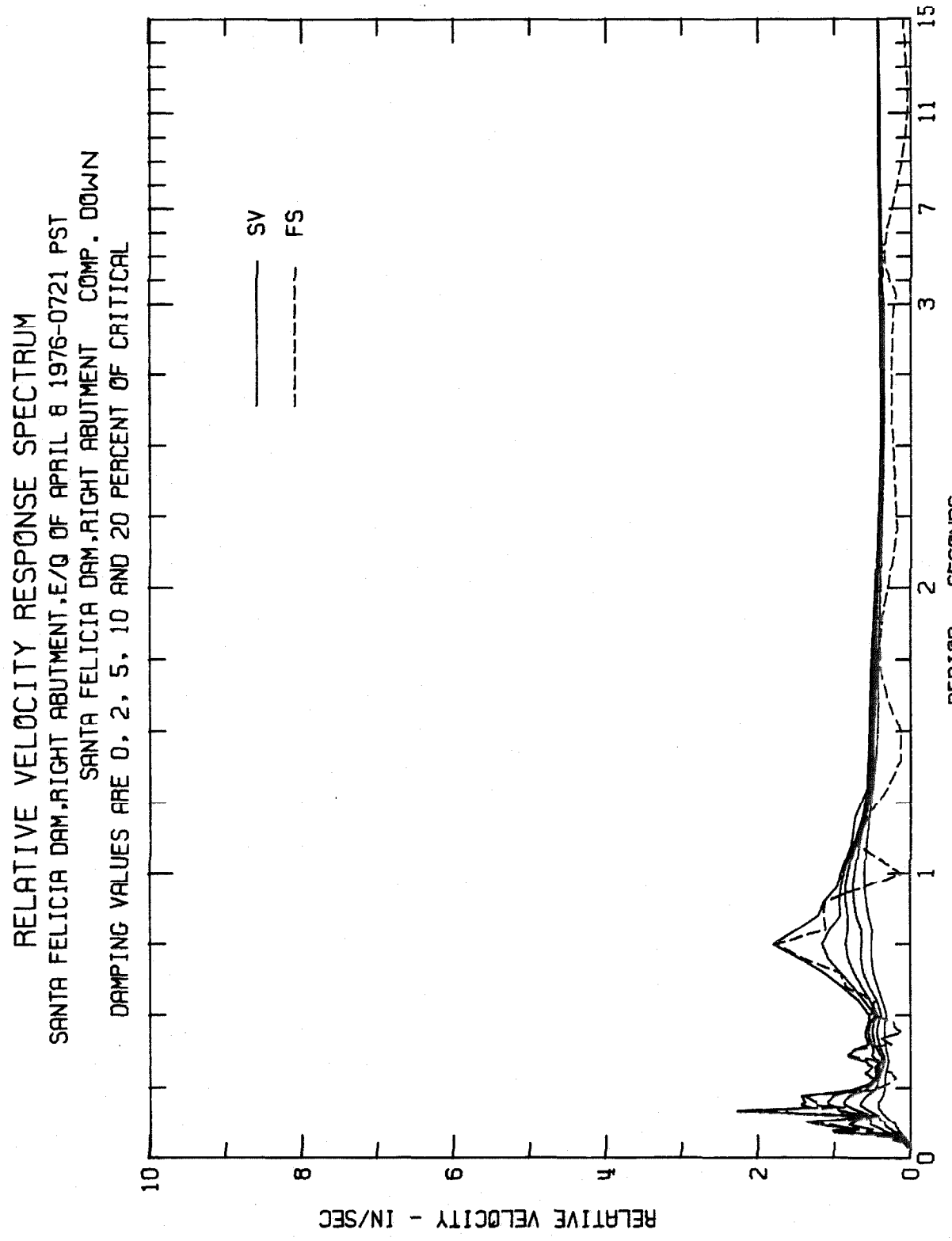
RELATIVE VELOCITY RESPONSE SPECTRUM
SANTA FELICIA DAM,RIGHT ABUTMENT,E/Q OF APRIL 8 1976-0721 PST
SANTA FELICIA DAM,RIGHT ABUTMENT COMP. DOWN
DAMPING VALUES ARE 0, 2, 5, 10 AND 20 PERCENT OF CRITICAL
SV
FS
RELATIVE VELOCITY - IN/SEC
PERIOD - SECONDS
0
2
4
6
8
10
1
3
7
11
15

Fig. A-14

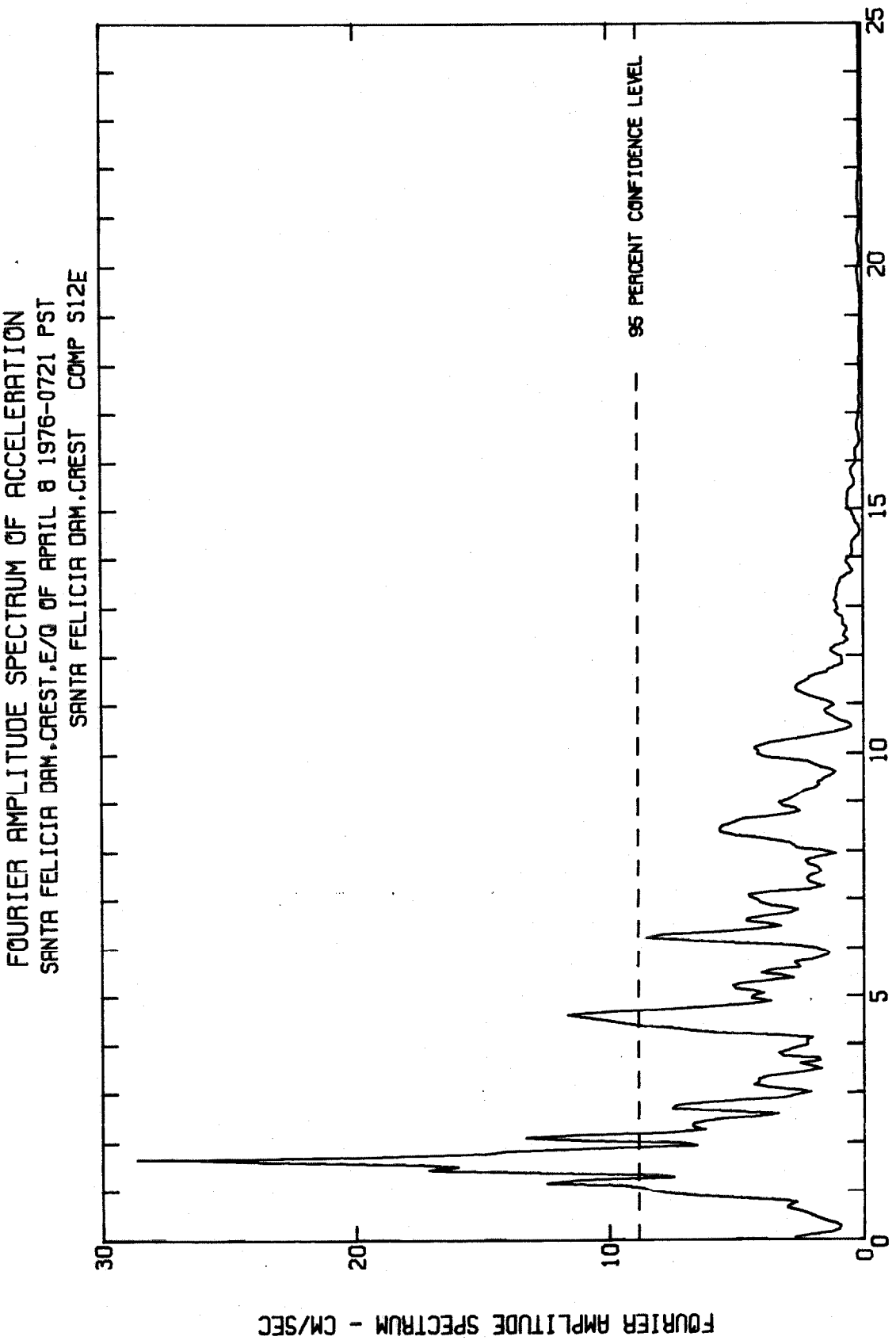
FOURIER AMPLITUDE SPECTRUM OF ACCELERATION
SANTA FELICIA DAM,CREST,E/O OF APRIL 8 1976-0721 PST
SANTA FELICIA DAM,CREST COMP S12E
95 PERCENT CONFIDENCE LEVEL
FOURIER AMPLITUDE SPECTRUM - CM/SEC
FREQUENCY - CPS
0
5
10
15
20
25
0
10
20
30

Fig. A-15

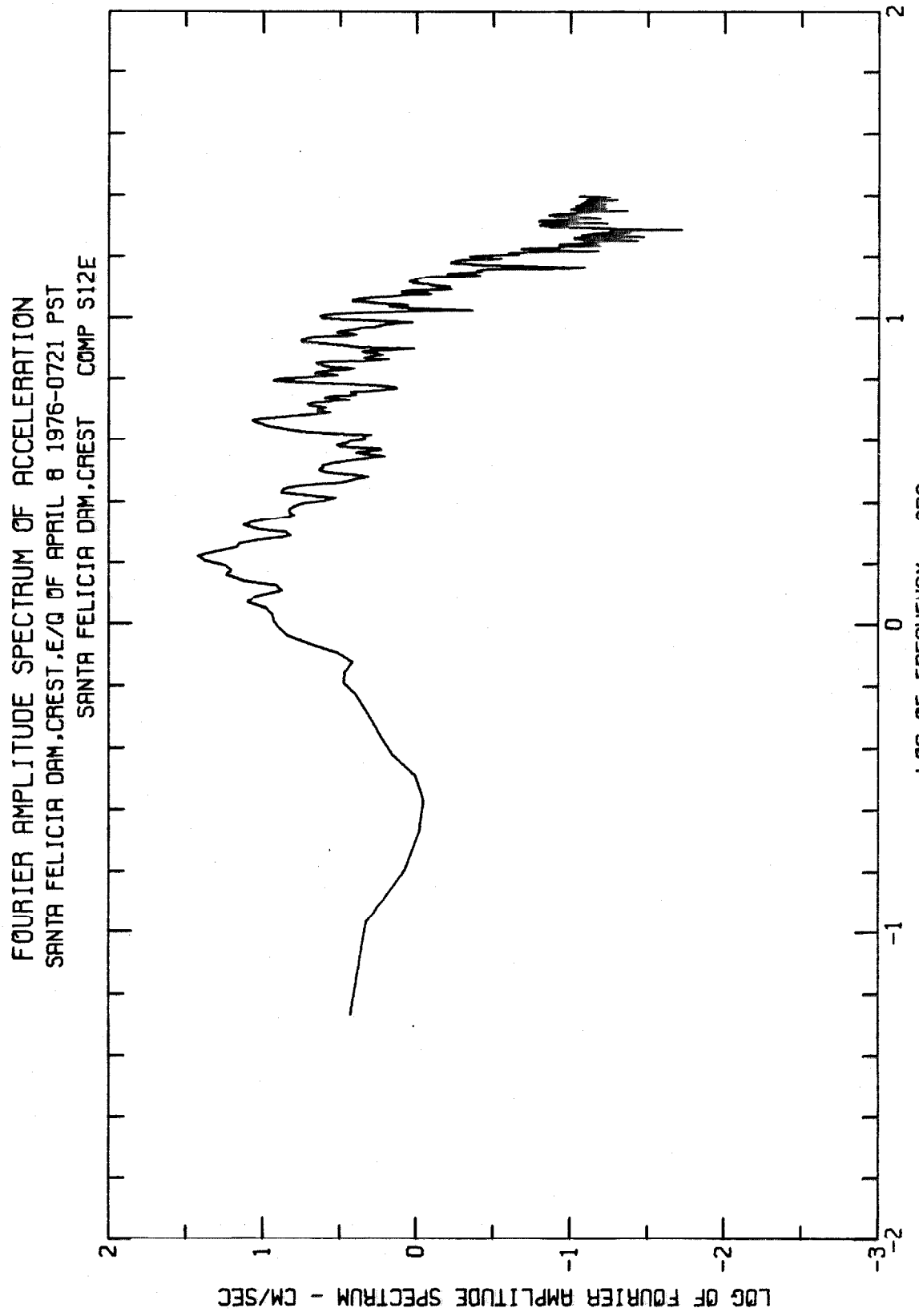
FOURIER AMPLITUDE SPECTRUM OF ACCELERATION
SANTA FELICIA DAM,CREST,E/O OF APRIL 8 1976-0721 PST
SANTA FELICIA DAM,CREST COMP S12E
LOG OF FOURIER AMPLITUDE SPECTRUM - CM/SEC
LOG OF FREQUENCY - CPS
2
1
0
-1
-2
-3
2
1
0
-1
-2

Fig.A-16

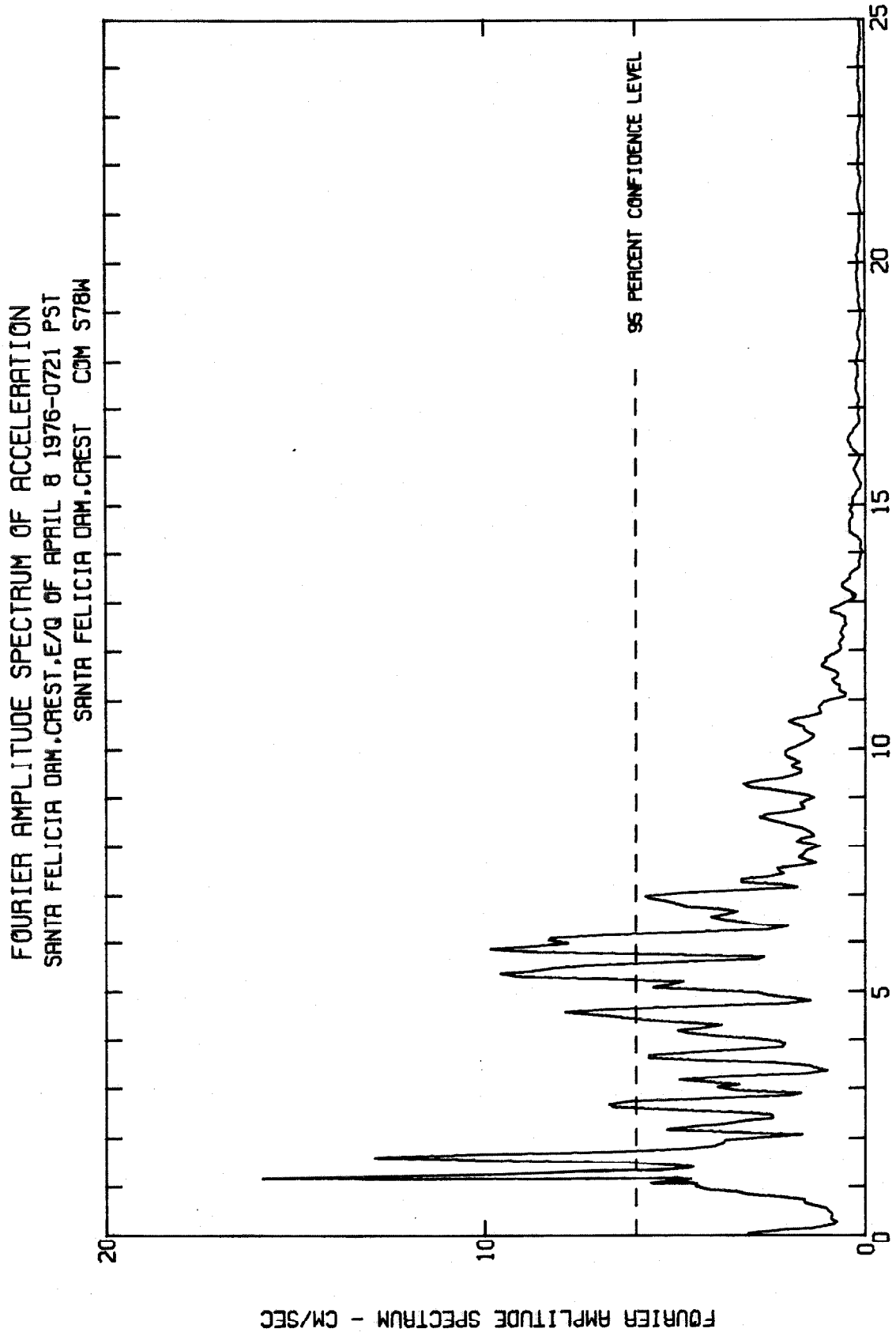
FOURIER AMPLITUDE SPECTRUM OF ACCELERATION
SANTA FELICIA DAM,CREST,E/O OF APRIL 8 1976-0721 PST
SANTA FELICIA DAM,CREST COM S78W
95 PERCENT CONFIDENCE LEVEL
FOURIER AMPLITUDE SPECTRUM - CM/SEC
FREQUENCY - CPS
0
5
10
15
20
25
0
10
20

Fig. A-17

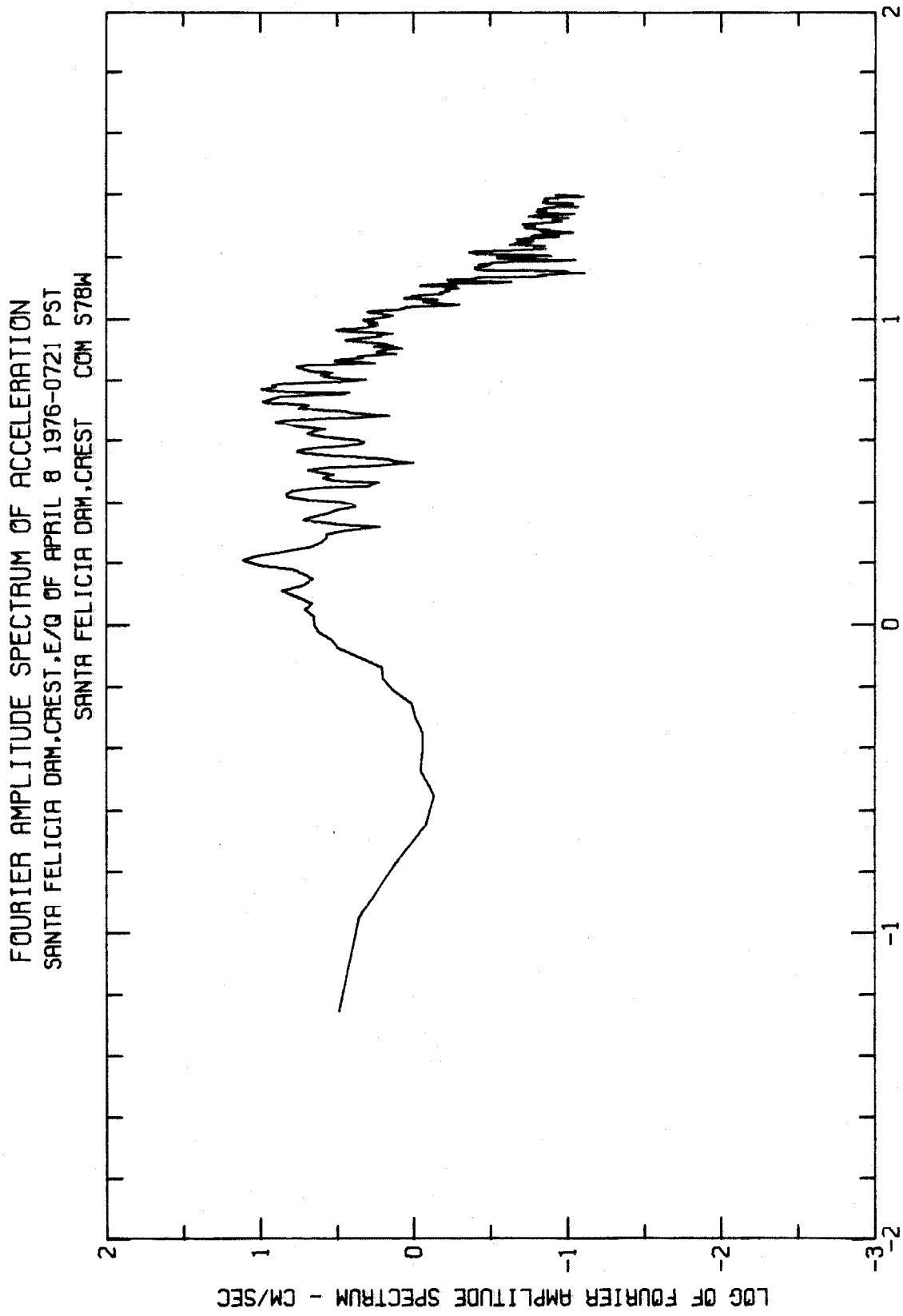
FOURIER AMPLITUDE SPECTRUM OF ACCELERATION
SANTA FELICIA DAM,CREST,E/Q OF APRIL 8 1976-0721 PST
SANTA FELICIA DAM,CREST COM S78W
LOG OF FOURIER AMPLITUDE SPECTRUM - CM/SEC
LOG OF FREQUENCY - CPS
2
1
0
-1
-2
-3
2
1
0
-1
-2

Fig. A-18

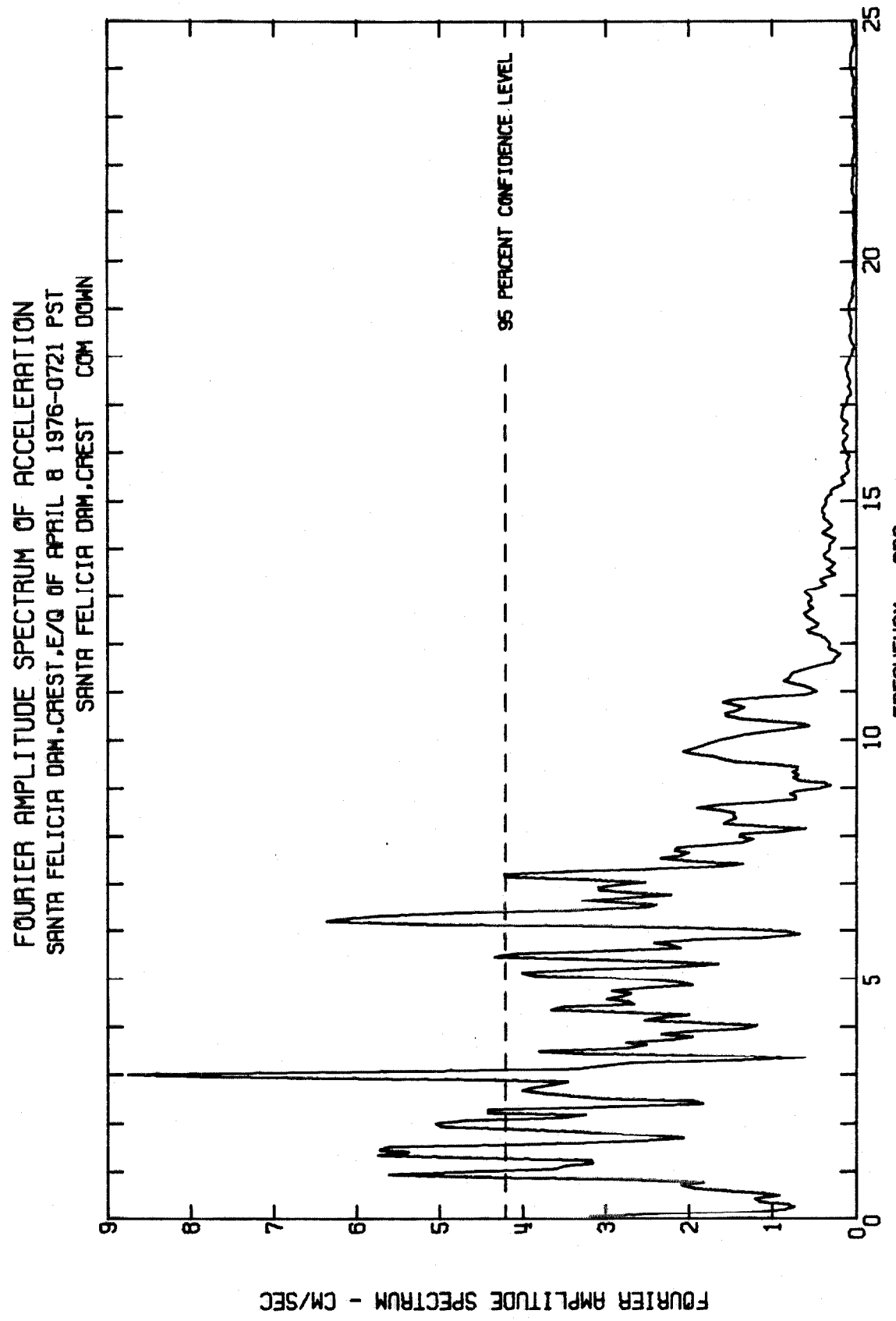
FOURIER AMPLITUDE SPECTRUM OF ACCELERATION
SANTA FELICIA DAM,CREST,E/Q OF APRIL 8 1976-0721 PST
SANTA FELICIA DAM,CREST COM DOWN
95 PERCENT CONFIDENCE LEVEL
FOURIER AMPLITUDE SPECTRUM - CM/SEC
FREQUENCY - CPS
0
1
2
3
4
5
6
7
8
9
0
5
10
15
20
25

Fig. A-19

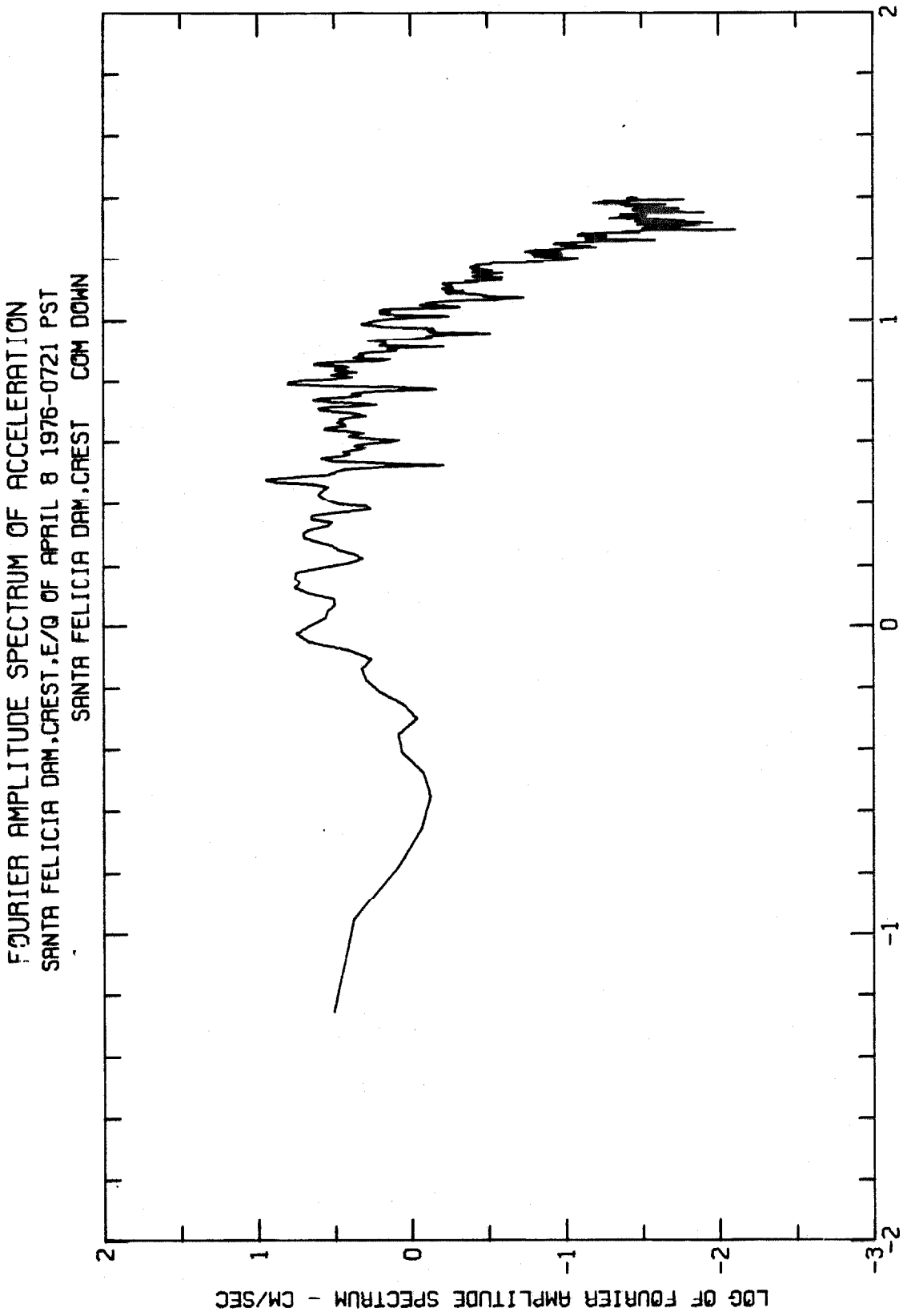
FOURIER AMPLITUDE SPECTRUM OF ACCELERATION
SANTA FELICIA DAM,CREST,E/Q OF APRIL 8 1976-0721 PST
SANTA FELICIA DAM,CREST COM DOWN
LOG OF FOURIER AMPLITUDE SPECTRUM - CM/SEC
LOG OF FREQUENCY - CPS
2
1
0
-1
-2
-3

Fig. A-20

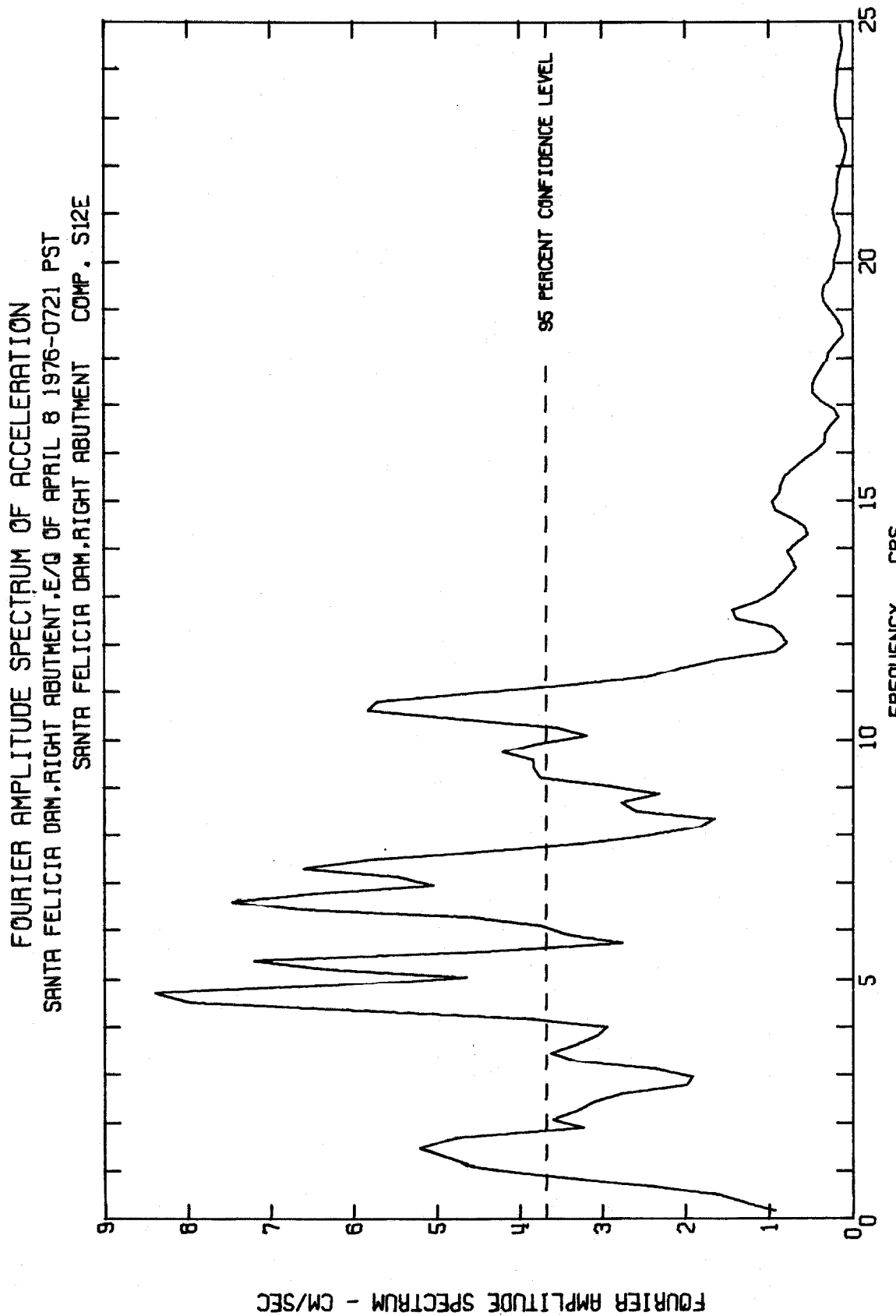
FOURIER AMPLITUDE SPECTRUM OF ACCELERATION
SANTA FELICIA DAM,RIGHT ABUTMENT,E/Q OF APRIL 8 1976-0721 PST
SANTA FELICIA DAM,RIGHT ABUTMENT COMP. S12E
95 PERCENT CONFIDENCE LEVEL
FOURIER AMPLITUDE SPECTRUM - CM/SEC
FREQUENCY - CPS
0
1
2
3
4
5
6
7
8
9
0
5
10
15
20
25

Fig. A-21

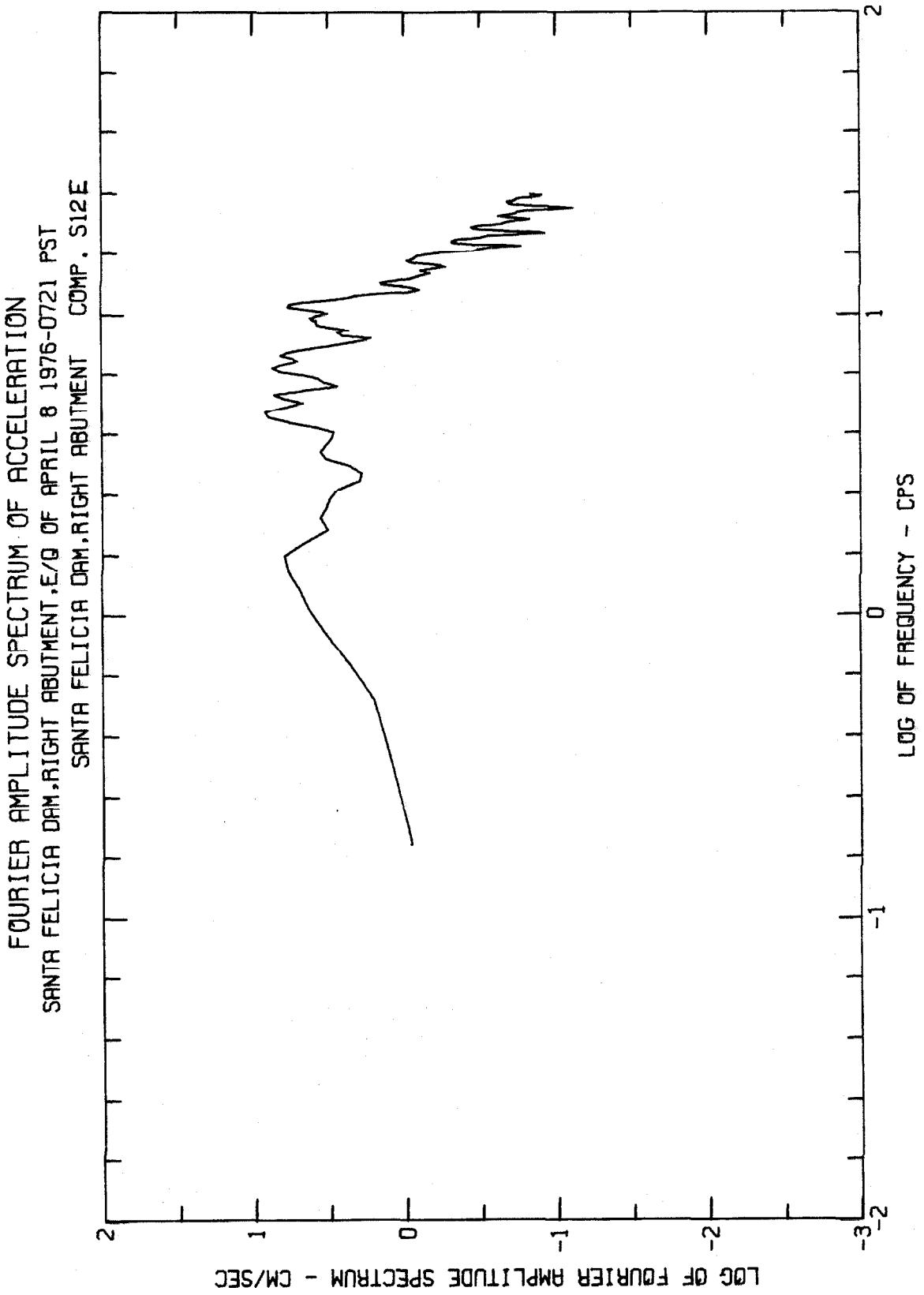
FOURIER AMPLITUDE SPECTRUM OF ACCELERATION
SANTA FELICIA DAM,RIGHT ABUTMENT,E/O OF APRIL 8 1976-0721 PST
SANTA FELICIA DAM,RIGHT ABUTMENT COMP. S12E
LOG OF FOURIER AMPLITUDE SPECTRUM - CM/SEC
LOG OF FREQUENCY - CPS
2
1
0
-1
-2
-3
2
1
0
-1
-2

Fig. A-22

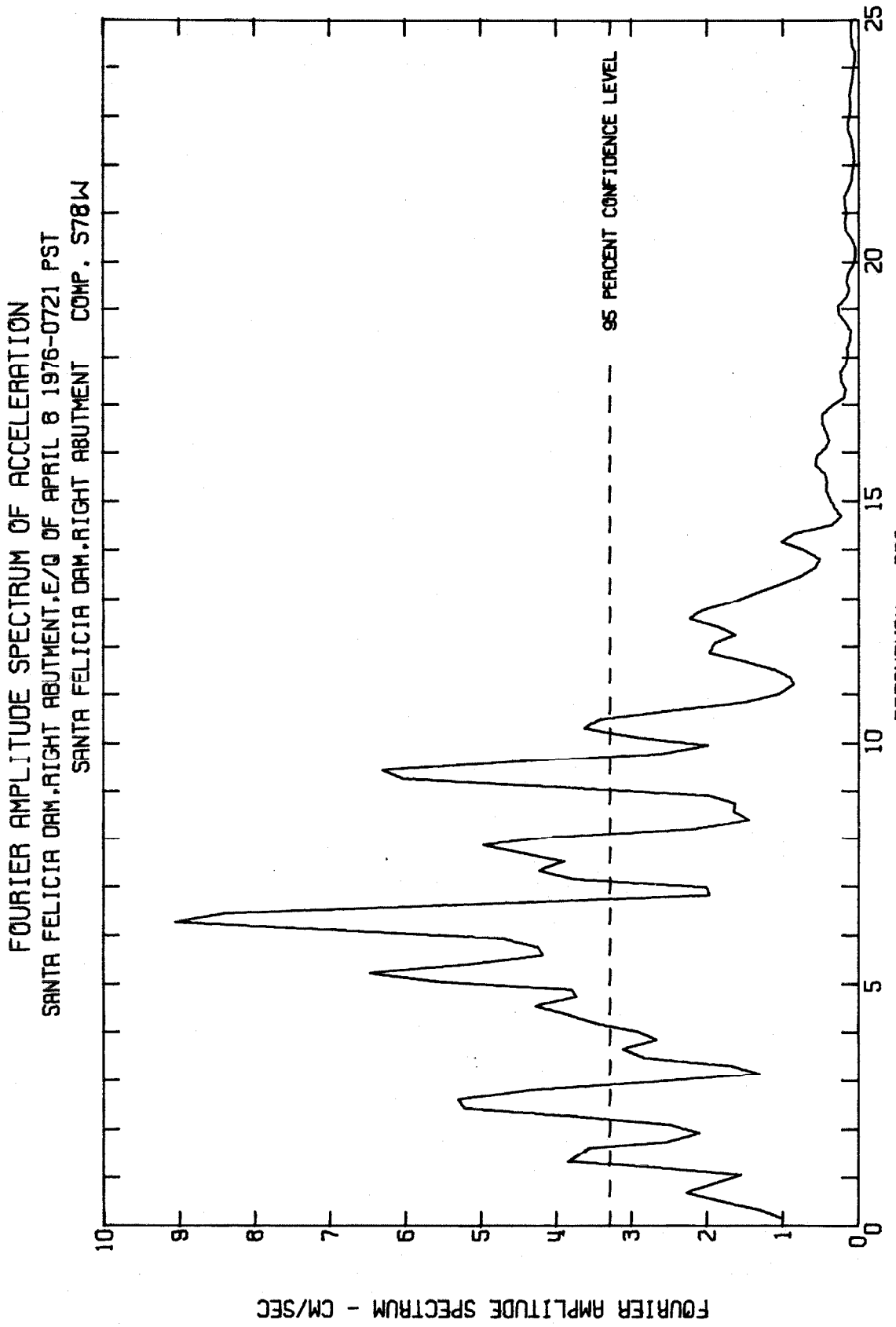
FOURIER AMPLITUDE SPECTRUM OF ACCELERATION
SANTA FELICIA DAM,RIGHT ABUTMENT,E/Q OF APRIL 8 1976-0721 PST
SANTA FELICIA DAM,RIGHT ABUTMENT COMP. S78W
95 PERCENT CONFIDENCE LEVEL
FOURIER AMPLITUDE SPECTRUM - CM/SEC
FREQUENCY - CPS
0
1
2
3
4
5
6
7
8
9
10
0
5
10
15
20
25

Fig. A-23

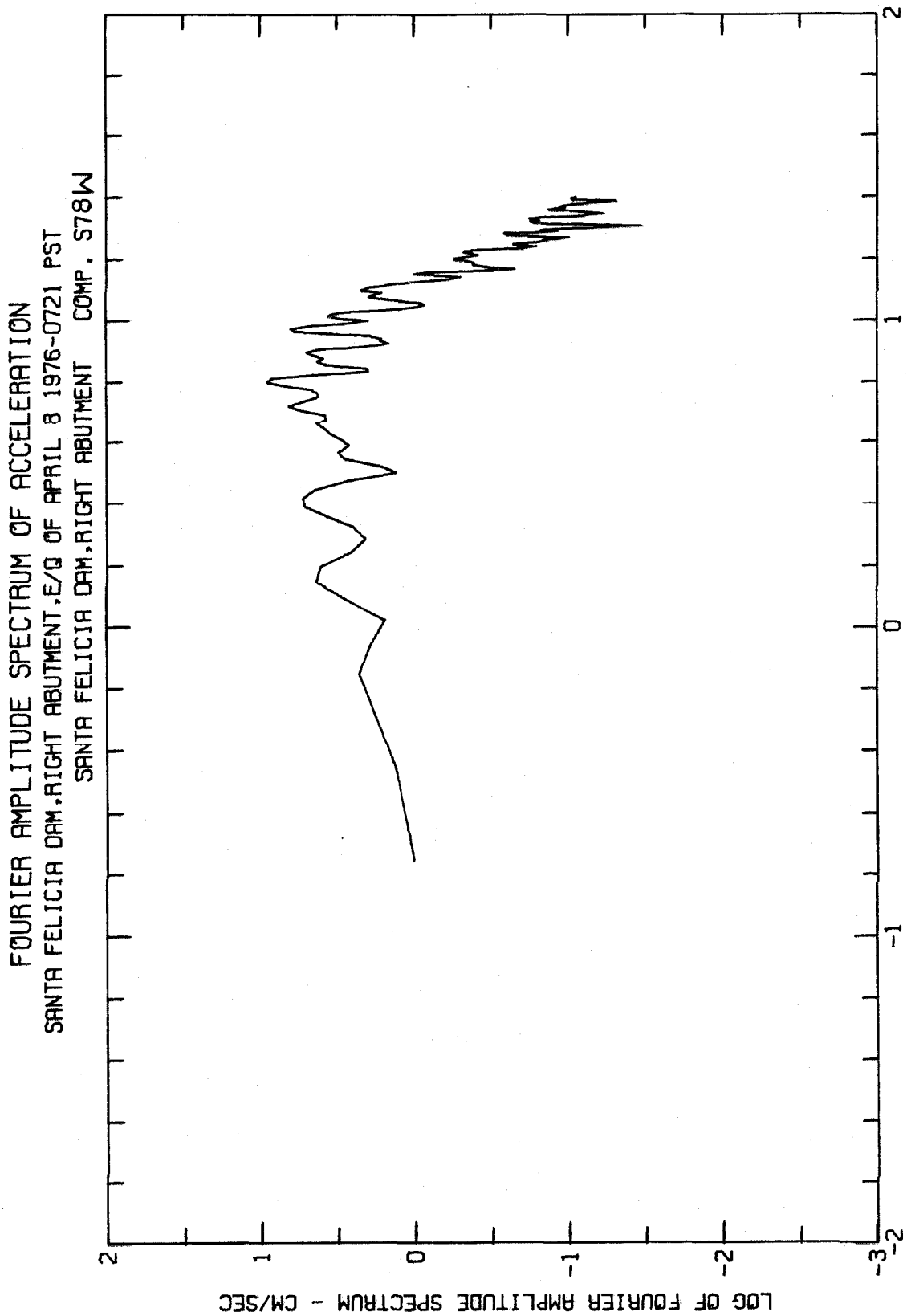
FOURIER AMPLITUDE SPECTRUM OF ACCELERATION
SANTA FELICIA DAM,RIGHT ABUTMENT,E/Q OF APRIL 8 1976-0721 PST
SANTA FELICIA DAM,RIGHT ABUTMENT COMP. S78W
LOG OF FOURIER AMPLITUDE SPECTRUM - CM/SEC
LOG OF FREQUENCY - CPS
2
1
0
-1
-2
-3
2
1
0
-1
-2

Fig. A-24

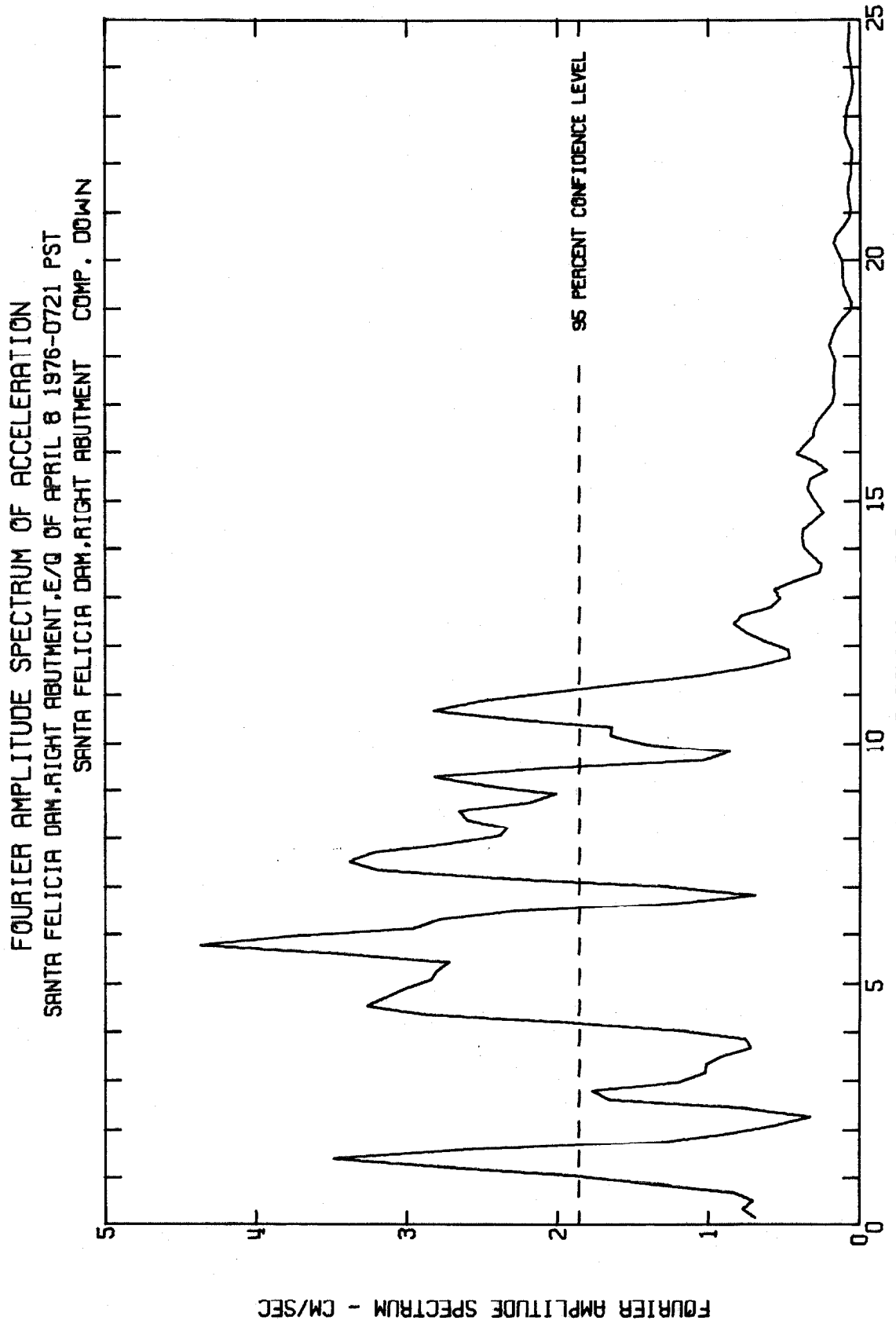
FOURIER AMPLITUDE SPECTRUM OF ACCELERATION
SANTA FELICIA DAM,RIGHT ABUTMENT,E/Q OF APRIL 8 1976-0721 PST
SANTA FELICIA DAM,RIGHT ABUTMENT COMP. DOWN
95 PERCENT CONFIDENCE LEVEL
FOURIER AMPLITUDE SPECTRUM - CM/SEC
FREQUENCY - CPS
0
5
10
15
20
25
1
2
3
4
5

Fig. A-25

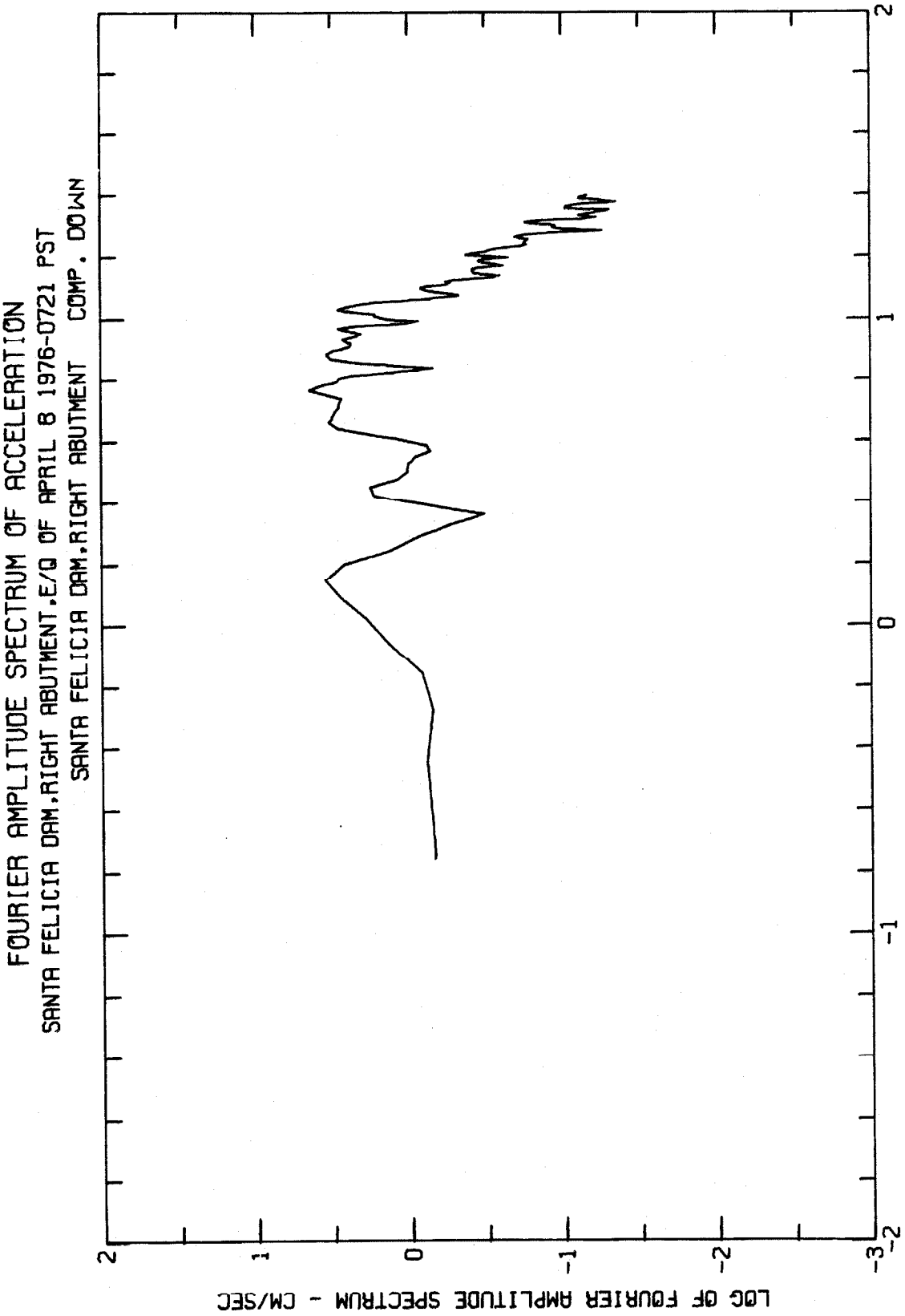
FOURIER AMPLITUDE SPECTRUM OF ACCELERATION
SANTA FELICIA DAM,RIGHT ABUTMENT,E/Q OF APRIL 8 1976-0721 PST
SANTA FELICIA DAM,RIGHT ABUTMENT COMP. DOWN
LOG OF FOURIER AMPLITUDE SPECTRUM - CM/SEC
LOG OF FREQUENCY - CPS
2
1
0
-1
-2
-3
-2
-1
0
1
2

Fig. A-26

APPENDIX B

Previously Available Data on the Shear Moduli and Damping Factors for Sands and Saturated Clays

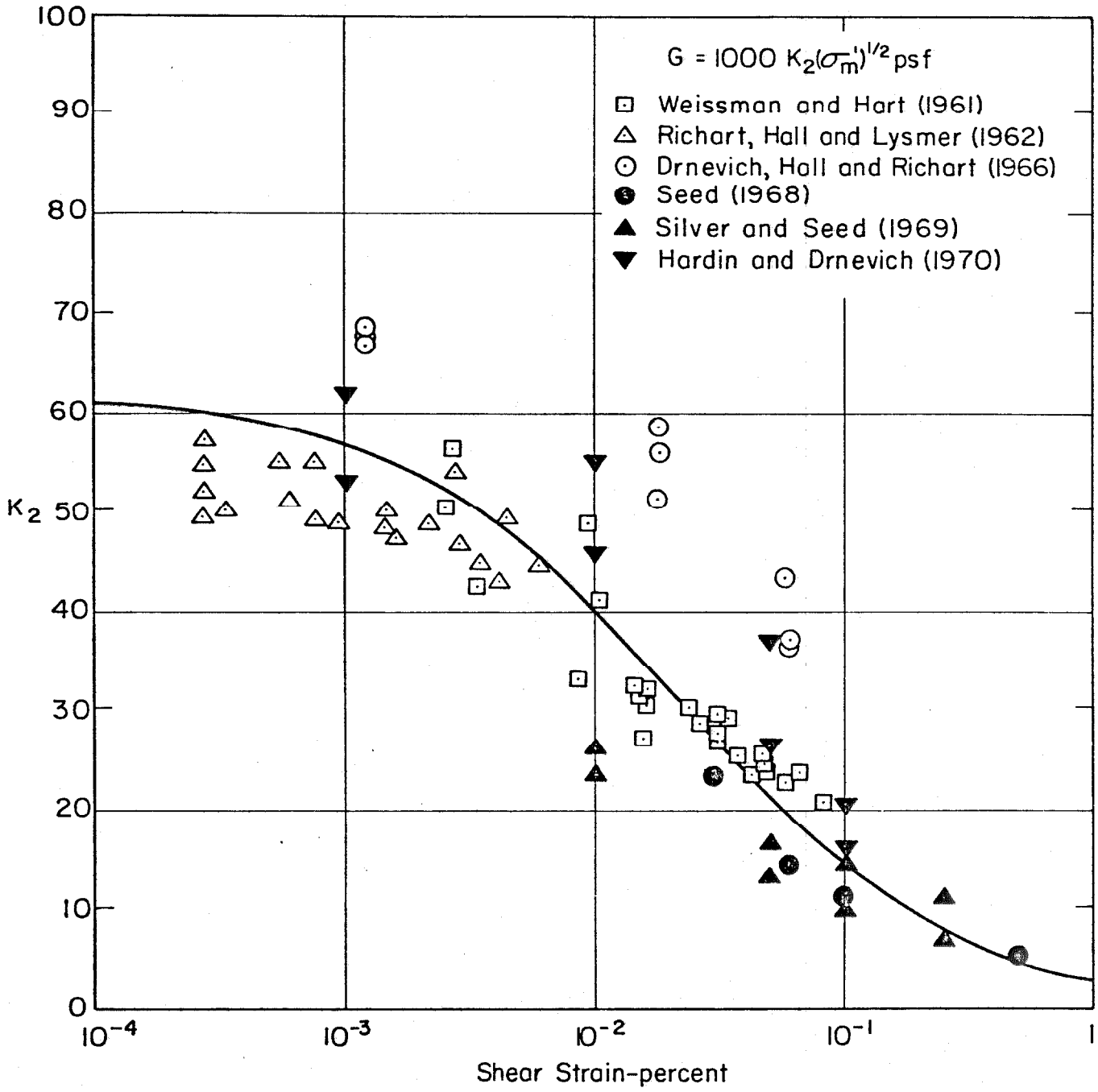

SHEAR MODULI OF SANDS AT RELATIVE DENSITY OF ABOUT 75 %.

(After Seed and Idriss, 1970)

Fig. B-1

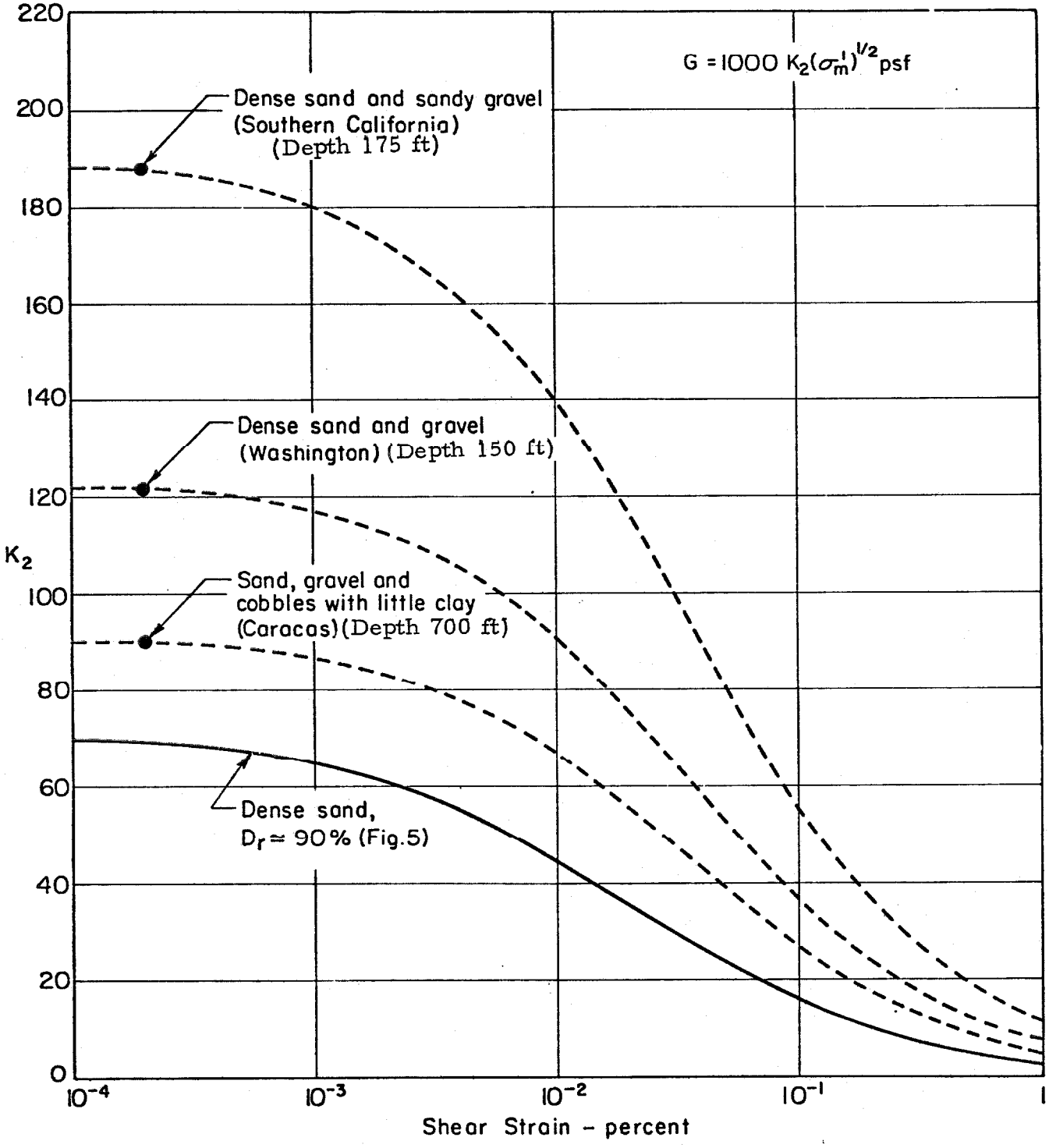

MODULI DETERMINATIONS FOR GRAVELLY SOILS.
(After Seed and Idriss, 1970)

Fig. B-2

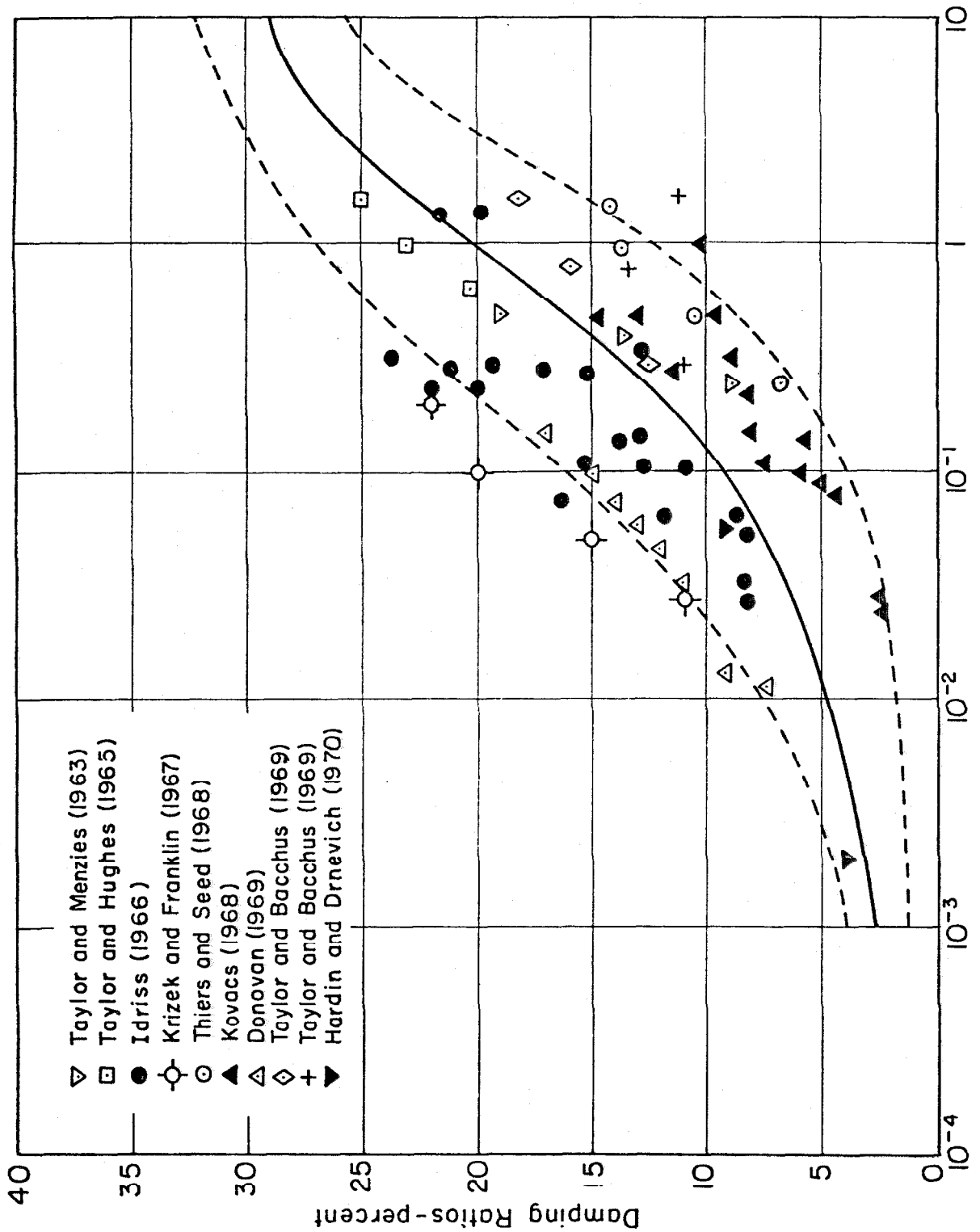

DAMPING RATIOS FOR SATURATED CLAYS.
(After Seed and Idriss, 1970)

Fig. B-3

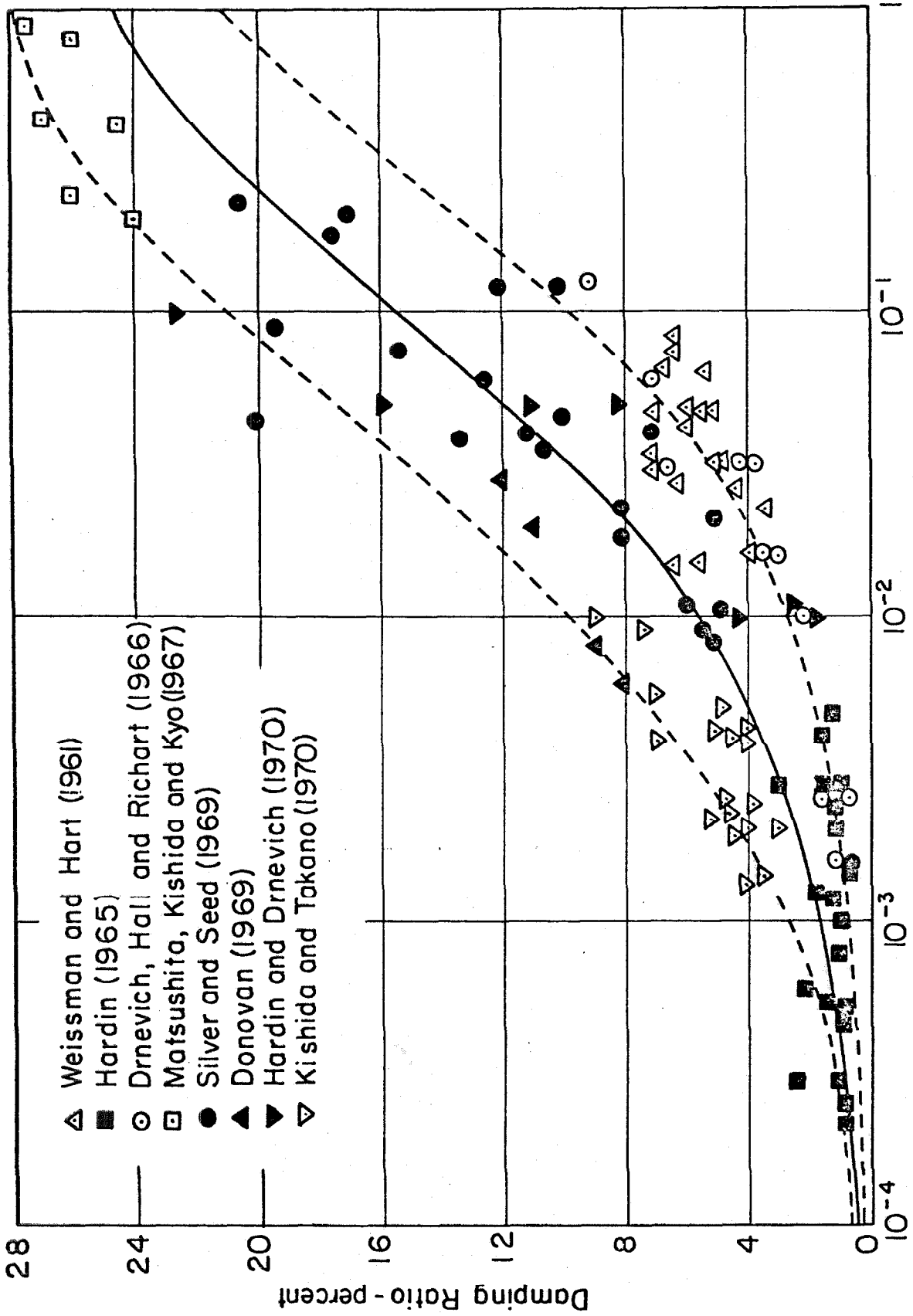

DAMPING RATIOS FOR SANDS.
(After Seed and Idriss, 1970)

Fig. B-4